

# UNCONVENTIONAL PHASES AND PHASE TRANSITIONS IN FRUSTRATED MAGNETS

A Thesis

*submitted to the*

Tata Institute of Fundamental Research, Mumbai

*for*

the degree of Doctor of Philosophy in Physics

*by*

**Animesh Nanda**

International Centre for Theoretical Sciences

Tata Institute of Fundamental Research

Bengaluru, 560097, India

January 2023

(Final version submitted in June 2023)



## DECLARATION

This thesis is a presentation of my original research work. Wherever contributions of others are involved, every effort is made to indicate this clearly, with due reference to the literature, and acknowledgement of collaborative research and discussions.

The work was done under the guidance of Prof. Subhro Bhattacharjee, at the International Centre for Theoretical Sciences, Tata Institute of Fundamental Research, Bangalore.



**Animesh Nanda**

In my capacity as supervisor of the candidate's thesis, I certify that the above statements are true to the best of my knowledge.



**Prof. Subhro Bhattacharjee**

Date: 27<sup>th</sup> June 2023

**Dedicated to my family**

*for years of support and keeping confidence in me*

## PUBLICATIONS

- Nanda, A., Dhochak, K. and Bhattacharjee, S., 2020. Phases and Quantum Phase Transitions in an Anisotropic Ferromagnetic Kitaev-Heisenberg- $\Gamma$  magnet. [Physical Review B, 102, p.235124.](#)
- Nanda, A., Agarwala, A. and Bhattacharjee, S., 2021. Phases and Quantum Phase Transitions in Anisotropic Antiferromagnetic Kitaev-Heisenberg- $\Gamma$  magnet. [Physical Review B, 104, p.195115.](#)

## ACKNOWLEDGEMENTS

I would like to express my deepest gratitude to Prof. Subhro Bhattacharjee for introducing the fascinating subject of quantum spin liquid and frustrated magnetism. I am indebted for his continuous support during various stages of my graduate school and for guiding me thoroughly through the exciting world of condensed matter physics.

During the course of my graduate school, I got the opportunity to collaborate with Prof. Kusum Dhochak and Prof. Adhip Agarwala, which gave me immense learning opportunities. I am grateful to both of them for their guidance, support, and constructive feedback. I would also like to thank Prof. R Loganayagam, and Prof. Sumilan Banerjee, for being part of my thesis monitoring committee and providing me with valuable feedback from time to time.

I am grateful to fellow group members for numerous insightful and stimulating discussions. I benefited from the discussions with Adhip Agarwala, Abhishodh Prakash, Kusum Dhochak, Aabhaas Vineet Mallik, Arnab Seth, Basudeb Mondal, Monica Bapna, and Sambuddha Sanyal. I am also grateful to my friends Chandan Jana, Avijit Das, Kohinoor Ghosh, Ajit Kumar Mehta, Subhadip Chakraborti, Priyanka Maity, Arghya Das, Akhil Sivakumar, and Joydeep Chakravarty for their constant support and well wishes.

I would further like to acknowledge the support from the Department of Atomic Energy, Government of India, for funding my fellowship, and ICTS-TIFR for providing me with the infrastructure for my research work. I participated in many conferences at ICTS, IISc, IMSc, and ICTP, I thank the organizers of these conferences for giving me the opportunity to interact with many people and exchange ideas.

Last but not the least, ICTS academic & administrative staff, canteen, and other facility staff ensured my graduate school was easier and hassle-free through their efficient services, I am indebted to them for their constant and silent support.

I thank all my friends and well-wisher for making my graduate school a memorable one.

## TABLE OF CONTENTS

### Chapter 1: Introduction and background

1.1	Introduction . . . . .	2
1.2	Outline and summary of the central results . . . . .	5

### Chapter 2: Generalized Heisenberg-Kitaev Model : Anisotropic Toric code limit

2.1	Low energy degrees of freedom in the anisotropic limit . . . . .	9
2.2	Symmetries of the low energy doublet . . . . .	11
2.2.1	Symmetries of the low energy doublet in FM anisotropic limit . . . . .	12
2.2.2	Symmetries of the low energy doublet in AFM anisotropic limit . . . . .	12
2.3	The effective Hamiltonian in FM anisotropic limit . . . . .	13
2.4	The effective Hamiltonian in AFM anisotropic limit . . . . .	15

### Chapter 3: Phases and Phase diagram in anisotropic limit

3.1	Phases and Phase diagram in FM anisotropic limit . . . . .	17
3.1.1	Toric code limit : $J = \Gamma = 0$ and canonical representation . . . . .	17
3.1.2	Heisenberg Limit : $\Gamma = K = 0$ . . . . .	20
3.1.3	Pseudo-dipolar limit: $J = K = 0$ : . . . . .	21
3.2	Phases and Phase diagram in AFM anisotropic limit . . . . .	22
3.2.1	Toric code limit $J = \Gamma = 0$ . . . . .	23
3.2.2	Heisenberg Limit: $\Gamma = K = 0$ . . . . .	23
3.2.3	The pseudo-dipolar limit $J = K = 0$ . . . . .	26

## **Chapter 4: Numerical results: FM Anisotropic Kitaev model**

4.1	Numerical results for FM Anisotropic Kitaev model . . . . .	37
-----	---	----

## **Chapter 5: Numerical results: AFM Anisotropic Kitaev model**

5.1	Phase diagram : Exact diagonalisations . . . . .	44
5.2	Exact diagonalisation study of stacked cluster chain in context of $\Gamma$ -limit of anisotropic AFM Kitaev model . . . . .	49

## **Chapter 6: Gauge theory description of the phases and phase transitions**

6.1	Gauge theory description of the phases . . . . .	54
6.2	$Z_2$ QSL from the Magnetic Order . . . . .	60

## **Chapter 7: Field Theory**

7.1	Phase transition in FM anisotropic Kitaev limit . . . . .	65
7.1.1	Phase transition between QSL and the spin ordered phase . . . . .	65
7.1.2	Effect of an external Zeeman field . . . . .	78
7.1.3	Phase Transition between QSL and the trivial paramagnet . . . . .	80
7.2	Phase transition in AFM anisotropic Kitaev limit . . . . .	90
7.2.1	Phase transition between QSL and the spin ordered phase . . . . .	90
7.2.2	Transition between large $\Gamma$ phase and $Z_2$ QSL . . . . .	97
7.2.3	Transition between spin-ordered phase and large $\Gamma$ phase . . . . .	98

## **Chapter 8: Summary and Outlook**

8.1	Summary . . . . .	99
-----	-------------------	----

## **Appendices**

### **Appendix A: Symmetry transformations**

A.1	Symmetry transformation in the anisotropic limit of FM Kitaev model . . . . .	102
A.2	Symmetry transformation in the anisotropic limit of AFM Kitaev model . . . . .	107

**Appendix B: Degenerate perturbation theory to obtain the toric code contribution in FM Kitaev model**

B.1	Low energy degrees of freedom . . . . .	108
B.2	First order contribution . . . . .	109
B.3	Fourth order contribution: Toric code . . . . .	110

**Appendix C:  $J - K$  Hamiltonian in AFM anisotropic limit**

C.1	$JK$ Hamiltonian in AFM anisotropic limit : a generic $\tau^x$ -field study . . . . .	112
-----	---	-----

**Appendix D: Additional comments and results on  $\Gamma$ -limit of AFM anisotropic model**

D.1	Summary of the 1D cluster phase ( $Z_2 \times Z_2$ SPT) . . . . .	115
D.2	$\mathcal{W}$ transformation . . . . .	119
D.3	Excitations and their dynamics in the pure $\Gamma$ limit . . . . .	120
D.4	Boundary modes of large $\Gamma$ Hamiltonian . . . . .	123
D.5	Effect of perturbations on the boundary modes . . . . .	125
D.6	Additional numerical results for the $\Gamma$ limit . . . . .	126

**Appendix E: Additional results in the anisotropic limit of the AFM Kitaev model**

E.1	Additional numerical results for the $KJT$ Hamiltonian . . . . .	128
E.2	Gauge Mean Field Theory . . . . .	128
E.3	Symmetry transformations of the soft modes . . . . .	130
E.4	Symmetry transformation of the gauge fields . . . . .	131
E.5	The phases . . . . .	131
E.6	The details of the mutual $Z_2$ gauge theory formulation . . . . .	133

**Appendix F: A possible transition between the  $Z_2$  QSL and a cluster SPT**

F.1 Transition between  $Z_2$  QSL and a cluster SPT . . . . . 135

**References**

## ABSTRACT

The theory of second-order phase transition is one of the cornerstones of modern statistical physics and condensed matter theory. Continuum field theory based on the order parameter, whose non-zero average breaks the symmetry of the Hamiltonian spontaneously captures the physics near the phase transition point. However, such local order parameter-based descriptions can not capture the physics of phase transition involving long-range entanglement phases having emerging gauge fields and deconfined degrees of freedom. In this work, we study the spin-1/2 generalized Heisenberg-Kitaev- $\Gamma$  model in the anisotropic (Toric code) limit involving a  $Z_2$  quantum spin liquid (QSL), which shows the signature of long-range entanglement and fractionalized excitations. Using a combination of exact diagonalization calculations and field-theoretic analysis we map out the phases proximate to the  $Z_2$  QSL and associated quantum phase transitions to reveal the complete phase diagram as a function of the Heisenberg, the Kitaev, and the pseudo-dipolar interactions in the anisotropic limit of ferromagnetic and anti-ferromagnetic Kitaev interaction.

In the ferromagnetic case, we find a  $Z_2$  QSL, spin-ordered, and a trivial paramagnetic phase. The transition between the QSL and the spin-ordered phase belongs to a self-dual modified Abelian Higgs field theory while that between the spin liquid and the trivial paramagnet belongs to a self-dual  $Z_2$  gauge theory. Both these transitions are examples of deconfined quantum critical points. In the anisotropic limit of antiferromagnetic Kitaev, we also find the presence of gapped  $Z_2$  QSL and the spin-ordered as well as a paramagnetic phase. Here, however, the paramagnetic phase is proximate to a gapless critical point of a system described by an equal superposition of differently oriented stacked one-dimensional  $Z_2 \times Z_2$  symmetry-protected topological phase. Similar to the ferromagnetic case, the Heisenberg limit stabilizes symmetry-breaking magnetic orders, while the phase transition between  $Z_2$  QSL and pseudo-dipolar limit is known to be a first order phase transition.

Interestingly, both the spin liquid and the spin-ordered phases have easily identifiable counterparts in the isotropic limit and the present calculations can shed insights into the corresponding transitions in the material relevant isotropic limit.

# CHAPTER 1

## INTRODUCTION AND BACKGROUND

### 1.1 Introduction

The correlated electron problem is an active area of research that surprises us with a plethora of novel phases and interesting phase transitions between them. [1, 2] In the Mott insulator regime of electronic materials, a strong Hubbard repulsion leads to localized electron moment, the exchange interactions give rise to low energy effective spin systems. [1, 3] Such spin systems, at low temperatures, undergo ordering giving rise to various magnetically ordered phases like a ferromagnet, antiferromagnetic, etc. [4, 5] In these systems, below the ordering temperature the large thermal entropy is quenched via spontaneous symmetry breaking in the thermodynamic limit. The paradigmatic local order parameter based Landau-Ginzburg-Wilson (LGW) theory to describe the phase transition between such a magnetically ordered phase and a thermal disordered phase which encapsulates the fluctuation of order parameters near the phase transition point, provides a comprehensive description of the critical point. [4–6]

Interestingly, competing spin-spin exchange interactions can suppress such magnetic orders at a low temperature, leading to a quantum paramagnet which *quenches* the thermal entropy via long-range entanglement (LRE). [7, 8] A fallout of this LRE are exotic low energy properties such as symmetry and statistics fractionalization in two spatial dimensions, and the emergence of dynamic gauge fields. [9–11] These phases are dubbed as quantum spin liquid (QSL). [7, 9] This raises an important question regarding the description of the QSL and phase transitions out of it. Such a phase or a transition out of it can not be described by the conventional local order parameter-based LGW theories as the latter do not capture the non-trivial entanglement structure and its fallout such as fractionalization [5, 12, 13]. The correct theory of the phase and associated transitions has to take into account the fractional excitations and the possible topological orders. [5].

Recently, it has been understood that the presence of the spin-orbit coupling (SOC) in the magnets containing active elements with higher atomic numbers enhances various competing interactions via a delicate balance between the electronic correlation, SOC and, crystal field effects. These competing interactions can enhance quantum fluctuations in the system, which

ultimately leads to novel quantum ground states. Prime examples are the spin-orbit coupled layered honeycomb magnets such as  $A_2\text{IrO}_3$  ( $A \equiv \text{Na, La, K}$ ), and  $\alpha\text{-RuCl}_3$  with the effective spin description is in terms of a local  $J_{eff} = 1/2$  moment. [14] Pioneering work by Jackeli and Khaliullin in 2009 [15] showed a bond-dependent interaction akin to Kitaev’s honeycomb model [16] can be realized in these materials. Interestingly, in a subset of such magnets which ultimately order (at very low temperatures), the low-temperature properties bear unconventional experimental signatures similar to fractionalized excitations[7, 9–11, 17–22] expected in a QSL. A framework to describe these properties starts by positing that these systems are proximate to the quantum phase transition between a spin-ordered phase and a QSL, albeit just on the ordered side. The finite temperature properties of such a *proximate QSL* phase then may account for, among others, the neutron scattering of honeycomb lattice magnet  $\alpha\text{-RuCl}_3$ [23–27] and rare-earth pyrochlore  $\text{Yb}_2\text{Ti}_2\text{O}_7$ . [28–32]

The case of  $\alpha\text{-RuCl}_3$  is particularly interesting where a collinear Zig-Zag spin order is stabilized below  $T \sim 7$  K.[23–27] However, recent neutron scattering experiments reveal that unusually intense diffused spin excitations resembling that of the two-particle fractionalized spinon continuum of a QSL survive well above the spin ordering temperature.[23–25] Further, in an in-plane Zeeman field, the spin order gives away to a field-induced partially-polarised paramagnet[33, 34] with unusual spin dynamics[35, 36] and quantized thermal-Hall conductivity and oscillation in longitudinal thermal conductivity [37, 38]. This has led to the suggestion the zero Zeeman field Zig-Zag order in this material occurring below 7 K[23] is fragile and proximate to a  $Z_2$  QSL with ultra short-ranged spin correlations[39]– which supports fractionalized Majorana excitations and  $Z_2$  fluxes.[16]

Within the proximate-spin liquid scenario, therefore, the quantum phase transition between the Zig-Zag spin ordered phase and the  $Z_2$  QSL then affects the low-temperature physics of  $\alpha\text{-RuCl}_3$ . On generic grounds, such transitions[12] cannot be captured within the conventional order parameter based description.[40] Further, the  $Z_2$  QSL is separated from a trivial paramagnet (one without topological order and fractionalized excitations) through a different and distinct quantum phase transition. In the case of this latter transition, an order parameter based description is completely unavailable. If the transitions are continuous– as is pertinent to the present work– the correct critical theory has to essentially account for the fractionalization and topological order[41, 42] in the  $Z_2$  QSL in addition to any possible spin order. Several examples of such *deconfined critical points*[5, 6] are known.

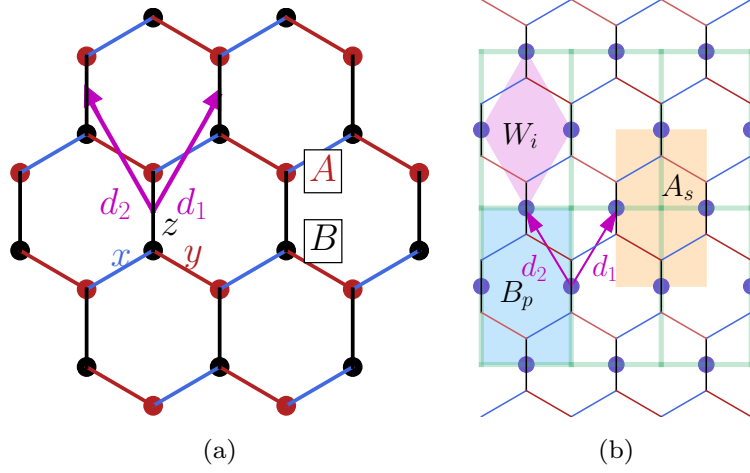


Figure 1.1: (a) Kitaev's honeycomb model is described on a bipartite hexagonal lattice with two sublattices A (red) and B (black). The spin exchanges are defined on three bonds labeled by  $x, y, z$  (shown in blue, red, and black lines respectively). (b) The anisotropic limit in the  $z$  direction leads to a square lattice where new degrees of freedom  $\tau$  (shown in grayish blue) sit on the bonds. Lattice vectors  $\mathbf{d}_1$  and  $\mathbf{d}_2$  are  $(\frac{1}{2}, \frac{1}{2})$  and  $(-\frac{1}{2}, \frac{1}{2})$  defined in the units of square lattice bond length which are assumed to be same in the horizontal and vertical direction.

The minimal spin Hamiltonian that can capture the above physics of  $\alpha$ -RuCl<sub>3</sub> is given by the so-called Heisenberg-Kitaev-Pseudodipolar ( $JK\Gamma$ ) Hamiltonian[15, 43–45]

$$H = J \sum_{\langle p,q \rangle} \boldsymbol{\sigma}_p \cdot \boldsymbol{\sigma}_q + \sum_{\langle p,q \rangle \alpha} [\Gamma_\alpha [\sigma_p^\beta \sigma_q^\gamma + \sigma_q^\beta \sigma_p^\gamma] - K_\alpha \sigma_p^\alpha \sigma_q^\alpha] \quad (1.1)$$

where  $\alpha = x, y, z$  refers to the  $x, y, z$  bonds of the honeycomb lattice respectively (see Fig. 1.1) and  $\sigma_p^\alpha$  denotes Pauli matrices representing spin-1/2 operator on the site of the honeycomb lattice.  $\langle pq \rangle$  refers to nearest neighbours while  $\langle pq \rangle \alpha$  refers to nearest neighbours along  $\alpha$ -bonds. Note that for a given  $\alpha; \beta, \gamma (= x, y, z) \neq \alpha$ . Remarkably, in addition to  $\alpha$ -RuCl<sub>3</sub>, the Hamiltonian in Eq. 1.1 can effectively describe the magnetic properties of several other strong spin-orbit coupled magnets on honeycomb lattice[15, 43, 44] that include honeycomb iridates [43, 46–50] as well as three-dimensional harmonic iridates.[26, 51–55] The material relevant isotropic limit ( $K_x = K_y = K_z$ ) has a rich phase diagram including a direct phase transition between the QSL and collinear spin ordered phases.[43, 44, 56–63]

Kitaev's honeycomb model [16] ( $J = \Gamma = 0$  in Eq. 1.1) is one of the few known exactly solvable models with a QSL ground state, which hosts fractionalized Majorana excitations and static  $Z_2$  fluxes. In an interesting anisotropic limit:  $|K_z| \gg |K_x| = |K_y| (\equiv |K|), |\Gamma|, |J|$  in Eq. 1.1, the QSL survives for  $J = \Gamma = 0$ , but the Majorana fermions acquire an extremely large gap ( $\sim |K_z|$ ) so that the  $Z_2$  fluxes become the low energy degrees of freedom. This is

the so-called toric code (TC) limit which realizes a gapped topological ordered  $Z_2$  QSL, with bosonic Ising electric ( $e$ ) and magnetic ( $m$ ) excitations and a fermionic excitation which is the bound state of  $e$  and  $m$  forming the low energy spectrum. The  $e$  and  $m$  excitations see each other as a source of  $\pi$ -flux (mutual semion).

Within this anisotropic setting, starting from TC limit (where  $J = \Gamma = 0$ ) on increasing  $J$  and  $\Gamma$ , the  $Z_2$ -QSL gives away to other phases, providing an opportunity to understand the phase transitions out of the  $Z_2$  QSL phase. Also, the understanding of such phase transitions in the anisotropic limit may provide us useful insights into the nature of the phase transition in the isotropic limit and thereby shed light on the finite temperature properties of candidates such as  $\text{RuCl}_3$  to ascertain the validity of the *proximate QSL* scenario. In this thesis, with the twin motivations above, we study the phases and phase transitions in the anisotropic limit of Eq. 1.1 to reveal the rich physics of such magnets. In the next section, we outline the structure of the thesis.

## 1.2 Outline and summary of the central results

The rest of the thesis is organized as follows, in the next chapter 2, we discuss the various energy scales of the Eq. 1.1 and set up the anisotropic limit for both ferromagnetic (FM,  $K_\alpha > 0$ ) and antiferromagnetic (AFM,  $K_\alpha < 0$ ) Kitaev coupling. We then identify the low energy degree of freedom in each case and discuss their symmetries. Finally, towards the end of this chapter, we use the degenerate perturbation theory, to find out the low energy effective Hamiltonian for FM and AFM Kitaev model. While the detailed calculation of symmetries of low energy degree of freedom and the perturbation theory is relegated to appendices A and B respectively.

In the next chapter 3, we discuss the relevant phases in both the FM and AFM anisotropic limit. In the case of the anisotropic limit of the FM Kitaev model, we show the system stabilizes the  $Z_2$  QSL ( $J = \Gamma = 0$  limit), symmetry-breaking magnetic orders by turning on Heisenberg coupling ( $J$ ), and a paramagnetic phase as we turn on pseudo-dipolar coupling ( $\Gamma$ ) (see Fig. 3.1). Similarly, in the AFM Kitaev model's anisotropic limit, the three phases are  $Z_2$  QSL, symmetry-breaking magnetic order, and a paramagnetic phase in the respective parameter regime (see Figs. 3.9). Both in FM and AFM anisotropic limits, the symmetry-breaking magnetic orders in terms of the underline  $\sigma$ -spins (of Eq. 1.1) are also found in the isotropic limit of the Kitaev honeycomb model. [44, 63]. The paramagnetic phase in the pseudo-dipolar ( $\Gamma$ ) limit of the FM case is akin to the nematic phase found in the isotropic limit. [62]

The pseudo-dipolar limit of the AFM Kitaev model is even more interesting, in this limit, the leading order interactions lead to a superposition of stacked  $Z_2 \times Z_2$  Symmetry-Protected Topological (SPTs) chains with edge modes and special sub-system symmetries which are weakly lifted by higher-order interactions. The equal superposition of SPT leads to a gapless critical point according to our symmetry analysis and finite size exact diagonalization calculations (presented in a later chapter). The gapless point, accordingly to our analysis, is fragile and immediately opens up a small gap due to higher-order perturbations. We show this phase is smoothly connected to a paramagnetic phase allowed by the symmetries of the AFM anisotropic limit. In terms of the underlying  $\sigma$ -spins, this paramagnet forms a singlet or triplet phase, depending upon the sign of the corresponding energy scale.

In chapter 4, we present the exact diagonalization based numerical results for FM anisotropic limit on finite spin clusters containing 12 – 32  $\tau$ -spins to further confirm the expectation for the phase diagram. We find out the phase boundaries between the  $Z_2$ -QSL, symmetry-breaking magnetic order, and paramagnetic phase by closely following the fidelity susceptibility and spectral gap. Furthermore, we characterize the phases using topological entanglement entropy [64, 65], two-point spin-spin correlator, and magnetization. In Fig. 4.5, we obtain the numerical phase diagram focusing on the third quadrant of Fig. 3.1. In the subsequent chapter 5, we obtain a similar phase diagram for the anisotropic limit of the AFM Kitaev model in Fig. 5.5. In the second part of this chapter (section 5.2) we further provide the supporting numerical studies focusing on the pseudo-dipolar limit ( $\Gamma$ ) of the AFM Kitaev model. We show by turning the higher order corrections in this limit the gapless point proximate to  $Z_2 \times Z_2$  SPT is smoothly connected to the paramagnet allowed by the symmetry. Further numerical evidences are relegated to appendix C, D.3, D.5, and E.1.

In chapter 6, a  $Z_2$  lattice gauge theory capturing  $e$  and  $m$  excitations of the  $Z_2$  QSL is introduced and their symmetry transformations are analyzed for both FM and AFM case. Due to the similarity of the  $Z_2$  QSL Hamiltonian in these two different limits, the gauge theory remains the same, however, a difference in the symmetry transformations of the gauge charges and fields transcends from the different symmetry transformations of the low energy degrees of freedom. In the later part of this chapter, in section 6.2, we give a prescription to obtain the  $Z_2$  QSL starting from a symmetry-broken magnetic order. We show that starting with a symmetry-broken magnetic order, the proliferation of selective domain walls with a specific sign structure leads to a  $Z_2$  QSL, which can not be connected to the product state. This is quite opposite to an

indiscriminate condensation of all the domain walls, ultimately leading to a trivial paramagnet, i.e. a product state. [66]

In the penultimate chapter 7, we provide the field theory of the phase transition out of the  $Z_2$  QSL. A canonical way to understand the emergence of short-range entangled (with or without spontaneous symmetry breaking) phases from a QSL is in terms of the condensation of the deconfined excitations of the QSL which in this case are  $Z_2$   $e$  and  $m$  charges. These bosonic  $Z_2$  charges ( $e$  and  $m$ ) are conserved modulo 2 and see each other as a source of  $\pi$  flux (mutual semions). In the case of the FM Kitaev model, in section 7.1.1, we start with the phase transition between  $Z_2$  QSL and symmetry breaking magnetic order (Eq. 7.2), using the gauge charges and fields defined in previous chapter 6, we use a gauge choice we identify the time-reversal partner soft modes from the dispersion of low energy  $e$  and  $m$  charges in Eq. 7.13 and 7.14. The symmetry transformations of the gauge charge further give rise to the symmetry transformations of these soft modes in Eq. 7.15.

Interestingly, we find the non-trivial implementation of the time-reversal symmetry (Eq. 6.10) and translation (Eq. 6.8) under  $\mathbf{T}_{d_1}$  and  $\mathbf{T}_{d_2}$  (Fig. 1.1) on the gauge charges. The latter leads to the permutation symmetry  $e \leftrightarrow m$ — an example of an *anyon permutation symmetry*. These soft modes transform under the symmetries as a pair of complex bosons,  $\Phi_e, \Phi_m$  (Eq. 7.13 and 7.14) up to a quartic term that reduces the symmetry to  $Z_4$  from  $U_e(1) \times U_m(1)$ . Crucially, however, anyon permutation  $\Phi_e \leftrightarrow \Phi_m$  leads to a self-dual structure of the critical theory. The mutual semionic statistics between the  $\Phi_e$  and  $\Phi_m$  soft modes are implemented within a mutual  $U(1) \times U(1)$  Chern Simons (CS) theory resulting in a self-dual 3D Euclidean action (Eq. 7.20) with Lagrangian

$$\begin{aligned} \mathcal{L} = & |(\partial_\mu - iA_\mu)\Phi_e|^2 + |(\partial_\mu - iB_\mu)\Phi_m|^2 + u(|\Phi_e|^2 + |\Phi_m|^2) + v(|\Phi_e|^4 + |\Phi_m|^4) \\ & - \lambda [(\Phi_e)^4 + (\Phi_e^*)^4 + (\Phi_m)^4 + (\Phi_m^*)^4] + w [(\Phi_e\Phi_m)^2 + (\Phi_e\Phi_m^*)^2 + \text{c.c.}] + \frac{i}{\pi}\epsilon^{\mu\nu\lambda}A_\mu\partial_\nu B_\lambda \end{aligned}$$

Where,  $A$ , &  $B$  are the  $U(1)$  gauge fields, which minimally couple to  $\Phi_e$  and  $\Phi_m$  respectively, while the last term in above Eq. takes care of the mutual semionic statistics.

For  $u > 0$   $\Phi_e$  and  $\Phi_m$  are gapped and the low energy effective action is given by the last term— the mutual CS action. This phase is nothing but the  $Z_2$  QSL with gapped  $e$  and  $m$  charges. The phase,  $u < 0$ , on the other hand, is characterized by finite collinear spin order characterized by the gauge invariant order parameters given by Eq. 7.29 that breaks time-reversal symmetry.

Using particle-vortex duality we can map the above action to a modified Abelian Higgs model (MAHM) which, at  $u = 0$  describes the transition. We note that the  $U_e(1) \times U_m(1)$  breaking anisotropy terms may be irrelevant at the critical point but relevant in the spin-ordered phases. An external Zeeman field lifts the symmetry of the two time-reversal partners by allowing a second order term (Eq. 7.50) of the form  $-h_z [(\Phi_e)^2 + (\Phi_e^*)^2 + (\Phi_m)^2 + (\Phi_m^*)^2]$ , see section 7.1.2. While the  $Z_2$  QSL remains intact the spin-ordered phase gets affected and is now continuously connected to the polarised phase (for  $J < 0$ ) or undergoes a spin-flop transition into a polarised phase for  $J \sim |h_z| > 0$ .

For the pseudo-dipolar in FM Kitaev model (section 7.1.3),  $\Gamma$ , perturbations similarly we get a pair of complex scalar modes,  $(\tilde{\Phi}_e, \tilde{\Phi}_m)$  (Eq. 7.59 and 7.60), which now are time reversal invariant. The projective symmetry group (PSG) of the soft modes allows for a second-order term (Eq. 7.64) similar to the Zeeman case. However, now the Higgs phase corresponds to a time reversal symmetric trivial paramagnet. In fact, we find a continuous interpolation of the soft modes driven by the Zeeman perturbation and the pseudo-dipolar perturbations by identifying the residual symmetries when both these terms are simultaneously present (Eq. 7.78). The second-order anisotropic term acts like a pairing term in a superconductor and reduces the gauge group down to  $Z_2$  from  $U(1)$  at the critical point. The transition, therefore, belongs to  $Z_2$  gauge theory on the self-dual line. The schematic phase diagram for the FM anisotropic limit is given in Fig. 3.1.

In the case of AFM anisotropic limit discussed in section 7.2.1, the field theory for the transition between  $Z_2$  QSL and symmetry breaking magnetic order (Heisenberg limit,  $J$ ) in AFM anisotropic limit is similar to the FM case. However, due to the difference in symmetry transformation between the low energy degrees of freedom in FM and AFM cases (see Eq. 2.11 and 2.12), in the Heisenberg limit ( $J$ ) we have paramagnetic field contribution. In appendix C, we provide a numerical study using a generic energy scale for this paramagnetic contribution and show despite the presence of this paramagnetic term we are inside a symmetry-breaking magnetic order in the extreme Heisenberg limit. Furthermore, the phase transition between  $Z_2$  QSL and the pseudo-dipolar limit (paramagnetic phase) is known to be of a first-order phase transition, [67, 68] hence, we do not expect any universal physics, except noting that this transition has a fundamentally different character from FM anisotropic limit.

Finally, in chapter 8, we finally summarise all the results and conclude the thesis. The details of various calculations are further given in the Appendices.

**CHAPTER 2**  
**GENERALIZED HEISENBERG-KITAEV MODEL : ANISOTROPIC TORIC CODE**  
**LIMIT**

**2.1 Low energy degrees of freedom in the anisotropic limit**

The gapped  $Z_2$  QSL stabilized in the anisotropic [69] limit is the starting point of our analysis. It is obtained by neglecting the Heisenberg ( $J$ ) and the pseudo-dipolar ( $\Gamma$ ) couplings in the Hamiltonian in Eq. 1.1 and considering one of the three Kitaev couplings to be much larger than the other two. [16] Depending on which Kitaev coupling we choose we get three equivalent gapped  $Z_2$  QSLs whose properties are related by appropriately rotating the underlying honeycomb lattice by  $\pm 2\pi/3$  about the center of the hexagon. For the rest of the paper, we shall take the Kitaev couplings on the  $z$ -bonds of Fig. 1.1 to be stronger than that of the  $x$  and  $y$  bonds.

In the presence of  $J$  and  $\Gamma$ , our analysis of the anisotropic limit starts with the derivation of the correct low energy effective Hamiltonian from Eq. 1.1 in the limit of  $|K_z| \gg |J|, |K_x|, |K_y|, |\Gamma_\alpha|$ . To this end we write the Hamiltonian in Eq. 1.1 as [16, 70]

$$\mathcal{H}^X = \mathcal{H}_0^X + \mathcal{V}^X, \quad (2.1)$$

in the above  $X = FM, AFM$ , depending upon the sign of  $K_\alpha$  in Eq. 1.1, e.g., for ferromagnetic Kitaev limit ( $K_\alpha > 0$ )

$$\mathcal{H}_0^{FM} = -(K_z - J) \sum_{\langle i,j \rangle, z} \sigma_i^z \sigma_j^z \quad (2.2)$$

and  $\mathcal{V}^X$  stands for the rest of the terms in Eq. 1.1 which can be treated as perturbation in this limit. For  $\mathcal{V}^X = 0$  the system breaks up into isolated bonds and each bond has two ground states. The nature of these ground states depends crucially on the sign of  $K_z$ .

For  $K_z > 0$ , *i.e.* the *ferromagnetic* case, the two spins participating in the bond are both parallel to each other. Let us denote these states in the  $\sigma^z$  basis by [16]

$$|\uparrow\uparrow\rangle \equiv |+\rangle, \quad |\downarrow\downarrow\rangle \equiv |-\rangle \quad (2.3)$$

where the first (second) spin belongs to sub-lattice  $A(B)$  of Fig. 1.1. The two excited states are given by

$$|\uparrow\downarrow\rangle, \quad |\downarrow\uparrow\rangle \quad (2.4)$$

where the excitation energy is  $2K_z$ . For the  $K_z < 0$ , *i.e.* the *antiferromagnetic* case, the role of the two sets of the doublet is reversed. In this case, the effective low energy Hamiltonian is obtained by re-writing Eq. 1.1 as  $\mathcal{H}^{AFM} = \mathcal{H}_0^{AFM} + \mathcal{V}^{AFM}$  where  $\mathcal{H}_0^{AFM}$  is given by

$$\mathcal{H}_0^{AFM} = (|K_z| + J) \sum_{\langle p,q \rangle, z} \sigma_p^z \sigma_q^z \quad (2.5)$$

Similar to the FM case, for  $\mathcal{V}^{AFM} = 0$  the system breaks up into isolated bonds, each with two ground states. However, contrary to the FM in Eq. 2.3 and 2.4, in the present AFM case of  $\mathcal{H}_0^{AFM}$ , the two spins on each  $z$ -bond are anti-aligned with respect to each other in the ground state manifold. So the ground states are:

$$|+\rangle \equiv |\uparrow\downarrow\rangle ; \quad |-\rangle \equiv |\downarrow\uparrow\rangle \quad (2.6)$$

which is exactly opposite to the FM case in Eq. 2.3. Also, the excited states of Eq. 2.5 are

$$|\uparrow\uparrow\rangle, \quad |\downarrow\downarrow\rangle \quad (2.7)$$

We now define  $\tau^z$  operators for each  $z$ -bond to capture the ground state manifold,  $\tau^z |\pm\rangle = \pm |\pm\rangle$  for both the cases of *ferromagnetic* ( $K_\alpha > 0$ ) and *anti-ferromagnetic* ( $K_\alpha < 0$ ). In terms of the underlying  $\sigma$  spins,

$$\tau^z = \begin{cases} (\sigma_A^z + \sigma_B^z)/2 & \text{FM}(K_z > 0) \\ (\sigma_A^z - \sigma_B^z)/2 & \text{AFM}(K_z < 0) \end{cases} \quad (2.8)$$

where the subscripts  $A$  and  $B$  label the two spins belonging to the two different sub-lattices participating in a particular  $z$ -bond (Fig. 1.1). If there are  $N_z$  number of  $z$  bonds then there are  $2N_z$ ,  $\sigma$ -spins and hence  $N_z$ ,  $\tau$ -spins. The  $\tau$ -spin span a rhombic lattice with  $\mathbf{d}_1$  &  $\mathbf{d}_2$  as the lattice vectors, as shown in Fig. 1.1 (and also Fig. A.3 in Appendix A.1).

The ground state of  $H_0$  is clearly  $2^{N_z}$ -fold degenerate. Depending on the various coupling parameters in  $\mathcal{V}$ , it breaks this degeneracy either by selecting an ordered ground state through quantum *order-by-disorder*[71] or through *disorder-by-disorder*[72] to a QSL by macroscopic superposition of the states within the degenerate manifold leading to long-range quantum en-

tanglement. We wish to understand the nature of such ordered or disordered phases along with the nature of possible intervening quantum phase transitions.

The effective low energy Hamiltonian below the  $\sim K_z$  scale can then be gotten using the strong coupling expansion in  $1/|K_z|$  from the perturbation series

$$\mathcal{H}_{eff} = \mathcal{P} [\mathcal{V} + \mathcal{V}\mathcal{G}\mathcal{V} + \dots] \mathcal{P} \quad (2.9)$$

where  $\mathcal{P}$  is the projector on the ground-state manifold of  $\mathcal{H}_0$  and  $\mathcal{G} = (1 - \mathcal{P}) \frac{1}{(E - \mathcal{H}_0)} (1 - \mathcal{P})$  is the propagator in the excited manifold.

Before describing our strong-coupling calculations, however, it is useful to understand the action of the various symmetries on the  $\tau^\alpha$  spins which will form an essential ingredient in our analysis. It is also worthwhile to note that for both FM and AFM anisotropic limit we use the same  $\tau^\alpha$ -notation. However, these degrees of freedom are defined differently as evident from Eq. 2.8, and we mark FM and AFM in the Hamiltonian to clarify the context whenever required.

## 2.2 Symmetries of the low energy doublet

The lattice points of the rhombic lattice on whose sites the  $\tau$ -spins reside (see Fig. 1.1 and also Fig. A.3 in the Appendix A.1) are given by

$$i \equiv (i_1, i_2) = i_1 \mathbf{d}_1 + i_2 \mathbf{d}_2, \quad (2.10)$$

with the two diagonal translation vectors  $\mathbf{d}_1$  &  $\mathbf{d}_2$  of the rhombic lattice as shown in Fig. 1.1. Alternatively, we can choose a Cartesian coordinate system (given by  $\hat{\mathbf{x}} = \mathbf{d}_1 - \mathbf{d}_2$  and  $\hat{\mathbf{y}} = \mathbf{d}_1 + \mathbf{d}_2$ ) with a two site-basis to describe the spins. We shall alternatively use both these descriptions whenever suitable.

Starting from the symmetries of the isotropic system (Eq. 1.1) on the honeycomb lattice (see Appendix A.1) and focusing on the FM anisotropic limit, we find the following generators of symmetries for the anisotropic limit :

- Time reversal,  $\mathcal{T}$ .
- Lattice translations in the honeycomb plane,  $T_{d_1}$  and  $T_{d_2}$ . Under translation  $T_{d_1} : (i_1, i_2) \rightarrow (i_1 + 1, i_2)$  and  $T_{d_2} : (i_1, i_2) \rightarrow (i_1, i_2 + 1)$ .

- Reflection about  $z$ -bond of the honeycomb lattice,  $\sigma_v$  for which we have  $\sigma_v : (i_1, i_2) \rightarrow (-i_2, -i_1)$ .
- $\pi$ -rotation about the  $z$ -bond,  $C_{2z}$  which gives  $C_{2z} : (i_1, i_2) \rightarrow (i_2, i_1)$ .

Note that due to spin-orbit coupling, the spin quantization axes and the real space are coupled and we choose the same convention as You *et. al.* in Ref. [73] to understand the symmetry transformations. Further, in addition to the symmetries listed above, we find it convenient to use the additional symmetry

- $\pi$ -rotation about the honeycomb lattice hexagon center,  $R_\pi = C_{2z}\sigma_v$

### 2.2.1 Symmetries of the low energy doublet in FM anisotropic limit

The action of the above symmetry transformations on the ground state doublets are given by (see Appendix A.1 for details) :

$$\begin{aligned}
\mathcal{T} : \quad & \{\tau_i^x, \tau_i^y, \tau_i^z\} \rightarrow \{\tau_i^x, \tau_i^y, -\tau_i^z\} \\
T_{\mathbf{d}_j} : \quad & \{\tau_i^x, \tau_i^y, \tau_i^z\} \rightarrow \{\tau_{i+\mathbf{d}_j}^x, \tau_{i+\mathbf{d}_j}^y, \tau_{i+\mathbf{d}_j}^z\} \\
\sigma_v : \quad & \{\tau^x, \tau^y, \tau^z\}_{(i_1, i_2)} \rightarrow \{-\tau^x, \tau^y, -\tau^z\}_{(-i_2, -i_1)} \\
C_{2z} : \quad & \{\tau^x, \tau^y, \tau^z\}_{(i_1, i_2)} \rightarrow \{-\tau_j^x, \tau_j^y, -\tau_j^z\}_{(i_2, i_1)} \\
R_\pi : \quad & \{\tau^x, \tau^y, \tau^z\}_{(i_1, i_2)} \rightarrow \{\tau^x, \tau^y, \tau^z\}_{(-i_1, -i_2)}
\end{aligned} \tag{2.11}$$

It is crucial to notice that,  $\tau^\alpha$ 's are *non-Kramers doublets*. Hence any on-site (time reversal odd) magnetic ordering that can be described within this limit, has to be an ordering of  $\tau^z$ . This also means that an external Zeeman field can only couple to  $\tau^z$  at linear order as is characteristic to such non-Kramers systems.

### 2.2.2 Symmetries of the low energy doublet in AFM anisotropic limit

Similar to the FM case we obtain the symmetry transformations of AFM  $\tau$ -doublet:

$$\begin{aligned}
\mathcal{T} : \quad & \{\tau_i^x, \tau_i^y, \tau_i^z\} \rightarrow \{\tau_i^x, \tau_i^y, -\tau_i^z\} \\
T_{\mathbf{d}_j} : \quad & \{\tau_i^x, \tau_i^y, \tau_i^z\} \rightarrow \{\tau_{i+\mathbf{d}_j}^x, \tau_{i+\mathbf{d}_j}^y, \tau_{i+\mathbf{d}_j}^z\} \\
\sigma_v : \quad & \{\tau^x, \tau^y, \tau^z\}_{(i_1, i_2)} \rightarrow \{\tau^x, \tau^y, \tau^z\}_{(-i_2, -i_1)} \\
C_{2z} : \quad & \{\tau^x, \tau^y, \tau^z\}_{(i_1, i_2)} \rightarrow \{\tau_j^x, -\tau_j^y, -\tau_j^z\}_{(i_2, i_1)} \\
R_\pi : \quad & \{\tau^x, \tau^y, \tau^z\}_{(i_1, i_2)} \rightarrow \{\tau^x, -\tau^y, -\tau^z\}_{(-i_1, -i_2)}
\end{aligned} \tag{2.12}$$

Please refer to the appendix A.2 for more details on the symmetry transformation. With the symmetries, we now start to analyze the low energy effective theories for the Hamiltonian (Eq. 1.1) in the anisotropic limit for the ferromagnetic ( $K_\alpha > 0$ ) case.

### 2.3 The effective Hamiltonian in FM anisotropic limit

For the Isotropic model with ferromagnetic Kitaev exchanges ( $K_x = K_y = K_z > 0$ ), with increasing Heisenberg coupling,  $J$ , the Kitaev spin liquid gives way to a ferromagnetic (for  $J < 0$ ) or a stripy spin ordered (for  $J > 0$ ) (Fig. 3.2) phase. The situation with the pseudo-dipolar interactions are much less clear and recently both the possibilities of QSL and a lattice nematic has been suggested[61, 62] in related models.

Here we show, similar results can also be obtained in the anisotropic limit, the effective Hamiltonian in the anisotropic limit is obtained through degenerate perturbation theory as outlined in Eq. 2.9. For the FM anisotropic limit, *i.e.*  $K_x = K_y = K > 0$ ,  $\Gamma_\alpha = \Gamma$  (where  $\alpha = x, y, z$ ), we derive the effective low energy Hamiltonian for the  $\tau$ -spins till fourth-order perturbation theory which captures the QSL, the proximate spin ordered phases as well as possible trivial paramagnets. The effective low energy Hamiltonian for the  $\tau$ -spins is given by

$$\mathcal{H}_{eff}^{FM} = \mathcal{H}_{[1]}^{FM} + \mathcal{H}_{[2]}^{FM} + \mathcal{H}_{[3]}^{FM} + \mathcal{H}_{[4]}^{FM} \tag{2.13}$$

where,

$$\mathcal{H}_{[1]}^{FM} = \left[ 2\Gamma \left( 1 - \frac{\Gamma^2}{\Delta^2} \right) - \frac{2\Gamma^2 \delta^2}{\Delta^3} \right] \sum_i \tau_i^y \tag{2.14}$$

is the *single spin* interaction. The index  $i$  now denotes the bonds of a square lattice as shown in Fig. 1.1. We have used

$$\delta = K - J \quad \text{and} \quad \Delta = K_z - J \quad (2.15)$$

for clarity. Note that the linear term in  $\tau^y$  in Eq. 2.14 is time reversal invariant and is proportional to  $\Gamma$  and hence is zero when  $\Gamma = 0$ . This term, as we shall see below, makes the  $Z_2$  QSL unstable to a trivial paramagnet as  $\Gamma$  is increased.

The other terms  $a = 2, 3, 4$  in the Hamiltonian  $\mathcal{H}_{[a]}$  involve interactions among two, three, and four spins respectively. Odd-spin terms are generically allowed due to the non-Kramers nature of the  $\tau$ -spins.

In writing the higher order terms we use the convention: each plaquette of the rhombic lattice is associated with its left edge such that we denote the spin on the left edge as  $\tau_i$  (Fig. 1.1). Using the definition of  $\mathbf{d}_1$  and  $\mathbf{d}_2$ , the topmost spin is then given by  $\tau_{i+d_1}$  while the other two spins, the one on the right and the one on the bottom are  $\tau_{i+d_1-d_2}$  and  $\tau_{i-d_2}$  respectively. With this, the two spin interactions are given by

$$\begin{aligned} \mathcal{H}_{[2]}^{FM} = & \left[ J - \frac{J\delta}{2\Delta} - \frac{J^3\delta + J\delta^3}{8\Delta^3} \right] \sum_{\langle ij \rangle} \tau_i^z \tau_j^z + \left[ \frac{J^2\delta^2}{2\Delta^3} \right] \sum_i \tau_i^z \tau_{i+d_1-d_2}^z \\ & - \left[ \frac{5J^2\delta^2}{8\Delta^3} \right] \sum_i (\tau_i^x \tau_{i+d_1-d_2}^x + \tau_i^y \tau_{i+d_1-d_2}^y) \\ & - \left[ \frac{J^2\delta^2}{4\Delta^3} \right] \sum_i \tau_{i+d_1}^z \tau_{i-d_2}^z - \left[ \frac{J^2\delta^2}{8\Delta^3} - \frac{\Gamma^2 J}{\Delta^2} \right] \sum_i (\tau_{i+d_1}^z \tau_{i-d_1}^z + \tau_{i+d_2}^z \tau_{i-d_2}^z) \end{aligned} \quad (2.16)$$

The leading term (proportional to  $J$ ) is an Ising interaction which, as we shall see drives the transition from the  $Z_2$  QSL to a spin-ordered phase. Unlike the trivial paramagnet above, this spin-ordered phase breaks time-reversal symmetry as well as lattice point groups symmetries  $\sigma_v$  and  $C_{2z}$  (Eq. 2.11) discussed in section 2.2.1.

The three spin interactions are given by

$$\begin{aligned}
\mathcal{H}_{[3]}^{FM} = & \left[ \frac{\Gamma^2}{\Delta} + \frac{7\Gamma^2\delta^2 - 4\Gamma^4}{4\Delta^3} \right] \sum_i (\tau_{i+d_1}^z \tau_i^x \tau_{i-d_1}^z - \tau_{i+d_2}^z \tau_i^x \tau_{i-d_2}^z) \\
& - \left[ \frac{\Gamma^2}{\Delta} - \frac{4\Gamma^4 - 6\Gamma^2\delta^2 + J^2\Gamma^2}{4\Delta^3} \right] \sum_i \tau_{i+d_1}^z \tau_{i-d_2}^z (\tau_i^y + \tau_{i+d_1-d_2}^y) \\
& + \left[ \frac{\Gamma^3}{\Delta^2} - \frac{\Gamma^4 + 3\Gamma^2\delta^2}{2\Delta^3} \right] \sum_i (\tau_i^z \tau_{i+d_1-d_2}^x - \tau_{i+d_1-d_2}^z \tau_i^x) (\tau_{i+d_1}^z - \tau_{i-d_2}^z) \\
& + \left[ \frac{J\Gamma^2}{\Delta^2} \right] \sum_i \tau_{i+d_1-d_2}^z \tau_i^z (\tau_{i+d_1}^y + \tau_{i-d_2}^y)
\end{aligned} \tag{2.17}$$

These third-order terms, along with others renormalize the energy of various excitations in both the QSL as well as the ordered phases and trivial paramagnet. However, we expect that they do not change the qualitative nature of the phase diagram.

Finally, the four spin interactions are given by

$$\mathcal{H}_{[4]}^{FM} = - \left[ \frac{J^4 + \delta^4}{16\Delta^3} \right] \sum_i \tau_i^y \tau_{i+d_1-d_2}^y \tau_{i+d_1}^z \tau_{i-d_2}^z - \left[ \frac{J^2\delta^2}{8\Delta^3} \right] \sum_i \tau_i^x \tau_{i+d_1-d_2}^x \tau_{i+d_1}^z \tau_{i-d_2}^z \tag{2.18}$$

where the first term is nothing but the Toric code Hamiltonian (exactly solvable for  $J = 0$ ) that has a  $Z_2$  QSL ground state.[16, 69] In appendix B we discuss the detailed calculation to obtain the first term in the above Eq. along with the first order contribution coming from pseudo-dipolar and Heisenberg energy scale.

Thus we have the entire effective Hamiltonian in the FM anisotropic limit which is consistent with the symmetries up to the fourth order of perturbation theory in  $1/K_z$  that incorporates the physics of all the relevant phases.

## 2.4 The effective Hamiltonian in AFM anisotropic limit

The low energy effective Hamiltonian for AFM anisotropic limit (up to fourth order in perturbation theory) is given by

$$\mathcal{H}_{\text{eff}}^{AFM} = \mathcal{H}_{[1]}^{AFM} + \mathcal{H}_{[2]}^{AFM} + \mathcal{H}_{[3]}^{AFM} + \mathcal{H}_{[4]}^{AFM} \tag{2.19}$$

where 1 – 4 represents the number of spins operators involved. The *single spin* terms are given by

$$\mathcal{H}_{[1]}^{AFM} = 2J \left( 1 - \frac{\Gamma^2}{\tilde{\Delta}^2} \right) \sum_i \tau_i^x \quad (2.20)$$

where  $\tilde{\delta} = J + |K|$ ,  $\tilde{\Delta} = |K_z| + J$ .

*Two-spin* contributions are:

$$\begin{aligned} \mathcal{H}_{[2]}^{AFM} = & - \left[ J + \frac{J\tilde{\delta}}{2\tilde{\Delta}} + \frac{\tilde{\delta}^3 J + \tilde{\delta} J^3}{8\tilde{\Delta}^3} \right] \sum_{\langle i,j \rangle} \tau_i^z \tau_j^z + \frac{J^2 \tilde{\delta}^2}{2\tilde{\Delta}^3} \sum_i \tau_i^z \tau_{i+d_1-d_2}^z - \left[ \frac{2\Gamma^3}{\tilde{\Delta}^2} + \frac{J^2 \tilde{\delta}^2}{4\tilde{\Delta}^3} \right] \sum_i \tau_{i+d_1}^z \tau_{i-d_2}^z \\ & - \frac{J^2 \tilde{\delta}^2}{8\tilde{\Delta}^3} \sum_i (\tau_{i+d_1}^z \tau_{i-d_1}^z + \tau_{i+d_2}^z \tau_{i-d_2}^z) + \frac{\tilde{\delta} J \Gamma^2}{\tilde{\Delta}^3} \sum_i (\tau_i^x \tau_{i+d_1-d_2}^y - \tau_i^y \tau_{i+d_1-d_2}^x) \\ & - \frac{5J^2 \tilde{\delta}^2}{8\tilde{\Delta}^3} \sum_i (\tau_i^x \tau_{i+d_1-d_2}^x + \tau_i^y \tau_{i+d_1-d_2}^y) \end{aligned} \quad (2.21)$$

*Three spin* contributions are:

$$\begin{aligned} \mathcal{H}_{[3]}^{AFM} = & \sum_i \left( \left[ \frac{\Gamma^2}{\tilde{\Delta}} - \frac{(\Gamma)^4}{\tilde{\Delta}^3} + \frac{7\Gamma^2 \tilde{\delta}^2}{4\tilde{\Delta}^3} \right] (\tau_{i+d_1}^z \tau_i^x \tau_{i-d_1}^z + \tau_{i+d_2}^z \tau_i^x \tau_{i-d_2}^z) \right. \\ & + \left[ \frac{\Gamma^2}{\tilde{\Delta}} - \frac{4\Gamma^4 + J^2 \Gamma^2}{4\tilde{\Delta}^3} + \frac{3\Gamma^2 \tilde{\delta}^2}{2\tilde{\Delta}^3} \right] (\tau_{i+d_1}^z \tau_i^y \tau_{i-d_2}^z - \tau_{i+d_2}^z \tau_i^y \tau_{i-d_1}^z) \\ & - \left[ \frac{\Gamma^4}{2\tilde{\Delta}^3} + \frac{3\Gamma^2 \tilde{\delta}^2}{2\tilde{\Delta}^3} \right] \sum_i (\tau_i^z \tau_{i-d_2}^z \tau_{i+d_1-d_2}^x + \tau_{i+d_1-d_2}^z \tau_{i+d_1}^z \tau_i^x - \tau_i^z \tau_{i+d_1}^z \tau_{i+d_1-d_2}^x - \tau_{i+d_1-d_2}^z \tau_{i-d_2}^z \tau_i^x) \\ & + \frac{J\Gamma^2}{\tilde{\Delta}^2} \sum_i (\tau_i^z \tau_{i+d_1}^z \tau_{i+d_1-d_2}^y - \tau_{i+d_1-d_2}^z \tau_{i-d_2}^z \tau_i^y + \tau_i^z \tau_{i-d_2}^z \tau_{i+d_1-d_2}^y - \tau_{i+d_1-d_2}^z \tau_{i+d_1}^z \tau_i^y) \\ & + \frac{\Gamma^3}{\tilde{\Delta}^2} \sum_i (\tau_{i+d_1}^z \tau_i^x \tau_{i+d_2}^z + \tau_{i-d_1}^z \tau_i^x \tau_{i-d_2}^z) \end{aligned} \quad (2.22)$$

*Four spins* contributions are:

$$\mathcal{H}_{[4]}^{AFM} = - \left[ \frac{\tilde{\delta}^4}{16\tilde{\Delta}^3} + \frac{J^4}{16\tilde{\Delta}^3} \right] \sum_i \tau_{i+d_1}^z \tau_{i-d_2}^z \tau_i^y \tau_{i+d_1-d_2}^y - \frac{J^2 \tilde{\delta}^2}{8\tilde{\Delta}^3} \sum_i \tau_{i+d_1}^z \tau_{i-d_2}^z \tau_i^x \tau_{i+d_1-d_2}^x \quad (2.23)$$

Following the two effective Hamiltonians in both FM and AFM anisotropic limit we now proceed to discuss the phases in different parameter regimes of both the Hamiltonian.

## CHAPTER 3

### PHASES AND PHASE DIAGRAM IN ANISOTROPIC LIMIT

With the above effective low energy Hamiltonians equations 2.13 and 2.19 for FM and AFM limit respectively, we now study the phase diagram as a function of  $J/|K|$  vs  $\Gamma/|K|$ .

#### 3.1 Phases and Phase diagram in FM anisotropic limit

The central result of this analysis for FM limit is shown in the schematic phase diagram of Fig. 3.1. We will discuss the above phase diagram as well as study the possible phase transitions using a combination of various field theoretic techniques and exact diagonalization calculations on small spin clusters in this thesis.

Before delving into the detailed analysis that results in the phase diagram, let us focus on the different limits to gain insights into the phase diagram. This will also allow us to understand the nature of the low-energy modes near the phase transitions.

##### 3.1.1 Toric code limit : $J = \Gamma = 0$ and canonical representation

In this limit the Hamiltonian in Eq. 2.13 becomes

$$\mathcal{H}_{J=\Gamma=0}^{FM} = - J_{TC} \sum_i W_i \quad (3.1)$$

With  $J_{TC} = \frac{K^4}{16|K_z|^3}$ , and  $W_i \equiv \tau_{i+d_1}^z \tau_{i-d_2}^z \tau_i^y \tau_{i+d_1-d_2}^y$  is the plaquette operator shown on the lattice (see Fig. 1.1). This is exactly equivalent to the Toric code model[69] albeit in the *Wen's representation*. [74] While the details of this limit are well known, [16, 69] we briefly summarise them for completion as well as to set up the notations that will be useful for our calculations.

Eq. 3.1 is brought into a familiar form by the following site-dependent rotation– rotate all the spins on the horizontal bonds (Fig. 1.1) of the square lattice by  $U_h = \exp[i\tau^z \pi/4]$  and on the vertical bonds by  $U_v = \exp[-i\pi(\tau^x + \tau^y + \tau^z)/(3\sqrt{3})]$ . [16] This gives

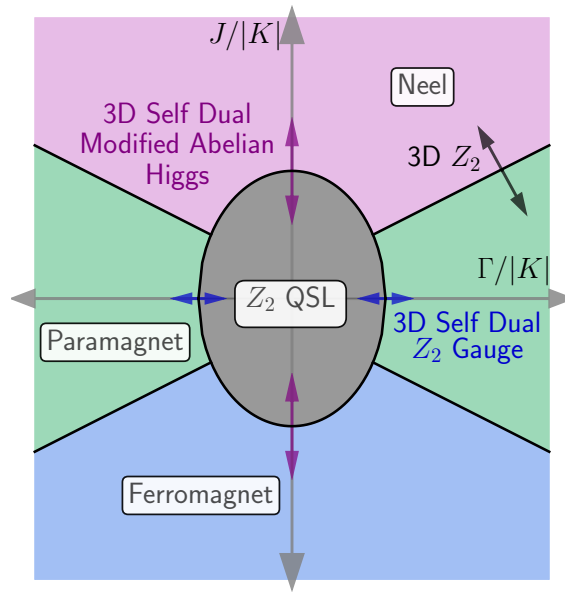


Figure 3.1: Schematic phase diagram of the anisotropic FM Kitaev limit. At origin, i.e.  $\Gamma = J = 0$  is the  $Z_2$  QSL, that survives the small perturbation with respect to  $\Gamma/|K|$ ,  $J/|K|$ . However, it finally gives way to the magnetically ordered phases (driven by the Heisenberg coupling,  $J$ ) or a trivial product paramagnet (driven by the pseudo-dipolar coupling  $\Gamma$ ). The field theoretic analysis leads to an understanding of the nature of the deconfined quantum phase transition between the QSL and the spin-ordered phase or the trivial paramagnet, in addition to the regular quantum phase transition associated with spontaneous symmetry breaking— as mentioned in the plot above.

$$\begin{aligned}
\{\tau_i^x, \tau_i^y, \tau_i^z\} &\rightarrow \{-\tilde{\tau}_i^y, \tilde{\tau}_i^x, \tilde{\tau}_i^z\} \quad \forall i \in \text{horizontal. bonds} \\
\{\tau_i^x, \tau_i^y, \tau_i^z\} &\rightarrow \{\tilde{\tau}_i^y, \tilde{\tau}_i^z, \tilde{\tau}_i^x\} \quad \forall i \in \text{vertical bonds}
\end{aligned} \tag{3.2}$$

where we denote the rotated basis by  $\tilde{\tau}^\alpha$ . Eq. 3.1 then assumes the canonical Toric code form[16, 69]

$$\tilde{\mathcal{H}}_{J=\Gamma=0}^{FM} = - J_{TC} \left[ \sum_s A_s + \sum_p B_p \right] \tag{3.3}$$

where the indices  $s, p$  denote star and plaquette respectively on the square lattice in Fig. 1.1 with  $A_s = \prod_{i \in s} \tilde{\tau}_i^x$ ,  $B_p = \prod_{i \in p} \tilde{\tau}_i^z$ . [16, 69] This stabilizes a topologically ordered  $Z_2$  QSL[16, 69] with excitations being gapped bosonic  $Z_2$  *electric* ( $e$ ) and *magnetic* ( $m$ ) charges residing on the vertices and plaquettes of the square lattice (Fig. 1.1) respectively. Crucially, the  $e$  and  $m$  charges have mutual semionic statistics,[69] *i.e.*, they see each other as a source of Aharonov-Bohm flux of  $\pi$ . It is useful to remind ourselves the exact ground states wave-function of a system at this point which is given by[69]

$$|\Psi_{G.S.}^{\text{Toric}}\rangle = \prod_s \left( \frac{\mathbb{I} + A_s}{2} \right) |0_z\rangle \tag{3.4}$$

where

$$|0_z\rangle = \bigotimes_i |+\rangle_i \tag{3.5}$$

represents the reference all up-state in the  $\tilde{\tau}^z$  basis. Three other ground states on a 2-tori can be generated from the above state by operating with the following Wilson-loop operators along the two non-trivial loops in the 2-tori :

$$\mathcal{L}_{x(y)}^e = \prod_{i \in l_{x(y)}} \tilde{\tau}_i^z ; \quad \mathcal{L}_{x(y)}^m = \prod_{i \in l_{x(y)}^*} \tilde{\tau}_i^x \tag{3.6}$$

$\mathcal{L}_{x(y)}^e$  ( $\mathcal{L}_{x(y)}^m$ ) is product over  $\tilde{\tau}^z$  ( $\tilde{\tau}^x$ ) on the closed loop  $l_{x(y)}$  ( $l_{x(y)}^*$ ) defined on the links of the direct(dual) lattice along horizontal and vertical directions respectively. These operators have

eigenvalues of  $\pm 1$ . The four ground states of TC model are labeled by  $(\mathcal{L}_x^e = \pm 1, \mathcal{L}_x^e = \pm 1)$ . In this notation, the ground state  $|\Psi_{G.S.}^{\text{Tor}}\rangle$  in Eq. 3.4 is labeled as  $|1, 1\rangle$ . The other three states are  $|1, -1\rangle = \mathcal{L}_x^m |\Psi_{G.S.}^{\text{Tor}}\rangle$ ,  $|-1, 1\rangle = \mathcal{L}_y^m |\Psi_{G.S.}^{\text{Tor}}\rangle$  and  $|-1, -1\rangle = \mathcal{L}_x^m \mathcal{L}_y^m |\Psi_{G.S.}^{\text{Tor}}\rangle$ .

The QSL is gapped and hence survives small Heisenberg and pseudo-dipolar perturbations as shown in Fig. 3.1. However, due to these perturbations, the  $e$  and  $m$  charges gain dispersion. The low energy effective description of the  $Z_2$  QSL in the continuum limit is captured by a  $U(1) \times U(1)$  mutual CS theory[13, 41, 42, 75] given by Eq. 7.18 which correctly implements the semionic statistics between the gapped  $e$  and  $m$  excitations of the  $Z_2$  QSL.

On cranking up the Heisenberg ( $J$ ) and/or the pseudo-dipolar ( $\Gamma$ ) couplings, however, the QSL ultimately gives way to other phases. Starting with the QSL, we can understand the possible destruction of the QSL by condensing the  $e$  and  $m$  charges.[66] This leads to different short-ranged entangled phases without or without spontaneously broken symmetries whose exact nature depends on the quantum numbers of the soft modes of the  $e$  and  $m$  charges that condense. This, in turn, is dictated by the energetics and the nature of the microscopic couplings,  $J$ , and  $\Gamma$ . Indeed we find that while the Heisenberg interactions,  $J$ , lead to a time reversal symmetry broken magnetically ordered phase, the pseudo-dipolar term,  $\Gamma$ , gives rise to a trivial product paramagnet.

### 3.1.2 Heisenberg Limit : $\Gamma = K = 0$

Another instructive and tractable limit is when both the pseudo-dipolar ( $\Gamma$ ) and the Kitaev  $x$  and  $y$  exchanges ( $K$ ) are absent. The effective Hamiltonian in FM anisotropic limit (Eq. 2.13) becomes

$$\mathcal{H}_{\Gamma=K=0}^{\text{FM}} = J \sum_{\langle i,j \rangle} \tau_i^z \tau_j^z + \mathcal{O} [(J^4/\Delta^3)] \quad (3.7)$$

In the limit where  $K_z$  (*i.e.*  $\Delta \rightarrow \infty$ ) is the largest energy scale in which the above Hamiltonian is valid, the leading term is clearly given by the first term. This leads to ferromagnetic or Neel ordering for the  $\tau^z$  spins depending on the sign of  $J$ . Higher order (in  $J/\Delta$ ) terms though introduce fluctuations, however, are expected to retain the above magnetic ordering. The same conclusion is also obtained in the limit  $\Gamma = 0$  and  $J = K$  such that  $\delta = 0$ .

It is interesting to note that the Neel order (for  $J > 0$ ) in terms of the  $\tau^z$  spins is actually

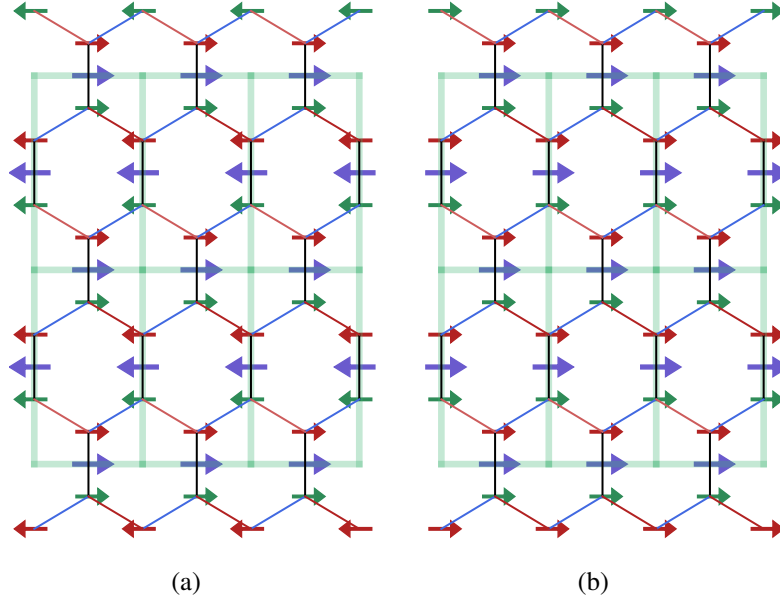


Figure 3.2: **(a) Stripy order:** For  $J > 0$ , Neel ordered state of the  $\tau$ -spins shown in blue arrows. For the  $\sigma$ -spin in the underlying honeycomb lattice, the magnetic ordering is shown, which is consistent Eq. 2.3. This  $\sigma^z$  ordering is nothing but the stripy phase. **(b) Ferromagnetic order** for  $J < 0$ : in  $\tau^z$  basis all the spins point to the same direction and equivalently for all the  $\sigma^z$  spins.

the stripy order in terms of the original  $\sigma^z$  of the underlying honeycomb lattice as shown in Fig. 3.2(a). Similarly, for  $J < 0$ , the ferromagnetic ordering in terms of  $\tau^z$  transforms into a ferromagnetic ordering in terms of the underlying  $\sigma^z$  as shown in Fig. 3.2 (b). Noticeably these are exactly the spin orders found in the immediate vicinity of the Isotropic Kitaev QSL with ferromagnetic exchanges.[43, 44]

Hence we expect a direct transition between the Ising ferromagnet (or antiferromagnet) and the  $Z_2$  QSL.[66, 76]

### 3.1.3 Pseudo-dipolar limit: $J = K = 0$ :

Finally, we consider the effect of only the  $\Gamma$  term on the  $\tau$  spins. From Eq. 2.13, we put  $J = K = 0$ , then we get

$$\mathcal{H}_{(J=K=0)}^{FM} = 2\Gamma \sum_i \tau_i^y + \mathcal{O}[(\Gamma^2/\Delta)] \quad (3.8)$$

In the  $\Gamma/\Delta \rightarrow 0$  limit, only the first term survives which is just non-interacting spins in a “magnetic field”. The ground state is a product state,  $|0; \Gamma_{\pm}\rangle = \otimes_j |\mp 1_y\rangle_j$ . In terms of  $z$ -basis

it is defined as  $|\mp_y\rangle = \frac{|+1_z\rangle \mp | -1_z\rangle}{\sqrt{2}}$ .

Also, it is worthwhile to go to the rotated basis (Eq. 3.2) whence the first term of Eq. 3.8 becomes

$$\tilde{\mathcal{H}}_{J=K=0}^{FM} = 2\Gamma \left[ \sum_{i \in V} \tilde{\tau}_i^z + \sum_{i \in H} \tilde{\tau}_i^x \right] \quad (3.9)$$

As an aside, it is interesting to note that, though explicitly broken in the anisotropic limit that we consider this work, the two above states have finite  $z$ -bond-spin-nematic correlations as measured from the expectation value of the operator

$$\hat{Q}_{ii'}^{\alpha\beta} = \left( \frac{\sigma_i^\alpha \sigma_{i'}^\beta + \sigma_i^\beta \sigma_{i'}^\alpha}{2} - \frac{\delta_{\alpha\beta}}{3} \sigma_i \cdot \sigma_{i'} \right) \quad (3.10)$$

We find

$$\langle \pm | {}_y \hat{Q}_{ii'}^{\alpha\beta} | \pm \rangle_y = \begin{bmatrix} -\frac{1}{3} & \mp 1 & 0 \\ \mp 1 & -\frac{1}{3} & 0 \\ 0 & 0 & \frac{2}{3} \end{bmatrix} \quad (3.11)$$

which describes a nematic with principle axis along  $\hat{\mathbf{n}} = [1\bar{1}0]$  for  $\Gamma < 0$  and is along  $\hat{\mathbf{n}} = [110]$  for  $\Gamma > 0$ . However, as stated above, this does not break any symmetry of the anisotropic Hamiltonian spontaneously and hence represents a featureless paramagnetic phase with gapped excitations which is continuously connected to the product state. Indeed signatures of such a nematic phase were numerically observed in the isotropic  $K - \Gamma$  model recently[62] where the rotational symmetry  $\sigma_h C_6$  of the extended Kitaev model is spontaneously broken down by the development of the nematic order.

### 3.2 Phases and Phase diagram in AFM anisotropic limit

Having isolated the different terms in the effective Hamiltonian for AFM anisotropic limit, we now discuss their effects in stabilizing different phases in order to develop the theory for the associated phase transitions.

### 3.2.1 Toric code limit $J = \Gamma = 0$

The full Hamiltonian in AFM anisotropic limit is given in Eq. 2.19, which in the limit:  $J = \Gamma = 0$  becomes:

$$\mathcal{H}_{J=\Gamma=0}^{AFM} = - J_{TC} \sum_i W_i \quad (3.12)$$

It is crucial to note that, both the  $W_i$  contribution is coming from the so-called six-spin hexagon contribution, which are the conserved degrees of freedom of the original Kitaev model [16]. These conserved quantities are giving rise to similar Toric code contributions both in FM and AFM anisotropic limits. After a bond dependent unitary rotations as defined in Eq. 3.2 (see also [16, 69]) becomes

$$\tilde{\mathcal{H}}_{J=\Gamma=0}^{AFM} = - J_{TC} \left[ \sum_s A_s + \sum_p B_p \right] \quad (3.13)$$

Where  $A_s = \prod_{i \in s} \tilde{\tau}_i^x$ ,  $B_p = \prod_{i \in p} \tilde{\tau}_i^z$ .  $\tilde{\tau}^\alpha$  denotes the rotated operators and Eq. 3.13 represents Kitaev's toric code model [69]. The symmetry transformations for  $\tilde{\tau}$  spins are given in the table A.3 in Appendix A.2.

The physics of the above limit of the Hamiltonian is discussed in section 3.1.1. In this limit too the above Hamiltonian stabilizes a  $Z_2$ -QSL ground state, albeit the definition of the  $\tilde{\tau}$ -spins are different from the Eq. 3.3.

### 3.2.2 Heisenberg Limit: $\Gamma = K = 0$

Deep inside the anisotropic limit, *i.e.*  $|K_z| \rightarrow \infty$ , as evident from Eq. 2.19, the leading order contribution (up to the linear order  $J$ ) arising from the Heisenberg perturbation is given by

$$\mathcal{H}_{\Gamma=K=0}^{AFM} = -J \sum_{\langle i,j \rangle} \tau_i^z \tau_j^z + 2J \sum_i \tau_i^x + \mathcal{O} [(J^4/\Delta^3)] \quad (3.14)$$

where the first term is the Ising interactions that favor ferromagnetic (Neel) ordering of the  $\tau^z$ -spins for  $J > 0$  ( $J < 0$ ). Qualitatively, this is similar to the FM-Kitaev case 3.1.2, with an important difference in terms of the underlying  $\sigma$  spins of the honeycomb magnet– the

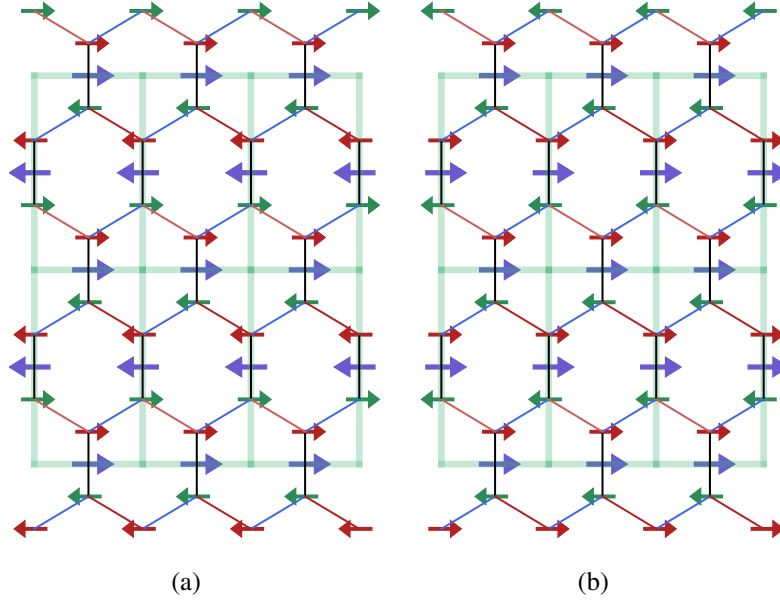


Figure 3.3: Configuration of  $\sigma$  and  $\tau$  spins. **(a) Zig-zag order:** For  $J < 0, \Gamma = 0, K = 0$  an AFM state is realized for  $\tau$  spins on  $z$  links of the honeycomb lattice, which is denoted by the blue arrows. While the  $\sigma$  spins are denoted by the red (green) arrow for the  $A$  ( $B$ ) sub-lattice, this corresponds to a *zig-zag* order for the  $\sigma$  spins. Where the left (right) blue arrow means  $\tau^z = +1(-1)$  state and the left (right) red/green arrow means  $\sigma^z = +1(-1)$  state. **(b) Neel order:** For  $J > 0$  a FM state is realized for the  $\tau$  spins, which corresponds to a *Neel* order for  $\sigma$  spins.

ferromagnetic (Neel) ordering for the  $\tau^z$  spins correspond to the Neel (Zig-Zag) ordering for the underlying  $\sigma^z$  spins as shown in Fig. 3.3.

The second term, representing the transverse field in the leading order of Heisenberg coupling, however, suggests a curious possibility of the Heisenberg perturbations stabilizing a paramagnetic state of  $\tau$ -spins polarised in the  $\tau^x$  direction. Very interestingly, in terms of the underlying  $\sigma$ -spins of the honeycomb lattice, this is given by

$$\begin{aligned}
 |\psi_+\rangle &= \otimes_{pp'} \left( \frac{|\uparrow_p \downarrow_{p'}\rangle - |\downarrow_p \uparrow_{p'}\rangle}{\sqrt{2}} \right) ; \text{ for } J > 0 \\
 |\psi_-\rangle &= \otimes_{pp'} \left( \frac{|\uparrow_p \downarrow_{p'}\rangle + |\downarrow_p \uparrow_{p'}\rangle}{\sqrt{2}} \right) ; \text{ for } J < 0
 \end{aligned} \tag{3.15}$$

which are singlet and triplet states respectively for  $pp'$  that denotes the  $z$ -bond (see Eq. 2.8). Therefore, following section 3.1.3 the bond-nematic order parameter:

$$\hat{Q}_{pp'}^{\alpha\beta} = \left( \frac{\sigma_p^\alpha \sigma_{p'}^\beta + \sigma_p^\beta \sigma_{p'}^\alpha}{2} - \frac{\delta_{\alpha\beta}}{3} \boldsymbol{\sigma}_p \cdot \boldsymbol{\sigma}_{p'} \right) \quad (3.16)$$

is non-zero. In particular, for the  $|\psi_-\rangle$ , we have

$$\langle \psi_- | \hat{Q}_{pp'}^{\alpha\beta} | \psi_- \rangle = \begin{bmatrix} \frac{2}{3} & 0 & 0 \\ 0 & \frac{2}{3} & 0 \\ 0 & 0 & -\frac{4}{3} \end{bmatrix} \quad (3.17)$$

On the other hand for  $|\psi_+\rangle$ , singlet dimers are present on the  $z$ -bonds of the honeycomb lattice. In absence of spin-rotation symmetry, for non-Kramers doublets both these orders represent lattice nematic.

While in Eq. 3.14 the couplings of the transverse field and the Ising term both are proportional to  $J$ , on considering higher order contributions of the perturbation theory (see Eq. 2.19 and Eq. 2.20-2.23) they are differently renormalized and it is, therefore, useful to consider them at independent parameters and study the generalized phase diagram where the strength of the Ising term ( $\equiv J_{\text{Ising}}$ ) and the magnetic field term ( $\equiv h$ ) is independently varied (see Fig. 3.4). In this generalized model for  $h \rightarrow \infty$  limit we obtain the two above polarised phases for the  $\tau$  spins that correspond to a direct product state of singlets and triplets on the  $z$  bonds for the  $\sigma$ -spins.

Detailed discussion regarding this model is relegated to Appendix C, where it is shown that under unitary transformations this system is equivalent to a problem of perturbing a toric code Hamiltonian with a transverse field and a  $x$ - $z$  Ising term (see Eq. C.3). For this model, our numerical studies show three prominent phases (qualitatively shown in Fig. 3.4) – (i) ferromagnet (FM), (ii) paramagnet (PM) and (iii)  $Z_2$  QSL. While the FM and PM are separated by a  $3D$ -Ising transition; the  $Z_2$  QSL and the paramagnet are separated by a first order line [67, 68]. The nature of the transition between  $Z_2$  QSL and the FM is a self-dual modified Abelian Higgs transition as is discussed below.

Therefore, in the present case, in principle, there can be two possible ways of destroying the  $Z_2$  QSL leading to a spin-ordered phase (in the Heisenberg limit) via tuning the Heisenberg interactions– (1) a direct second-order quantum phase transition into the spin ordered

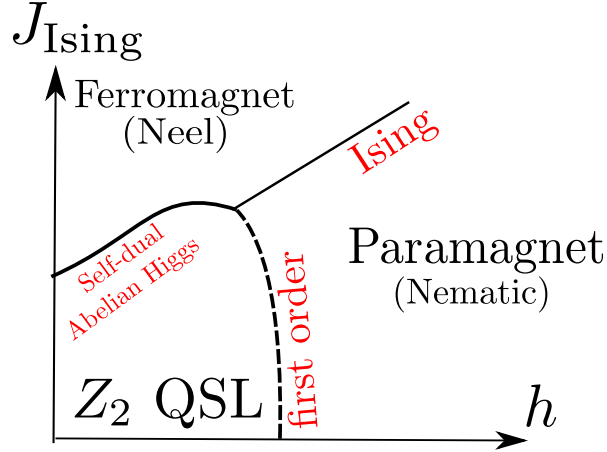


Figure 3.4: A single or a two-step transition from the  $Z_2$  QSL as a function of Heisenberg coupling into a magnetically ordered state (Eq. 3.14). In the leading order of perturbation,  $h \sim 2J$  and  $J_{\text{Ising}} = J$  where  $J$  is the strength of the Heisenberg perturbation as defined in Eq. 1.1. The transition from the  $Z_2$  QSL to a paramagnet in the parallel field is a first order transition[68] where the transition at  $J_{\text{Ising}} = 0$  is a self dual point. We expect this first-order transition to be stable to Ising perturbation since our numerical results do not show any significant change of behavior (see Appendix C).

phase, and (2) a two-step transition where the QSL first goes into a polarised trivial paramagnet through a first-order transition and finally into the spin-ordered state via a  $3D$ -Ising transition. For the purely transverse field Ising model on a square lattice (Eq. 3.14), existing variational and cluster Monte-Carlo calculations [77–80] shows the strength of the transverse field  $\approx 3J$  is the critical point for the phase transition between the symmetry broken  $\tau^z$  magnetically ordered state, i.e.  $\langle \tau_i^z \rangle \neq 0$  and the paramagnet state, i.e.  $\langle \tau_i^z \rangle = 0$ . So for Eq. 3.14, we expect a single-step transition which is supported by our exact diagonalization results on finite spin clusters presented in Appendix C.

### 3.2.3 The pseudo-dipolar limit $J = K = 0$

A novel and the most interesting limit of the anisotropic antiferromagnetic model is obtained when the pseudo-dipolar interactions dominate. The leading order effect of such perturbation in the  $|K_z| \rightarrow \infty$  limit is given by the second order perturbation theory leading to the effective Hamiltonian from Eq. 2.19. The full Hamiltonian up to fourth order perturbation is given in Eq. 3.18) given by

$$\begin{aligned}
\mathcal{H}_{J=K=0}^{AFM} = & \left[ \frac{\Gamma^2}{|K_z|} - \frac{\Gamma^4}{|K_z|^3} \right] \sum_i (\tau_{i+d_1}^z \tau_i^x \tau_{i-d_1}^z + \tau_{i+d_2}^z \tau_i^x \tau_{i-d_2}^z) \\
& + \left[ \frac{\Gamma^2}{|K_z|} - \frac{\Gamma^4}{|K_z|^3} \right] \sum_i (\tau_{i+d_1}^z \tau_i^y \tau_{i-d_2}^z - \tau_{i+d_2}^z \tau_i^y \tau_{i-d_1}^z) - \frac{2\Gamma^3}{|K_z|^2} \sum_i \tau_{i+d_1}^z \tau_{i-d_2}^z \\
& - \left[ \frac{\Gamma^4}{2|K_z|^3} \right] \sum_i (\tau_i^z \tau_{i-d_2}^z \tau_{i+d_1-d_2}^x + \tau_{i+d_1-d_2}^z \tau_{i+d_1}^z \tau_i^x - \tau_i^z \tau_{i+d_1}^z \tau_{i+d_1-d_2}^x - \tau_{i+d_1-d_2}^z \tau_{i-d_2}^z \tau_i^x) \\
& + \frac{\Gamma^3}{|K_z|^2} \sum_i (\tau_{i+d_1}^z \tau_i^x \tau_{i+d_2}^z + \tau_{i-d_1}^z \tau_i^x \tau_{i-d_2}^z)
\end{aligned} \tag{3.18}$$

### Stacked cluster chains

The pseudo-dipolar limit up to the second order is best described as a combination of four Hamiltonian of the stacked one-dimensional cluster chains, which we will discuss now. Unlike the Heisenberg perturbations (Eq. 3.14) or the  $\Gamma$  perturbations in the ferromagnetic Kitaev as discussed in section 3.1.3, the above term does not get contributions at the first order level. This allows for non-trivial spin interactions through the three spin terms. Notably, due to the unusual implementation of time reversal symmetry (see Eq. 2.12), the above three spin terms are symmetry allowed.

We now discuss the rich structure of the Hamiltonian in Eq. 3.18 up to the second order perturbation ( $\frac{\Gamma^2}{|K_z|}$ ). To this end, we re-write it as

$$\mathcal{H}_{J=K=0}^{AF} = \frac{\Gamma^2}{|K_z|} (H_1 + H_2 + H_3 + H_4) \tag{3.19}$$

with

$$\begin{aligned}
H_1 &= \sum_i \tau_{i+d_1}^z \tau_i^x \tau_{i-d_1}^z \\
H_2 &= \sum_i \tau_{i+d_2}^z \tau_i^x \tau_{i-d_2}^z \\
H_3 &= \sum_{i \in V} (\tau_{i+d_1}^z \tau_i^y \tau_{i-d_2}^z) - \sum_{i \in H} (\tau_{i+d_2}^z \tau_i^y \tau_{i-d_1}^z) \\
H_4 &= \sum_{i \in H} (\tau_{i+d_1}^z \tau_i^y \tau_{i-d_2}^z) - \sum_{i \in V} (\tau_{i+d_2}^z \tau_i^y \tau_{i-d_1}^z)
\end{aligned} \tag{3.20}$$

where  $H$ , &  $V$  denote the set of sites belonging to the horizontal and vertical bonds respectively.

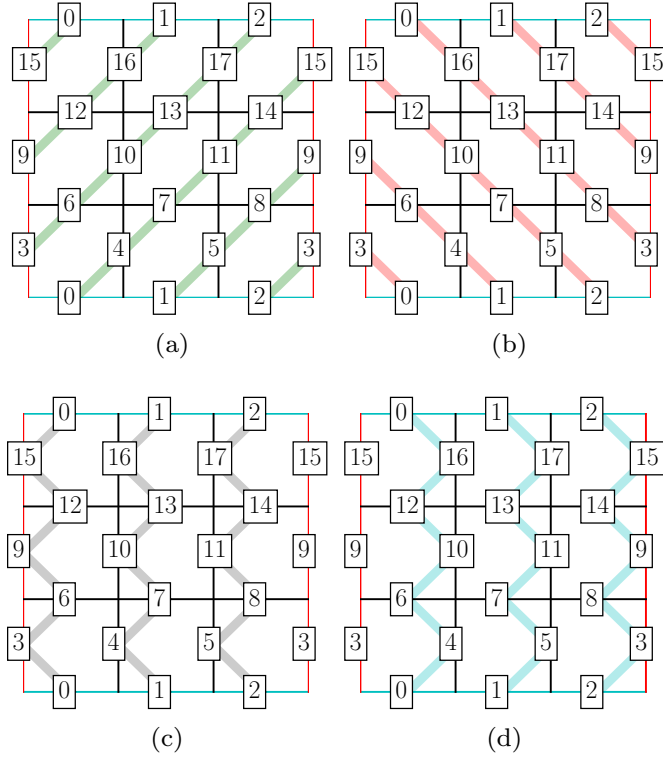


Figure 3.5: Four stacked cluster spin chains : The panels **(a)**, **(b)**, **(c)**, **(d)** represent the four Hamiltonians in Eq. 3.20 in PBC.

We immediately note that each of these Hamiltonians represents a set of stacked one-dimensional cluster spin-1/2 chains arranged in a particular direction. This is shown in Fig. 3.5. While  $H_1$  and  $H_2$  are stacked cluster chains oriented at  $\frac{\pi}{4}$  and  $\frac{-\pi}{4}$  in the lattice plane,  $H_3$  and  $H_4$  are oriented vertically with the chains being displaced by a lattice constant with respect to each other.

If the Hamiltonians are considered independently, as discussed in Appendix D.1, at this leading order each decoupled chain has an enhanced  $Z_2 \times Z_2$  symmetry and stabilizes a gapped symmetry protected topological (SPT) phase protected by this symmetry [81–85]. As a result each chain supports a zero energy localized spin-1/2 at the edge of each chain. Each stacking pattern of these cluster Hamiltonians in Eq. 3.20,  $H_\alpha$  ( $\alpha = 1, 2, 3, 4$ ), therefore, results in a weak-SPT phase [81] whose edge mode structure depends on the shape of the cluster chosen, as expected (see Table. 3.1 and Appendix D.2).

The full Hamiltonian in the pseudo-dipolar limit (Eq. 3.19), however, is an equal-weight superposition of the four stackings. In order to understand this, it is useful to consider the interpolating Hamiltonian

Hamiltonian	PBC	$x$ -CBC	$y$ -CBC	OBC
$H_1$	1	$2^{2L_x}$	$2^{2L_y}$	$2^{2(L_x+L_y)-2}$
$H_2$	1	$2^{2L_x}$	$2^{2L_y}$	$2^{2(L_x+L_y)-2}$
$H_3$	1	$2^{2L_x}$	1	$2^{2L_x}$
$H_4$	1	$2^{2L_x}$	1	$2^{2(L_x+L_y)-2}$

Table 3.1: Ground state degeneracies for various stacked cluster Hamiltonians  $H_1, H_2, H_3, H_4$  (see Eq. 3.20) when placed under various boundary conditions. PBC (OBC) is the usual periodic (open) boundary condition on a torus, while  $x$ -CBC ( $y$ -CBC) is a cylindrical boundary condition with  $x(y)$  direction being periodic. The details are discussed in Appendix. D.2.

$$\begin{aligned}
H(\lambda_1, \lambda_2) &= \lambda_2 ((2 - \lambda_1)H_1 + \lambda_1 H_2) \\
&\quad + (2 - \lambda_2) ((2 - \lambda_1)H_3 + \lambda_1 H_4)
\end{aligned} \tag{3.21}$$

parameterized by  $\lambda_1$  and  $\lambda_2$  – such that in the  $(\lambda_1, \lambda_2)$  plane, the points  $(0, 2)$ ,  $(2, 2)$ ,  $(0, 0)$  and  $(2, 0)$  are identified with  $H_1, H_2, H_3$  and  $H_4$  respectively while, up to multiplicative factors,  $\mathcal{H}_{(J=K=0)}^{AF}$  is given by  $(1, 1)$ . This is illustrated in Fig. 3.6 and explained below. However, we note that on this plane the symmetry of  $\pi$ -rotation about the  $z$ -bond,  $C_{2z}$  results in  $H_1 \leftrightarrow H_2$  and  $H_3 \leftrightarrow H_4$  and thus constraining  $\lambda_1 = 1$  on the plane while  $\lambda_2$  being free to be renormalized by higher order terms. We shall especially focus on this line while discussing the phase diagram.

The interpolating Hamiltonian of Eq. 3.21 in the entire  $(\lambda_1, \lambda_2)$  has some special symmetry and energetic features. While these properties are not stable to higher order perturbations (see Eq. 3.18), not only such structures are interesting in their own rights as we shall see below, but also, these *weakly broken* symmetries provide important insights into the nature of the phase in this pure  $\Gamma$  limit. Hence, we now discuss these special symmetries.

The generic non-Kramers time-reversal symmetry is generated by (see table 2.12) the operator  $\mathcal{T} = \prod_{i \in H, V} \tau_i^x \mathcal{K}$  (where  $\mathcal{K}$  is the complex conjugation operator). However Eq. 3.21 enjoys an enhanced *sub-lattice* time-reversal symmetry generated by the operators

$$\mathcal{T}_H = \prod_{i \in H} \tau_i^x \mathcal{K}_i, \quad \mathcal{T}_V = \prod_{i \in V} \tau_i^x \mathcal{K}_i \tag{3.22}$$

where the products in the first and second expressions run over the horizontal and vertical bonds

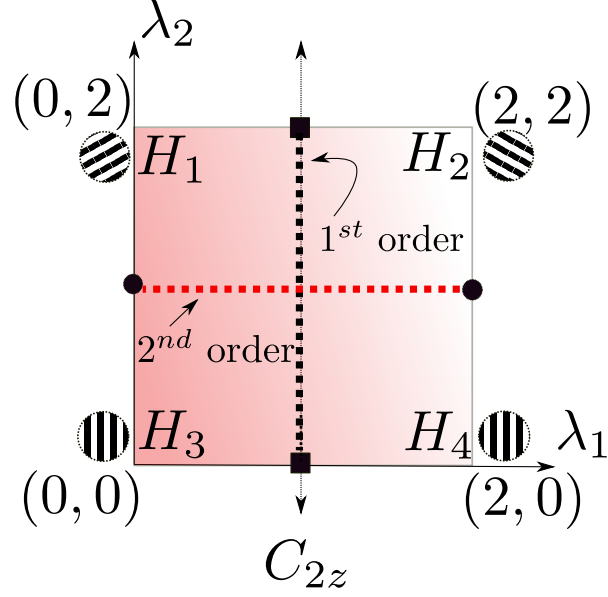


Figure 3.6: Anticipated phase diagram for the Hamiltonian in Eq. 3.21. The four corners are the exact limit of the stacked cluster SPTs (given in Eq. 3.20) which are oriented in different directions and shown in Fig. 3.5.  $C_{2z}$  symmetry transforms  $H_1 \leftrightarrow H_2$  and  $H_3 \leftrightarrow H_4$ . The phase transitions at  $\lambda_2 = 0$  ( $\lambda_1 = 0$ ) as a function of  $\lambda_1$  ( $\lambda_2$ ) is a first(second) order transition which is expected to be stable when  $\lambda_2 \neq 0$  ( $\lambda_1 \neq 0$ ) (see text).

respectively. Thus this plane enjoys a global  $Z_2 \times Z_2$  symmetry.

The Hamiltonian in Eq. 3.21, however, has an even larger set of *sub-system symmetries* which is most apparent after a unitary rotation defined on a set of bonds, followed by a global unitary rotation. The following transformation [81, 86–89]

$$\mathcal{W} \equiv \prod_i U_{i,i+d_1} \quad (3.23)$$

where we define a bond-dependent (direction independent) unitary operator

$$U_{ij} = \frac{1}{2} \left( 1 + \tau_i^z + \tau_j^z - \tau_i^z \tau_j^z \right) \quad (3.24)$$

renders

$$\mathcal{W} : \tau_i^x \rightarrow \tau_{i-d_1}^z \tau_i^x \tau_{i+d_1}^z ; \quad \tau_i^z \rightarrow \tau_i^z. \quad (3.25)$$

This when followed by a global rotation

$$\mathcal{V} : \{ \tau_i^x, \tau_i^y, \tau_i^z \} \rightarrow \{ \eta_i^y, \eta_i^z, \eta_i^x \} \quad (3.26)$$

leads to

$$H_\alpha \rightarrow \tilde{H}_\alpha = (\mathcal{V}\mathcal{W}) H_\alpha (\mathcal{V}\mathcal{W})^{-1} \quad (3.27)$$

where  $\eta_i^\alpha$  is the new spin degrees of freedom. Note that while the transformation  $\mathcal{V}$  is not essential, as we shall see below, it simplifies parts of our analysis.

The resultant transformed Hamiltonians are given by

$$H_1 \rightarrow \tilde{H}_1 = \sum_i \eta_i^y \quad (3.28)$$

$$H_2 \rightarrow \tilde{H}_2 = \sum_i \eta_i^y \eta_{i+d_1}^x \eta_{i-d_1}^x \eta_{i+d_2}^x \eta_{i-d_2}^x \quad (3.29)$$

$$H_3 \rightarrow \tilde{H}_3 = \sum_{i \in V} \eta_{i-d_1}^x \eta_i^z \eta_{i-d_2}^x - \sum_{i \in H} \eta_{i+d_2}^x \eta_i^z \eta_{i+d_1}^x \quad (3.30)$$

$$H_4 \rightarrow \tilde{H}_4 = \sum_{i \in H} \eta_{i-d_1}^x \eta_i^z \eta_{i-d_2}^x - \sum_{i \in V} \eta_{i+d_2}^x \eta_i^z \eta_{i+d_1}^x \quad (3.31)$$

Therefore under this particular transformation, the four differently stacked weak cluster SPTs respectively get mapped to a  $y$ -paramagnet (PM) ( $\tilde{H}_1$ ), strong sub-system symmetry protected topological phase (SSPT) ( $\tilde{H}_2$ ) of the topological plaquette Ising model [81, 90], and two horizontally stacked weak cluster SPTs ( $\tilde{H}_3$  and  $\tilde{H}_4$ ). We have explicitly checked that the transformation when defined for an open system restores the correct number of zero modes in both  $H_\alpha$  and  $\tilde{H}_\alpha$ . A discussion about the transformation  $\mathcal{W}$  (Eq. 3.23) and the way it acts on the boundary Hamiltonians in an open system see Appendix D.2. The cluster SPT is briefly discussed in Appendix D.1.

In the transformed basis, the Hamiltonian (Eq. 3.21) is invariant under the following set of *anti-unitary subsystem symmetries* that are generated by

$$\tilde{P}T_{h_n} = \prod_{i \in n^{th} \text{ Hor. line}} \eta_i^z \mathcal{K}_i \quad (3.32)$$

$$\tilde{P}T_{v_n} = \prod_{i \in n^{th} \text{ Vert. line}} \eta_{i-d_1}^x \mathcal{K}_{i-d_1} \eta_i^z \mathcal{K}_i \eta_{i+d_1}^x \mathcal{K}_{i+d_1} \quad (3.33)$$

where in Eq. 3.32 (3.33),  $h_n(v_n)$  denotes the  $n^{th}$  horizontal (vertical) line which either can pass through the horizontal (vertical) bonds or cut through the vertical (horizontal) bonds of the square lattice (see Fig. 3.7) and  $\mathcal{K}_i$  is the local complex conjugation operation which acts

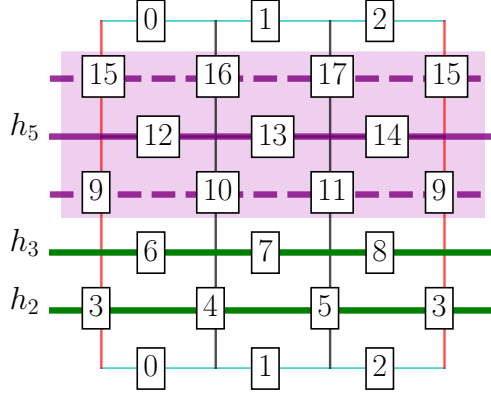


Figure 3.7: The anti-unitary symmetry operator in Eq. 3.32 is shown as a single green continuous line ( $h_n$ ), for example,  $h_3$  passes through the horizontal bonds (spins 6, 7, 8) and  $h_2$  passes through the vertical bonds (spins 3, 4, 5). The symmetry operator in the Eq. 3.34 is shown using the three magenta lines. The dashed (continuous) line shows the unitary (anti-unitary) operation.

on-site  $i$ .

In terms of the untransformed basis (by Eq. 3.27), Eq. 3.32 and 3.33 can be obtained from Eqs. 3.25 and 3.26 and are given respectively by

$$PT_{h_n} = \prod_{i \in n^{th} \text{Hor. line}} \tau_{i+d_1}^z \tau_i^x \tau_{i-d_1}^z \mathcal{K}_i \quad (3.34)$$

$$PT_{v_n} = \prod_{i \in n^{th} \text{Vert. line}} \tau_{i+d_1}^z \mathcal{K}_{i+d_1} \tau_i^x \mathcal{K}_i \tau_{i-d_1}^z \mathcal{K}_{i-d_1} \quad (3.35)$$

Note that both Eq. 3.34 and 3.35 involve the same transformation on horizontal/vertical stacks of three consecutive spins separated by,  $T_{d_1}$ , *i.e.* translation along  $d_1$ . However, while for the horizontal stacking in Eq. 3.34, the conjugation operator acts only on the spin in the middle, for the vertical stacking in Eq. 3.35 they act on all the spins involved.

In addition, along the  $\lambda_2 = 2$  line the system has another set of subsystem symmetries generated by :

$$\tilde{P}T'_{v_n} = \prod_{i \in n^{th} \text{Vert. line}} \eta_i^z \mathcal{K}_i \quad (3.36)$$

Similar to the Eq. 3.34, we can write this symmetry in the original spin basis of Eq. 3.20 as a combination of unitary and anti-unitary symmetry, now in the vertical direction which is

$$PT'_{v_n} = \prod_{i \in n^{th} \text{Vert. line}} \tau_{i+d_1}^z \tau_i^x \tau_{i-d_1}^z \mathcal{K}_i \quad (3.37)$$

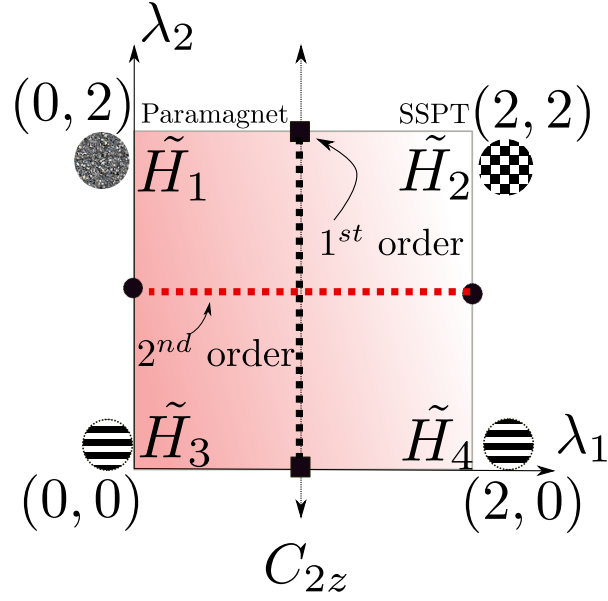


Figure 3.8: Phase diagram corresponding to the Hamiltonian given in Eq. 3.21 after the transformation defined in Eq. 3.27, also see Fig. 3.6.

We shall later return to the constraints imposed by these sub-system symmetries. However, as briefly discussed in Appendix D.3, due to the particular non-Kramers nature of the time reversal symmetry the above subsystem symmetries do not constrain the dispersion of excitations unlike fractons [91, 92].

The above transformation (Eq. 3.27) allows for new insights into the phase diagram of the pure  $\Gamma$  Hamiltonian given by Eq. 3.19. In particular, the transitions along the four boundaries, as shown in Fig. 3.8, can be immediately read off from existing literature. These are as follows :

- The transition between  $\tilde{H}_1$  and  $\tilde{H}_2$  along the  $\lambda_2 = 2$  line is between a trivial paramagnet and a two-dimensional SSPT respectively. This transition is known to be first order [87, 93] and occurs at  $\lambda_1 = 1$ . In the un-transformed basis, we note that this represents a transition between two stacked cluster models,  $H_1$  and  $H_2$ . Remarkably, the effective dimensional reduction at the critical point is far from apparent in this un-transformed basis.

There exists a transformation similar to Eq. 3.27 which transforms, on the  $\lambda_2 = 0$  line,  $H_3$  to a trivial transverse field paramagnet and  $H_4$  to an SSPT. The discussion of the above paragraph then can be immediately applied to the  $\lambda_2 = 0$  line. (Notably, such a transformation map  $H_1$  and  $H_2$  to weak cluster SPTs.)

Therefore at  $\lambda_1 = 1$ , both  $\lambda_2 = 0, 2$  are first-order transition points. This implies that the

phase diagram in  $(\lambda_1, \lambda_2)$  phase has a reflection symmetry about  $\lambda_2 = 1$  line.

- The transition from  $\tilde{H}_1$  to  $\tilde{H}_3$  along the  $\lambda_1 = 0$  line is between a trivial paramagnet and decoupled one-dimensional cluster chains. This is a self-dual transition at  $\lambda_2 = 1$  that is described by a  $SO(2)_1$  conformal field theory (CFT) with central charge,  $c = 1$  [94, 95]. Given the existence of sub-system symmetry operators, it may seem that dynamics of the excitations from the  $\tilde{H}_3$  state is constrained. As is discussed in Appendix D.3 we show that the antiunitary character of these subsystem symmetries effectively renders the dynamics to be free, especially on the  $\lambda_1 = 0$  line. Again, as above, in the un-transformed basis, the above transition is between two stacked cluster models,  $H_1$  and  $H_3$ , again, with non-obvious effective dimensional reduction at the critical point.

A yet third set of transformations similar to Eq. 3.27 transforms  $H_2$  to a transverse paramagnet and  $H_4$  to a stacked cluster SPT. This immediately allows us to import the above physics of  $\lambda_1 = 0$  and apply it to the case of  $\lambda_1 = 2$  line. Further, the rotation about the  $z$ -bond ( $C_{2z}$  symmetry, see table 2.12) leads to  $(\lambda_1, \lambda_2) \rightarrow (2 - \lambda_1, \lambda_2)$  which also leads to the same conclusion regarding the phases and phase transitions.

The above discussion of the phases sharpen the questions about the quantum phase transitions between the  $Z_2$  QSL and the spin-ordered or a trivial paramagnetic phase as a function of  $J/K$  and  $\Gamma/K$  respectively as indicated in Fig. 3.1. However, before moving on to the critical field-theory of quantum phase transition, we present our preliminary numerical calculations in the form of exact diagonalization on finite spin clusters in section 5.2. This provides further insights into the nature of the soft  $e$  and  $m$  modes which then is used to construct the critical theory.

Our numerical studies on small spin clusters reveal the general structure of the phase diagram indicating that the  $Z_2$  QSL is destroyed via proliferation and condensation of its gauge charges—both electric and magnetic. While the transition to the paramagnetic phase in the large  $\Gamma$  limit turns out to be discontinuous, the continuous transition to the spin-ordered state (from the QSL) is driven by Heisenberg coupling via a deconfined critical point. We construct a critical continuum field theory in terms of the soft modes of the electric and magnetic charges via a mutual  $Z_2$  Chern-Simons (CS) theory and show that the direct transition between the QSL and the spin-ordered phase is described by a self-dual modified Abelian Higgs field theory—

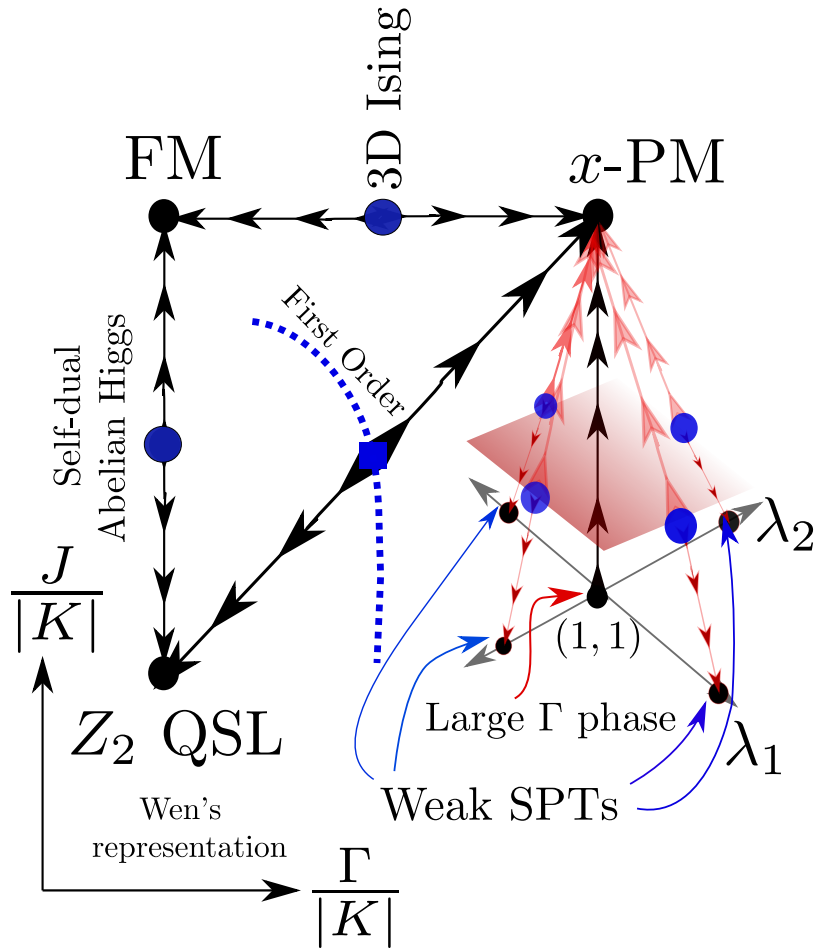


Figure 3.9: Schematic depiction of the phases and phase transitions which are accessible within the parameter space of the complete  $KJ\Gamma$  Hamiltonian (see Eq. 2.19) in the anisotropic limit of anti-ferromagnetic Kitaev model.

in agreement with the critical theory obtained by us in the ferromagnetic case using a mutual  $U(1)$  CS theory in section 7. The overall summary of our phase diagram is then illustrated in Fig. 3.9.

## CHAPTER 4

### NUMERICAL RESULTS: FM ANISOTROPIC KITAEV MODEL

#### 4.1 Numerical results for FM Anisotropic Kitaev model

We perform exact diagonalization calculations on finite spin clusters[96, 97]. For the present purpose, we focus on the third quadrant of the phase diagram (Fig. 3.1). For this, we take the minimal Hamiltonian from Eqs. 3.7 and 3.8 which captures the leading perturbations to the QSL (Eq. 3.1) arising due to the Heisenberg and the pseudo-dipolar terms. The Hamiltonian that interpolates between the different limits is given by

$$\begin{aligned} \mathcal{H}^{FM}(t_1, t_2) = & - (1 - t_1)(1 - t_2)\mathcal{H}_{TCM}^{FM} \\ & - t_1(1 - t_2)\mathcal{H}_{\Gamma}^{FM} - t_2(1 - t_1)\mathcal{H}_{zz}^{FM} \end{aligned} \quad (4.1)$$

where to compare with the couplings introduced above, we note  $\mathcal{H}_{TCM}^{FM} \equiv \frac{1}{J_{TC}}\mathcal{H}_{J=\Gamma=0}^{FM}$ ,  $\mathcal{H}_{\Gamma}^{FM} \equiv \frac{1}{2\Gamma}\mathcal{H}_{J=K=0}^{FM}$  and  $\mathcal{H}_{zz}^{FM} \equiv \frac{1}{J}\mathcal{H}_{\Gamma=K=0}^{FM}$ , defined in Eqs. 3.1, 3.7 and 3.8 respectively and  $t_1 = \frac{2\Gamma}{J_{TC}+2\Gamma}$ ;  $t_2 = \frac{J}{J_{TC}+J}$ .

In this parameter space, at the points  $(t_1, t_2) = (0, 0), (1, 0), (0, 1)$  the  $\mathcal{H}^{FM}(t_1, t_2)$  becomes  $\mathcal{H}_{TCM}^{FM}$ ,  $\mathcal{H}_{\Gamma}^{FM}$  and  $\mathcal{H}_{zz}^{FM}$  respectively. We perform exact diagonalization (ED) for  $2 \times 3, 3 \times 3, 5 \times 2, 4 \times 3, 5 \times 3$  and  $4 \times 4$  clusters with periodic boundary conditions (PBC) such that they contain 12 – 32 spins.

To make an estimate of the phase boundaries in the system, we calculate ground state fidelity susceptibility and spectral gap. The numerical results for representative parameter sets, as discussed below, are plotted in Fig. 4.1 and 4.2 respectively. The three different phases are then characterized by calculating the Topological entanglement entropy[64, 65] that characterises the  $Z_2$  QSL, the magnetization,  $\langle \tau^y \rangle$ , that characterizes the trivial paramagnet and the two-point correlator  $\langle \tau_i^z \tau_j^z \rangle$  that characterizes the ferromagnet. These are then plotted in representative parameter regimes in Fig. 4.4. A combination of the above signatures results in the phase diagram given by Fig. 4.5 which should then be compared with the third quadrant of the schematic phase diagram in Fig. 3.1.

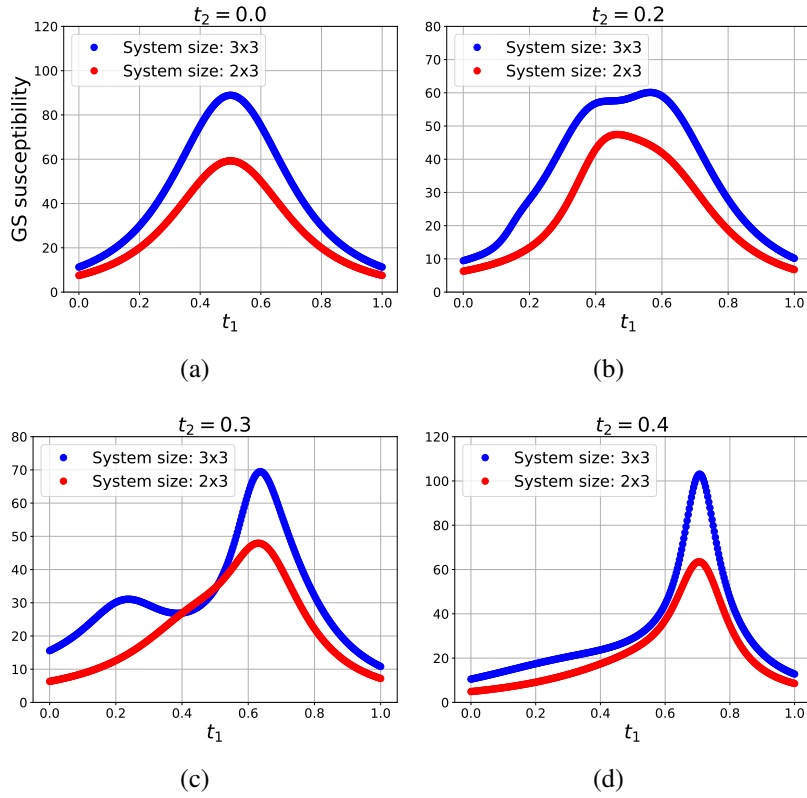


Figure 4.1: Peak in the absolute value of  $\frac{\partial^2 E_{GS}}{\partial t_1^2}$ , for different  $t_2$ s. **(a)**  $t_2 = 0.0$  **(b)**  $t_2 = 0.2$  **(c)**  $t_2 = 0.3$  **(d)**  $t_2 = 0.4$ . The blue and red dots are for the system size  $3 \times 3$  and  $2 \times 3$  respectively, we see the height of the peak increase as we increase the system size. In the thermodynamic limit, the peaks are expected to diverge.

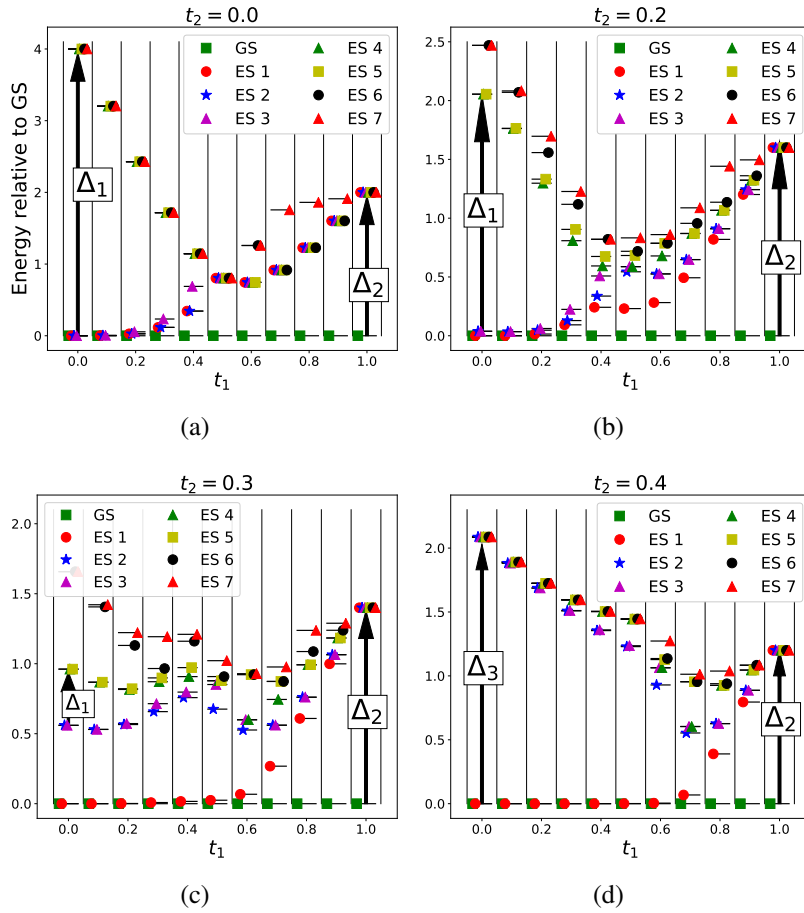


Figure 4.2: Change of excitation gaps along  $t_1$ , for different  $t_2$ 's. **(a)**  $t_2 = 0.0$  **(b)**  $t_2 = 0.2$  **(c)**  $t_2 = 0.3$  **(d)**  $t_2 = 0.4$ . GS (ES  $j$ ) stands for ground state ( $j$ th excited state).  $\Delta_1$ ,  $\Delta_2$  &  $\Delta_3$  are the excitation gaps above the  $Z_2$  QSL, paramagnetic (PM) and ferromagnetic (FM) GS respectively.

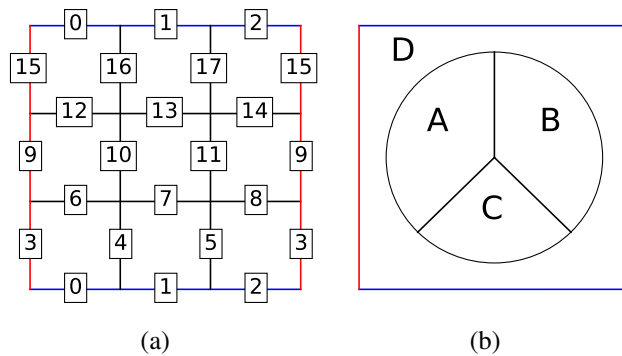


Figure 4.3: **(a)** The  $3 \times 3$  cluster with 18 spins, the blue and red edges are identified due to PBC **(b)** Geometry of the four sub-systems, for the calculation of the topological entanglement entropy.

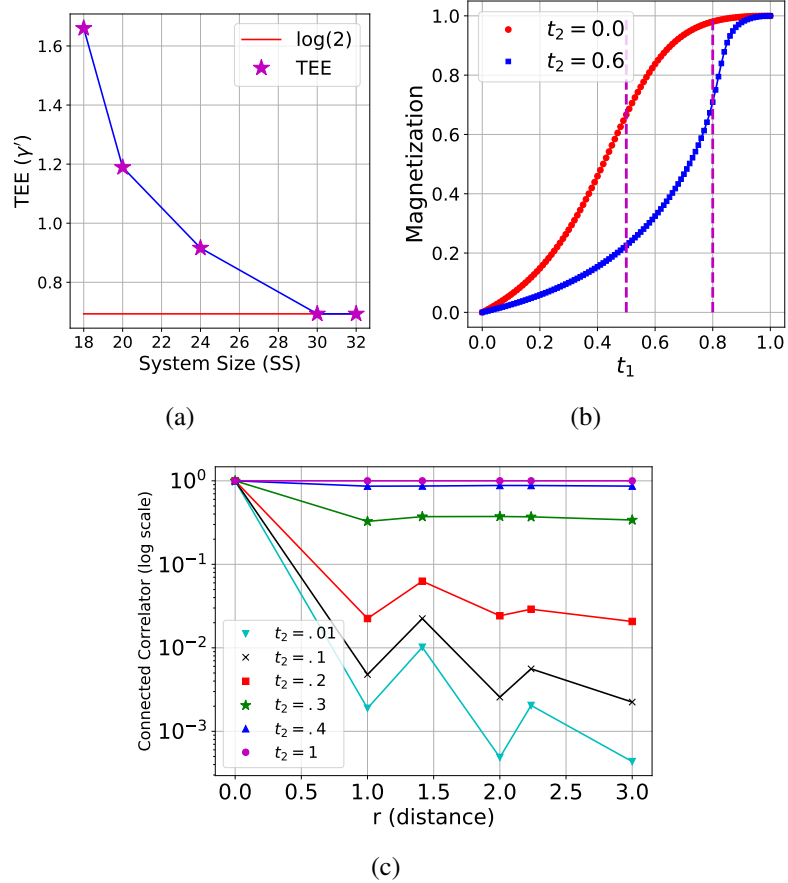


Figure 4.4: **(a)** The topological entanglement entropy (TEE) for increasing system sizes (see text). The considered system sizes are  $3 \times 3$ ,  $5 \times 2$ ,  $4 \times 3$ ,  $5 \times 3$  and  $4 \times 4$  which have 18, 20, 24, 30 & 32 spins respectively. Only the  $3 \times 3$  cluster is shown in Fig. 4.3(a). **(b)** Magnetization in the  $\Gamma$ -direction, as a function of  $t_1$  for constant  $t_2 = 0.0$  &  $0.6$ , along the red dashed lines in the Fig. 4.5. The dashed magenta line shows the phase transition points along  $t_1$ , obtained from the phase diagram in Fig. 4.5 for the respective  $t_2$  values. **(c)** Plot of the normalized correlation function as a function of distance for different values of  $t_2$  (with  $t_1 = 0$ , see text for more details). Deep inside the FM phase, the correlation does not decay, beyond  $t_2 = 0.3$  the correlation decays exponentially.

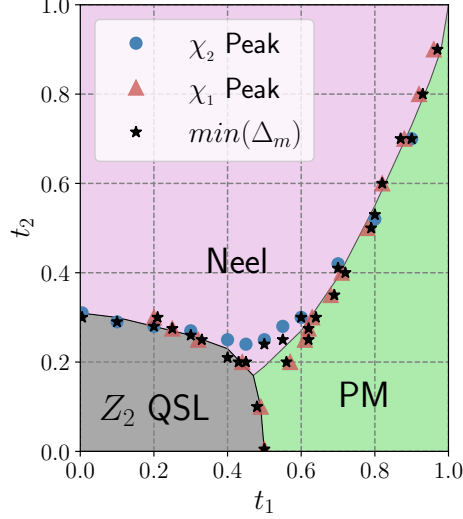


Figure 4.5: Numerically obtained phase diagram focusing on the third quadrant of Fig. 3.1. The phase transition points are obtained from the gap analysis and the GS susceptibility peak for the cluster  $4 \times 3$  (Fig. 4.3(a)). The magnetization plots in Fig. 4.4(b) are along the red dashed lines:  $t_2 = 0.0$  &  $0.6$ .

**Fidelity Susceptibility :** An estimate of the phase boundaries can be obtained from the study of the response of the ground state energy due to the change in the parameters  $t_1$  and  $t_2$  through the fidelity susceptibility[98]:  $\chi_\lambda = -\partial^2 E_{GS}/\partial\lambda^2$  (with  $\lambda = t_1, t_2$ ). In the Fig. 4.1 ((a)-(d)) we plot  $|\chi_{t_1}|$  as a function of  $t_1$  for four different representative values of  $t_2$ . The peaks, which increase with system size indicate possible phase transitions. Similar peaks are observed in  $\chi_{t_2}$  (not shown). The position of the peaks is plotted in Fig. 4.5 which gives an estimate of the phase boundaries.

**Ground state degeneracy and spectral gap :** A related way to characterize the phase boundaries is obtained by tracking the closing of the spectral gap. The corresponding results are shown in Fig. 4.2 ((a)-(d)) as a function of  $t_1$  for the same values of  $t_2$  as  $\chi_{t_1}$  figures in the upper panel.

$t_1 = 0, t_2 = 0$  corresponds to the exactly solvable Toric code limit which has  $Z_2$  QSL ground state, similarly at  $(t_1 = 1, t_2 = 0)$ , we have spin polarized ground state (paramagnetic phase). In the Toric code limit the system is expected to have four fold degenerate ground state. In the spin polarized limit, there is no GS degeneracy. The gap closing gives us an estimate of the transition which is again plotted in the numerical phase diagram of Fig. 4.5. The general agreement of the susceptibility data and the gap data is noticeable.

Fig. 4.2(a) shows for  $t_2 = 0$  the evolution of gap at different  $t_1$ . At  $t_1 = 0$  we have the

exactly solvable Toric code model with a  $Z_2$  QSL ground state with the gap scale is  $\Delta_1$ , above the four fold degenerate ground state which is exactly equal to 4 for the pure Toric code model in accordance with the expectation. The gap closes around  $t_1 = 0.5$  and towards  $t_1 = 1$  another gap,  $\Delta_2$  opens up, which is above the trivial spin polarized paramagnetic ground state. In the 4.2(b) and 4.2(c), for  $t_2 = 0.2$  and  $0.3$  respectively, the size of the gap and the closing point along  $t_1$  changes significantly. In both the cases the perturbation to the Toric code model lifts the four fold degeneracy of the topologically ordered QSL ground state via finite size effects. Finally in 4.2(d), at  $t_2 = 0.4$ , the two fold degeneracy at  $t_2 \sim 0$  originates from the two possible time reversal partners describing the ferromagnetic state which spontaneously breaks time reversal symmetry as discussed in the previous section. The gap above the ground state manifold is given by  $\Delta_3$ . At  $t_1 \approx 0.7$  this gap closes so that the system goes into paramagnetic phase signalled by the unique time reversal symmetric ground state as seen in the figure.

Having gotten an estimate of the phase boundaries, we now turn to further characterisation of the phases.

**Topological Entanglement Entropy :** In the  $Z_2$  QSL, the entanglement entropy ( $S_A$ ) between a sub-system ( $A$ ), and its compliment ( $\bar{A}$ ) follows the area law with a sub-leading topological correction given by[64, 65]

$$S_A(L) = \alpha L - \tilde{\gamma}(L) ; \tilde{\gamma}(L) = \log(2) + O(1/L) \quad (4.2)$$

Where  $\alpha$  is a non-universal constant and  $L$  is the length of the boundary between  $A$  &  $\bar{A}$ . In the limit  $L \rightarrow \infty$  the TEE saturates to  $\log(2) \approx 0.693$ . By partitioning the whole system into 4 sub-systems in a particular way, as shown in Fig. 4.3(b), the constant part of the TEE can be extracted as[64, 65]

$$\begin{aligned} -\gamma' &= S_A + S_B + S_C + S_{ABC} - S_{AB} - S_{BC} - S_{AC} \\ &= \log(2) + \sum_{\beta} O(1/L_{\beta}) \end{aligned} \quad (4.3)$$

where  $\beta$  is the different choices of combinations of the sub-system, such as  $\beta = A, AB$  and so on. In Fig. 4.4(a) the  $\gamma'$  is shown as a function of increasing system (SS) size, which is denoted by the total number of spins in a cluster, for the higher system size TEE saturates to  $\log(2)$ . The clusters considered here are  $3 \times 3, 5 \times 2, 4 \times 3, 5 \times 3$  &  $4 \times 4$  which have 18,

20, 24, 30 & 32 spins respectively. For the smallest system with 18 spins, the sub-systems (A, B, C in Fig. 4.3(b)) has 3-4 spins, whereas for the largest system size considered here with 32 spins, the sub-systems has 7-8 spins.

**Transverse magnetisation along  $\Gamma$  :** To characterise the trivial paramagnet, we calculate the magnetisation along  $\Gamma$ , *i.e.*  $\langle \tau_i^y \rangle$ . For two representative values of  $t_2 = 0.0$  and  $0.6$ , this has been plotted as a function of  $t_1$  in Fig. 4.4(b). In the  $(t_1, t_2)$  parameter space, these are along the red dotted lines in the Fig. 4.5. For both the values of  $t_2$ , in the limit  $t_1 = 1$ , the system is in PM phase, where the magnetization saturates to 1. The magnetization decreases along with the decreasing  $t_1$ , eventually being zero in the limit  $t_1 = 0$ . However for two different values of  $t_2$ , the magnetization changes differently. From the Fig. 4.5, we see for  $t_2 = 0.0$  ( $0.6$ ) the phase transition is around  $t_1 \approx 0.5$  ( $0.8$ ), the magenta lines in Fig. 4.4(b) denote the corresponding  $t_1$  values for phase transition.

**The two point correlator for the ferromagnetic order parameter :** To characterize the ferromagnet, connected correlator  $c(r) = \langle \tau_i^z \tau_{i+r}^z \rangle - \langle \tau_i^z \rangle \langle \tau_{i+r}^z \rangle$  is used where  $\langle \dots \rangle$  denotes the ground state expectation value. The normalised  $c(r)$  is plotted as a function of distance in Fig. 4.4(c) for different values of  $t_2$  with  $t_1$  being zero. This is along the  $t_2$  axis of Fig. 4.5. In the FM phase, starting from the  $t_2 = 1$  until  $t_2 = 0.4$  the spins are correlated. Below  $t_2 = 0.3$ , the correlation falls off exponentially, however due to small system size it is difficult to extract the correlation length.

The above exact diagonalisation, is severely limited by system size. However, it has well understood limits. The results suggest possibility of direct transitions out of the  $Z_2$  QSL into the symmetry broken ferromagnet or the symmetric trivial paramagnet. The results are summarised in Fig. 4.5 which is in rough agreement with the expectation of Fig. 3.1.

In the section 7.1, we present our understanding of the unconventional quantum phase transitions assuming that they are continuous. To successfully describe the transition, we need to obtain a description of the non-trivial low energy excitations of the QSL and their behaviour determines the critical theory. This naturally takes the form of a gauge theory coupled with matter matter fields.

## CHAPTER 5

### NUMERICAL RESULTS: AFM ANISOTROPIC KITAEV MODEL

#### 5.1 Phase diagram : Exact diagonalisations

Having discussed the phases in the different limits in section 3.2, we now study the phase boundaries via ED on finite spin clusters. For this we use the interpolating Hamiltonian:

$$\begin{aligned} \mathcal{H}^{AFM}(\tilde{t}_1, \tilde{t}_2) = & (1 - \tilde{t}_1)(1 - \tilde{t}_2)\bar{\mathcal{H}}_{(J=\Gamma=0)}^{AFM} \\ & + \tilde{t}_2(1 - \tilde{t}_1)\bar{\mathcal{H}}_{(\Gamma=K=0)}^{AFM} + \tilde{t}_1(1 - \tilde{t}_2)\bar{\mathcal{H}}_{(J=K=0)}^{AFM} \end{aligned} \quad (5.1)$$

Where  $\bar{\mathcal{H}}_X^{AFM}$  is defined as  $\mathcal{H}_X^{AFM}$  with a unit energy scale and  $X$  being the various limits in the parameter regimes of  $K$ ,  $J$ , &  $\Gamma$ . The explicit forms of the Hamiltonians( $\mathcal{H}_X^{AFM}$ ) are given in Eqs. 3.12, 3.14, and 3.19. The rescaled parameters are:

$$\tilde{t}_1 = \frac{\Gamma^2/|K_z|}{J_{TC} + \Gamma^2/|K_z|}; \quad \tilde{t}_2 = \frac{J}{J_{TC} + |J|} \quad (5.2)$$

Similar to the FM case discussed in section 4, in this parameter space, at the points,  $(\tilde{t}_1, \tilde{t}_2) = (0, 0), (0, 1), (1, 0)$  the  $\mathcal{H}(\tilde{t}_1, \tilde{t}_2)$  are Toric code, the Heisenberg and the pseudo-dipolar limit respectively. We perform ED for system sizes of up to 32 spins with periodic boundary conditions (PBC). Following the discussion on the FM case (chapter 4), we calculate the following quantities to estimate the phase boundaries as well as the nature of the phases– (1) *Ground state fidelity susceptibility*, (2) *Spectral gaps*, (3) *Topological entanglement entropy*, (4) *Magnetization*, and, (5) *Spin-spin correlation*. In addition, we use *Plaquette expectation*, i.e. the expectation value of  $W_i$  operator (following Eq. 3.12) to determine the phase boundaries in the parameter space of  $(\tilde{t}_1, \tilde{t}_2)$ .

**1. Ground state fidelity susceptibility ( $\chi_1, \chi_2$ ) :** As introduced in the chapter 4, this is the double derivative of the ground state energy  $E_{GS}$  as a function of any of the parameters  $\tilde{t}_1$  and  $\tilde{t}_2$ :  $\chi_1 = |\frac{\partial^2 E_{GS}}{\partial \tilde{t}_1^2}|$  and  $\chi_2 = |\frac{\partial^2 E_{GS}}{\partial \tilde{t}_2^2}|$ . The behavior of the fidelity susceptibility for fixed values of  $\tilde{t}_1$  as a function of  $\tilde{t}_2$  and vice-versa shows pronounced peaks (see Fig. 5.1) showing transitions

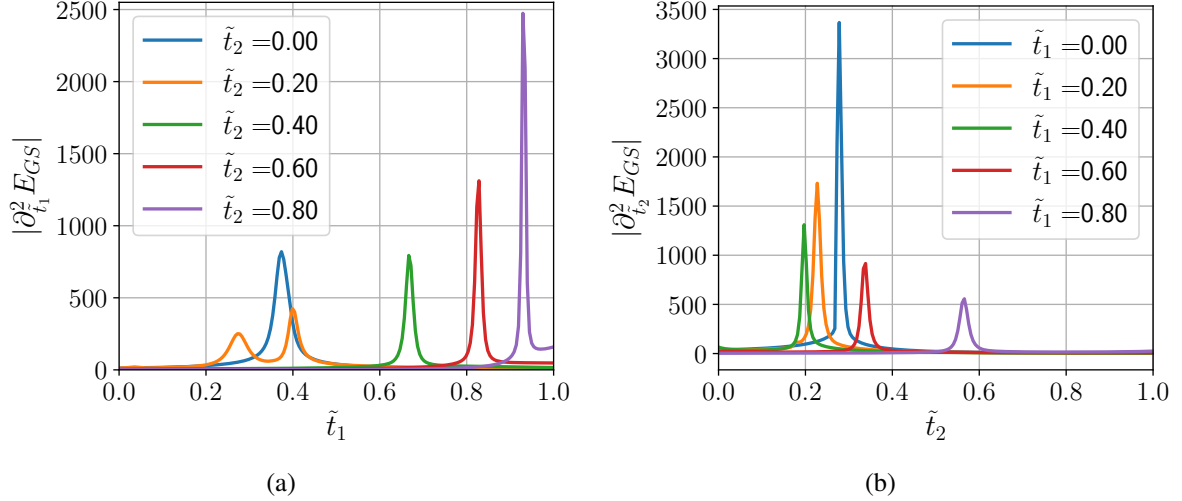


Figure 5.1: Behavior of ground state susceptibility for Eq. 5.1. (a)  $\chi_1$  along the  $\tilde{t}_1$  direction for constant values of  $\tilde{t}_2$ . (b)  $\chi_2$  along the  $\tilde{t}_2$  direction for various values of  $\tilde{t}_1$ . ( $N = 2L_x L_y$  for  $L_x \times L_y = 4 \times 3$ )

between the  $Z_2$  QSL (stabilized by  $\bar{\mathcal{H}}_{(J=\Gamma=0)}^{AFM}$ ), the ferromagnet (stabilized by  $\bar{\mathcal{H}}_{(\Gamma=K=0)}^{AFM}$ ) and the large  $\Gamma$  phase stabilized by  $\bar{\mathcal{H}}_{(J=K=0)}^{AFM}$ . The position of these peaks is plotted in Fig. 5.5 to demarcate the phase boundaries.

**2. Spectral gap ( $\Delta_m$ ):** Further insights into the nature of phases and phase boundaries are obtained from the bulk spectral gap of the low-lying energy eigenstates,  $\Delta_m$ , – the gap between the  $m^{th}$  excited state and the ground state. For instance, in the FM state  $\Delta_1 \sim$  zero given the expected two-fold degenerate ground states (pertaining to two symmetry broken states in the thermodynamic limit), while in the  $Z_2$  QSL one expects  $\Delta_1 - \Delta_3 \sim$  zero since the latter has a 4 fold topological degeneracy on a torus. One expects no such degeneracy for the large  $\Gamma$  phase since it is a gapless point where the bulk states would show gaps due to finite-size effects. All these expectations are correctly borne out in our numerical results shown in Fig. 5.2, where the behavior  $\Delta_1 - \Delta_5$  helps to demarcate the various phases.

Furthermore, the minimum bulk gap ( $\min(\Delta_m)$ ) coincides with the susceptibility peaks (see Fig.5.5) which serves as a self-consistent check for the phase boundaries for our finite spin clusters.

**3. Topological entanglement entropy ( $\gamma$ ):** As discussed in chapter 4, the non-trivial entanglement of the gapped  $Z_2$  QSL can be captured via the topological entanglement entropy ( $\equiv \gamma$ ). In order to distill this it is useful to employ the Kitaev-Preskil prescription[64, 65] where the

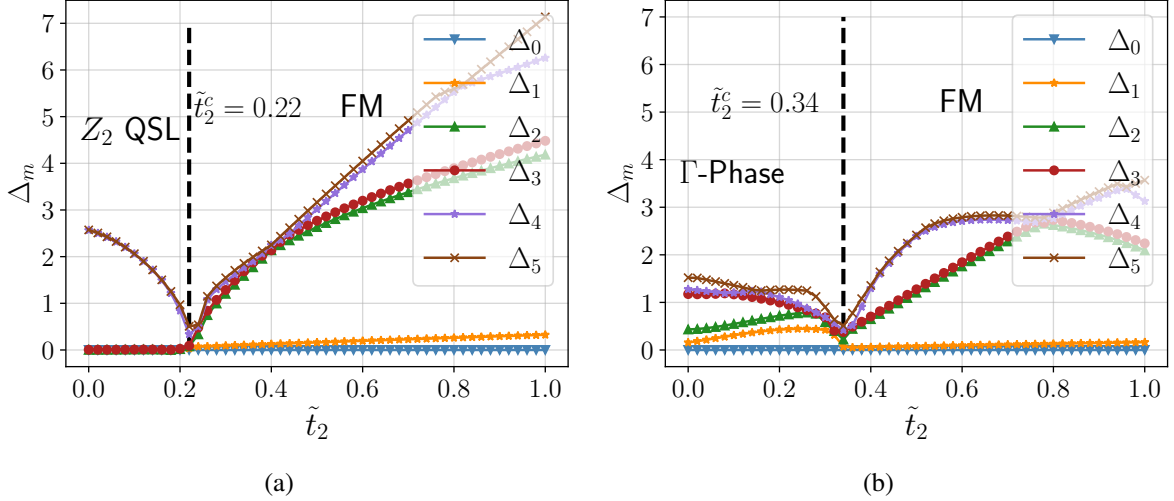


Figure 5.2: Low energy spectra to excited states from the ground state where  $\Delta_m$  defines the gap between the  $m^{\text{th}}$  excited state and the ground state is shown as a function of  $\tilde{t}_2$  for constant values of  $\tilde{t}_1$  (see Eq. 5.1). In (a)  $\tilde{t}_1 = 0.2$  and (b)  $\tilde{t}_1 = 0.6$ . The system size is  $(L_x, L_y) = (4, 3)$  with  $N = 2L_x L_y$  spins.

area law contributions cancel perfectly (see chapter 4). The behavior of  $\gamma$  as a function of  $\tilde{t}_1$  for  $\tilde{t}_2 = 0$  is shown in Fig. 5.3(a). One finds that while  $\gamma \sim \log(2)$  in the  $Z_2$  QSL,  $\gamma \sim 0$  in the  $\Gamma$  phase reflecting that the latter has no topological order of a gapped spin liquid state. To investigate the area law contributions in the various phases it is useful to calculate, for a given spin cluster, the bipartite entanglement entropy ( $S_A(L)$ ) of any subpart of volume  $A$  with a linear boundary of size  $L$  and fit it to this functional form (also see Eq. 4.3)

$$S_A(L) = \alpha L - \gamma + O(1/L) \quad (5.3)$$

where  $\alpha$ ,  $\gamma$  are the coefficients of the area law entanglement, and the topological entanglement entropy respectively [64, 65, 99]. The behavior of  $\alpha$  is also shown in Fig. 5.3(a) reflecting that both  $Z_2$  QSL and large  $\Gamma$  phase has finite area law contributions. It is worthwhile to point out that  $\gamma$  obtained by fitting Eq. 5.3 ( $\equiv \gamma_{\text{Fit}}$ ) seems to show a finite value in the large  $\Gamma$  phase, however, is a spurious artifact of the fitting scheme as has been pointed out in [100] for stacked/cluster SPT like states. It is pertinent to point out that in the large  $\Gamma$  phase we often find a curvature in the behavior of  $S$  as a function of  $L$  which may suggest a logarithmic correction [101]. However, in our limited ED calculations, it is hard to separate out if this is due to the gapless nature of the  $(\lambda_1, \lambda_2)$  point or a finite correlation length in the large  $\Gamma$  phase. Some additional results in other parameter regimes are discussed in Appendix E.1.

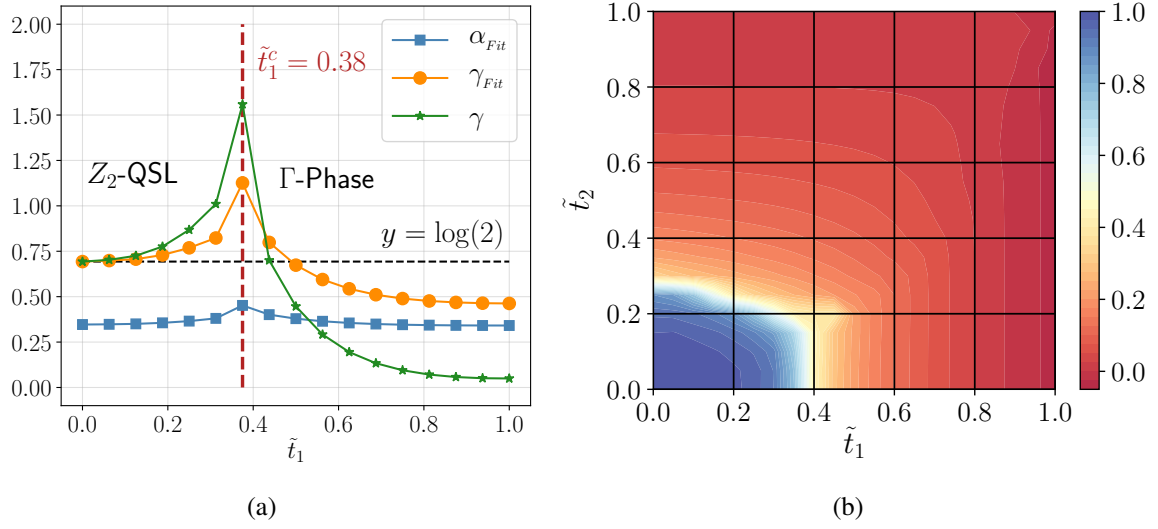


Figure 5.3: (a) The bipartite entanglement entropy in the  $\Gamma K$  direction ( $\tilde{t}_2 = 0$  line in Eq. 5.1) follows an area law, i.e.  $S_A(L) = \alpha L$ , however, in the  $Z_2$ -QSL phase this is supplemented by a topological correction ( $\gamma$ ). Calculations done on a  $((L_x, L_y) = (5, 3))$  cluster. (b) Average of the plaquette ( $W_i$  in Eq. 3.12) expectation value for the ground state of Eq. 5.1 in the  $(\tilde{t}_1, \tilde{t}_2)$  plane (for a  $((L_x, L_y) = (3, 3))$  spin cluster).

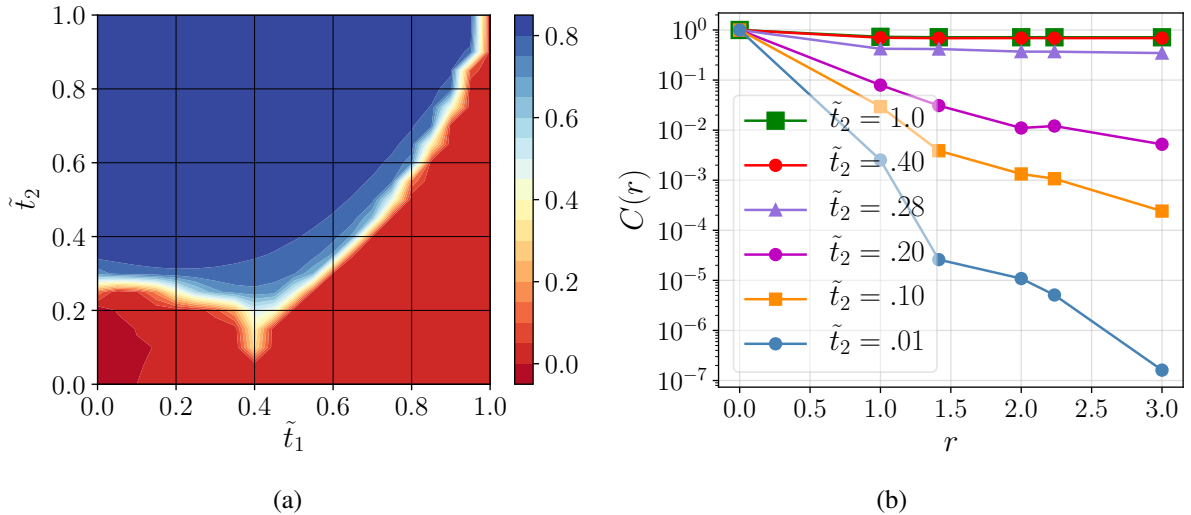


Figure 5.4: (a) Behavior of  $M_z = \frac{1}{N} \sum_i \langle \tau_i^z \rangle$  in the  $\tilde{t}_1, \tilde{t}_2$  parameter regime of Eq. 5.1. To characterize the ferromagnet state we apply a weak symmetry breaking perturbation ( $\sim \frac{\tilde{t}_2(1-\tilde{t}_1)}{100} \sum_i \tau_i^z$ ). (b) Behavior of connected correlator  $C(r) = \langle \tau_i^z \tau_{i+r}^z \rangle - \langle \tau_i^z \rangle \langle \tau_{i+r}^z \rangle$  over the ground state of Eq. 5.1 for different values of  $\tilde{t}_2$  for  $\tilde{t}_1 = 0$ . (System size,  $L_x = 3, L_y = 3$ )

**4. Plaquette expectation ( $w$ ):** The non-trivial topological entanglement entropy of the QSL is closely related to the type of topological order realized. As discussed above in the section 3.2.1 the low energy excitations of the QSL are gapped bosonic Ising electric and magnetic charges [16, 69] whose density is encoded by the plaquette spin operators  $W_i \equiv \tau_{i+d_1}^z \tau_{i-d_2}^z \tau_i^y \tau_{i+d_1-d_2}^y$  (see Eq.3.12). We plot the expectation value of such average charge density  $w = \sum_i \frac{1}{N} \langle W_i \rangle$  in Fig. 5.3(b) for the entire  $\tilde{t}_1, \tilde{t}_2$  plane (where the expectation value is taken over the ground state). Clearly, in the QSL the ground state does not contain any charges resulting in  $w \approx 1$  which gives away to  $w \approx 0$  in both the spin ordered as well as the large  $\Gamma$  phase showing that in the ground states of these phases the charges proliferate.

This provides an important clue into the mechanism of the phase transitions out of the QSL via the proliferation and condensation of the gauge charges. We use these soft modes to construct our critical theory for the phase transition in the next section.

**5. Magnetization ( $M_z$ ):** While the QSL does not break any symmetry spontaneously, the spin-ordered phase, on the other hand, is characterized by symmetry breaking captured by a finite magnetization  $M_z = \frac{1}{N} \sum_i \langle \tau_z \rangle$  which is calculated in the presence of a small symmetry breaking field ( $\sim \frac{\tilde{t}_2(1-\tilde{t}_1)}{100} \sum_i \tau_i^z$ ). The resultant plot is shown in Fig. 5.4(a). Clearly, the complete FM region shows a finite  $M_z$  while both the  $Z_2$  liquid and the large  $\Gamma$  phase show no such feature. Thus we expect that this region spontaneously breaks symmetry in the thermodynamic limit as the symmetry-breaking field is taken to zero as our calculation of the spin-spin correlations (below) indicates.

**6. Spin-spin correlation:** To further characterize the ferromagnet, connected correlator  $C(r) = \langle \tau_i^z \tau_{i+r}^z \rangle - \langle \tau_i^z \rangle \langle \tau_{i+r}^z \rangle$  is evaluated over the ground state in *absence* of any perturbing field. An exponentially falling correlation signals no magnetic order while a long-range ordered state will show that  $C(r)$  takes a finite value. The behavior of  $C(r)$  as a function of  $r$  is shown in Fig. 5.4(b) for different values of  $t_2$  with  $t_1$  being zero showing the systems realize a long-range magnetic order in the FM state.

The above numerical results, when taken together, lead to the phase diagram as shown in Fig. 5.5 which illustrates the three phases and the intervening transitions. In the rest of the thesis, we investigate the nature of the intervening phase transitions and develop its field theory.

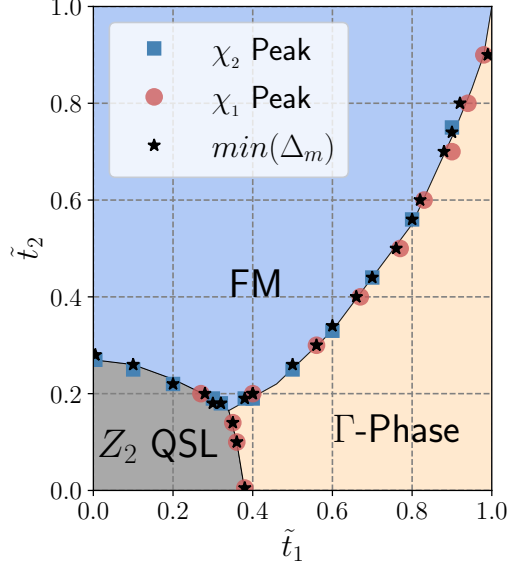


Figure 5.5: Phase diagram of Eq. 5.2 for  $\tilde{t}_1, \tilde{t}_2 \in [0, 1]$  for the complete  $\text{KJ}\Gamma$  Hamiltonian. The phase boundaries are obtained by analyzing ground state fidelity susceptibility and values where the gaps to the bulk excited states ( $\equiv \Delta_m$ ) (see text) take the minimum value ( $\min(\Delta_1)$ ) of a 24 spin ( $L_x = 4, L_y = 3$ ) cluster.

## 5.2 Exact diagonalisation study of stacked cluster chain in context of $\Gamma$ -limit of anisotropic AFM Kitaev model

Continuing the discussion of the pseudo-dipolar limit of the anisotropic AFM Kitaev model in section 3.2.3, here we present results from ED-based numerical analysis.

In Fig. 5.6(a) we show the ground state (GS) susceptibility [98] discontinuous peak along the  $\lambda_1$  for various constant  $\lambda_2$  values between 0 and 0.8. We can clearly see for  $\lambda_2 = 0$  line the sudden jump in the susceptibility at  $\lambda_1 = 1$  is indicating a first-order phase transition [87, 93] expected between the SSPT and the trivial paramagnet. On departing from the  $\lambda_2 = 0$  line, the weight of the discontinuous peak monotonically comes down as we approach  $\lambda_2 = 1$  indicating that the discontinuous nature of the transition weakens as we approach  $\lambda_2 = 1$  and disappears at this point. However, our present calculations cannot discern if the discontinuity persists all the way to  $\lambda_2 = 1$ . Similar physics is observed coming down from the  $\lambda_2 = 2$  line (not shown). It is pertinent to point out that given the limited system sizes accessible in ED, there are significant even-odd (commensurability) effects in all regions of the phase diagram. This, therefore, makes the role of symmetries and various transformations, even more, crucial to understand the nature of the phases.

The above first-order transition is in stark contrast with the transition obtained by tuning

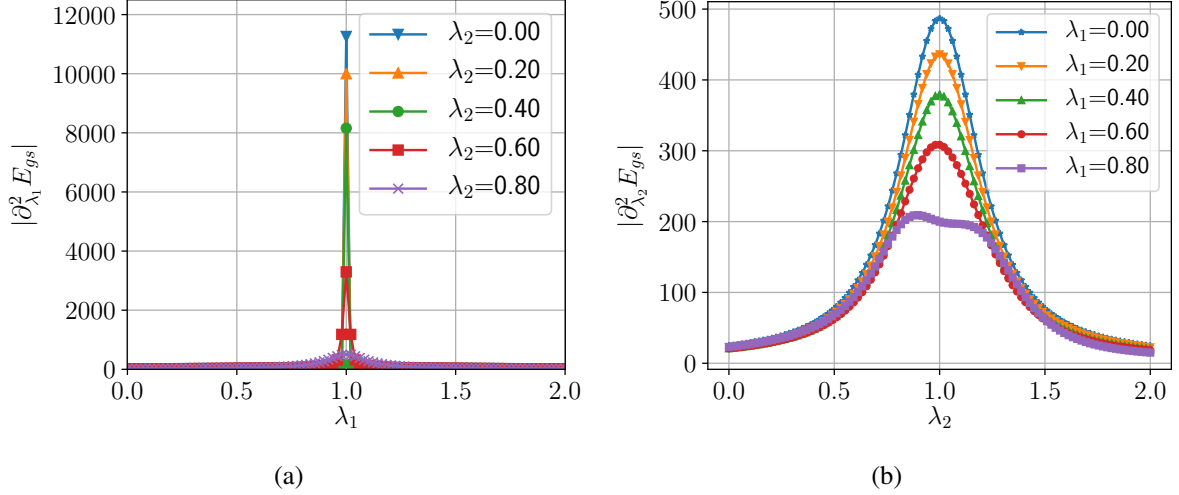


Figure 5.6: (a) Ground state (GS) susceptibility as the absolute value of the second derivative of the GS energy ( $E_{gs}$ ) with respect to  $\lambda_1$  for constant  $\lambda_2$  values for the Hamiltonian given in Eq. 3.21 (b) Ground state susceptibility along  $\lambda_2$  for constant  $\lambda_1$  values. Both results are for an 18 spin cluster with  $L_x = 3$  and  $L_y = 3$  and PBC geometry.

$\lambda_2$  as shown in Fig. 5.6(b). Here the susceptibility shows a peak without a shoulder (*i.e.*, a sudden jump) indicative of a continuous transition at  $\lambda_2 = 1$ . Indeed for  $\lambda_1 = 0$ , this transition originates from a stack of cluster chains and is described by decoupled  $(1 + 1)$  dimensional critical point of  $SO_1(2)$  CFT [94, 95] with a description in terms of Majorana fermions (see Appendix D.1). The continuous nature of the transition persists for larger values of  $\lambda_1$  until close to the  $\lambda_1 = 1$  whence the peak bifurcates indicating the possibility of opening up of an intermediate phase in the vicinity of  $\lambda_1 = 1$ . However, our present numerical calculations are limited by system size to probe this aspect. As we discuss below, we expect this intermediate phase, even if it exists, to be very fragile due to a large number of special symmetries (see the discussion above) in the  $(\lambda_1, \lambda_2)$  plane. Again we find a similar picture on the  $\lambda_1 > 1$  region due to the  $\pi$ -rotation about the z-bond symmetry  $C_{2z}$ , (see Eq. 2.12).

Right at the point  $\lambda_1 = \lambda_2 = 1$ , our present ED calculations reveal a bulk gapless phase. This is shown in Fig. Fig. 5.7(a) where we plot the bulk gap to the four lowest excitations as a function of the few systems sizes to indicate that the gap to these excitations vanishes almost linearly in inverse system size. The contour plot of the bulk gap to the first excited state in the entire  $(\lambda_1, \lambda_2)$  plane is shown in Fig. 5.7(b). This shows that gap indeed closes along the  $\lambda_1 = 1$  and  $\lambda_2 = 1$  lines with the former leading to a first-order transition and the later leading to a second-order transition. This separates the plane into four phases as shown in Fig. 3.6 and 3.8.

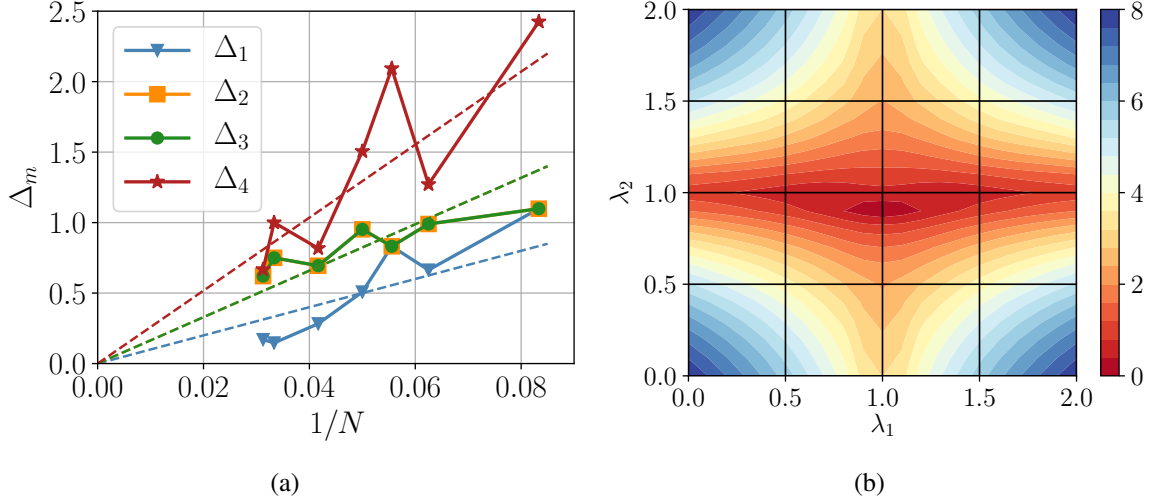


Figure 5.7: (a) Scaling of energy gaps ( $\Delta_m$ ) to  $m^{\text{th}}$  excited state as a function of inverse system size ( $N = 2(L_x \times L_y)$ ) at pure  $\Gamma$  limit, i.e.  $(\lambda_1, \lambda_2) = (1, 1)$  (see Eq. 3.21) for systems sizes involving  $N = 12$  to  $N = 32$  spins. The dashed lines are guides to the eye. (b) The gap to the first excited state in the complete  $(\lambda_1, \lambda_2)$  plane for a  $4 \times 2$  cluster. Both results are for a PBC geometry.

As indicated above, the first-order transitions weaken near the  $\lambda_1 = \lambda_2 = 1$  and possibly lead to a bulk gapless phase right at that point. Remarkably, our ED calculations on systems with open boundary conditions show that at this point, in addition to the gapless bulk modes the system has an additional  $2^{2L_x}$  exact zero energy Ising boundary modes on the top and bottom boundary which do not hybridize with the bulk gapless modes due to special subsystem symmetries (Eq. 3.35). A detailed discussion on the anomalous character of these symmetry operations in the  $(\lambda_1, \lambda_2)$  plane is discussed in Appendix D.4. Such gapless phases with boundary modes have recently been discussed in the context of symmetry-enriched criticality in one dimension [102, 103] and more recently for related two-dimensional phases [104], however to the best of our knowledge none of these phases lie in the intersection of such weak SPTs as here.

We now turn to the important question regarding the nature of the possible gapless phase at  $\lambda_1 = \lambda_2 = 1$  with extra sub-system symmetry-protected zero energy boundary modes. At the outset, such a gapless phase is rather remarkable in a system with no continuous symmetries and hence would be rather novel if found to be stable. As noted above, whether such a gapless phase is limited to only a single point or extends over a finite region is not clear from our present ED calculations due to severe finite size effects, however as we shall discuss now, we think it is the former and this gapless point is rather fragile.

The first clue to the fragility of this gapless point comes from the rather fine-tuned nature of the Hamiltonian in Eq. 3.21 which allows for a whole class of sub-system symmetries not present in the microscopic Hamiltonian and are an artifact of keeping just the second order terms in  $\Gamma$ . For example, on considering the higher order ( $\mathcal{O}(\Gamma^3/|K_z|^3)$  in perturbation theory) term for the  $\Gamma$ -Hamiltonian (see Eq. 3.18), such sub-system symmetries are explicitly broken. However, they serve as important approximate symmetries in discerning the general structure of the phase diagram in the  $(\lambda_1, \lambda_2)$  plane— particularly the gapped part of the phase diagram. However, for the gapless part of the phase diagram, the absence of these sub-system symmetries is rather subtle. Indeed the boundary modes are susceptible to symmetry-breaking perturbations or to boundary interactions which can lead to spontaneous symmetry-breaking at the boundary. A discussion of such symmetry-breaking terms on the boundary Hamiltonian of the large  $\Gamma$  phase is shown in section D.4.

To check the stability of the gapless point at  $\lambda_1 = \lambda_2 = 1$ , we added simple perturbations that explicitly break the sub-system symmetries, but are still allowed by the microscopic symmetries and studied the fate of such a Hamiltonian. In particular, we performed ED on

$$H(\delta_1, \delta_2) = (1 - \delta_1)(1 - \delta_2)H(1, 1) - \delta_1(1 - \delta_2) \sum_i \tau_i^x - \delta_2(1 - \delta_1) \sum_{\langle ij \rangle} \tau_i^z \tau_j^z \quad (5.4)$$

where  $H(1, 1)$  is the Hamiltonian which belongs to the general Hamiltonian given in Eq. 3.21 with  $(\lambda_1, \lambda_2) = (1, 1)$ , the second term represents a  $x$ -field and the third term is a nearest neighbor Ising exchange in the  $z$  direction, both of which are allowed within the microscopic symmetries (see Eq. 2.12).

Fig. 5.8 shows the ground state fidelity as a function of the two interpolating parameters, where we find that while a finite size system shows a GS susceptibility ( $|\frac{\partial^2 E_{gs}}{\partial \delta_1^2}|$ ) peak suggesting a phase transition – the peak falls significantly with the inclusion of an Ising coupling suggesting that the large  $\Gamma$  phase is indeed smoothly connected to a  $x$ -paramagnet *without* any intervening phase transition within the symmetry allowed parameter space. A further insight into the nature of the phase is— as more systematically discussed in the next section we also find that the phase has no topological entropy content and is short-range entangled (see Fig. 5.3). Interestingly as the system is tuned to a paramagnet this topological entropy content continues to remain zero showing that the phase is smoothly connected to a trivial state. The behavior of the energy gaps ( $\Delta_m$ ) as well as the topological entanglement entropy (see Eq. 5.3) are shown

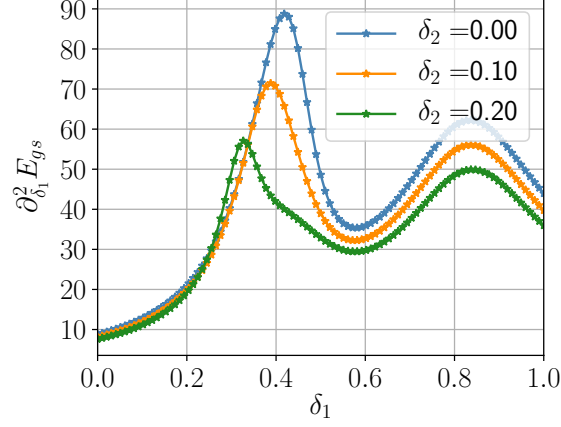


Figure 5.8: Behavior of GS susceptibility as the large  $\Gamma$  phase is tuned to a  $x$  paramagnet in presence of varying strengths of Ising perturbation ( $\sim \delta_2$ ), see Eq. 5.4. The results are for a system size  $N = 16, L_x = 2, L_y = 4$  with PBC geometry.

in Fig. D.7 in Appendix D.6.

Together with the above signatures of the  $\Gamma$  phase, we conclude that the  $\lambda_1 = \lambda_2 = 1$  is a fine-tuned point which even while it is itself gapless, gets gapped out immediately by generic microscopic symmetry allowed perturbations and the resultant gapped phase is continuously connected to a trivial paramagnet. This insight as will discuss later will guide both the nature of the phase and the nature of transitions in the complete  $KJ\Gamma$  parameter space.

## CHAPTER 6

### GAUGE THEORY DESCRIPTION OF THE PHASES AND PHASE TRANSITIONS

#### 6.1 Gauge theory description of the phases

As the first step towards the gauge theory description, we find it convenient to separate the  $e$  and  $m$  charges, and this is done by rotating the spins as outlined in Eq. 3.2. Also, following the nature of the similarity between FM and AFM anisotropic model in the case of TC Hamiltonian (see Eq. 3.3 and 3.13), the gauge theory description will be same for both the limit. However, we should keep in mind that the definition of  $\tau$ -spins (and  $\tilde{\tau}$ -spins) is different as described in Eq. 2.8.

Following usual techniques,[70, 105] we introduce the Ising variables,  $\mu^\alpha$ , on the sites and  $\rho^\alpha$  on the bonds of the square lattice (Fig. 1.1) as follows :

$$\tilde{\tau}_i^z = \mu_a^x \rho_{ab}^z \mu_b^x, \quad \tilde{\tau}_i^x = \rho_{ab}^x \quad (6.1)$$

with the Gauss's law constraint

$$\prod_{b \in +_a} \rho_{ab}^x = \mu_a^z = \prod_{i \in +_a} \tilde{\tau}_i^x \quad (6.2)$$

where  $a(\equiv (a_x, a_y))$  and  $b$  denote sites the square lattice (fig. 1.1) joined by the bond  $i$  where  $\tilde{\tau}_i$  sits. For  $N$  sites, there are  $2N$ ,  $\tau^\alpha$ -spins sitting on the bonds. Hence the total dimension of the Hilbert space is  $2^{2N}$ . In terms of the gauge theory, there are  $N$   $\mu$ -spins and  $2N$   $Z_2$  gauge potentials  $\rho$  leading to a total degree of freedom of  $2^N \times 2^{2N}$  which form a redundant description. However, for each site, there is one Gauss's law constraint (Eq. 6.2) leading to  $\frac{2^{2N} \times 2^{2N}}{2^N} = 2^{2N}$  physical degree of freedom equivalent to that of the  $\tau$  spins. Thus the above mapping leads to a faithful representation.

The physical picture for the above mapping is easy to understand. The Gauss's law shows that  $\mu_a^z = +1(-1)$  denotes the absence (presence) of an  $e$  charge at the sites of the square lattice in Fig. 1.1. Therefore,  $\mu_a^x$ 's are the creation/annihilation operators for  $e$  charges at the

sites, and  $\rho_{ab}^x$ 's are the electric fields of the  $Z_2$  gauge theory whose flux is related to the density of the electric charges  $\mu_a^z$  through the Gauss's law. Finally, from Eq. 6.1, we get

$$\prod_{i \in \square} \tilde{\tau}_i^z = \prod_{ab \in \square} \rho_{ab}^z \quad (6.3)$$

This is nothing but the  $m$  excitations now given by the lattice curl of the  $Z_2$  gauge potential.

At this point, it is useful to also introduce the dual gauge fields where the  $m$  charges are explicit. This is obtained using the standard  $Z_2$  version of the electromagnetic duality[106]

$$\tilde{\tau}_i^x = \tilde{\mu}_a^x \tilde{\rho}_{\bar{a}\bar{b}}^z \tilde{\mu}_{\bar{b}}^x; \quad \tilde{\tau}_i^z = \tilde{\rho}_{\bar{a}\bar{b}}^x \quad (6.4)$$

where the  $m$  charge creation operators,  $\tilde{\mu}_a^x$  are now defined on the sites of the dual lattice, denoted by  $\bar{a} \equiv T_{\mathbf{d}_1}(a) \equiv (\bar{a}_x, \bar{a}_y)$  and  $\bar{b}$  (we use the bar above the symbol to denote dual lattice sites), obtained by joining the centers of the direct square lattice of Fig. 1.1 such that in the above expression the bond of the direct lattice denoted by  $i$  is bisected by the dual bond joining the sites  $\bar{a}$  and  $\bar{b}$ . The dual gauge fields,  $\tilde{\rho}_{\bar{a}\bar{b}}^\alpha$ , reside on the links of the dual lattice, and the dual Gauss's law is given by

$$\prod_{\bar{b} \in +\bar{a}} \tilde{\rho}_{\bar{a}\bar{b}}^x = \tilde{\mu}_{\bar{a}}^z = \prod_{i \in \square_{\bar{a}}} \tilde{\tau}_i^z \quad (6.5)$$

Therefore in this dual representation,  $\tilde{\rho}_{\bar{a}\bar{b}}^x$  is the magnetic field of the  $Z_2$  gauge theory whose divergence is equal to the  $m$  charge  $\tilde{\mu}_{\bar{a}}^z$  at the site of the dual plaquette. As previously, the dual representation along with the dual Gauss's law span the physical Hilbert space. This is further clarified by the relation between the direct and the dual degrees of freedom which is obtained by comparing Eq. 6.1 and 6.4, which gives

$$\rho_{ab}^x = \tilde{\mu}_a^x \tilde{\rho}_{\bar{a}\bar{b}}^z \tilde{\mu}_{\bar{b}}^x \quad (6.6)$$

where the  $(ab)$  bond on the direct lattice bisect the dual bond  $(\bar{a}\bar{b})$ , and

$$\begin{aligned}
\prod_{b \in +_a} \rho_{ab}^x &= \mu_a^z = \prod_{\langle \bar{a}\bar{b} \rangle \in \square_a} \tilde{\rho}_{\bar{a}\bar{b}}^z \\
\prod_{\bar{b} \in +_{\bar{a}}} \tilde{\rho}_{\bar{a}\bar{b}}^x &= \tilde{\mu}_{\bar{a}}^z = \prod_{\langle ab \rangle \in \square_{\bar{a}}} \rho_{ab}^z
\end{aligned} \tag{6.7}$$

The last equation encodes that while the  $e$  and  $m$  charges are bosons, they see each other as a source of  $\pi$  fluxes. In fact, these equations are actually not independent but are related to each other through duality.

We can use either of the representations discussed above. However, it is often useful to introduce both the charges explicitly, each coupled to its own gauge field and the mutual semionic statistics is then represented by a mutual  $Z_2$  Chern-Simons (SC) action or, [107, 108] in the continuum limit, a mutual  $U(1) \times U(1)$  CS theory.[13, 41, 42, 75]

At this point it is worthwhile to note, although the gauge theory description for FM and AFM TC limits are the same, the symmetry transformation of the  $\tau$ -spins are different. While the symmetry transformations of  $\tau$ -spins are provided in Eq. 2.11 and 2.12 for FM and AFM limits respectively, after the rotation to  $\tilde{\tau}$  (Eq. 3.2) the symmetry transformations are discussed in the appendix A.1 and A.2 for the FM and AFM cases respectively.

### Action of the symmetries on the gauge charges and the gauge fields in FM case

Having expressed the elementary excitations, the gauge charges, of the QSL, we now turn to the action of symmetries on them. From Eq. 2.11, we get the symmetry transformations of the rotated spins  $\tilde{\tau}$ s using Eq. 3.2 (Table A.2 in Appendix A.1).

**Lattice Translations** : Under both the translations, along the directions  $\mathbf{d}_1$  and  $\mathbf{d}_2$  (see Fig. 1.1), the plaquettes and the vertices are interchanged. Hence the  $e$  and  $m$  charges are interchanged (the original square lattice and its dual get interchanged). This is thus an example of an anyon permutation symmetry.[109] The translation symmetry acts on the gauge degrees of freedom in the following manner.

$$\begin{aligned}
T_{\mathbf{d}_j} : \quad & \{\mu^x, \mu^z\}_a \rightarrow \{\tilde{\mu}^x, \tilde{\mu}^z\}_{T_{\mathbf{d}_j}(a)} \\
& \{\tilde{\mu}^x, \tilde{\mu}^z\}_{\bar{a}} \rightarrow \{\mu^x, \mu^z\}_{T_{\mathbf{d}_j}(\bar{a})} \\
& \{\rho^x, \rho^z\}_{ab} \rightarrow \{\tilde{\rho}^x, \tilde{\rho}^z\}_{T_{\mathbf{d}_j}(ab)} \\
& \{\tilde{\rho}^x, \tilde{\rho}^z\}_{\bar{a}\bar{b}} \rightarrow \{\rho^x, \rho^z\}_{T_{\mathbf{d}_j}(\bar{a}\bar{b})}
\end{aligned} \tag{6.8}$$

For translation along the cartesian axes, the lattice vectors are given by  $\hat{x} = \mathbf{d}_1 - \mathbf{d}_2$  and  $\hat{y} = \mathbf{d}_1 + \mathbf{d}_2$ . Under this, the gauge charges and potentials transform as

$$\begin{aligned}
T_{\hat{x}(\hat{y})} : \quad & \{\mu^x, \mu^z\}_a \rightarrow \{\mu^x, \mu^z\}_{a+\hat{x}(\hat{y})} \\
& \{\tilde{\mu}^x, \tilde{\mu}^z\}_{\bar{a}} \rightarrow \{\tilde{\mu}^x, \tilde{\mu}^z\}_{\bar{a}+\hat{x}(\hat{y})} \\
& \{\rho^x, \rho^z\}_{\bar{a}\bar{b}} \rightarrow \{\rho^x, \rho^z\}_{\bar{a}+\hat{x}(\hat{y}), \bar{b}+\hat{x}(\hat{y})} \\
& \{\tilde{\rho}^x, \tilde{\rho}^z\}_{\bar{a}\bar{b}} \rightarrow \{\tilde{\rho}^x, \tilde{\rho}^z\}_{\bar{a}+\hat{x}(\hat{y}), \bar{b}+\hat{x}(\hat{y})}
\end{aligned} \tag{6.9}$$

**Time Reversal :** The bond-dependent rotation of Eq. 3.2 implies that in the rotated basis, natural to the Toric code QSL, on the vertical bonds, the  $\tau^x$  is odd under time reversal, whereas on the vertical bonds  $\tau^z$  continues to remain time-reversal odd. This endows the gauge charges and the gauge fields with non-trivial transformation under time reversal which depends on their spatial location and is given by

$$\begin{aligned}
\mathcal{T} : \quad & \{\mu^x, \mu^z\}_a \rightarrow \{\mu^x, \mu^z\}_a \\
& \{\tilde{\mu}^x, \tilde{\mu}^z\}_{\bar{a}} \rightarrow \{\tilde{\mu}^x, \tilde{\mu}^z\}_{\bar{a}} \\
& \{\rho^x, \rho^z\}_{ab} \rightarrow \{(-1)^{a_y+b_y} \rho^x, (-1)^{a_x+b_x} \rho^z\}_{ab} \\
& \{\tilde{\rho}^x, \tilde{\rho}^z\}_{\bar{a}\bar{b}} \rightarrow \{(-1)^{\bar{a}_y+\bar{b}_y} \tilde{\rho}^x, (-1)^{\bar{a}_x+\bar{b}_x} \tilde{\rho}^z\}_{\bar{a}\bar{b}}
\end{aligned} \tag{6.10}$$

**Reflections about  $z$  bond,  $\sigma_v$  :**

$$\begin{aligned}
\sigma_v : \quad & \{\mu^x, \mu^z\}_a \rightarrow \{\mu^x, \mu^z\}_{\sigma_v(a)} \\
& \{\tilde{\mu}^x, \tilde{\mu}^z\}_a \rightarrow \{\tilde{\mu}^x, \tilde{\mu}^z\}_{\sigma_v(a)} \\
& \{\rho^x, \rho^z\}_{ab} \rightarrow \{(-1)^{a_y+b_y} \rho^x, (-1)^{a_x+b_x} \rho^z\}_{\sigma_v(ab)} \\
& \{\tilde{\rho}^x, \tilde{\rho}^z\}_{\bar{a}\bar{b}} \rightarrow \{(-1)^{\bar{a}_y+\bar{b}_y} \tilde{\rho}^x, (-1)^{\bar{a}_x+\bar{b}_x} \tilde{\rho}^z\}_{\sigma_v(\bar{a}\bar{b})}
\end{aligned} \tag{6.11}$$

**$\pi$ -rotation about the  $z$ -bond,  $C_{2z}$  :**

$$\begin{aligned}
C_{2z} : \quad & \{\mu^x, \mu^z\}_{\mathbf{a}} \rightarrow \{\mu^x, \mu^z\}_{C_{2z}(\mathbf{a})} \\
& \{\tilde{\mu}^x, \tilde{\mu}^z\}_{\bar{\mathbf{a}}} \rightarrow \{(-1)^{\bar{a}_x} \tilde{\mu}^x, \tilde{\mu}^z\}_{C_{2z}(\bar{\mathbf{a}})} \\
& \{\rho^x, \rho^z\}_{ab} \rightarrow \{(-1)^{a_y+b_y} \rho^x, (-1)^{a_x+b_x} \rho^z\}_{C_{2z}(ab)} \\
& \{\tilde{\rho}^x, \tilde{\rho}^z\}_{\bar{a}\bar{b}} \rightarrow \{(-1)^{\bar{a}_y+\bar{a}_y} \tilde{\rho}^x, (-1)^{\bar{a}_x+\bar{b}_x} \tilde{\rho}^z\}_{C_{2z}(\bar{a}\bar{b})}
\end{aligned} \tag{6.12}$$

$\pi$ -rotation honeycomb lattice centre,  $R_\pi$  :

$$\begin{aligned}
 R_\pi : \quad & \{\mu^x, \mu^z\}_a \rightarrow \{\mu^x, \mu^z\}_{R_\pi(a)} \\
 & \{\tilde{\mu}^x, \tilde{\mu}^z\}_{\bar{a}} \rightarrow \{\tilde{\mu}^x, \tilde{\mu}^z\}_{R_\pi(\bar{a})} \\
 & \{\rho^x, \rho^z\}_{ab} \rightarrow \{\rho^x, \rho^z\}_{R_\pi(ab)} \\
 & \{\tilde{\rho}^x, \tilde{\rho}^z\}_{\bar{a}\bar{b}} \rightarrow \{\tilde{\rho}^x, \tilde{\rho}^z\}_{R_\pi(\bar{a}\bar{b})}
 \end{aligned} \tag{6.13}$$

With this, we are in a position to investigate the nature of the phase transition out of the  $Z_2$  QSL discussed in the section 3.1.1. The phase transitions out of  $Z_2$ -QSL to the associated symmetry-breaking magnetic order and to the paramagnetic phase are discussed in section 7.1, which is related to the schematic phase diagram is summarized in Fig. 3.1. To this end, it is worthwhile to continue the symmetry transformations of the gauge charges and fields in the case of the AFM Kitaev model which we discuss next.

Action of the symmetries on the gauge charges and the gauge fields in AFM case

Following the symmetry transformation of the  $\tilde{\tau}$ -spins in table A.3 in appendix A.2, we will now discuss the transformation rules for the gauge charges and gauge fields.

**Lattice Translations** : Under both the translations, along the directions  $\mathbf{d}_1$  and  $\mathbf{d}_2$  (see Fig. 1.1), the plaquettes and the vertices are interchanged. Hence the  $e$  and  $m$  charges are interchanged.

$$\begin{aligned}
 T_{\mathbf{d}_j} : \quad & \{\mu^x, \mu^z\}_a \rightarrow \{\tilde{\mu}^x, \tilde{\mu}^z\}_{T_{\mathbf{d}_j}(a)} \\
 & \{\tilde{\mu}^x, \tilde{\mu}^z\}_{\bar{a}} \rightarrow \{\mu^x, \mu^z\}_{T_{\mathbf{d}_j}(\bar{a})} \\
 & \{\rho^x, \rho^z\}_{ab} \rightarrow \{\tilde{\rho}^x, \tilde{\rho}^z\}_{T_{\mathbf{d}_j}(ab)} \\
 & \{\tilde{\rho}^x, \tilde{\rho}^z\}_{\bar{a}\bar{b}} \rightarrow \{\rho^x, \rho^z\}_{T_{\mathbf{d}_j}(\bar{a}\bar{b})}
 \end{aligned} \tag{6.14}$$

For translation along the cartesian axes, the lattice vectors are given by  $\hat{x} = \mathbf{d}_1 - \mathbf{d}_2$  and  $\hat{y} = \mathbf{d}_1 + \mathbf{d}_2$ . Under this, the gauge charges and potentials transform as

$$\begin{aligned}
 T_{\hat{x}(\hat{y})} : \quad & \{\mu^x, \mu^z\}_a \rightarrow \{\mu^x, \mu^z\}_{a+\hat{x}(\hat{y})} \\
 & \{\tilde{\mu}^x, \tilde{\mu}^z\}_{\bar{a}} \rightarrow \{\tilde{\mu}^x, \tilde{\mu}^z\}_{\bar{a}+\hat{x}(\hat{y})} \\
 & \{\rho^x, \rho^z\}_{\bar{a}\bar{b}} \rightarrow \{\rho^x, \rho^z\}_{\bar{a}+\hat{x}(\hat{y}), \bar{b}+\hat{x}(\hat{y})} \\
 & \{\tilde{\rho}^x, \tilde{\rho}^z\}_{\bar{a}\bar{b}} \rightarrow \{\tilde{\rho}^x, \tilde{\rho}^z\}_{\bar{a}+\hat{x}(\hat{y}), \bar{b}+\hat{x}(\hat{y})}
 \end{aligned} \tag{6.15}$$

**Time Reversal :** Due the bond dependent nature of the  $\tilde{\tau}$  transformation the gauge degrees of freedoms transform as:

$$\begin{aligned} & \{\mu^x, \mu^z\}_a \rightarrow \{\mu^x, \mu^z\}_a \\ \mathcal{T} : & \{\tilde{\mu}^x, \tilde{\mu}^z\}_{\bar{a}} \rightarrow \{\tilde{\mu}^x, \tilde{\mu}^z\}_{\bar{a}} \\ & \{\rho^x, \rho^z\}_{ab} \rightarrow \{(-1)^{a_y+b_y}\rho^x, (-1)^{a_x+b_x}\rho^z\}_{ab} \\ & \{\tilde{\rho}^x, \tilde{\rho}^z\}_{\bar{a}\bar{b}} \rightarrow \{(-1)^{\bar{a}_y+\bar{b}_y}\tilde{\rho}^x, (-1)^{\bar{a}_x+\bar{b}_x}\tilde{\rho}^z\}_{\bar{a}\bar{b}} \end{aligned} \quad (6.16)$$

**Reflections about  $z$  bond,  $\sigma_v$  :** This transformation is different compared to the ferromagnetic case:

$$\begin{aligned} & \{\mu^x, \mu^z\}_a \rightarrow \{\mu^x, \mu^z\}_{\sigma_v(a)} \\ \sigma_v : & \{\tilde{\mu}^x, \tilde{\mu}^z\}_a \rightarrow \{\tilde{\mu}^x, \tilde{\mu}^z\}_{\sigma_v(a)} \\ & \{\rho^x, \rho^z\}_{ab} \rightarrow \{\rho^x, \rho^z\}_{\sigma_v(ab)} \\ & \{\tilde{\rho}^x, \tilde{\rho}^z\}_{\bar{a}\bar{b}} \rightarrow \{\tilde{\rho}^x, \tilde{\rho}^z\}_{\sigma_v(\bar{a}\bar{b})} \end{aligned} \quad (6.17)$$

**$\pi$ -rotation about the  $z$ -bond,  $C_{2z}$  :** This transformation is also different compared to the ferromagnetic case:

$$\begin{aligned} & \{\mu^x, \mu^z\}_a \rightarrow \{\mu^x, \mu^z\}_{C_{2z}(a)} \\ C_{2z} : & \{\tilde{\mu}^x, \tilde{\mu}^z\}_{\bar{a}} \rightarrow \{\tilde{\mu}^x, \tilde{\mu}^z\}_{C_{2z}(\bar{a})} \\ & \{\rho^x, \rho^z\}_{ab} \rightarrow \{-\rho^x, -\rho^z\}_{C_{2z}(ab)} \\ & \{\tilde{\rho}^x, \tilde{\rho}^z\}_{\bar{a}\bar{b}} \rightarrow \{-\tilde{\rho}^x, -\tilde{\rho}^z\}_{C_{2z}(\bar{a}\bar{b})} \end{aligned} \quad (6.18)$$

**$\pi$ -rotation about honeycomb lattice centre,  $R_\pi$  :** We can obtain the transformation rules from the Eq. 6.17 and 6.18

$$\begin{aligned} & \{\mu^x, \mu^z\}_a \rightarrow \{\mu^x, \mu^z\}_{R_\pi(a)} \\ R_\pi : & \{\tilde{\mu}^x, \tilde{\mu}^z\}_{\bar{a}} \rightarrow \{\tilde{\mu}^x, \tilde{\mu}^z\}_{R_\pi(\bar{a})} \\ & \{\rho^x, \rho^z\}_{ab} \rightarrow \{-\rho^x, -\rho^z\}_{R_\pi(ab)} \\ & \{\tilde{\rho}^x, \tilde{\rho}^z\}_{\bar{a}\bar{b}} \rightarrow \{-\tilde{\rho}^x, -\tilde{\rho}^z\}_{R_\pi(\bar{a}\bar{b})} \end{aligned} \quad (6.19)$$

Having discussed the symmetry transformations of the gauge charges and gauge fields for both FM and AFM limit, in chapter 7 we discuss the theory of phase transition out of  $Z_2$  QSL phase. In the rest of this chapter, we will try to understand a complementary analysis to obtain the  $Z_2$ -QSL starting from a symmetry-breaking ground state. To gain insight, we start with the

ferromagnetic order in the  $\tau$ -spins for the FM Kitaev model ( $J < 0$  in Eq. 3.7), and so how to obtain a  $Z_2$  QSL by selectively proliferating the domain walls.

## 6.2 $Z_2$ QSL from the Magnetic Order

While we will later study a controlled field theory for the transition into the magnetically ordered phase from the  $Z_2$  QSL in chapter 7, it is interesting to understand how to obtain a  $Z_2$  QSL by disordering the magnetic order. Specifically, the  $Z_2$  QSL can be understood as the selective proliferation of the domain wall (DW) of the magnetically ordered state, in contrast to the indiscriminate proliferation of all the domain walls that gives a trivial paramagnet.

As mentioned above in section 3.1.2 for the anisotropic limit of FM Kitaev model, in the limit  $J = 0$ , the ground state wave function of TC model in the rotated basis is given by Eq. 3.4. On the other hand, for  $J_{TC} = 0$ , when the Hamiltonian is just the first term of Eq. 3.7, albeit in the rotated basis, the two-fold degenerate ground states. (To be specific, let us consider  $J < 0$  such that the ground state in the un-rotated basis is a ferromagnet)

$$|\Psi_{FM}^\pm\rangle = \bigotimes_i |\psi_i^\pm\rangle \quad (6.20)$$

where

$$|\psi_i^\pm\rangle = \begin{cases} \begin{cases} | +1_{\tilde{z}}\rangle & \forall i \in H \\ | +1_{\tilde{x}}\rangle & \forall i \in V \end{cases} \\ \begin{cases} | -1_{\tilde{z}}\rangle & \forall i \in H \\ | -1_{\tilde{x}}\rangle & \forall i \in V \end{cases} \end{cases} \quad (6.21)$$

for the two time-reversal partner ground states, in the  $\tilde{\tau}$ -spins.

Generalizing the ideas of Ref. [66], we can think about obtaining the QSL from the spin-ordered state by selectively proliferating the domain walls of the latter. Consider taking the above ferromagnetic ground state wave function in the rotated basis and project it in the zero  $e$  and  $m$  sector as follows

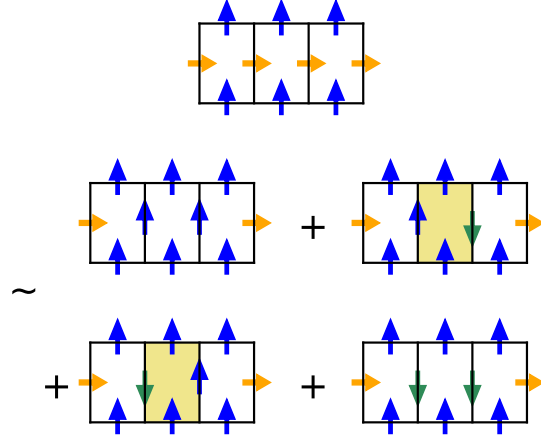


Figure 6.1: The  $|\Psi_{FM}^+\rangle$  state for one plaquette expanded in the  $\tilde{\tau}^z$ -basis. It is clear that for two of the contributing terms there is a magnetic charge,  $B_p = -1$  as marked in yellow. Blue (green) arrows stand for  $\tilde{\tau}^z = 1(-1)$  state. Orange arrows stand for  $\tilde{\tau}^x = 1$  state.

$$|\Psi^+\rangle = \left[ \prod_s \left( \frac{1 + A_s}{2} \right) \right] \left[ \prod_p \left( \frac{1 + B_p}{2} \right) \right] |\Psi_{FM}^+\rangle \quad (6.22)$$

We note that the two projectors commute with each other. For a plaquette  $|\Psi_{FM}^+\rangle$  is shown in Fig. 6.1 when expanded in the  $\tilde{\tau}^z$ -basis. It is clear that on applying the  $B_p$  operator to this plaquette, the amplitudes of the two contributions that have a  $m$  charge ( $B_p = -1$ ) do not survive the projection of  $\prod_p (1 + B_p)/2 (\equiv \mathcal{S}_B)$ . Extending this argument, we conclude that the on a torus, acting  $\mathcal{S}_B$  on  $|\psi_{FM}^+\rangle$  leads to, up to normalization,

$$\prod_{x_j} \left[ \prod_{p \in j^{th} \text{ row}} \left( \frac{1 + B_p}{2} \right) \right] |\Psi_{FM}^+\rangle \approx \prod_{x_j} \left( 1 + \mathcal{L}_{x_j}^m \right) |0_z\rangle \quad (6.23)$$

where  $|0_z\rangle$  is defined in Eq. 3.5.  $\mathcal{L}_{x_j}^m$  are the horizontal Wilson loops (see Eq. 3.6) for each row in the square lattice, with  $x_j$  being the row index. Thus it consists of closed loops of down spins on the vertical bonds running along the horizontal direction along the rows. In the above equation, the product on the right-hand side is expanded to obtain

$$\begin{aligned} & \left( 1 + \sum_{x_j} \mathcal{L}_{x_j}^m + \sum_{x_j \neq x_k} \mathcal{L}_{x_j}^m \mathcal{L}_{x_k}^m + \dots \right) |0_z\rangle \\ &= \left( \sum_e [\mathcal{L}_{x_k}^m \dots] + \sum_o [\mathcal{L}_{x_k}^m \dots] \right) |0_z\rangle \end{aligned} \quad (6.24)$$

where in the last expression we have collected all the even (first summation) and the odd (second summation) powers of the  $\mathcal{L}^m$  operators separately. From Eq. 6.22, it is easy to see that on application of  $\prod_s(1 + A_s)/2(\equiv \mathcal{S}_A)$ , this leads to an equal weight superposition of the  $Z_2$  QSL ground states belonging to two topological sectors, *i.e.*,

$$|\Psi^+\rangle \sim |1, 1\rangle + |1, -1\rangle \quad (6.25)$$

Clearly from Eq. 6.25,  $\mathcal{L}_y^e |\psi^+\rangle \approx |1, 1\rangle - |1, -1\rangle$ , this helps us to get :

$$|\Psi_{G.S.}^{\text{Toric}}\rangle \equiv |1, 1\rangle \approx (1 + \mathcal{L}_y^e) \mathcal{S}_A \mathcal{S}_B |\Psi_{FM}^+\rangle. \quad (6.26)$$

The above equation connects the QSL with the spin-ordered state and the operators can be interpreted in terms of the domain walls of the spin-ordered state. Expanding the right-hand side of the above equation, we get

$$|\Psi_{G.S.}^{\text{Toric}}\rangle \sim (1 + \mathcal{L}_y^e) (1 + (A_{s_1} \cdots A_{s_m})(B_{p_1} \cdots B_{p_n})) |\Psi_{FM}^+\rangle \quad (6.27)$$

The first term  $(1 + \mathcal{L}_y^e) |\Psi_{FM}^+\rangle$  is a superposition of the ordered state with periodic boundary and twisted boundary conditions (see Fig. 6.2(a)) along the  $x$  direction on the 2-tori for the spins on the vertical bonds (For the spins on the horizontal bonds both the states have periodic boundary conditions). Clearly, the position of the twist is a choice and does not affect the observables in the QSL state. The rest of the terms on the right-hand side are products of  $A_s$  and  $B_p$  operators and they have a straightforward interpretation in terms of the selected domain walls (defined as the location of frustrating bonds) of the spin order.[66] With the spins located on the bonds, the domain walls pass through the vertices of the square lattice of Fig. 1.1 and have two sub-lattice structure. As shown in Fig. 6.2(b)-(d),

the  $A_s$  and the  $B_p$  operators create domain walls respectively of the spin ordering on the horizontal and vertical bonds. An arbitrary product of only  $A_s$  or  $B_p$  operators creates such domain walls of the spin order and all these contributions have an amplitude with a positive sign as is explicit. For a combined set of  $A_s$  and  $B_p$  operators, the sign is given by  $(-1)^m$  where  $m$  denotes the total overlap of the horizontal bonds among the participating  $A_s$  and  $B_p$

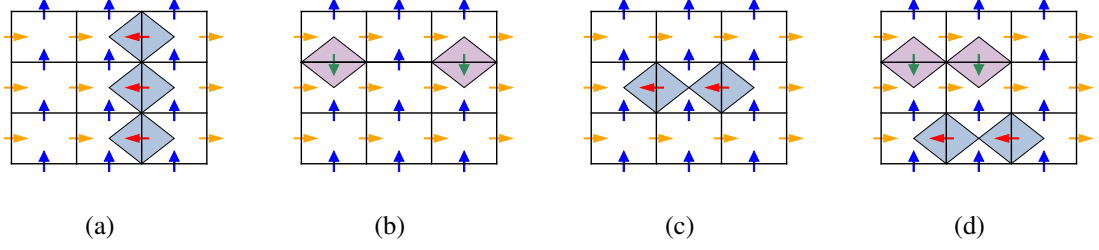


Figure 6.2: **(a)** Domain wall created by twisted boundary condition ( $\mathcal{L}_y^e$ ). An electric domain wall is created by the action of two neighboring  $A_s$  on  $|\Psi_{FM}^+\rangle$  is shown in **(b)**, whereas in **(c)**, a magnetic domain wall is created by a single  $B_p$  operator. **(d)** Both domain walls with even overlap (see text). **(e)** Both domain walls with odd overlaps, this contribution has a relative negative sign (see text). Red arrow denote  $\tilde{\tau}^x = -1$ , rest of the arrow definitions follow from Fig. 6.1

operators. The  $A_s$  and  $B_p$  in Fig. 6.2(d) has zero (even) overlap on the horizontal bond compare to the single (odd) overlap in Fig. 6.2(e). Thus we have

$$|\Psi_{G.S.}^{\text{Toric}}\rangle \sim |\Psi_{FM}\rangle + \sum_{\alpha} (-1)^{m_{\alpha}} |d_{\alpha}\rangle \quad (6.28)$$

where  $|d_{\alpha}\rangle$  denotes various domain wall states starting with the ferromagnetic state. Focusing on a single row of horizontal bonds, the application of two neighboring  $A_s$  only on this row (for reference Fig. 6.2(b)) leads to two disconnected domain walls. On application of further  $A_s$ s belonging to this row, more domain walls are either created or the ones that are already present get transported along the chain. As a result, the spin on any site on this row of horizontal bonds locally has an equal superposition of up and down spins (in  $\tilde{\tau}^z$ -basis). This is nothing but a state where the spins on this row of horizontal bonds are polarized along  $\tilde{\tau}^x$  leading to the gapping out of the  $e$  charge. An argument for the row of vertical bonds and the  $m$  charge would lead to a similar result. A calculation starting from  $|\psi_{FM}^-\rangle$  leads to equal weight superposition of the other two topological sectors of the QSL. Incidentally one can perform the above analysis starting with an all up state (in  $\tilde{\tau}^z$ -basis) as was considered in Ref. [66]. In that case, the action of  $B_p$  is trivial as the all up state is already in the zero  $m$  sector resulting in a  $Z_2$  QSL. Indeed the right-hand side of the Eq. 6.22 in that case can be interpreted in terms of the selective domain walls of the all up  $\tilde{\tau}^z$ -ferromagnet.

We can contrast Eq. 6.28 to the ground state of the trivial paramagnet obtained by arbitrarily proliferating the domain walls of the ferromagnetic state. Such a trivial paramagnet has a wave-

function of the form

$$|\Psi_{G.S.}^{\text{Trivial}}\rangle \sim |\Psi_{FM}\rangle + \sum_{\alpha} |\tilde{d}_{\alpha}\rangle \quad (6.29)$$

which crucially differs from Eq. 6.28 in nature along with the sign structure of the domain walls. Indeed  $|\Psi_{G.S.}^{\text{Trivial}}\rangle$  can be obtained from  $|\Psi_{FM}\rangle$  by proliferating trivial domain walls using the  $\tilde{\tau}_i^z(\tilde{\tau}_i^x)$  operators on the vertical (horizontal) bonds. Such domain wall states clearly lack the sign structure discussed above.

Inside the ferromagnetic phase, all types of domain walls are gapped. However, depending on the energetics of the microscopic model their energy costs are different. Hence as a function of various coupling terms, one can become energetically cheaper than the other within the ferromagnetic phase without causing a phase transition. This provides a crossover within the ferromagnetic phase similar to the U(1) case in three dimensions as discussed in Ref. [66]. In this light, it is clear that the Toric code interaction term such as in Hamiltonian in Eq. 7.1 favors *decorated* (by sign) domain walls energetically whose subsequent proliferation leads to the QSL. This also suggests that a different perturbation involving single-site spin operators can lead to a trivial paramagnet starting from the FM. This, we argue below is exactly what the  $\Gamma$  term does.

To this end, we begin with the phase transition along the line of vertical and horizontal axes of the phase diagram in Fig. 3.1 starting with the transition between the  $Z_2$  QSL and the spin-ordered state brought about by the Heisenberg interactions and followed by the description of the transition between the QSL and the trivial paramagnet tuned by the pseudo-dipolar term. Here we note that as indicated previously, we expect that the transition between the ferromagnet and the trivial paramagnet is described by a transverse field Ising model whose transition is well understood and belongs to the well known 3d Ising universality class.

## CHAPTER 7

### FIELD THEORY

In this chapter, we discuss the theory of phase transitions out of  $Z_2$ -QSL. In the first part of this chapter, we start with the various phase transitions between the phases in the anisotropic limit of the FM Kitaev model (section 3.1), for which the schematic phase diagram is summarized in Fig. 3.1, subsequently, we discuss the phase transitions between the various phases in AFM Kitaev model, the phases are described in section 3.2 and Fig. 3.9.

#### 7.1 Phase transition in FM anisotropic Kitaev limit

##### 7.1.1 Phase transition between QSL and the spin ordered phase

Along the vertical axis of Fig. 3.1 at  $\Gamma = 0$ , there are two competing phases– the  $Z_2$  QSL for  $J \sim 0$  and the spin ordered phase in the Heisenberg limit,  $J/|K| \gg 1$ . While, as we already described, the QSL can be understood in terms of the selective proliferation of domain walls of the spin-ordered phase, to understand the phase transition between them, it is much more convenient to start with the QSL and obtain the description of the transition in terms of the soft modes, as a function of  $J$ , of its excitations– the  $e$  and  $m$  charges.

To understand this transition we re-write the minimal Hamiltonian (in  $\Gamma = 0$  limit) in the rotated basis (Eq. 3.2) to obtain

$$\tilde{\mathcal{H}}_{\Gamma=0}^{FM} = J \sum_{\langle i,j \rangle, (i \in H; j \in V)} \tilde{\tau}_i^z \tilde{\tau}_j^x - J_{TC} \left[ \sum_s A_s + \sum_p B_p \right] \quad (7.1)$$

where  $A_s$  and  $B_p$  are defined below Eq. 3.3. We note that the perturbation by the Heisenberg term is different from that considered in Ref. [105] of [110] as in the present case a term like  $\tilde{\tau}_i^{z(x)} \tilde{\tau}_j^{z(x)}$  (where  $i \in V$  and  $j \in H$ ) is forbidden by time reversal.

To the leading order in  $J$ , the pertinent Hamiltonian is given by Eq. 7.1 which generates the dispersion for the localized (in the exactly solvable Toric code limit) bosonic  $e$  and  $m$  charges eventually resulting in soft-modes which condense to give rise to the spin order as we shall show below. We neglect the higher order terms in  $J$  and later shall return to them to understand their effects.

In terms of the gauge charges of Eq. 6.1, the Hamiltonian in Eq. 7.1 becomes

$$\tilde{\mathcal{H}}_{\Gamma=0}^{FM} = J \sum_{\langle ab \rangle \in H; \langle bc \rangle \in V} [\mu_a^x \rho_{ab}^z \mu_b^x] [\rho_{bc}^x] - J_{TC} \sum_a \mu_a^z - J_{TC} \sum_p \prod_{\langle ab \rangle \in p} \rho_{ab}^z \quad (7.2)$$

The second and the third term represents the energy costs for creating  $e$  and  $m$  charges respectively. Indeed for  $J = 0$ , the theory is nothing but an even Ising gauge theory[111] that describes the  $Z_2$  QSL.

The first term, on the other hand, creates and mobilizes both  $e$  and  $m$  charges. Of central importance for our purpose is the particular form of the hopping term– both  $e$  and  $m$  charges, once created, can only disperse along the horizontal directions (with reference to Fig. 1.1) at this leading order of  $J$ . A somewhat similar effect was observed in doped isotropic Kitaev model.[112] The decoupling of various horizontal electric and magnetic “chains” lead to a dimensional reduction in this order. However, different such chains, as we shall see below, get coupled by higher order terms. This generically leads to anisotropic kinetic energy for the  $e$  and  $m$  charges and hence one expects anisotropic correlation lengths.

### Gauge mean field theory

We start our analysis by decoupling the first term in Eq. 7.2 within gauge mean field theory[113] where we systematically neglect the gauge fluctuations. A mean-field decoupling of the gauge charges and the gauge fields in the  $e$  and  $m$  sectors for the first term in Eq. 7.2:

$$[\mu_a^x \rho_{ab}^z \mu_b^x] [\rho_{bc}^x] \rightarrow \langle \mu_a^x \rho_{ab}^z \mu_b^x \rangle \rho_{bc}^x + \mu_a^x \rho_{ab}^z \mu_b^x \langle \rho_{bc}^x \rangle, \text{ gives}$$

$$\tilde{\mathcal{H}}_{\Gamma=0}^{FM} \rightarrow \tilde{\mathcal{H}}_{\Gamma=0}^{\text{GMFT}} = \tilde{\mathcal{H}}_{\Gamma=0}^{\text{GMFT}}(e) + \tilde{\mathcal{H}}_{\Gamma=0}^{\text{GMFT}}(m) \quad (7.3)$$

where

$$\tilde{\mathcal{H}}_{\Gamma=0}^{\text{GMFT}}(e) = \sum_{\langle ab \rangle \in H} J_{ab} \mu_a^x \rho_{ab}^z \mu_b^x - J_{TC} \sum_a \mu_a^z \quad (7.4)$$

describes the  $e$  sector with

$$J_{ab} = J [\langle \rho_{b,b-\hat{y}}^x \rangle + \langle \rho_{b,b+\hat{y}}^x \rangle + \langle \rho_{a,a-\hat{y}}^x \rangle + \langle \rho_{a,a+\hat{y}}^x \rangle] \quad (7.5)$$

being the effective coupling and

$$\tilde{\mathcal{H}}_{\Gamma=0}^{\text{GMFT}}(m) = \sum_{\langle \bar{a}\bar{b} \rangle \in H} J_{\bar{a}\bar{b}} \tilde{\mu}_{\bar{a}}^x \tilde{\rho}_{\bar{a}\bar{b}}^z \tilde{\mu}_{\bar{b}}^x - J_{TC} \sum_{\bar{a}} \tilde{\mu}_{\bar{a}}^z \quad (7.6)$$

describes the  $m$  sector with

$$J_{\bar{a}\bar{b}} = J \left[ \langle \tilde{\rho}_{\bar{b},\bar{b}-\hat{y}}^x \rangle + \langle \tilde{\rho}_{\bar{b},\bar{b}+\hat{y}}^x \rangle + \langle \tilde{\rho}_{\bar{a},\bar{a}-\hat{y}}^x \rangle + \langle \tilde{\rho}_{\bar{a},\bar{a}+\hat{y}}^x \rangle \right] \quad (7.7)$$

Clearly, at this order in  $J$ , the  $e$  and  $m$  sectors completely decouple into a series of transverse field Ising chains in the horizontal direction in Fig. 1.1. For the horizontal direction, we can choose a gauge

$$\rho_{a,a+\hat{x}}^z = \tilde{\rho}_{\bar{a},\bar{a}+\hat{x}}^z = +1 \quad (7.8)$$

as these links do not cross. The  $Z_2$  QSL is then the paramagnetic phase of this decoupled transverse field Ising chains where the  $e$  and  $m$  charges are both gapped. The Heisenberg term gives kinetic energy to both the  $e$  and  $m$  charges in the horizontal direction which then develops soft modes which condense to give rise to  $\langle \mu^x \rangle \neq 0$  and  $\langle \tilde{\mu}^x \rangle \neq 0$  for the respective chains.

For the above gauge, the soft mode develops at zero momentum as shown in Fig. 7.1(a) for both the  $e$  and  $m$  sectors. This can be denoted by

$$\hat{\nu}_e^{(1)} = 1; \quad \hat{\nu}_m^{(1)} = 1 \quad (7.9)$$

for the  $e$  sector on the direct lattice and  $m$  sector on the dual lattice respectively.

Application of time reversal symmetry (see Eq. 6.10) gives the time reversal partner soft mode for both the  $e$  and  $m$  sectors as shown in Fig. 7.1(b) which are given by

$$\hat{\nu}_e^{(2)} = e^{i\pi x}; \quad \hat{\nu}_m^{(2)} = e^{i\pi X} \quad (7.10)$$

for the  $e$  sector and  $m$  sectors. The cartesian coordinates of the direct and dual lattices are given by  $(x, y)$  and  $(X, Y)$  with  $X = x + 1/2$  and  $Y = y + 1/2$ . Other symmetries do not generate any further soft modes and hence the transition out of the QSL into the spin-ordered phase is described in terms of the above soft modes.

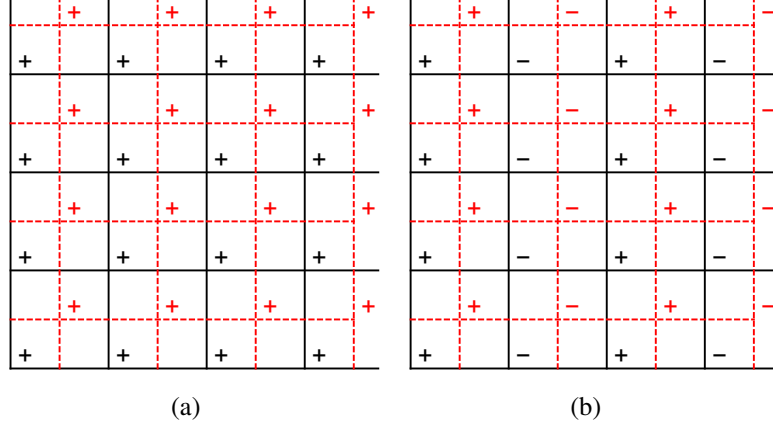


Figure 7.1: The electric (black) and the magnetic (red) soft modes on the direct and dual lattice respectively. The  $\pm$  denotes  $\mu^x = \pm 1$  and  $\tilde{\mu}^x = \pm 1$  respectively. Fig. (a) and (b) show the two time-reversal partners respectively,  $(\hat{\nu}_e^{(1)}, \hat{\nu}_e^{(2)})$  for the electric and  $(\hat{\nu}_m^{(1)}, \hat{\nu}_m^{(2)})$  the magnetic sectors.

### Soft modes

The soft mode expansion for the  $e$  sector is therefore given by[75, 108, 114]

$$\Psi_e(\mathbf{r}, \tau) = \phi_e^{(1)}(\mathbf{r}, \tau) \hat{\nu}_e^{(1)} + \phi_e^{(2)}(\mathbf{r}, \tau) \hat{\nu}_e^{(2)} \quad (7.11)$$

where  $(\phi_e^{(1)}(\mathbf{r}, \tau), \phi_e^{(2)}(\mathbf{r}, \tau))$  are real fields that represent amplitudes of the electric soft modes. Similarly, for the  $m$  sector, the soft mode expansion is given by

$$\Psi_m(\mathbf{r}, \tau) = \phi_m^{(1)}(\mathbf{r}, \tau) \hat{\nu}_m^{(1)} + \phi_m^{(2)}(\mathbf{r}, \tau) \hat{\nu}_m^{(2)} \quad (7.12)$$

where  $(\phi_m^{(1)}(\mathbf{r}, \tau), \phi_m^{(2)}(\mathbf{r}, \tau))$  are real amplitudes of the magnetic soft modes.

The Higg's phase obtained by condensation of a combination of the above modes is nothing but the spin-ordered phase as we shall see below, while the “uncondensed” phase represents the  $Z_2$  QSL. However, due to the non-trivial projective symmetry group (PSG) transformation of the soft modes under various symmetries of the system and due to the non-trivial mutual semionic statistics between the  $e$  and the  $m$  excitations, the construction of the critical theory requires careful analysis starting with the PSG analysis of the soft mode amplitudes. To this end, it is useful to define the complex soft mode amplitudes

$$\Phi_e = \phi_e^{(1)} + i\phi_e^{(2)} = |\Phi_e|e^{i\theta_e} \quad (7.13)$$

and

$$\Phi_m = \phi_m^{(1)} + i\phi_m^{(2)} = |\Phi_m|e^{i\theta_m} \quad (7.14)$$

where we have suppressed the arguments for clarity. Now, for the different symmetries considered in Eqs. 6.8-6.13, we have

$$\begin{aligned} \mathbf{T}_{d_1} : & \begin{cases} \Phi_e \rightarrow \Phi_m \\ \Phi_m \rightarrow \Phi_e^* \end{cases} & \mathbf{T}_{d_2} : & \begin{cases} \Phi_e \rightarrow \Phi_m^* \\ \Phi_m \rightarrow \Phi_e \end{cases} \\ \mathbf{T}_x : & \begin{cases} \Phi_e \rightarrow \Phi_e^* \\ \Phi_m \rightarrow \Phi_m^* \end{cases} & \mathbf{T}_y : & \begin{cases} \Phi_e \rightarrow \Phi_e \\ \Phi_m \rightarrow \Phi_m \end{cases} \\ \mathcal{T} : & \begin{cases} \Phi_e \rightarrow -i\Phi_e \\ \Phi_m \rightarrow -i\Phi_m \end{cases} & \sigma_v : & \begin{cases} \Phi_e \rightarrow i\Phi_e^* \\ \Phi_m \rightarrow i\Phi_m^* \end{cases} \\ C_{2z} : & \begin{cases} \Phi_e \rightarrow i\Phi_e^* \\ \Phi_m \rightarrow i\Phi_m^* \end{cases} & R_\pi : & \begin{cases} \Phi_e \rightarrow \Phi_e \\ \Phi_m \rightarrow \Phi_m^* \end{cases} \end{aligned} \quad (7.15)$$

where we have considered the origin of the coordinates to be centered at the site of the direct lattice. Clearly under  $\mathbf{T}_{d_1}$  and  $\mathbf{T}_{d_2}$  the  $e$  and  $m$  soft modes transform into each other— as mentioned above— due to the fact that the horizontal and vertical bonds interchange under these transformations. This is an example of anyon permutation symmetry.[109, 115] Due to this, the mass of the  $e$  and  $m$  excitations are forced to be the same in the critical theory.

The gauge invariant spin order parameter can be constructed out of the above soft modes[75, 108, 114] by considering the symmetry transformation, as

$$\begin{aligned} \tilde{\tau}_i^z &\sim |\Phi_e|^2 \cos(2\theta_e) \quad \forall i \in \text{Horizontal bonds} \\ \tilde{\tau}_i^x &\sim |\Phi_m|^2 \cos(2\theta_m) \quad \forall i \in \text{Vertical bonds} \end{aligned} \quad (7.16)$$

Among other transformations, it is clear from the symmetry transformation table that, as expected, the above two spin order parameters are odd under time-reversal symmetry,  $\mathcal{T}$ .

A crucial ingredient missing from the above analysis of the soft modes is the mutual semionic statistics of the electric and magnetic modes. This can either be implemented using a  $U(1) \times U(1)$  mutual Chern-Simons (CS) theory[13, 41, 42, 75] or a slightly more microscopic mutual  $Z_2$  CS theory.[107, 108] Here we shall use the  $U(1) \times U(1)$  formalism.

## Mutual semionic statistics and the $U(1) \times U(1)$ mutual Chern-Simons action

Within the  $U(1) \times U(1)$  mutual CS formalism,[41, 75, 116] the mutual semionic statistics between the  $e$  and  $m$  charges is implemented by introducing two internal  $U(1)$  gauge fields  $A_\mu$  and  $B_\mu$  that are minimally coupled to the electric ( $\Phi_e$ ) and magnetic ( $\Phi_m$ ) soft modes respectively. The PSG transformations of these fields are obtained from the fact that they are minimally coupled to  $\Phi_e$  and  $\Phi_m$  respectively. For the different symmetries in Eqs. 6.8-6.13, this leads to

$$\begin{aligned}
 \mathbf{T}_{\mathbf{d}_1} : & \begin{cases} A_\mu \rightarrow B_\mu \\ B_\mu \rightarrow -A_\mu \end{cases} & \mathbf{T}_{\mathbf{d}_2} : & \begin{cases} A_\mu \rightarrow -B_\mu \\ B_\mu \rightarrow A_\mu \end{cases} \\
 \mathbf{T}_{\mathbf{x}} : & \begin{cases} A_\mu \rightarrow -A_\mu \\ B_\mu \rightarrow -B_\mu \end{cases} & \mathbf{T}_{\mathbf{y}} : & \begin{cases} A_\mu \rightarrow A_\mu \\ B_\mu \rightarrow B_\mu \end{cases} \\
 \mathcal{T} : & \begin{cases} A_\mu \rightarrow -A_\mu, \\ B_\mu \rightarrow -B_\mu \end{cases} \\
 \sigma_v : & \begin{cases} A_x \rightarrow -A_x, \quad A_y \rightarrow A_y, \quad A_\tau \rightarrow -A_\tau \\ B_x \rightarrow -B_x, \quad B_y \rightarrow B_y, \quad B_\tau \rightarrow -B_\tau \end{cases} \\
 C_{2z} : & \begin{cases} A_x \rightarrow A_x, \quad A_y \rightarrow -A_y, \quad A_\tau \rightarrow -A_\tau \\ B_x \rightarrow B_x, \quad B_y \rightarrow -B_y, \quad B_\tau \rightarrow -B_\tau \end{cases} \\
 R_\pi : & \begin{cases} A_x \rightarrow -A_x, \quad A_y \rightarrow -A_y, \quad A_\tau \rightarrow A_\tau \\ B_x \rightarrow B_x, \quad B_y \rightarrow B_y, \quad B_\tau \rightarrow -B_\tau \end{cases} \tag{7.17}
 \end{aligned}$$

The mutual  $U(1) \times U(1)$  CS action in continuum in  $(2+1)$  dimensions is then given by[41, 75]

$$\mathcal{S}_{CS} = \frac{i}{\pi} \int d^2\mathbf{r}d\tau \epsilon^{\mu\nu\lambda} A_\mu \partial_\nu B_\lambda \tag{7.18}$$

where  $\mu, \nu, \lambda = x, y, \tau$ . It is easy to see that the above action implements the semionic statistics,[117] for example, by extremizing  $\mathcal{S}_{CS}$  with respect to  $A_\mu$  in presence of a static  $e$  charge density,  $\rho_e$ , which gives

$$\rho_e = \frac{1}{\pi} (\partial_x B_y - \partial_y B_x) \tag{7.19}$$

Therefore the  $m$  charge,  $\Phi_m$ , sees an odd number of  $e$  charge as a source of  $\pi$  flux as expected for a  $Z_2$  QSL. Note that both  $A_\mu$  and  $B_\mu$  have their respective Maxwell terms. However such terms are irrelevant in presence of the CS term and the respective photons gain mass.[117] Using the symmetry transformation in Eq. 7.17, we find that the CS action (Eq. 7.18) is odd under  $\mathcal{T}$  and  $R_\pi$ . However, we note that since the attachment of  $\pi$  and  $-\pi$  fluxes are equivalent, the above CS theory is in accordance with these symmetries.[75]

### The critical theory

With this, we can now write down the continuum critical action which is given by

$$\mathcal{S}_c = \int d^2\mathbf{r}d\tau \mathcal{L} + \mathcal{S}_{CS} \quad (7.20)$$

where  $\mathcal{S}_{CS}$  is given by Eq. 7.18 and

$$\mathcal{L} = \mathcal{L}_e + \mathcal{L}_m + \mathcal{L}_{em} \quad (7.21)$$

with

$$\mathcal{L}_e = |(\partial_\mu - iA_\mu)\Phi_e|^2 + u|\Phi_e|^2 + v|\Phi_e|^4 - \lambda [(\Phi_e)^4 + (\Phi_e^*)^4] \quad (7.22)$$

$$\mathcal{L}_m = |(\partial_\mu - iB_\mu)\Phi_m|^2 + u|\Phi_m|^2 + v|\Phi_m|^4 - \lambda [(\Phi_m)^4 + (\Phi_m^*)^4] \quad (7.23)$$

$$\mathcal{L}_{em} = w [(\Phi_e\Phi_m)^2 + (\Phi_e\Phi_m^*)^2 + \text{c.c.}] \quad (7.24)$$

At this stage, it is useful to draw attention to three important features of the above critical theory. Firstly, at the GMFT level (Eqs. 7.4 and 7.6), different horizontal chains are decoupled. Hence the soft modes do not have any rigidity in the vertical direction. However, fluctuations beyond the GMFT level lead to interactions between different horizontal chains. This is clear from Eq. 7.2, where each horizontal chain of  $e$  charges is coupled with two  $m$  horizontal chains at  $Y = y \pm 1/2$ . Thus integrating out the high energy  $m$  modes generate interaction between neighboring electric chains and thereby provides effective dispersion to the electric soft mode along the vertical direction. Additional contributions to both horizontal and vertical dispersions

are further obtained from higher-order corrections of the perturbation theory. However, the above mechanism leads to anisotropic dispersion, and the couplings for horizontal and vertical directions for the kinetic terms are indeed different. However, such anisotropy can be scaled away by simultaneously re-scaling  $y$  (say) and the fields. Such anisotropy would be reflected in terms of correlation functions in terms of lattice unit of length.

Secondly, due to Eq. 7.15 and 7.17, the coupling constants of the  $e$  and  $m$  modes are equal. In particular, the mass is related to the microscopic coupling constants as  $u \sim (J_{\text{TC}} - J)$  for both the  $e$  and  $m$  charges. This ensures that both the  $e$  and  $m$  soft modes condense together unless the translation symmetries,  $\mathbf{T}_{d_1}$  and/or  $\mathbf{T}_{d_2}$  are spontaneously broken. In terms of the soft modes, this is then the continuum version of a  $Z_2$  anyon permutation symmetry which places very strong constraints on the structure of the critical theory and ensures the correct phases as well as phase transitions.

Finally, for  $\lambda = w = 0$ , the system conserves fluxes in both the  $e$  and  $m$  sectors,  $U_e(1)$  and  $U_m(1)$ , separately.[75] Since, due to the mutual CS term, the fluxes of  $A_\mu(B_\mu)$  are attached to  $m(e)$  particle densities, the above flux conservation results in charge conservation for both  $e$  and  $m$  charges. This is broken down when  $\lambda \neq 0$  to  $Z_4^e$  and  $Z_4^m$ . Further,  $w \neq 0$  indicates short-range interaction between the  $e$  and  $m$  soft modes as expected, say, from Eq. 7.2. Both these terms receive contributions from various terms in the perturbation theory and as such these coupling constants can be both positive or negative. For  $w \neq 0$  the symmetry is broken down further to  $Z_4$ . We note that, in principle, the  $\lambda$  term can be generated from the  $w$  term at the second order level due to the integration of high energy modes with  $\lambda \sim w^2/u > 0$ , but we keep both these symmetry-allowed terms as independent for our discussion.

### The phases

The critical theory clearly captures the two phases as expected. At the mean-field level, for  $u > 0$ , we have

$$\langle \Phi_e \rangle = \langle \Phi_m \rangle = 0 \tag{7.25}$$

Therefore both of them can be integrated out and the low energy effective theory is given by  $\mathcal{S}_{CS}$  (Eq. 7.18) which is the  $Z_2$  QSL with the right low energy spectrum consisting of the gapped electric and magnetic charges and a four-fold ground state degeneracy in the thermodynamic limit on a two-tori.[41, 75]

For  $u < 0$  both the electric and magnetic modes condense, *i.e.*,

$$\langle \Phi_e \rangle, \langle \Phi_m \rangle \neq 0 \quad (7.26)$$

Therefore both  $A_\mu$  and  $B_\mu$  gauge fields acquire mass through the Anderson-Higgs mechanism and hence their dynamics can be dropped. To understand the nature of this phase we note that the fourfold terms in Eqs. 7.22 and 7.23 becomes (using Eqs. 7.13 and 7.14)

$$\sim -\lambda (|\Phi_e|^4 \cos(4\theta_e) + |\Phi_m|^4 \cos(4\theta_m)) \quad (7.27)$$

Therefore, for  $\lambda > 0$  the free energy minima occurs for

$$\theta_e, \theta_m = 0, \pm\pi/2, \pi \quad (7.28)$$

which gives the two possible symmetry broken partner spin ordered states as is now evident from Eq. 7.16 with the spin order parameters being :

$$\begin{aligned} \langle \tilde{\tau}_i^z \rangle &\sim \langle |\Phi_e|^2 \cos(2\theta_e) \rangle \sim \pm 1 \quad \forall i \in \text{Horizontal bonds} \\ \langle \tilde{\tau}_i^x \rangle &\sim \langle |\Phi_m|^2 \cos(2\theta_m) \rangle \sim \pm 1 \quad \forall i \in \text{Vertical bonds} \end{aligned} \quad (7.29)$$

Further the state also breaks  $\sigma_v$  and  $C_{2z}$ . Note that the order parameter is indeed invariant under the  $Z_2$  gauge transformations and individual gauge charges are absent in the low energy spectrum in the spin-ordered phases due to the mutual CS term.

In this phase, the interaction between the electric and the magnetic modes (Eq. 7.24) can be written as

$$\mathcal{L}_{em} \sim w |\Phi_e|^2 |\Phi_m|^2 \cos(2\theta_e) \cos(2\theta_m) \quad (7.30)$$

For  $w < 0 (> 0)$ , this results in ferromagnetic (antiferromagnetic) spin ordering in terms of  $\tilde{\tau}^x$  (on horizontal bonds) and  $\tilde{\tau}^z$  (on the vertical bonds) giving rise to the two states shown in Fig. 3.2. The latter choice also breaks translation symmetry under  $\mathbf{T}_{d_1}$  and  $\mathbf{T}_{d_2}$  which interchanges a vertical and horizontal bond. The above phenomenology matches with the underlying microscopics for  $w \sim J$ . Therefore the above critical theory indeed reproduces the right phases.

It is interesting to note that for  $\lambda < 0$ , Eq. 7.27 shows that the free energy is minimised for

$$\theta_e, \theta_m = \pm\pi/4, \pm 3\pi/4 \quad (7.31)$$

It is easy to see that this phase is time-reversal symmetric. However, note that in such a state the order parameters

$$\langle |\Phi_e|^2 \sin(2\theta_e) \rangle, \langle |\Phi_m|^2 \sin(2\theta_m) \rangle \quad (7.32)$$

are non-zero. These order parameters however break translation symmetry in the horizontal direction,  $\mathbf{T}_x$ , and possibly represent some type of bond nematic state. However, for the type of microscopic model that we are concerned with– as our numerical calculations suggest– this bond nematic is not relevant and hence we shall not pursue it further.

### The critical point

We now turn to the critical point. It is useful to start by neglecting the anisotropic terms in the critical theory described by Eq. 7.21 by putting  $\lambda = w = 0$ . The critical action can then be written as

$$\mathcal{S} = \int d^2\mathbf{r}d\tau [\mathcal{L}_e + \mathcal{L}_m] + \mathcal{S}_{CS} \quad (7.33)$$

where in this limit

$$\mathcal{L}_e = |(\partial_\mu - iA_\mu)\Phi_e|^2 + u|\Phi_e|^2 + v|\Phi_e|^4 \quad (7.34)$$

$$\mathcal{L}_m = |(\partial_\mu - iB_\mu)\Phi_m|^2 + u|\Phi_m|^2 + v|\Phi_m|^4 \quad (7.35)$$

and  $\mathcal{S}_{CS}$  given by Eq. 7.18.

This class of mutual  $U(1) \times U(1)$  CS theories has been described in a number of different contexts.[41, 75, 116, 118] Most pertinent to our discussion is Ref. [75] where such theories were considered in the context of transitions out of a  $Z_2$  QSL– similar to the present case. However, there, in absence of the anyon-permutation symmetry that leads to a constraint on the masses as given in Eq. 7.37, the above class of transitions in that case turns out to be fine-tuned and in general separated by an intermediate  $e$ -Higgs or  $m$ -Higgs phase each characterized by

a distinct spontaneously broken symmetry. Hence the anyon-permutation symmetry due to the microscopic symmetry  $\mathbb{T}_{d_1(2)}$  (Eqs. 6.8 and 7.15) is crucial to protect the above critical point facilitating the direct phase transition in the present case.

Ref. [118] studied the lattice version of the above model for generic values of the coupling parameters including the self-dual line which is directly relevant to us. Along the self-dual line, it was found[118] the  $Z_2$  QSL phase gives way to a line of first-order transitions (separating the  $e$  and  $m$  condensates– not applicable to our work) before it leads to a  $e - m$  condensed phase which is characterized exactly through the order parameters as we find here (Eq. 7.16). The meaning of the line of first-order phase transition along the self-dual line is not clear in the present context since our severely system size limited numerics did not find any signature of it.

To gain complementary insights into the critical theory, it is useful to apply particle-vortex duality[119, 120] for bosons in  $(2 + 1)$  dimensions to either the  $e$  (in Eq. 7.34) or  $m$  (in Eq. 7.35) sector. Let us choose to dualise the  $m$  sector to get the dual of Eq. 7.35,

$$\mathcal{L}_m^D = |(\partial_\mu - ib_\mu)\Phi_m^D|^2 + u_D|\Phi_m^D|^2 + v_D|\Phi_m^D|^4 + \frac{i}{2\pi}\epsilon^{\mu\nu\lambda}b_\mu\partial_\nu B_\lambda \quad (7.36)$$

where  $\Phi_m^D$  is dual to the  $m$  soft mode,  $\Phi_m$  which is coupled to the internal gauge field  $b_\mu$ . In other words,  $\Phi_m^D$  is the vortex of the  $m$  field,  $\Phi_m$ .  $u_D$  and  $v_D$  are the respective couplings. It is clear that when the  $m$ -vortex condenses, *i.e.*,  $\langle\Phi_m^D\rangle \neq 0$ , then the  $m$ -charge,  $\Phi_m$ , is gapped, *i.e.*  $\langle\Phi_m\rangle = 0$ , and vice versa. Therefore on general grounds, we expect that at low energies, the dual couplings are given by

$$u_D = -\kappa u \quad v_D = \eta v \quad (7.37)$$

where  $\kappa, \eta > 0$  are proportionality constants and  $u, v$  are the coupling constants of the original theory of Eq. 7.35. This ensures that the  $m$ -vortex vacuum is mapped to the  $m$ -charge condensate and vice-versa. From Eq. 7.62 and 7.36 we can now integrate out  $B_\mu$  to get

$$b_\mu + 2A_\mu = 0 \quad (7.38)$$

which when put back into Eq. 7.36, gives

$$\mathcal{L}_m^D = |(\partial_\mu + i2A_\mu)\Phi_m^D|^2 - \kappa u|\Phi_m^D|^2 + \eta v|\Phi_m^D|^4 \quad (7.39)$$

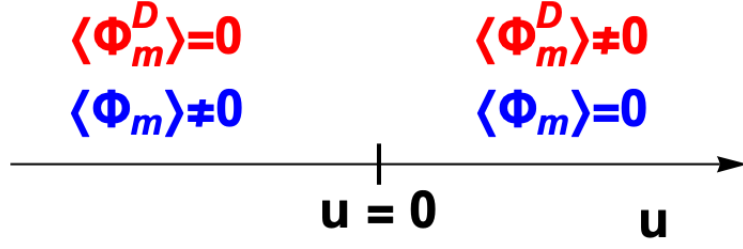


Figure 7.2: The phase diagram corresponding to the critical Lagrangian,  $\mathcal{L}_c$  in Eq. 7.41. At the mean-field level, the bare  $u = 0$  corresponds to the synchronized *condensing* and *gapping out* of  $\Phi_m^D$  and  $\Phi_e$  respectively as shown. While, this may appear fine-tuned, as explained in the text, the above picture is indeed generic and is protected by symmetry.

The critical action is now given by

$$\mathcal{S} = \int d^2\mathbf{r}d\tau \mathcal{L}_c \quad (7.40)$$

where

$$\begin{aligned} \mathcal{L}_c = & |(\partial_\mu - iA_\mu)\Phi_e|^2 + |(\partial_\mu + i2A_\mu)\Phi_m^D|^2 \\ & + u(|\Phi_e|^2 - \kappa|\Phi_m^D|^2) + v(|\Phi_e|^4 + \eta|\Phi_m^D|^4) + g(\epsilon^{\mu\nu\lambda}\partial_\nu A_\lambda)^2 \end{aligned} \quad (7.41)$$

where we have now explicitly written the Maxwell term for  $A_\mu$  with coupling constant  $g(> 0)$  in absence of any CS term. The resultant phase diagram is shown in Eq. 7.2 where  $\Phi_e$  ( $\Phi_m^D$ ) are condensed for  $u < 0$  ( $> 0$ ) with  $u = 0$  being the critical point where, as an increasing function of  $u$  across  $u = 0$  lead to simultaneous *condensation* and *un-condensation* (gapping out) of  $\Phi_m^D$  and  $\Phi_e$  respectively. Clearly, this is true irrespective of the renormalization of the bare mass-scale,  $u$ , and is not fine-tuned.

The  $\langle \Phi_m^D \rangle \neq 0$  phase represents the QSL where both the  $e$  and  $m$  charges are gapped. However due to the fact that  $\Phi_m^D$  carries charge-2 of the  $U(1)$  gauge field  $A_\mu$ , on condensing  $\Phi_m^D$  the gauge group is reduced to  $Z_2$  as is appropriate for the  $Z_2$  QSL. In this phase, both  $\Phi_e$  and  $\Phi_m$  exist as gapped excitations. To uncover the mutual semionic statistics, we remind ourselves that  $\Phi_m$  corresponds to  $\pi$ -flux of  $A_\mu$  due to the mutual CS term (Eq. 7.18). In the Higgs phase of  $\Phi_m^D$ , such fluxes are gapped. However, once excited, the  $\Phi_e$  charges are sensitive to it by virtue of their minimal coupling to  $A_\mu$  as given by Eq. 7.41. This description of the  $Z_2$  QSL is quite similar to that obtained by disordering a superconductor through condensation of *charge-2* vortices.[107, 114] Indeed in the present case all the *even* charges of  $A_\mu$  are condensed while the *odd* charges are gapped out which is equivalent to the conservation of the  $e$  and  $m$  charges

modulo 2— as expected in a  $Z_2$  QSL. The above description of the  $Z_2$  QSL remains unchanged even in the presence of the anisotropy terms in Eq. 7.21.

The spin-ordered state, on the other hand, is obtained for  $u < 0$  when both  $\Phi_e$  and  $\Phi_m$  (and hence  $\Phi_m^D$  is gapped) are condensed as we described earlier. The photon of  $A_\mu$  acquires a gap by the Anderson-Higgs mechanism. Indeed all odd charges of  $A_\mu$  are condensed in this spin-ordered phase. We, of course, could have performed the particle-vortex duality in the  $e$  sector in Eq. 7.34 to obtain an equivalent critical theory in terms of the  $m$  charges,  $\Phi_m$  and  $e$  vortices,  $\Phi_e^D$ . In particular, we get

$$\begin{aligned} \mathcal{L}_c^{\text{Dual}} = & |(\partial_\mu - iB_\mu)\Phi_m|^2 + |(\partial_\mu + i2B_\mu)\Phi_e^D|^2 \\ & + u(|\Phi_m|^2 - \kappa|\Phi_e^D|^2) + v(|\Phi_m|^4 + \eta|\Phi_e^D|^4) + g(\epsilon^{\mu\nu\lambda}\partial_\nu B_\lambda)^2 \end{aligned} \quad (7.42)$$

which is same as Eq. 7.41 once we identify the following mapping :

$$(\Phi_e, \Phi_m^D, A_\mu) \Leftrightarrow (\Phi_m, \Phi_e^D, B_\mu) \quad (7.43)$$

which shows that the critical theory is self-dual.[121]

Turning to the anisotropy terms in the critical action in Eq. 7.21 by considering  $\lambda, w \neq 0$  in Eqs. 7.22-7.24. Due to the symmetry under  $\mathbf{T}_{\mathbf{d}_{1(2)}}$ , we expect that the scaling dimension of the  $\Phi_e$  and  $\Phi_m$  are equal at the critical point. Hence, in order to judge the relevance of these quartic terms, for our formulation (Eq. 7.41), it is easiest to start with the  $(\Phi_m)^4$  term. From Eq. 7.36 and 7.38, that the current of  $\Phi_m$  is related to the flux of  $A_\mu$  as

$$j_m^\mu = \frac{1}{2\pi}\epsilon^{\mu\nu\lambda}\partial_\nu b_\lambda = -\frac{1}{\pi}\epsilon^{\mu\nu\lambda}\partial_\nu A_\lambda. \quad (7.44)$$

The anisotropic term breaks the  $O(2)$  symmetry of the  $m$  sector in Eq. 7.41 down to  $Z_4$  since four  $\Phi_m$  charges can be created/annihilated. Each such charge being proportional to  $\pi$  flux of  $A_\mu$  the  $(\Phi_m)^4$  term therefore corresponds to the *doubled monopole operator*[122] of  $A_\mu$ . For an Abelian Higgs model for a superconductor, such doubled monopoles may be irrelevant in a parameter regime[123] raising hope that the present transition may indeed be controlled by the  $\lambda = w = 0$ . However, the critical theory needs to be studied in further detail to settle this issue.

The critical point described by  $u = 0$  involving the simultaneous condensation and gapping out of the even and odd charges of  $A_\mu$  respectively and the gauge flux of  $A_\mu$  being conserved is novel and is expected to be different from the transition in Abelian Higgs model[120] on one hand and the transition in the dual Abelian Higgs model describing the condensation of paired vortices[107, 114] on the other.

The critical theory (Eq. 7.40) therefore suggests that the deconfined quantum phase transition between the  $Z_2$  QSL and the magnetically ordered phase is described by a modified self-dual modified Abelian Higgs model (MAHM) with conserved flux. In absence of the mutual CS term, the critical action in Eq. 7.20 describes an easy-plane non-compact projective field theory (easy-plane NCCP<sup>1</sup>) studied in Ref. [121] while the one with the mutual CS term was studied in Ref. [118]. In the second study— as mentioned before— it was found that the  $QSL$  and the  $e - m$  condensate phases are separated by a line of first-order transition along the self-dual line. The relevance of this line is not clear in the present context. Hence, at present, it is not clear to us whether the present self-dual modified Abelian Higgs model belongs to the same universality class at easy-plane NCCP<sup>1</sup>.

The transition, therefore, is an example of a deconfined quantum critical point.[5] The critical theory is not written in terms of the order parameters but the low energy degrees of freedom of the  $Z_2$  QSL. Characteristic of deconfined critical points, the spin order parameter is bilinear in terms of the critical field— the gauge charges. Therefore we expect a large anomalous dimension for the order parameter which naively should be twice that of the critical field. [121] The above critical theory is expected to be stable in presence of small  $\Gamma$  as it does not add any new symmetry-allowed terms to the critical theory at the lowest order, thus resulting in the phase diagram as shown in Fig. 3.1 for small  $\Gamma$ .

### 7.1.2 Effect of an external Zeeman field

So far we have neglected the experimentally relevant possibility of turning on an external magnetic field (we refer to it as a Zeeman field to avoid confusion) on Eq. 1.1 in the anisotropic limit. This perturbation in the isotropic limit is given by

$$H_{\text{Zeeman}}^{FM} = - \sum_i \mathbf{h} \cdot \boldsymbol{\sigma}_i \quad (7.45)$$

for the spins,  $\sigma_i^\alpha$  on the sites of the honeycomb lattice, where  $\mathbf{h} = (h_x, h_y, h_z)$  is the external

Zeeman field. In the anisotropic limit ( $|\mathbf{h}|/K_z$ ) that we are concerned with, the degenerate perturbation theory (Eq. 2.9) gives rise to the following addition in the leading order of  $\mathbf{h}$  to Eq. 2.13:

$$\mathcal{H}_z^{FM} = -2h_z \sum_i \tau_i^z \quad (7.46)$$

for the  $\tau$ -spins on the  $z$ -bond in the unrotated basis. This is clearly in agreement with the fact that  $\tau_i^z$  is the time reversal odd component of the non-Kramers doublet (Eq. 2.11). In the rotated basis (Eq. 3.2) becomes

$$\tilde{H}_z^{FM} = -2h_z \left[ \sum_{i \in H} \tilde{\tau}_i^z + \sum_{i \in V} \tilde{\tau}_i^x \right] \quad (7.47)$$

where the first sum is over the horizontal bonds and the second sum is over the vertical bonds. There are higher order terms in the above Zeeman field including cross terms involving the other perturbing terms in  $\mathcal{V}^{FM}$  of Eq. 2.1. We neglect the detailed structure of these higher-order time-reversal symmetry-breaking terms. Notice that the structure of the above term is “opposite” to that of the leading order pseudo-dipolar term given by Eq. 3.9 with a crucial difference that unlike Eq. 3.9, the present term in Eq. 7.47 is time reversal odd since the Zeeman field breaks the time-reversal symmetry. We explore this relationship between the Zeeman and the pseudo-dipolar perturbations in the next section in the context of the latter.

In terms of the gauge theory, Eq. 7.47 becomes

$$\begin{aligned} \tilde{\mathcal{H}}_z^{FM} = & -2h_z \sum_a \mu_a^x \rho_{a,a+\hat{x}}^z \mu_{a+\hat{x}}^x - J_{TC} \sum_a \mu_a^z \\ & - 2h_z \sum_{\bar{a}} \tilde{\mu}_{\bar{a}}^x \tilde{\rho}_{\bar{a},\bar{a}+\hat{x}}^x \tilde{\mu}_{\bar{a}+\hat{x}}^x - J_{TC} \sum_{\bar{a}} \tilde{\mu}_{\bar{a}}^z \end{aligned} \quad (7.48)$$

This, therefore, leads to the dispersion of the  $e$  and  $m$  charges along the horizontal direction which renormalizes the results of Eq. 7.4 and 7.6 for the  $e$  and  $m$  sectors respectively.

Crucially, however, it lifts the degeneracy of the two time-reversal partner soft modes in Eq. 7.11 and 7.12. This allows the following term in addition to the ones already in the soft mode critical action in Eq. 7.20

$$\mathcal{S}_z = \int d^x d\tau \mathcal{L}_z \quad (7.49)$$

where,

$$\begin{aligned}\mathcal{L}_z &= -\tilde{h} [(\Phi_e)^2 + (\Phi_e^*)^2 + (\Phi_m)^2 + (\Phi_m^*)^2] \\ &= -2\tilde{h} [|\Phi_e|^2 \cos(2\theta_e) + |\Phi_m|^2 \cos(2\theta_m)]\end{aligned}\tag{7.50}$$

with  $\tilde{h} \propto h_z$ . This clearly lifts the degeneracy between the two time-reversal invariant spin states. In presence of this second order term ( $\propto \cos 2\theta$ ), the fourth order  $Z_4$  anisotropy terms (proportional to  $\lambda \cos 4\theta$ ) in Eq. 7.22 and 7.23 can be neglected.

The  $Z_2$  QSL remains unchanged for  $u - \tilde{h} > 0$ . However, for  $u - \tilde{h} < 0$ , inside the spin-ordered phase, for  $\tilde{h} > 0 (< 0)$ , we have

$$\theta_e, \theta_m = 0, \pi(\pm\pi/2)\tag{7.51}$$

which is nothing but the polarised phase. This is indeed true for  $w < 0$  in the  $e-m$  coupling term in Eq. 7.24 or equivalently Eq. 7.85 where the  $\tilde{h} = 0$  state is a ferromagnet. However, for  $w > 0$ , where the  $\tilde{h} = 0$  ground state is antiferromagnetic, we expect a first-order spin-flop transition from the antiferromagnet to a polarised phase within the spin-ordered phase.

The critical point is given for  $u - \tilde{h} = 0$ . It turns out that for  $J < 0$ , this critical point is similar to that obtained by destabilizing the  $Z_2$  QSL using the pseudo-dipolar interactions,  $\Gamma$ . Hence to avoid repetition, we first develop the soft modes of the pseudo-dipolar limit and then return to discuss the critical point for both the Zeeman and the pseudo-dipolar limits together.

### 7.1.3 Phase Transition between QSL and the trivial paramagnet

Having understood the transition to the spin-ordered phase from the QSL in section 7.1.1 we now turn to the transition between the QSL and the trivial paramagnet accessed by tuning the  $\Gamma$  term (horizontal axis of the Fig. 3.1). Again a controlled description of the phase transition is achieved by starting with the QSL and understanding the fate of its excitations– the gauge charges. The effect of the Zeeman field– the topic of the last subsection– sheds crucial insight into this transition. This becomes even more clear by comparing the leading order perturbations due to the  $h_z$  (Eq. 7.47) and  $\Gamma$  (Eq. 3.9). It is clear that the reflection about the  $x = y$  line of the square lattice in Fig. 1.1 and passing through the sites maps all the vertical bonds to horizontal bonds and vice versa and thereby mapping Eq. 7.47 to Eq. 3.9 when we perform a concomitant transformation of  $h_z \rightarrow -\Gamma$ . We note that under the above reflection the Toric

code Hamiltonian (Eq. 3.3) remains unchanged. However, now the  $\tilde{\tau}^x(\tilde{\tau}^z)$  on the horizontal (vertical) bonds are time-reversal odd. This is in accordance with our previous observation that Eq. 3.9 is time-reversal even. As a consequence, a trivial time-reversal symmetric paramagnet is realized due to the pseudo-dipolar perturbations,  $\Gamma$ .

### Decoupled vertical Ising chains

Similar to the case of Heisenberg interactions, we first incorporate the leading order perturbation in  $\Gamma$  given by Eq. 3.9 to the QSL Hamiltonian in Eq. 3.3 in the rotated basis. In terms of the gauge fields and the gauge charges, this becomes

$$\begin{aligned} \tilde{\mathcal{H}}_{J=0}^{FM} = & 2\Gamma \sum_a \mu_a^x \rho_{a,a+\hat{y}}^z \mu_{a+\hat{y}}^x - J_{TC} \sum_a \mu_a^z \\ & + 2\Gamma \sum_{\bar{a}} \tilde{\mu}_{\bar{a}}^x \tilde{\rho}_{\bar{a},\bar{a}+\hat{y}}^x \tilde{\mu}_{\bar{a}+\hat{y}}^x - J_{TC} \sum_{\bar{a}} \tilde{\mu}_{\bar{a}}^z \end{aligned} \quad (7.52)$$

Contrast this with the effect of the Zeeman field given in Eq. 7.48. Here, evidently, the first (second) line denotes a series of now decoupled *vertical*, with respect to Fig. 1.1, transverse field Ising chains[124] representing the  $e(m)$  charges as opposed to the horizontal ones in Eq. 7.48. This can alternatively be looked up as a consequence of the  $x = y$  reflections discussed above which converts the horizontal chains to vertical chains. This leads to important differences, particularly regarding the nature of the phase that the QSL transits into due to the non-trivial projective implementation of the time-reversal symmetry (Eq. 6.10).

Similar to Eq. 7.8, we can choose the gauge

$$\rho_{a,a+\hat{y}}^z = \tilde{\rho}_{a,a+\hat{y}}^z = +1 \quad (7.53)$$

as these links do not cross. Thus we get, from Eq. 7.52

$$\tilde{\mathcal{H}}_{J=0} = 2\Gamma \sum_a \mu_a^x \mu_{a+\hat{y}}^x - J_{TC} \sum_a \mu_a^z + 2\Gamma \sum_{\bar{a}} \tilde{\mu}_{\bar{a}}^x \tilde{\mu}_{\bar{a}+\hat{y}}^x - J_{TC} \sum_{\bar{a}} \tilde{\mu}_{\bar{a}}^z \quad (7.54)$$

The paramagnetic phase of each vertical chain– both for  $e$  and  $m$  sectors– for  $\Gamma = 0$  is clearly the  $Z_2$  QSL. On increasing  $\Gamma$ , the electric and the magnetic charges now develop dispersions along the vertical direction and when the minima of such dispersion hits zero they condense destroying the QSL.

For  $\Gamma < 0(> 0)$  the soft mode for  $e$  and  $m$  sectors are given by a charge arrangement similar

to Fig. 7.1(a) (7.1(b)). However, very crucially, unlike the Heisenberg case of the previous section 7.1.1, these two soft modes are not degenerate because they are not time-reversal partners as is evident from Eq. 6.10. This will become more evident below. Anticipating the difference, we, therefore, denote these two soft modes as

$$\hat{\xi}_e^{(1)} = 1 \quad \hat{\xi}_e^{(2)} = e^{i\pi x} \quad (7.55)$$

for the  $e$  sector on the direct lattice and

$$\hat{\xi}_m^{(1)} = 1 \quad \hat{\xi}_m^{(2)} = e^{i\pi X} \quad (7.56)$$

for the  $m$  sector on the dual lattice.

Indeed, as discussed above, for a given choice of  $\Gamma$  the two states have different energies and hence we can completely work with one of the soft modes for each sign of  $\Gamma$ . This becomes more evident in the PSG analysis of the soft modes (see below) where we see that the two soft modes do not mix with each other under symmetry transformations. This, to draw a further analogy with the Zeeman perturbation, is like the lifting of the degeneracy of the two soft modes, of Eqs. 7.11 and 7.12, as discussed below Eq. 7.48. There, the existence of the time reversal symmetric point  $h_z = 0$  allows us to use a theory with two soft modes each in the  $e$  and  $m$  sector which is subsequently broken down further by the Zeeman field through Eq. 7.50 in the critical theory.

Similarly, we define a hypothetical  $\Gamma = 0$  situation where both these modes are degenerate as our starting point and then use a redundant description keeping both the soft modes and obtain the correct description for the phases and phase transition. We note that unlike in the Zeeman case, this hypothetical situation is not realized in our model and indeed is actually an unstable quantum ground state with  $\ln 2$  entropy per site as this does not break any symmetry of the anisotropic Hamiltonian. In the passing, we note that the soft modes result in two distinct nematic states as given in Eq. 7.50 and hence may be relevant to the isotropic/near isotropic limit of Eq. 1.1. However, here we use this limit only as a convenient starting point for our analysis of the critical theory.

### **Soft modes**

Similar to Eq. 7.11 and 7.12, we expand the gauge charges in terms of the soft modes. This

gives

$$\Psi_e(\mathbf{r}, \tau) = \tilde{\phi}_e^{(1)}(\mathbf{r}, \tau) \hat{\xi}_e^{(1)} + \tilde{\phi}_e^{(2)}(\mathbf{r}, \tau) \hat{\xi}_e^{(2)} \quad (7.57)$$

for the  $e$  sector and

$$\Psi_m(\mathbf{r}, \tau) = \tilde{\phi}_m^{(1)}(\mathbf{r}, \tau) \hat{\xi}_m^{(1)} + \tilde{\phi}_m^{(2)}(\mathbf{r}, \tau) \hat{\xi}_m^{(2)} \quad (7.58)$$

for the  $m$  sector. Here  $(\tilde{\phi}_e^{(1)}, \tilde{\phi}_e^{(2)})$  and  $(\tilde{\phi}_m^{(1)}, \tilde{\phi}_m^{(2)})$  are the new  $e(m)$  soft mode amplitudes. In order to obtain the PSG transformations we once again combine the two amplitudes of each sector as

$$\tilde{\Phi}_e = \tilde{\phi}_e^{(1)} + i\tilde{\phi}_e^{(2)} = |\tilde{\Phi}_e|e^{i\tilde{\theta}_e} \quad (7.59)$$

and

$$\tilde{\Phi}_m = \tilde{\phi}_m^{(1)} + i\tilde{\phi}_m^{(2)} = |\tilde{\Phi}_m|e^{i\tilde{\theta}_m} \quad (7.60)$$

The PSG transformations under different symmetries listed in Eqs. 6.8-6.13 are now given by

$$\begin{aligned} \mathbf{T}_{\mathbf{d}_1} : & \begin{cases} \tilde{\Phi}_e \rightarrow \tilde{\Phi}_m \\ \tilde{\Phi}_m \rightarrow \tilde{\Phi}_e^* \end{cases} & \mathbf{T}_{\mathbf{d}_2} : & \begin{cases} \tilde{\Phi}_e \rightarrow \tilde{\Phi}_m^* \\ \tilde{\Phi}_m \rightarrow \tilde{\Phi}_e \end{cases} \\ \mathbf{T}_x : & \begin{cases} \tilde{\Phi}_e \rightarrow \tilde{\Phi}_e^* \\ \tilde{\Phi}_m \rightarrow \tilde{\Phi}_m^* \end{cases} & \mathbf{T}_y : & \begin{cases} \tilde{\Phi}_e \rightarrow \tilde{\Phi}_e \\ \tilde{\Phi}_m \rightarrow \tilde{\Phi}_m \end{cases} \\ \mathcal{T} : & \begin{cases} \tilde{\Phi}_e \rightarrow \tilde{\Phi}_e^* \\ \tilde{\Phi}_m \rightarrow \tilde{\Phi}_m^* \end{cases} & \sigma_v : & \begin{cases} \tilde{\Phi}_e \rightarrow \tilde{\Phi}_e \\ \tilde{\Phi}_m \rightarrow \tilde{\Phi}_m \end{cases} \\ C_{2z} : & \begin{cases} \tilde{\Phi}_e \rightarrow \tilde{\Phi}_e \\ \tilde{\Phi}_m \rightarrow \tilde{\Phi}_m^* \end{cases} & R_\pi : & \begin{cases} \tilde{\Phi}_e \rightarrow \tilde{\Phi}_e \\ \tilde{\Phi}_m \rightarrow \tilde{\Phi}_m^* \end{cases} \end{aligned} \quad (7.61)$$

We shall find the Higgs phase resulting from condensing the above charges results in a trivial paramagnet.

### The mutual $U(1) \times U(1)$ CS critical theory

Using a redundant description by keeping both the soft modes in each of the electric and magnetic sectors allows us to extend the  $U(1) \times U(1)$  mutual CS formalism for this transition. In this case, the CS action is given by

$$\tilde{\mathcal{S}}_{CS} = \frac{i}{\pi} \int d^2\mathbf{r}d\tau \epsilon^{\mu\nu\lambda} \tilde{A}_\mu \partial_\nu \tilde{B}_\lambda \quad (7.62)$$

where now  $\tilde{A}_\mu$  and  $\tilde{B}_\mu$  are the internal  $U(1)$  gauge fields that couple minimally to the soft modes  $\tilde{\Phi}_e$  and  $\tilde{\Phi}_m$  respectively. The PSG of the gauge fields are given by

$$\begin{aligned} \mathbf{T}_{\mathbf{d}_1} : & \begin{cases} \tilde{A}_\mu \rightarrow \tilde{B}_\mu \\ \tilde{B}_\mu \rightarrow -\tilde{A}_\mu \end{cases} & \mathbf{T}_{\mathbf{d}_2} : & \begin{cases} \tilde{A}_\mu \rightarrow -\tilde{B}_\mu \\ \tilde{B}_\mu \rightarrow \tilde{A}_\mu \end{cases} \\ \mathbf{T}_{\mathbf{x}} : & \begin{cases} \tilde{A}_\mu \rightarrow -\tilde{A}_\mu \\ \tilde{B}_\mu \rightarrow -\tilde{B}_\mu \end{cases} & \mathbf{T}_{\mathbf{y}} : & \begin{cases} \tilde{A}_\mu \rightarrow \tilde{A}_\mu \\ \tilde{B}_\mu \rightarrow \tilde{B}_\mu \end{cases} \\ \mathcal{T} : & \begin{cases} \tilde{A}_\mu \rightarrow \tilde{A}_\mu \\ \tilde{B}_\mu \rightarrow \tilde{B}_\mu \end{cases} & & \\ \sigma_v : & \begin{cases} \tilde{A}_x \rightarrow \tilde{A}_x, \tilde{A}_y \rightarrow -\tilde{A}_y, \tilde{A}_\tau \rightarrow \tilde{A}_\tau \\ \tilde{B}_x \rightarrow \tilde{B}_x, \tilde{B}_y \rightarrow -\tilde{B}_y, \tilde{B}_\tau \rightarrow \tilde{B}_\tau \end{cases} & & \\ C_{2z} : & \begin{cases} \tilde{A}_x \rightarrow -\tilde{A}_x, \tilde{A}_y \rightarrow \tilde{A}_y, \tilde{A}_\tau \rightarrow \tilde{A}_\tau \\ \tilde{B}_x \rightarrow \tilde{B}_x, \tilde{B}_y \rightarrow -\tilde{B}_y, \tilde{B}_\tau \rightarrow -\tilde{B}_\tau \end{cases} & & \\ R_\pi : & \begin{cases} \tilde{A}_x \rightarrow -\tilde{A}_x, \tilde{A}_y \rightarrow -\tilde{A}_y, \tilde{A}_\tau \rightarrow \tilde{A}_\tau \\ \tilde{B}_x \rightarrow \tilde{B}_x, \tilde{B}_y \rightarrow \tilde{B}_y, \tilde{B}_\tau \rightarrow -\tilde{B}_\tau \end{cases} & & \end{aligned} \quad (7.63)$$

which are consistent with the CS action in Eq. 7.62 as before up to in inconsequential sign change under  $C_{2z}$ . The resultant critical field theory is

$$\tilde{\mathcal{S}}_c = \int d^2\mathbf{r}d\tau \mathcal{L} + \tilde{\mathcal{S}}_{CS} \quad (7.64)$$

where  $\tilde{\mathcal{S}}_{CS}$  is given by Eq. 7.62 and

$$\tilde{\mathcal{L}} = \tilde{\mathcal{L}}_e + \tilde{\mathcal{L}}_m + \tilde{\mathcal{L}}_{em} \quad (7.65)$$

with

$$\tilde{\mathcal{L}}_e = |(\partial_\mu - i\tilde{A}_\mu)\tilde{\Phi}_e|^2 + \tilde{u}|\tilde{\Phi}_e|^2 + \tilde{v}|\tilde{\Phi}_e|^4 - \tilde{\lambda} \left[ (\tilde{\Phi}_e)^2 + (\tilde{\Phi}_e^*)^2 \right] \quad (7.66)$$

$$\tilde{\mathcal{L}}_m = |(\partial_\mu - i\tilde{B}_\mu)\tilde{\Phi}_m|^2 + \tilde{u}|\tilde{\Phi}_m|^2 + \tilde{v}|\tilde{\Phi}_m|^4 - \tilde{\lambda} \left[ (\tilde{\Phi}_m)^2 + (\tilde{\Phi}_m^*)^2 \right] \quad (7.67)$$

$$\tilde{\mathcal{L}}_{em} = \tilde{w} \left[ (\tilde{\Phi}_e \tilde{\Phi}_m)^2 + (\tilde{\Phi}_e \tilde{\Phi}_m^*)^2 + \text{c.c.} \right] \quad (7.68)$$

Considerations similar to those noted below Eq. 7.24 for the case of Heisenberg perturbations, also apply here with an important difference that in the present case, the decoupled limit pertains to vertical Ising chains. In particular the mass term,  $u \sim J_{TC} - 2\Gamma$ .

Note that due to the presence of the second-order anisotropic term proportional to  $\lambda$  in the critical action given by Eq. 7.64, the discussion of the phases and phase transitions has an exact parallel with the case of the Zeeman term (Eq. 7.49)— a consequence of the  $x = y$  reflection as discussed above— with the difference being, in the present case the condensation of the soft modes lead to a time-reversal symmetric paramagnet.

### The phases

Turning to the phases, clearly, as before, the un-condensed phase for  $\tilde{u} - \tilde{\lambda} > 0$ , *i.e.*,

$$\langle \tilde{\Phi}_e \rangle = \langle \tilde{\Phi}_m \rangle = 0 \quad (7.69)$$

is the  $Z_2$  QSL with gapped  $e$  and  $m$  charges with mutual semionic statistics. For  $\tilde{u} - \tilde{\lambda} < 0$ , the both electric and magnetic charges condense, *i.e.*

$$\langle \tilde{\Phi}_e \rangle, \langle \tilde{\Phi}_m \rangle \neq 0 \quad (7.70)$$

This Higgs phase does not break time-reversal symmetry. Indeed, in terms of symmetry, the  $Z_2$  gauge invariant fields are given by

$$\begin{aligned} \tilde{\Phi}_e^2 + (\tilde{\Phi}_e^*)^2 &\sim |\tilde{\Phi}_e|^2 \cos(2\tilde{\theta}_e) \sim \tilde{\tau}_i^x \quad \forall i \in \text{Horizontal bonds} \\ \tilde{\Phi}_m^2 + (\tilde{\Phi}_m^*)^2 &\sim |\tilde{\Phi}_m|^2 \cos(2\tilde{\theta}_m) \sim \tilde{\tau}_i^z \quad \forall i \in \text{Vertical bonds} \end{aligned} \quad (7.71)$$

These should be contrasted with Eq. 7.16 which characterizes spin ordering. In spite of similar appearances, the above equations are exactly opposite in terms of the type of the bonds (vertical versus horizontal) with respect to that of Eq. 7.16, and this has a central effect in the nature of the resultant phase which for the present case is a symmetric non-degenerate paramagnet.

For  $\tilde{\lambda} > 0 (< 0)$  in Eq. 7.66 and 7.67, the free energy is minimised for

$$\tilde{\theta}_e, \tilde{\theta}_m = 0, \pi(\pm\pi/2) \quad (7.72)$$

This corresponds to ordering (see Eq. 7.71)

$$\begin{aligned} \tilde{\tau}_i^x &= \pm 1 \quad \forall i \in \text{Horizontal bonds} \\ \tilde{\tau}_i^z &= \pm 1 \quad \forall i \in \text{Vertical bonds} \end{aligned} \quad (7.73)$$

all of which are time reversal symmetric (see Table. A.2 in Appendix A.1). For each of these cases, the interaction between the  $e$  and  $m$  modes is given by Eq. 7.85, *i.e.*

$$\tilde{\mathcal{L}}_{em} \sim w |\tilde{\Phi}_e|^2 |\tilde{\Phi}_m|^2 \cos(2\tilde{\theta}_e) \cos(2\tilde{\theta}_m) \quad (7.74)$$

For  $w < 0 (> 0)$  the spin components as given in Eq. 7.73 are parallel (antiparallel). The latter case breaks translation by  $\mathbf{T}_{d_1}$  and  $\mathbf{T}_{d_2}$  which interchanges horizontal and vertical bonds and appears to be not relevant for the present case. The above phenomenology is consistent with the microscopic of Section 3.1.3 for  $\tilde{\lambda} \sim -\Gamma$ . This then completes the discussion of the two trivial paramagnets as shown in Fig. 3.1. We expect the above theory to be stable to small Heisenberg perturbations,  $J$ .

### Effects of Zeeman term and the critical point

Before discussing the critical point, we would like to understand the effect of the Zeeman term in this pseudo-dipolar limit which would throw critical insight into the nature of the transition both in the Zeeman limit of subsection 7.1.2 and the present pseudo-dipolar limit. The starting point is the previously mentioned observation of the leading order Zeeman terms and pseudo-dipolar terms mapping into each other under  $x = y$  reflection. This becomes more clear when we consider the leading Zeeman perturbing term given by Eq. 7.47 along with the

leading pseudo-dipolar perturbation given by Eq. 3.9 whence the net leading perturbation is given by

$$\mathcal{H}_{\Gamma-z}^{FM} = \sum_{i \in V} [2\Gamma \tilde{\tau}_i^z - 2h_z \tilde{\tau}_i^x] + \sum_{i \in H} [2\Gamma \tilde{\tau}_i^x - 2h_z \tilde{\tau}_i^z] \quad (7.75)$$

In particular for the limit  $h_z = -\Gamma$  the above Hamiltonian becomes

$$\mathcal{H}_{\Gamma-z} = 2\Gamma \sum_i [\tilde{\tau}_i^x + \tilde{\tau}_i^z] \quad (7.76)$$

In conjunction with the Toric code term in Eq. 3.3, this is exactly the Hamiltonian studied in Refs. [125], [126] and [127] for a Toric code QSL in a “magnetic” field along the self-dual line. While this inference is drawn on the basis of the leading order perturbations, in the spirit of the discussions presented, it leads to interesting possibilities, particularly in the light of the rich properties of the self-dual line as known from very systematic numerical calculations.[125] We shall return to this in a moment, but first let us notice that in presence of the Zeeman field, from the symmetry transformations in Eq. 2.11, it is clear that the residual symmetry of the system is generated by only  $\mathbf{T}_{d_1}$ ,  $\mathbf{T}_{d_2}$  (and hence  $\mathbf{T}_x$ ,  $\mathbf{T}_y$ ) and  $R_\pi$ . This is the reason for the exact match between the transformation tables of the soft modes  $(\Phi_e, \Phi_m)$  (Eq. 7.15) and  $(A_\mu, B_\mu)$  (Eq. 7.17) with  $(\tilde{\Phi}_e, \tilde{\Phi}_m)$  (Eq. 7.61) and  $(\tilde{A}_\mu, \tilde{B}_\mu)$  (Eq. 7.63) under  $\mathbf{T}_{d_1}$ ,  $\mathbf{T}_{d_2}$  (and hence  $\mathbf{T}_x$ ,  $\mathbf{T}_y$ ) and  $R_\pi$ . Indeed, we can introduce the following linear superposition of the soft modes

$$\chi_e = \frac{1}{\sqrt{\Gamma^2 + h_z^2}} [\Gamma \tilde{\Phi}_e - h_z \Phi_e] \quad (7.77)$$

$$\chi_m = \frac{1}{\sqrt{\Gamma^2 + h_z^2}} [\Gamma \tilde{\Phi}_m - h_z \Phi_m] \quad (7.78)$$

and their corresponding gauge fields

$$C_\mu = \frac{1}{\sqrt{\Gamma^2 + h_z^2}} [\Gamma \tilde{A}_\mu - h_z A_\mu] \quad (7.79)$$

$$D_\mu = \frac{1}{\sqrt{\Gamma^2 + h_z^2}} [\Gamma \tilde{B}_\mu - h_z B_\mu] \quad (7.80)$$

for the perturbation corresponding to Eq. 7.75 which interpolates between the two limits  $\Gamma = 0$  and  $h_z = 0$ . The left-hand side of the above equation, by construction, has the same transformation property as the right hand side under  $\mathbf{T}_{d_1}$ ,  $\mathbf{T}_{d_2}$  (and hence  $\mathbf{T}_x$ ,  $\mathbf{T}_y$ ) and  $R_\pi$ . Clearly, at the special value  $h_z = -\Gamma$ , corresponding to Eq. 7.76 whence the system enjoys a

reflection symmetry to the leading order, stands for an equal superposition of the two sets of soft modes.

Hence following the symmetry arguments as before, we can write a critical action as

$$\mathcal{S}_c^x = \int d^2\mathbf{r} d\tau \mathcal{L}_c^x + \mathcal{S}_{CS}^x \quad (7.81)$$

where

$$\mathcal{S}_{CS}^x = \frac{i}{\pi} \int d^2\mathbf{r} d\tau \epsilon^{\mu\nu\lambda} C_\mu \partial_\nu D_\lambda \quad (7.82)$$

and

$$\mathcal{L}_c^x = \mathcal{L}_e^x + \mathcal{L}_m^x + \mathcal{L}_{em}^x \quad (7.83)$$

with

$$\begin{aligned} \mathcal{L}_e^x &= |(\partial_\mu - iC_\mu)\chi_e|^2 + \tilde{u}|\chi_e|^2 + \tilde{v}|\chi_e|^4 - \tilde{\lambda} [(\chi_e)^2 + (\chi_e^*)^2] \\ \mathcal{L}_m^x &= |(\partial_\mu - iD_\mu)\chi_m|^2 + \tilde{u}|\chi_m|^2 + \tilde{v}|\chi_m|^4 - \tilde{\lambda} [(\chi_m)^2 + (\chi_m^*)^2] \end{aligned} \quad (7.84)$$

and

$$\mathcal{L}_{em}^x = \tilde{w} [(\chi_e\chi_m)^2 + (\chi_e\chi_m^*)^2 + \text{c.c.}] \quad (7.85)$$

which clearly interpolates between the two limits in Eqs. 7.64 (for  $h_z = 0$ ) and 7.49 (for  $\Gamma = 0$ ).

The discussions of the  $Z_2$  QSL for  $\tilde{u} - \tilde{\lambda} > 0$  and the trivial paramagnet for  $\tilde{u} - \tilde{\lambda} < 0$  now directly follow from our previous discussions. Note that the trivial paramagnet continuously deforms from the polarised state (for  $\Gamma = 0$ ) to a time-reversal symmetric trivial paramagnet (for  $h_z \rightarrow 0^+$ ) with the  $h_z = 0$  line being the time-reversal symmetric paramagnet.

The two-fold anisotropy term proportional to  $\lambda$  is given by Eq. 7.84 carries charge-2 under  $C_\mu$  and  $D_\mu$  respectively. Therefore this is like the pairing term in superconductors, albeit for bosons which breaks down the gauge group from  $U(1)$  to  $Z_2$ . [106, 128] However, we note that in our case the  $Z_2$  theory is naturally tuned to be along the self-dual line due to the  $e \leftrightarrow m$  symmetry. Indeed a similar action was proposed in Ref. [116] for the transition to from the

$Z_2$  QSL to a trivial paramagnet in the context of Toric code models. However, due to the absence of the  $e \leftrightarrow m$  symmetry, the masses and other coupling constants of the  $e$  sector were different from that of the  $m$  sector and thereby away from the self-dual line.

In particular, Eq. 7.76 corresponds to the exact numerical calculations of Refs. [125] and [126] and series expansion techniques of Ref. [127]. In the light of our present discussion, it is certainly worthwhile to understand if the entire range from  $h_z = 0$  to  $\Gamma = 0$  is given by the same physics as this would indicate an extremely interesting mapping of the physics under Zeeman perturbations to that of the pseudo-dipolar interactions. Of course, this conclusion is tentative at this point as the above mapping is drawn on the basis of the effects of the leading order perturbations and the effects of the higher order terms need to be taken into account in any systematic numerical calculation.

Assuming that the physics of the self-dual line is relevant for the present discussion, we now ask what do we know about this line? From the point of view of  $Z_2$  gauge theory with dynamic electric and magnetic charges, the  $e$ -Higgs and the  $m$ -Higgs (confined) phases are smoothly connected [128] with both phase transition belonging to  $3D - Z_2$  universality class and meeting at a multicritical point which merges with a line of first order transition along the self-dual line ending in a critical point. Series expansion techniques of Ref. [127] show that along the self-dual line, the charge gap,  $\Delta$ , for both the  $e$  and  $m$  sectors vanishes as  $\Delta \sim |h_z - h_z^c|^{z\nu}$  where the critical value of the field is estimated to be  $h_z^c \approx 0.34$  (for  $J_{TC} = 1$ ) and the exponent,  $z\nu \approx 0.69 - 0.70$  [127, 129]—different from the  $3D - Z_2$  value,  $(z\nu)_{3D-Z_2} = 0.6301$ . The first-order transition, on the other hand ends at  $h_c^{1st} \approx 0.42$ . [126] The above picture is confirmed by Monte Carlo calculations. [125, 126, 130, 131]

We end this section with two more comments. First, away from the self-dual line when either  $e$  or  $m$  charges condense, neglecting the gauge fluctuations of  $A_\mu$  and  $B_\mu$  at the critical point on the grounds that the CS term makes the respective photons massive results in a transition correctly belonging to the  $3D - Z_2$  universality class. [116] A similar mean-field assumption would lead to  $3D - XY$  transition in the present case with  $(z\nu)_{3D-XY} \approx 0.67155$ . [132] Second, recent series expansion calculations [129] and tensor-network based wave-function analysis [133] has been suggested that perturbations on the self-dual line in the vicinity of the multicritical point can open up a gapless phase with power-law correlations for the  $e$  and  $m$  charges with continuously varying exponents. However, in our severely finite-size limited ED results, we did not find any signatures of such a phase. The relevance of this physics to the

anisotropic Kitaev model in a magnetic field as well as the higher order terms neglected in Eq. 7.47 remains to be understood.

This concludes our discussion of the phases and phase transitions for the ferromagnetic Kitaev-Heisenberg- $\Gamma$  model in the anisotropic limit in reference to the discussion in section 3.1.

## 7.2 Phase transition in AFM anisotropic Kitaev limit

In this section, we will study the phase transitions between phases discussed in section 3.2, while the schematic phase diagram pertaining to this section is shown in Fig. 3.9

Our numerical studies leading to the phase diagram of Fig. 5.5 show that the phase transitions out of the QSL are brought about by the condensation of the Ising electric and magnetic charges. We now build on the above observation to develop field theories for phase transitions.

### 7.2.1 Phase transition between QSL and the spin ordered phase

Along the  $\Gamma = 0$  line ( $t_1 = 0$  line in Fig. 5.5), there are two competing phases– the  $Z_2$  QSL for  $J \sim 0$  and the spin-ordered phase in the Heisenberg limit,  $J/|K| \gg 1$ . To understand the phase transition between them, it is convenient to start with the QSL and obtain the description of the transition in terms of the soft electric and magnetic modes similar to section 7.1.1, as a function of  $J$ , of its excitations– the  $e$  and  $m$  charges. To the leading order in  $J$ , the Hamiltonian is given by Eq. 3.14, where, we neglect the higher order terms in  $J$ . Since at large  $J$  (depending on the sign) the system goes into a ferromagnet or anti-ferromagnet state for  $\tau$ -spins we, for now, ignore the transverse field term and look at the effect of the Ising exchange term on the Toric code Hamiltonian. Please refer to the numerical analysis in the appendix E.2 for further comments on this approximation.

In terms of the gauge charges and fields (see section 6.1), the Hamiltonian in Eq. 2.19 in the limit  $\Gamma = 0$  becomes:

$$\tilde{\mathcal{H}}_{\Gamma=0}^{AFM} = -J \sum_{\langle ab \rangle \in H; \langle bc \rangle \in V} [\mu_a^x \rho_{ab}^z \mu_b^x] [\rho_{bc}^x] - J_{TC} \sum_a \mu_a^z - J_{TC} \sum_p \prod_{\langle ab \rangle \in p} \rho_{ab}^z \quad (7.86)$$

Where  $a, b, c$  are the square lattice vertices (see Fig 1.1). Similar to the FM case (section 7.1.1) we identify the soft modes within a gauge mean field analysis (also see Appendix E.2) appropriately modified to the present symmetry considerations. As in the ferromagnetic case

(section 7.1.1) (see Appendix E.3), we get two soft modes for each of electric and magnetic sectors [75, 108, 114]:

$$\Psi_e(\mathbf{r}, \tau) = \phi_e^{(1)}(\mathbf{r}, \tau) \hat{\nu}_e^{(1)} + \phi_e^{(2)}(\mathbf{r}, \tau) \hat{\nu}_e^{(2)} \quad (7.87)$$

$$\Psi_m(\mathbf{r}, \tau) = \phi_m^{(1)}(\mathbf{r}, \tau) \hat{\nu}_m^{(1)} + \phi_m^{(2)}(\mathbf{r}, \tau) \hat{\nu}_m^{(2)} \quad (7.88)$$

where  $(\phi_e^{(1)}(\mathbf{r}, \tau), \phi_e^{(2)}(\mathbf{r}, \tau))$  (and  $(\phi_m^{(1)}(\mathbf{r}, \tau), \phi_m^{(2)}(\mathbf{r}, \tau))$ ) are real fields that represent amplitudes of the electric (magnetic) soft modes. Defining complex variables

$$\Phi_e = \phi_e^{(1)} + i\phi_e^{(2)} = |\Phi_e|e^{i\theta^e} \quad (7.89)$$

and

$$\Phi_m = \phi_m^{(1)} + i\phi_m^{(2)} = |\Phi_m|e^{i\theta^m} \quad (7.90)$$

provides us with the fields using which the critical field theory is formulated. The symmetry transformations of these fields are given in Eq. E.9, we notice that the transformation rules for the symmetries  $\sigma^v$  and  $R_\pi$  are different from the FM case (section 7.1.1) given the different implementation of microscopic symmetries.

Given the electric and magnetic charges see each other as a source of mutual  $\pi$ -flux due to their statistics such long-range statistical interactions need to be accounted for through an appropriate Chern-Simons term. In the FM case, as discussed in section 7.1.1, we presented a mutual  $U(1)$  gauge theory to account for this long-range statistical interaction. The same techniques can be applied to the present case as shown below. However, here we employ a somewhat more microscopic formulation using a mutual  $Z_2$  gauge theory formalism to obtain the same critical field theory. We discuss them in turn.

### Mutual $U(1)$ Chern Simons theory

The semionic statistics between the Ising electric and magnetic charges can be captured [16] using a mutual  $U(1)$  Chern-Simons term [41, 75, 116]

$$\mathcal{S}_{CS}^{U(1)} = \frac{i}{\pi} \int d^2\mathbf{r}d\tau \epsilon^{\mu\nu\lambda} A_\mu \partial_\nu B_\lambda \quad (7.91)$$

where  $\mu, \nu, \lambda = x, y, \tau$ , and  $A_\mu$  and  $B_\mu$  are  $U(1)$  gauge fields that couple to the electric and magnetic soft modes respectively. The symmetry transformations for the gauge fields  $A_\mu$  ( $B_\mu$ ) are given in Eq. E.11.

The critical theory is identical to the FM case and is given by

$$\mathcal{S}_c = \int d^2\mathbf{r}d\tau \mathcal{L} + \mathcal{S}_{CS}^{U(1)} \quad (7.92)$$

where  $\mathcal{S}_{CS}$  is given by Eq. 7.91 and

$$\mathcal{L} = \mathcal{L}_e + \mathcal{L}_m + \mathcal{L}_{em} \quad (7.93)$$

with

$$\mathcal{L}_e = |(\partial_\mu - iA_\mu)\Phi_e|^2 + u|\Phi_e|^2 + v|\Phi_e|^4 - \lambda [(\Phi_e)^4 + (\Phi_e^*)^4] \quad (7.94)$$

$$\mathcal{L}_m = |(\partial_\mu - iB_\mu)\Phi_m|^2 + u|\Phi_m|^2 + v|\Phi_m|^4 - \lambda [(\Phi_m)^4 + (\Phi_m^*)^4] \quad (7.95)$$

$$\mathcal{L}_{em} = w [(\Phi_e\Phi_m)^2 + (\Phi_e\Phi_m^*)^2 + \text{c.c.}] \quad (7.96)$$

Similar to the FM case (section 7.1.1) (see details in Appendix E.5) we find that while  $u > 0$  signifies the  $Z_2$  spin liquid state, ( $u < 0, \lambda < 0, w \neq 0 \propto \text{sgn}(J)$ ) specifies the spin symmetry broken ordered state, where the ordered states correspond to FM (AFM) for  $J > 0$  ( $J < 0$ ) in Eq. 3.14 for the  $\tau$  spins state, which translates into Neel (zig-zag) order for underlying  $\sigma$  spins (see Fig. 3.3).

### The Mutual $Z_2$ gauge theory

The soft modes of the Ising electric and magnetic charges in Eq. 7.89 and 7.90 respectively are charges under a  $Z_2$  gauge field and hence their mutual semionic statistics are naturally captured by a mutual  $Z_2$  CS theory as we describe below [107, 108]. This provides for connecting the more prevalent mutual  $U(1)$  approach described above [134] with a systematic  $Z_2$  approach. Indeed, the latter approach is generically more suited to faithfully capture the nature

of phase transitions. However, in the present case, we obtain the same continuum theory for the transition.

The starting point of the mutual  $Z_2$  formalism is obtaining a lattice version of the soft mode theory since the  $Z_2$  gauge fields are naturally formulated on the lattice. Hence using Eq. 7.89 and 7.90, we write the lattice low energy action as [128]

$$\mathcal{S} = \mathcal{S}_e + \mathcal{S}_m + \mathcal{S}_{CS} \quad (7.97)$$

where

$$\mathcal{S}_e = -t \sum_{ab} \rho_{ab} \cos(\theta_a^e - \theta_b^e) + \dots \quad (7.98)$$

is the electric action defined on the direct square lattice with  $\rho_{ab}$  being the  $Z_2$  link field with which it is minimally coupled,

$$\mathcal{S}_m = -t \sum_{\bar{a}\bar{b}} \tilde{\rho}_{\bar{a}\bar{b}} \cos(\theta_{\bar{a}}^m - \theta_{\bar{b}}^m) + \dots \quad (7.99)$$

is the magnetic action defined on the dual square lattice with  $\tilde{\rho}_{\bar{a}\bar{b}}$  being the dual  $Z_2$  gauge field and

$$\mathcal{S}_{CS} = i\frac{\pi}{4} \sum_{ab \in \square} (1 - \rho_{ab}) \left( 1 - \prod_{\bar{a}\bar{b} \in \square} \tilde{\rho}_{\bar{a}\bar{b}} \right) \quad (7.100)$$

is the Ising Chern-Simons action that implements the mutual semionic statistics between the electric and the magnetic charges[16].

Note that the hopping amplitude for both the electric and magnetic charges are fixed to be the same (denoted by  $t$  above) by the self-dual structure of the action since the electric and magnetic soft modes transform into each other under unit lattice translation (see section 7.1.1 and the discussion near Eq. E.9). Similarly  $(\dots)$  represents higher-order interaction terms that are highly constrained by the self-dual structure of the theory. We shall consider such interaction terms soon.

To proceed further we seek to dualize either the electric or the magnetic sectors both of

which are XY-fields and hence can be dualized using the particle-vortex duality [135, 136]. We choose to dualize the electric sector.

To this end, we re-write the electric action

$$\mathcal{S}_e = -t \sum_{ab} \cos \left( \theta_a^e - \theta_b^e + \frac{\pi}{2}(1 - \rho_{ab}) \right) \quad (7.101)$$

using Villain approximation [137] to obtain (the details are given in Appendix E.6)

$$\mathcal{S}'_e = \frac{1}{2t} \sum_{ab} L_{ab}^2 + iL_{ab} \left( \theta_a^e - \theta_b^e + \frac{\pi}{2}(1 - \rho_{ab}) \right) \quad (7.102)$$

where  $L_{ab}$  is an integer value link field. Further integration over  $\theta_a^e$  gives rise to the zero divergences (on a lattice) constraint on them, *i.e.*,

$$\nabla_j L_{ab} = 0 \quad (7.103)$$

which is solved by defining an integer field  $C_{\bar{a}\bar{b}}$  on the dual lattice through a lattice curl

$$L_{ab} = \nabla \times C_{\bar{a}\bar{b}} \quad (7.104)$$

Putting this together with  $\mathcal{S}_{CS}$  (Eq. 7.100), we have

$$\mathcal{S}_e + \mathcal{S}_{CS} = \sum_{\bar{a}\bar{b}} \frac{(\nabla \times C_{\bar{a}\bar{b}})^2}{2t} + i\frac{\pi}{2} \sum_{ab} [1 - \rho_{ab}] \left[ \nabla \times C_{\bar{a}\bar{b}} + \frac{1 - \prod_{\square} \tilde{\rho}_{\bar{a}\bar{b}}}{2} \right] \quad (7.105)$$

such that on integrating over  $\rho_{ab}$  we get the constraint which gives rise to

$$\prod_{\bar{a}\bar{b} \in \square} \tilde{\rho}_{\bar{a}\bar{b}} = (-1)^{(\nabla \times C_{\bar{a}\bar{b}})} \quad (7.106)$$

which can be solved by dividing  $C_{\bar{a}\bar{b}}$  into an even and an odd part as

$$C_{\bar{a}\bar{b}} = 2A_{\bar{a}\bar{b}} + \eta_{\bar{a}\bar{b}} \quad (7.107)$$

where  $\eta_{\bar{a}\bar{b}} = 0, 1$  and  $A_{\bar{a}\bar{b}} \in \mathbb{Z}$ , such that

$$\tau_{\bar{a}\bar{b}} = 1 - 2\eta_{\bar{a}\bar{b}} \quad (7.108)$$

In continuation with our soft mode treatment, we now implement the integer constraint on  $A_{\bar{a}\bar{b}}$  softly through the potential

$$-w \cos(2\pi A) \quad (w > 0) \quad (7.109)$$

such that the whole action (Eq. 7.97) becomes

$$\mathcal{S} = \sum_{\bar{a}\bar{b}} \frac{(\nabla \times C_{\bar{a}\bar{b}})^2}{2t\pi^2} - \sum_{\bar{a}\bar{b}} \tilde{\rho}_{\bar{a}\bar{b}} [w \cos(C_{\bar{a}\bar{b}} + \vartheta_{\bar{a}} - \vartheta_{\bar{b}}) + t \cos(\theta_{\bar{a}}^m - \theta_{\bar{b}}^m)] \quad (7.110)$$

where we have re-scaled  $C \rightarrow \pi C$  and have separated out a vortex field  $\vartheta_{\bar{a}}$  through a gauge choice [138–140]:  $\nabla \cdot C = 0$ . Integrating out  $\tilde{\rho}$ , we get, to the leading order

$$\begin{aligned} \mathcal{S} = & \frac{1}{2t\pi^2} \sum_{\bar{a}\bar{b}} (\nabla \times C_{\bar{a}\bar{b}})^2 + \frac{t^2}{4} \sum_{\bar{a}\bar{b}} \cos[2(\xi_{\bar{a}} - \xi_{\bar{b}}) - 2(\vartheta_{\bar{a}} - \vartheta_{\bar{b}})] \\ & + \frac{w^2}{4} \sum_{\bar{a}\bar{b}} \cos[2(\vartheta_{\bar{a}} - \vartheta_{\bar{b}} - C_{\bar{a}\bar{b}})] + \frac{tw}{2} \sum_{\bar{a}\bar{b}} \cos[\xi_{\bar{a}} - \xi_{\bar{b}} - C_{\bar{a}\bar{b}}] \end{aligned} \quad (7.111)$$

where we have defined

$$\xi = \theta^m + \vartheta \quad (7.112)$$

The continuum limit can be obtained by introducing bosonic fields

$$\varphi = e^{i2\vartheta}, \quad \chi = e^{-i\xi} \quad (7.113)$$

to get

$$\begin{aligned}
\mathcal{S} = & \frac{1}{2t\pi^2} \sum_{\bar{a}\bar{b}} (\nabla \times C_{\bar{a}\bar{b}})^2 + tw \sum_{\bar{a}\bar{b}} \chi_{\bar{a}}^* e^{-iC_{\bar{a}\bar{b}}} \chi_{\bar{b}} \\
& + \frac{w^2}{2} \sum_{IJ} \varphi_{\bar{a}}^* e^{i2C_{\bar{a}\bar{b}}} \varphi_{\bar{b}} + \frac{t^2}{2} \sum_{\bar{a}\bar{b}} (\chi_{\bar{a}}^* \chi_{\bar{b}})^2 (\varphi_{\bar{a}}^* \varphi_{\bar{b}})
\end{aligned} \tag{7.114}$$

such that the continuum action is given by

$$\mathcal{S}_{cont} = \int d^2\mathbf{x}d\tau \mathcal{L}_{cont} \tag{7.115}$$

where

$$\begin{aligned}
\mathcal{L}_{cont} = & |(\partial_\mu - iC_\mu)\chi|^2 + |(\partial_\mu + i2C_\mu)\varphi|^2 + V[\chi, \varphi] \\
& + g(\epsilon_{\mu\nu\lambda}\partial_\nu C_\lambda)^2
\end{aligned} \tag{7.116}$$

where  $V[\chi, \varphi]$  denotes the interactions between the modes that are allowed by symmetry. The above critical theory is exactly dual to Eq. 7.92. Indeed starting with Eq. 7.92, we can dualize the electric charges to get the above field theory as was shown for the FM case in section 7.1.1. Similarly, based on the symmetry transformations of the soft modes and in particular the permutation of the electric and the magnetic soft modes under translation, we have:

$$V[\chi, \varphi] = u(|\chi|^2 - |\varphi|^2) + v(|\chi|^4 + |\varphi|^2) + \tilde{w}|\chi|^4|\varphi|^2 + \dots \tag{7.117}$$

where the relative negative sign for the quadratic term is obtained by noting that  $\varphi$  is dual to the electric soft mode. Thus the transition belongs to a self-dual modified Abelian Higg's theory. This concludes our discussion of the deconfined critical point describing the quantum phase transition between the  $Z_2$  QSL and the spin-ordered phase. For a detailed discussion of this critical theory, we refer to section 7.1.1.

### A two-step or a single step transition

In the above discussion, we have presently ignored the transverse field term (see Eq. 3.14) which occurs with a strength of  $2J$  may potentially open up an intermediate phase as  $J$  is increased (see Fig. 3.4). We now focus on the viability of such a scenario.

The inclusion of the Heisenberg term leads to a perturbation of both an Ising term and a transverse field to the parent Toric code Hamiltonian in the strong anisotropic limit. In the complete parameter space, therefore we clearly have three phases (i) The  $Z_2$  QSL for the Toric code. (ii) The Ising ordered phase which breaks a  $Z_2$  symmetry stabilizing a Neel order for the original  $\sigma$  spins. (iii) A  $x$  paramagnet (in  $\tau$ s, also, see Fig. 3.4 and Fig. C.1).

Even while for  $\tau$  spins the paramagnet may seem featureless and trivially  $x$  polarized, in terms of underlying  $\sigma$  spins it is an intriguing state given the eigenstates correspond to  $\tau^x$  is essentially a singlet or a triplet bond

$$|\pm\rangle_x = \frac{1}{\sqrt{2}} \left( |\uparrow\downarrow\rangle \pm |\downarrow\uparrow\rangle \right) \quad (7.118)$$

ordered state on every  $z$  bond of the underlying honeycomb lattice. A polarized state in the  $\tau$  spins, therefore, corresponds to a direct product state of singlets on all  $z$  bonds which in turn corresponds to a lattice nematic state for the  $\sigma$  spins (see discussion in section 3.2.2). The analysis already provides some interesting insights. This present study in the anisotropic limit already leads to the fact that the transition from the Neel state to the lattice nematic phase is essentially an Ising transition. The transition from the  $Z_2$  liquid to the Neel phase is the self-dual modified Abelian Higgs transition. Now at infinite  $J$ , we know the system enters a Neel phase – this can either occur directly through a single-step transition or the route may entail an intermediate paramagnet phase which could then imply a two-step transition (see Fig. 3.4). A detailed numerical study of the Toric code Hamiltonian with a generalized Ising perturbation and a transverse field is given in appendix C. We find that in general, a Heisenberg perturbation in this strong anisotropic limit is in fact a single-step transition where the  $Z_2$  QSL undergoes a self-dual modified Abelian Higgs transition to a ferromagnet state.

### 7.2.2 Transition between large $\Gamma$ phase and $Z_2$ QSL

While the nature of the transition from a Toric code to the Neel state is captured in the framework discussed above - the transition from the  $Z_2$ -QSL to the paramagnet is quite interesting and we now discuss this transition. The  $Z_2$  QSL for the  $\tau$  spins is in Wen's representation [11] while the paramagnet it transits to is  $x$ -polarized which is adiabatically connected to the large- $\Gamma$  phase (see discussion in sections 3.2.3 and 5.2). Under a unitary rotation (see Eq. 3.2) while the QSL can be exactly mapped to the Kitaev's Toric code ground state (see Eq. 3.4), the paramagnet gets converted to  $y$ -polarized state. The nature of the transition from a Toric code

QSL to a transverse field in  $y$  direction is known to be a first-order transition [67, 68]. Given the first-order nature of this transition, we do not expect any universal physics, except noting that this transition has a fundamentally different character from our related FM study discussed in section 7.1.1, where the transition between the QSL and large  $\Gamma$  phase was a second order transition.

### 7.2.3 Transition between spin-ordered phase and large $\Gamma$ phase

This leaves us with the transition between the FM and the large  $\Gamma$  phase. Given the large  $\Gamma$  phase contains all the microscopic symmetries, we expect the transition from the large  $\Gamma$  to the FM transition to be of the Ising kind where a symmetry-breaking order gets developed at a critical value of Ising coupling. Our numerical estimation of the phase boundary shows that the transition from the large  $\Gamma$  phase to the FM occurs along the  $t_2 = \frac{t_1}{3-2t_1}$  curve. This corresponds to a critical value of  $J_c$  which quadratically increases with the strength of the  $\Gamma$  coupling strength ( $\Gamma^2/J_c|K_z| \sim 3$ ).

This completes our discussion of the phase transitions between the phases in the anisotropic limit of the AFM Kitaev model discussed in section 3.2, which is also summarized in Fig. 3.9.

## CHAPTER 8

### SUMMARY AND OUTLOOK

#### 8.1 Summary

In summary, starting with a well motivated and concrete microscopic model we obtain phase diagrams (both in FM and AFM cases) and the theory for unconventional quantum phase transitions out of a  $Z_2$  QSL phase. This is obtained via multi-step calculations to identify the right low energy degrees of freedom and the correct symmetry implementations using complementary methods such as exact diagonalization, strong coupling, and effective quantum field theory. In our present calculation for the anisotropic limit, we find that the transition between the  $Z_2$  QSL and the symmetry-breaking spin-ordered phase is given by a self-dual modified Abelian Higgs model whereas that between the QSL and the trivial paramagnet is given by a self-dual  $Z_2$  gauge theory. The self-duality owes its origin to the anyon permutation symmetry which protects the structure of the critical theory. It would be interesting to understand other examples of such anyon permutation symmetry protected phase transitions. Finally, the phase diagram in figures 4.5 and 5.5 allows for interesting multicritical points where all the three phases—topological, symmetry broken, and trivial—meet. The nature of the multicritical point is worth investigating.

Interestingly, the different phases in the material relevant isotropic phase diagram for the generalized Kitaev model are also present in the anisotropic limit. While, even in the  $\alpha$ - $\text{RuCl}_3$  and other materials, the strength of the three Kitaev interactions are not the same, our calculation is not applicable in its present form but gives useful insights. In the current form of our calculation, we have ignored the Majorana degrees of freedom of the Kitaev honeycomb model due to the higher energy scale. In the isotropic phase transition, these gapless Majorana plays an important role along with the  $Z_2$  fluxes of the Kitaev model [16]. Given the correspondence of the QSL and the spin-ordered phases, it is tempting to conclude that the soft modes in the anisotropic limit indeed play an important role—along with the gapless Majorana—to determine the critical theory for the isotropic point. Outcomes of calculations along these lines would be interesting.

Despite the similarity like the deconfined critical point phase transition in the large Heisen-

berg coupling ( $J$ ) limit, there is an important difference between the FM and AFM Kitaev anisotropic limit for the large pseudo-dipolar coupling ( $\Gamma$ ). Although the large  $\Gamma$  phase in both the FM and AFM limit turns out to be a trivial paramagnet, the crucial differences between the microscopic symmetry transformations lead to the fact that the large  $\Gamma$  limit in the AFM case is proximate to a gapless critical point of a system described by an equal superposition of differently oriented stacked one-dimensional  $Z_2 \times Z_2$  symmetry protected topological phases. Interestingly, earlier works in the pseudo-dipolar limit for isotropic Kitaev limit have found a similar gapless phase [101]. Our numerical calculations on finite system size we find the  $\Gamma$  phase is critical & unstable and is smoothly connected to symmetry allowed paramagnetic phase, which doesn't have a topological correction to the entanglement entropy, a signature of the gapped entangled phase [122]. However, a detailed study is needed to understand the nature of this gapless phase proximate to the stacked SPTs and its connection to the isotropic  $\Gamma$  limit.

# Appendices

## APPENDIX A

### SYMMETRY TRANSFORMATIONS

#### A.1 Symmetry transformation in the anisotropic limit of FM Kitaev model

Since the Kitaev model is realized in spin-orbit coupled systems, the magnetic moment transforms non-trivially under spin and real space rotations. Following Ref. [73] we embed the honeycomb in a cube as shown in Fig. A.1. The generators of the symmetries (Fig. A.2) for the underlying honeycomb lattice are given by

- Time reversal symmetry,  $\mathcal{T}$ , where the  $\sigma^\alpha$  spins transform as Kramers doublets in all the known candidate materials.
- Translations in the honeycomb plane,  $T_{d_1}$  and  $T_{d_2}$ .
- $C_6$  rotation about  $[111]$  about the center of the hexagon, followed by reflection,  $\sigma_h$ , about the honeycomb plane ( $\equiv \sigma_h C_6$ ).
- Reflection,  $\sigma_v$ , about the  $x = y$  plane.

In the anisotropic limit,  $\mathcal{T}, T_{d_1}, T_{d_2}$  and  $\sigma_v$  remain intact while  $\sigma_h C_6$  is absent. However, the combination  $C_{2z} = (\sigma_h C_6)^2 \sigma_v (\sigma_h C_6)^{-1}$  is still a symmetry. Further, in addition to the above symmetries, we find it useful to consider the  $\pi$ -rotation about  $[111]$  through the center of the hexagon, namely  $R_\pi = (\sigma_h C_6)^3 = C_{2z} \sigma_v$ .

The non-trivial transformation of the  $\sigma$  spins under various symmetries (except for the two translations which are rather straightforward) is given in Table A.1. It is now easy to work out the action of the surviving symmetries on the  $\tau$  spins as shown in Fig. A.3.

**Time reversal Symmetry,  $\mathcal{T}$  :** For the  $\sigma$  spins, the time-reversal symmetry is implemented by the regular operator  $i\sigma^y \mathcal{K}$  where  $\mathcal{K}$  is the conjugation operator. Therefore, using Eq. 2.8, under time reversal :

$$\mathcal{T} : \{|+\rangle, |-\rangle\} \rightarrow \{|-\rangle, |+\rangle\} \quad (\text{A.1})$$

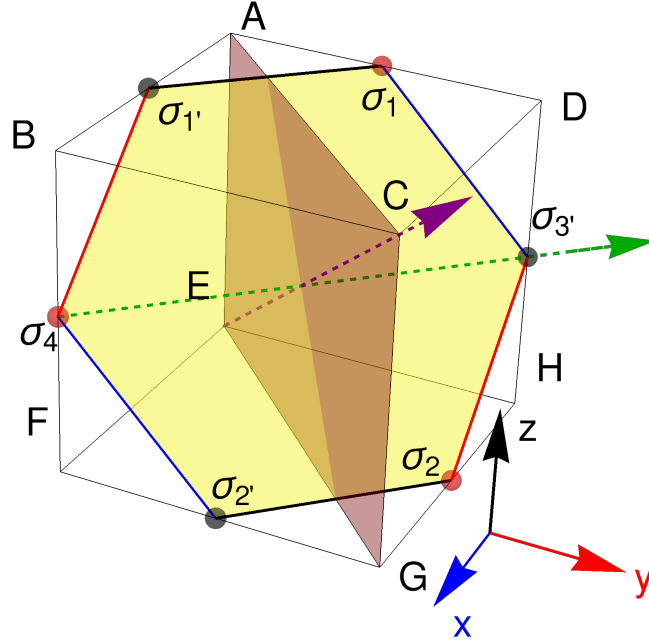


Figure A.1: The hexagon embedded in a cube with the cartesian  $[111]$  direction being normal to the hexagon plane. The red and black sub-lattice structure of the  $\sigma$ -spins are same as in Fig. A.2. Green dashed arrow along  $[\bar{1}10]$  direction is the  $\pi$ -rotation axis,  $C_{2z}$ . A light red plane cutting two of the z-bonds is the mirror reflection,  $\sigma_v$ . The purple dashed arrow along  $[111]$  direction is the six-fold rotation supplemented by the mirror reflection about the honeycomb plane,  $\sigma_h C_6$ .

Symmetry	1	1'	2	2'	3	3'	4	4'	$\sigma^x$	$\sigma^y$	$\sigma^z$
$\mathcal{T}$	1	1'	2	2'	3	3'	4	4'	$-\sigma^x$	$-\sigma^y$	$-\sigma^z$
$\sigma_h C_6$	1'	4	3'	2	5'	1	2'	8	$\sigma^z$	$\sigma^x$	$\sigma^y$
$\sigma_v$	1'	1	2'	2	4'	4	3'	3	$-\sigma^y$	$-\sigma^x$	$-\sigma^z$
$C_{2z}$	2	2'	1	1'	3	3'	4	4'	$-\sigma^y$	$-\sigma^x$	$-\sigma^z$
$R_\pi$	2'	2	1'	1	4'	4	3'	3	$\sigma^x$	$\sigma^y$	$\sigma^z$

Table A.1: The time reversal and point group symmetry operations on the  $\sigma$ -spin of the central hexagon of the Fig. A.2. The second, to fifth columns, indicate the transformations of the lattice labels while the last column shows the spin space rotations.

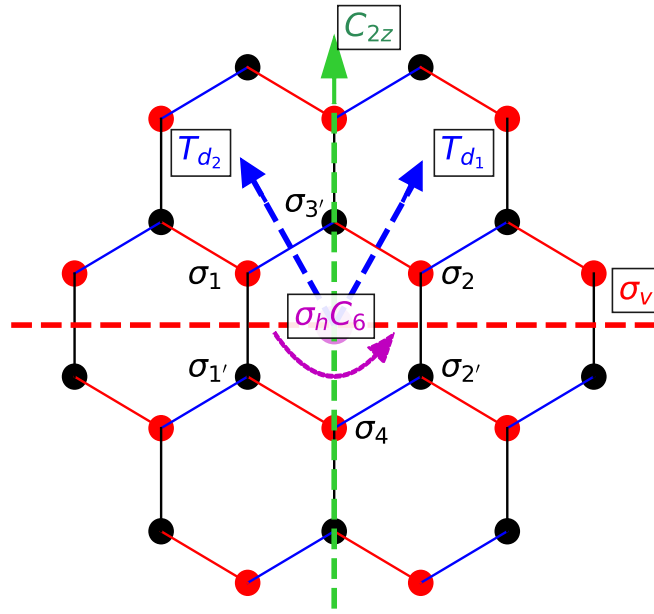


Figure A.2: Symmetries with respect to the hexagonal plane. Refer to Fig. A.1 for more details.

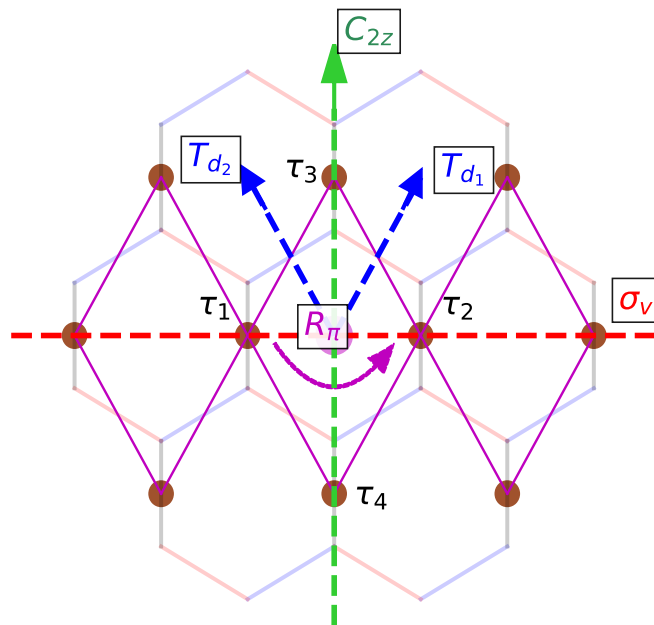


Figure A.3: In the anisotropic limit the  $\sigma$ -spin gives rise to  $\tau$ -spins, they are labeled by the brown spheres at the vertices of the rhombic lattice (magenta lines). Also, the honeycomb lattice is shown in the background. The relevant symmetries are shown following the convention of Fig. A.2.

**Reflection symmetry,  $\sigma_v$  :** Following Table A.1, we define the symmetry transformation operator for the  $\sigma$  spins as

$$\sigma_v(11') = \hat{\mathbb{E}}(11') e^{-i \frac{\hat{n}_v \cdot \vec{\sigma}_1 \pi}{2}} e^{-i \frac{\hat{n}_v \cdot \vec{\sigma}_{1'} \pi}{2}} \quad (\text{A.2})$$

where  $\hat{\mathbb{E}}((11'))$  is the exchange operator between the 1 & 1' and  $\hat{n}_v = \frac{1}{\sqrt{2}}(-1, 1, 0)$ . This gives rise to the following transformation:

$$\sigma_v(11') : \{|+\rangle_1, |-\rangle_1\} \rightarrow \{i|-\rangle_1, -i|+\rangle_1\} \quad (\text{A.3})$$

**Rotation about the z-bond,  $C_{2z}$  :** From Table A.1 we focus on the pair  $\sigma_{1'}$  and  $\sigma_{2'}$  which are mapped into each other under the symmetry transformation. This gives

$$C_{2z}(1'2') = \hat{\mathbb{E}}(1'2') e^{-i \frac{\hat{n}_{2z} \cdot \vec{\sigma}_{1'} \pi}{2}} e^{-i \frac{\hat{n}_{2z} \cdot \vec{\sigma}_{2'} \pi}{2}} \quad (\text{A.4})$$

with  $\hat{n}_{2z} = \hat{n}_v$ . For the  $\tau$ -spins we therefore have

$$C_{2z}(12; 1'2') : \{|+\rangle_{1(2)}, |-\rangle_{1(2)}\} \rightarrow \{i|-\rangle_{2(1)}, -i|+\rangle_{2(1)}\} \quad (\text{A.5})$$

**Rotation about the center of the hexagon,  $R_\pi$  :** From Table A.1, this transformation does not mix the spin components, but, it introduces lattice transformation including the interchange of the two sub-lattices. From Fig. A.2, focusing on the spins  $\sigma_{1(1')}$  and  $\sigma_{2(2')}$ , the exchange operators  $\mathbb{E}(12')$  and  $\mathbb{E}(1'2)$  are defined, they exchange between  $\sigma_1$  &  $\sigma_{2'}$  and  $\sigma_2$  &  $\sigma_{1'}$ . The effect of the symmetry operation on the  $\tau^z$  basis state is as follows

$$R_\pi(12'; 1'2) : \{|+\rangle_{1(2)}, |-\rangle_{1(2)}\} \rightarrow \{|+\rangle_{2(1)}, |-\rangle_{2(1)}\} \quad (\text{A.6})$$

The above transformations result in the symmetry table as summarised in Eq. 2.11. Due to the difference in rotation (see Eq. 3.2), the  $\tilde{\tau}$ -spins on horizontal and vertical bonds of the square lattice transform differently under the symmetries. This is summarised in Table A.2.

**Accidental symmetry for  $\Gamma = 0$**  Apart from the symmetries listed above, as mentioned in the main text, there are accidental symmetries present for the Hamiltonian in Eq. 1.1 in the

Symmetry	$\tilde{\tau}_h^x$	$\tilde{\tau}_h^y$	$\tilde{\tau}_h^z$	$-\tilde{\tau}_v^x$	$\tilde{\tau}_v^y$	$\tilde{\tau}_v^z$
$\mathcal{T}$	$\tilde{\tau}_h^x$	$\tilde{\tau}_h^y$	$-\tilde{\tau}_h^z$	$-\tilde{\tau}_{v'}^x$	$\tilde{\tau}_{v'}^y$	$\tilde{\tau}_{v'}^z$
$\sigma_v$	$\tilde{\tau}_{h'}^x$	$-\tilde{\tau}_{h'}^y$	$-\tilde{\tau}_{h'}^z$	$-\tilde{\tau}_{v'}^x$	$-\tilde{\tau}_{v'}^y$	$\tilde{\tau}_{v'}^z$
$C_{2z}$	$\tilde{\tau}_{h'}^x$	$-\tilde{\tau}_{h'}^y$	$-\tilde{\tau}_{h'}^z$	$-\tilde{\tau}_{v'}^x$	$-\tilde{\tau}_{v'}^y$	$\tilde{\tau}_{v'}^z$
$R_\pi$	$\tilde{\tau}_{h'}^x$	$\tilde{\tau}_{h'}^y$	$\tilde{\tau}_{h'}^z$	$\tilde{\tau}_{v'}^x$	$\tilde{\tau}_{v'}^y$	$\tilde{\tau}_{v'}^z$
$T_{d_j}$	$\tilde{\tau}_{v_j}^z$	$-\tilde{\tau}_{v_j}^y$	$\tilde{\tau}_{v_j}^x$	$\tilde{\tau}_{h_j}^z$	$-\tilde{\tau}_{h_j}^y$	$\tilde{\tau}_{h_j}^x$

Table A.2: Symmetry transformations of the  $\tilde{\tau}$  spins on the horizontal ( $h$ ) and vertical ( $v$ ) bonds for FM anisotropic limit.

limit  $\Gamma = 0$ . These are  $\pi$ -rotation about the spin  $x$ ,  $y$  &  $z$ -axis:

$$\begin{aligned}
R_\pi^x &: \{\sigma^x, \sigma^y, \sigma^z\} \rightarrow \{\sigma^x, -\sigma^y, -\sigma^z\} \\
R_\pi^y &: \{\sigma^x, \sigma^y, \sigma^z\} \rightarrow \{-\sigma^x, \sigma^y, -\sigma^z\} \\
R_\pi^z &: \{\sigma^x, \sigma^y, \sigma^z\} \rightarrow \{-\sigma^x, -\sigma^y, \sigma^z\}
\end{aligned} \tag{A.7}$$

These transformations act on the  $\tau$ -spins states in the following way:

$$\begin{aligned}
R_\pi^x &: \{|+\rangle, |-\rangle\} \rightarrow \{|-\rangle, |+\rangle\} \\
R_\pi^y &: \{|+\rangle, |-\rangle\} \rightarrow \{-|-\rangle, -|+\rangle\} \\
R_\pi^z &: \{|+\rangle, |-\rangle\} \rightarrow \{|+\rangle, |-\rangle\}
\end{aligned} \tag{A.8}$$

While the rotation about the spin  $z$ -axis results in identity transformation in the  $\tau$ -spins, clearly the other two transformations act as a  $\pi$ -rotation about the  $\tau^x$ , as

$$R_\pi^\alpha : \{\tau_i^x, \tau_i^y, \tau_i^z\} \rightarrow \{\tau_i^x, -\tau_i^y, -\tau_i^z\} \tag{A.9}$$

In a rotated basis this leads to

$$R_\pi^\alpha : \{\tilde{\tau}_i^x, \tilde{\tau}_i^y, \tilde{\tau}_i^z\} \rightarrow \{-\tilde{\tau}_i^x, \tilde{\tau}_i^y, -\tilde{\tau}_i^z\} \quad \forall i \tag{A.10}$$

Symmetry	$\tilde{\tau}_h^x$	$\tilde{\tau}_h^y$	$\tilde{\tau}_h^z$	$\tilde{\tau}_v^x$	$\tilde{\tau}_v^y$	$\tilde{\tau}_v^z$
$\mathcal{T}$	$\tilde{\tau}_h^x$	$\tilde{\tau}_h^y$	$-\tilde{\tau}_h^z$	$-\tilde{\tau}_v^x$	$\tilde{\tau}_v^y$	$\tilde{\tau}_v^z$
$\sigma_v$	$\tilde{\tau}_{h'}^x$	$\tilde{\tau}_{h'}^y$	$\tilde{\tau}_{h'}^z$	$\tilde{\tau}_{v'}^x$	$\tilde{\tau}_{v'}^y$	$\tilde{\tau}_{v'}^z$
$C_{2z}$	$-\tilde{\tau}_{h'}^x$	$\tilde{\tau}_{h'}^y$	$-\tilde{\tau}_{h'}^z$	$-\tilde{\tau}_{v'}^x$	$\tilde{\tau}_{v'}^y$	$-\tilde{\tau}_{v'}^z$
$R_\pi$	$-\tilde{\tau}_{h'}^x$	$\tilde{\tau}_{h'}^y$	$-\tilde{\tau}_{h'}^z$	$-\tilde{\tau}_{v'}^x$	$\tilde{\tau}_{v'}^y$	$-\tilde{\tau}_{v'}^z$
$T_{d_j}$	$\tilde{\tau}_{h'}^z$	$-\tilde{\tau}_{h'}^y$	$\tilde{\tau}_{h'}^x$	$\tilde{\tau}_{v'}^z$	$-\tilde{\tau}_{v'}^y$	$\tilde{\tau}_{v'}^x$

Table A.3: Symmetry transformation of the  $\tilde{\tau}$  spins on the horizontal ( $h$ ) and vertical ( $v$ ) links of the AFM anisotropic limit (see Fig. 1.1). Where  $v'$  &  $h'$  denotes the lattice points transformation,  $h' \equiv \mathcal{S}(h)$  &  $v' \equiv \mathcal{S}(v)$  for  $\mathcal{S} \equiv \{\mathcal{T}, \sigma_v, C_{2z}, R_\pi, T_{d_{1(2)}}\}$ .

For the electric and magnetic charges as well as the gauge fields this leads to

$$\begin{aligned}
R_\pi^\alpha : \quad & \{\mu^x, \mu^z\}_a \rightarrow \{\mu^x, \mu^z\}_a \\
& \{\tilde{\mu}^x, \tilde{\mu}^z\}_{\bar{a}} \rightarrow \{\tilde{\mu}^x, \tilde{\mu}^z\}_{\bar{a}} \\
& \{\rho^x, \rho^z\}_{ab} \rightarrow \{-\rho^x, -\rho^z\}_{ab} \\
& \{\tilde{\rho}^x, \tilde{\rho}^z\}_{\bar{a}\bar{b}} \rightarrow \{-\tilde{\rho}^x, -\tilde{\rho}^z\}_{\bar{a}\bar{b}}
\end{aligned} \tag{A.11}$$

and hence for the soft modes and the gauge fields we get

$$R_\pi^\alpha : \begin{cases} \Phi_e \rightarrow i\Phi_e^* \\ \Phi_m \rightarrow i\Phi_m^* \\ A_\mu \rightarrow -A_\mu \\ B_\mu \rightarrow -B_\mu \end{cases} \tag{A.12}$$

However, we do not use these accidental symmetries in our calculations. We note however that our calculation is consistent with this symmetry in the limit when  $\Gamma = 0$ .

## A.2 Symmetry transformation in the anisotropic limit of AFM Kitaev model

Similar to the above section A.1 for the FM case, we can find out the symmetry transformations of the  $\tau$ -spins, the symmetry transformations for this case are summarized in Eq. 2.12. Also, following the Eq. 3.2, after the rotation to the  $\tilde{\tau}$ -spins the symmetry transformations of the  $t\tau$ -spins on horizontal and vertical bonds of the square lattice are changed, this is summarized in table A.3.

## APPENDIX B

### DEGENERATE PERTURBATION THEORY TO OBTAIN THE TORIC CODE CONTRIBUTION IN FM KITAEV MODEL

#### B.1 Low energy degrees of freedom

In this section, we will provide the detailed calculation of the three most important contributions using degenerate perturbation theory in the anisotropic limit of the FM Kitaev model, these are respectively pseudo-dipolar (first order in  $\Gamma$ ), Heisenberg (first order in  $J$ ) and Kitaev contribution (fourth order in  $K$ , *i.e.*  $\sim \frac{\delta^4}{\Delta^3}$ , see Eq. 2.15). These contributions are given in Eq. 2.14, in the first term in Eq. 2.16, and the first term in Eq. 2.18 respectively.

Following the definition of the low energy degrees of freedom in Eq. 2.3 and excited states in Eq. 2.3 on each z-bond of the honeycomb lattice (see Fig. 1.1), we define a projector operator to the ground state on each z-bond, along with the associated identity operator:

$$\mathbb{P}_{ii'} = (|\uparrow\uparrow\rangle\langle\uparrow\uparrow| + |\downarrow\downarrow\rangle\langle\downarrow\downarrow|)_{ii'} ; \quad \mathbb{I}_{ii'} = \mathbb{P}_{ii'} + (|\uparrow\downarrow\rangle\langle\uparrow\downarrow| + |\downarrow\uparrow\rangle\langle\downarrow\uparrow|)_{ii'} = \mathbb{P}_{ii'} + \mathbb{Q}_{ii'} \quad (\text{B.1})$$

Where  $ii'$  denotes the z-bonds of the honeycomb lattice, and  $i \in A$  ( $i' \in B$ ) sub-lattice (refer to the Fig. 1.1). They follow the usual relationships of projector algebra

$$\mathbb{P}_{ii'}^2 = \mathbb{P}_{ii'} , \quad \mathbb{Q}_{ii'}^2 = \mathbb{Q}_{ii'} , \quad \mathbb{P}_{ii'}\mathbb{Q}_{ii'} = 0 \quad (\text{B.2})$$

With the help of the above projector on each z-bond, we can define the  $\tau$ -spin in terms of the underlying  $\sigma$ -spin.

$$\begin{aligned} \mathbb{I}_i &= \mathbb{P}_{ii'} (\sigma_i^z \otimes \sigma_{i'}^z) \mathbb{P}_{ii'} = \mathbb{P}_{ii'} (\mathbb{I}_i \otimes \mathbb{I}_{i'}) \mathbb{P}_{ii'} \\ \tau_i^z &= \mathbb{P}_{ii'} (\mathbb{I}_i \otimes \sigma_{i'}^z) \mathbb{P}_{ii'} = \mathbb{P}_{ii'} (\sigma_i^z \otimes \mathbb{I}_{i'}) \mathbb{P}_{ii'} \\ \tau_i^x &= \mathbb{P}_{ii'} (\sigma_i^x \otimes \sigma_{i'}^x) \mathbb{P}_{ii'} = -\mathbb{P}_{ii'} (\sigma_i^y \otimes \sigma_{i'}^y) \mathbb{P}_{ii'} \\ \tau_i^y &= \mathbb{P}_{ii'} (\sigma_i^x \otimes \sigma_{i'}^y) \mathbb{P}_{ii'} = \mathbb{P}_{ii'} (\sigma_i^y \otimes \sigma_{i'}^x) \mathbb{P}_{ii'} \end{aligned} \quad (\text{B.3})$$

Where  $\mathbb{I}_i$  is the identity operator on each z-bonds in the  $\tau$ -spin space. The above definitions are complimentary to the definition of the  $\tau^z$ -spin provided in Eq. 2.8 for FM case.

Finally, to set up the calculations we write the contributions in degenerate perturbation

theory up to fourth order of  $1/\Delta$  in more details (see Eq. 2.9):

$$\begin{aligned}
\mathcal{H}_{eff}^{FM} = & \mathbb{P}\mathcal{V}^{FM}\mathbb{P} + \mathbb{P}\mathcal{V}^{FM}\mathbb{R}\mathcal{V}^{FM}\mathbb{P} + \mathbb{P}\mathcal{V}^{FM}\mathbb{R}\mathcal{V}^{FM}\mathbb{R}\mathcal{V}^{FM}\mathbb{P} \\
& + \left[ \mathbb{P}\mathcal{V}^{FM}\mathbb{R}\mathcal{V}^{FM}\mathbb{R}\mathcal{V}^{FM}\mathbb{R}\mathcal{V}^{FM}\mathbb{P} \right. \\
& \left. - \frac{1}{2} \left( \mathbb{P}\mathcal{V}^{FM}\mathbb{R}^2\mathcal{V}^{FM}\mathbb{P}\mathcal{V}^{FM}\mathbb{R}\mathcal{V}^{FM}\mathbb{P} + \mathbb{P}\mathcal{V}^{FM}\mathbb{R}\mathcal{V}^{FM}\mathbb{P}\mathcal{V}^{FM}\mathbb{R}^2\mathcal{V}^{FM}\mathbb{P} \right) \right] + \dots
\end{aligned} \tag{B.4}$$

where  $\mathbb{P} = \otimes_{ii'} \mathbb{P}_{ii'}$  is the global projection operator in the ground state degenerate sector of the  $\mathcal{H}_0^{FM}$  (see Eq. 2.2), and  $\mathbb{R} = \frac{\mathbb{I} - \mathbb{P}}{E_0 - \mathcal{H}_0^{FM}}$ ,  $\mathbb{I} = \otimes_{ii'} \mathbb{I}_{ii'}$  and  $E_0$  is the energy of ground state manifold due to  $\mathcal{H}_0^{FM}$ . It is also worthwhile to note that, since the  $\mathcal{V}^{FM}$  acting on  $\mathbb{P}$  is taken out of the ground state manifold, the denominator of  $\mathbb{R}$  is non-zero. In case of FM Kiteav model, we write the  $\mathcal{V}^{FM}$  defined in Eq. 2.1 in more details:

$$\begin{aligned}
\mathcal{V}^{FM} = & \sum_{\langle ii' \rangle_z} \{ K (\sigma_i^x \sigma_{i'}^x + \sigma_i^y \sigma_{i'}^y) + \Gamma (\sigma_i^x \sigma_{i'}^y + \sigma_{i'}^x \sigma_i^y) \} \\
& + \sum_{\langle ij' \rangle_x} \{ -(K - J) \sigma_i^x \sigma_{j'}^x + J \sigma_i^y \sigma_{j'}^y + J \sigma_i^z \sigma_{j'}^z + \Gamma (\sigma_i^y \sigma_{j'}^z + \sigma_{j'}^y \sigma_i^z) \} \\
& + \sum_{\langle ij' \rangle_y} \{ -(K - J) \sigma_i^y \sigma_{j'}^y + J \sigma_i^x \sigma_{j'}^x + J \sigma_i^z \sigma_{j'}^z + \Gamma (\sigma_i^x \sigma_{j'}^z + \sigma_{j'}^x \sigma_i^z) \}
\end{aligned} \tag{B.5}$$

With the above understanding, we calculate the first-order contribution in Eq. B.4 in more detail in the next sections.

## B.2 First order contribution

We start with the pseudo-dipolar contribution in Eq. B.5, clearly using Eq. B.3 the second term in the first summation in Eq. B.5 gives:

$$\mathbb{P} \Gamma (\sigma_i^x \sigma_{i'}^y + \sigma_{i'}^x \sigma_i^y) \mathbb{P} \Rightarrow 2\Gamma \tau_i^y \tag{B.6}$$

Similarly, from the Heisenberg contribution in Eq. B.5 on each x and y bond, we get:

$$\mathbb{P} \left( \sum_{\langle ij' \rangle_x} J \sigma_i^z \sigma_{j'}^z + \sum_{\langle ij' \rangle_y} J \sigma_i^z \sigma_{j'}^z \right) \mathbb{P} \Rightarrow J \sum_{\langle ij \rangle} \tau_i^z \tau_j^z \tag{B.7}$$

while,  $\mathbb{P} \sigma_i^y \sigma_{j'}^y \mathbb{P} = \mathbb{P} \sigma_i^x \sigma_{j'}^x \mathbb{P} = 0$ . Noticeably, these two contributions are provided in Eq.

2.14 and in the first term of 2.16 along with their higher order energy correction respectively.

### B.3 Fourth order contribution: Toric code

We now try to understand the first term in Eq. 2.18, which is the so-called TC contribution in Wen's representation. [74] To this end, we define four Kitaev contributions on the hexagon (see central hexagon in Fig. A.2)

$$A_1 = \sigma_4^x \sigma_2^x ; A_2 = \sigma_1^x \sigma_3^x ; B_1 = \sigma_1^y \sigma_4^y ; B_2 = \sigma_3^y \sigma_2^y \quad (\text{B.8})$$

In total, 24 different permutations of these  $A_1, A_2, B_1, B_2$  are possible in Eq. B.4, which will give rise to the TC contribution. We can easily find out the operator content in terms of  $\tau$ -spins, using Eq. B.4 and B.3, we get:

$$\begin{aligned} \mathbb{P}A_1\mathbb{R}A_2\mathbb{R}B_1\mathbb{R}B_2\mathbb{P} &\sim \mathbb{P}(\sigma_2^x \sigma_4^x)(\sigma_3^x \sigma_1^x)(\sigma_1^y \sigma_4^y)(\sigma_3^y \sigma_2^y)\mathbb{P} \\ &\sim \mathbb{P}(\sigma_2^x \sigma_2^y)(i\sigma_4^z)(i\sigma_3^z)(\sigma_1^x \sigma_1^y)\mathbb{P} \sim (-)\tau_3^z \tau_4^z \tau_1^y \tau_2^y \end{aligned} \quad (\text{B.9})$$

Where we have ignored the energy contribution in the denominator of  $\mathbb{R}$ , we have listed all the denominators for 24 possible permutations in table B.1. Crucially out of the three possible terms in the fourth order contributions in Eq. B.4, for each permutation either solely the first term or the last two terms have a non-zero contribution.

Finally, we collect all the permutations to get the below TC contribution

$$\left(12 - \left(\frac{8}{2} + 4\right)\right) \frac{(K - J)^4}{64 \times (K_z - J)^3} (-)\tau_3^z \tau_4^z \tau_1^y \tau_2^y = -\frac{\delta^4}{16\Delta^3} \tau_3^z \tau_4^z \tau_1^y \tau_2^y \quad (\text{B.10})$$

We can now see the above is one of the contributions up to the fourth order of perturbation theory which is present in the first term in Eq. 2.18.

$V_1$	$V_2$	$V_3$	$V_4$	Denominator
$A_1$	$A_2$	$B_1$	$B_2$	$-(4)(8)(4)$
$A_1$	$A_2$	$B_2$	$B_1$	$-(4)(8)(4)$
$A_1$	$B_1$	$A_2$	$B_2$	$-(4)(4)(4)$
$A_1$	$B_2$	$B_1$	$A_2$	$+(4)(4)(4)$
$A_1$	$B_1$	$B_2$	$A_2$	$+(4)(4)(4)$
$A_1$	$B_2$	$A_2$	$B_1$	$+(4)(4)(4)$
$A_2$	$A_1$	$B_1$	$B_2$	$-(4)(8)(4)$
$A_2$	$A_1$	$B_2$	$B_1$	$-(4)(8)(4)$
$B_1$	$A_1$	$A_2$	$B_2$	$+(4)(4)(4)$
$B_2$	$A_1$	$B_1$	$A_2$	$+(4)(4)(4)$
$B_1$	$A_1$	$B_2$	$A_2$	$-(4)(4)(4)$
$B_2$	$A_1$	$A_2$	$B_1$	$+(4)(4)(4)$
$A_2$	$B_1$	$A_1$	$B_2$	$+(4)(4)(4)$
$A_2$	$B_2$	$A_1$	$B_1$	$-(4)(4)(4)$
$B_1$	$A_2$	$A_1$	$B_2$	$+(4)(4)(4)$
$B_2$	$B_1$	$A_1$	$A_2$	$-(4)(8)(4)$
$B_1$	$B_2$	$A_1$	$A_2$	$-(4)(8)(4)$
$B_2$	$A_2$	$A_1$	$B_1$	$+(4)(4)(4)$
$A_2$	$B_1$	$B_2$	$A_1$	$+(4)(4)(4)$
$A_2$	$B_2$	$B_1$	$A_1$	$+(4)(4)(4)$
$B_1$	$A_2$	$B_2$	$A_1$	$+(4)(4)(4)$
$B_2$	$B_1$	$A_2$	$A_1$	$-(4)(8)(4)$
$B_1$	$B_2$	$A_2$	$A_1$	$-(4)(8)(4)$
$B_2$	$A_2$	$B_1$	$A_1$	$-(4)(4)(4)$

Table B.1: Permutations of  $A_1$ ,  $A_2$ ,  $B_1$ , &  $B_2$ .

## APPENDIX C

### $J - K$ HAMILTONIAN IN AFM ANISOTROPIC LIMIT

#### C.1 $JK$ Hamiltonian in AFM anisotropic limit : a generic $\tau^x$ -field study

The generalization of the Hamiltonian for the antiferromagnetic Kitaev model in the strong anisotropic limit with the Heisenberg term (Eqs. 3.13 and 3.14) is given by

$$\begin{aligned} \mathcal{H}_{\Gamma=0}^{AF} = & h_{\text{eff}} \sum_i \tau_i^x - J_{\text{eff}} \sum_{\langle i,j \rangle} \tau_i^z \tau_j^z \\ & - J_{\text{eff}}^{\text{TC}} \sum_i \tau_{i+d_1}^z \tau_{i-d_2}^z \tau_i^y \tau_{i+d_1-d_2}^y \end{aligned} \quad (\text{C.1})$$

where  $J_{\text{eff}}$ ,  $h_{\text{eff}}$  and  $J_{\text{eff}}^{\text{TC}}$  are the strengths of the Ising term, magnetic field and of the quartic term respectively. On transforming the above Hamiltonian via a unitary rotation in Eq. 3.2 followed by  $\tilde{\tau}_i^y \rightarrow -\tilde{\tau}_i^y$  on the horizontal bonds, we get

$$\begin{aligned} \mathcal{H}_{\Gamma=0}^{AF} = & h_{\text{eff}} \sum_i \tilde{\tau}_i^y - J_{\text{eff}} \sum_{\langle i,j \rangle, i \in H, j \in V} \tilde{\tau}_i^z \tilde{\tau}_j^x \\ & - J_{\text{eff}}^{\text{TC}} \left( \sum_s A_s + \sum_p B_p \right) \end{aligned} \quad (\text{C.2})$$

which now takes the form of the toric code Hamiltonian when perturbed by a *transverse* magnetic field and an Ising perturbation, although of a  $\tilde{\tau}^z \tilde{\tau}^x$  kind. This Hamiltonian, in parts, has been a subject of recent numerical studies [67, 68]; and we now investigate it further to develop a field-theoretic understanding of the phases and intervening phase transitions. To understand this phase diagram numerically we define two interpolating parameters:  $\epsilon_1$  and  $\epsilon_2$ , and study the following Hamiltonian

$$\begin{aligned} \mathcal{H}' = & \epsilon_1(1 - \epsilon_2) \sum_i \tilde{\tau}_i^y - \epsilon_2(1 - \epsilon_1) \sum_{\langle i,j \rangle, i \in H, j \in V} \tilde{\tau}_i^z \tilde{\tau}_j^x \\ & - (1 - \epsilon_1)(1 - \epsilon_2) \left( \sum_s A_s + \sum_p B_p \right) \end{aligned} \quad (\text{C.3})$$

which interpolates between the exact toric code Hamiltonian ( $\epsilon_1 = \epsilon_2 = 0$ ), a  $z - x$  ferromagnet ( $\epsilon_1 = 0, \epsilon_2 = 1$ ) and a  $y$  paramagnet ( $\epsilon_1 = 1, \epsilon_2 = 0$ ). We perform exact diagonalization

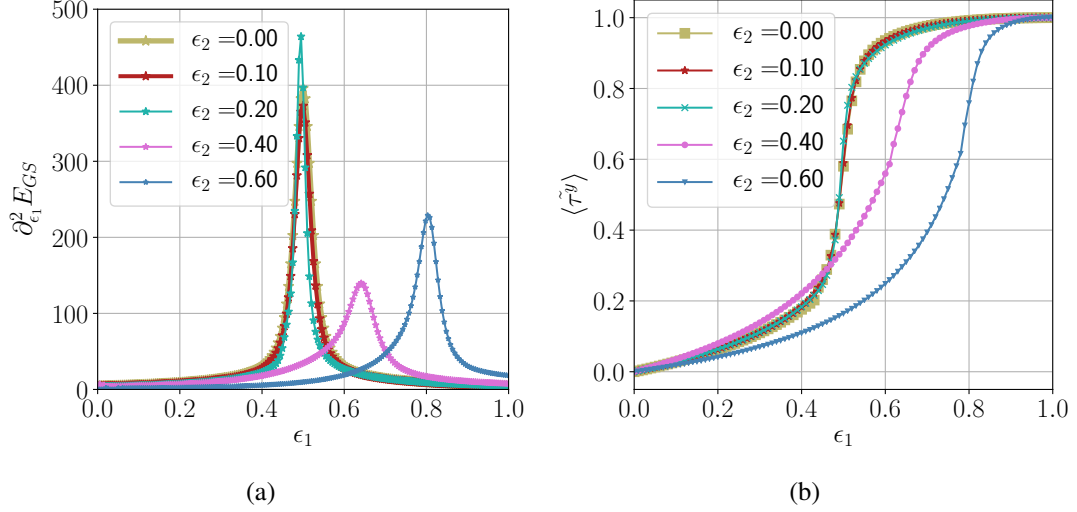


Figure C.1: The absolute value of ground state (GS) susceptibility ( $\frac{\partial^2 E_{GS}}{\partial \epsilon_1^2}|_{\epsilon_2}$ ) (a) and the absolute value of  $\tilde{\tau}^y$ -magnetization (b) as a function of  $\epsilon_1$  for constant values of  $\epsilon_2$  are shown for the Hamiltonian given in Eq. C.3.

(ED) studies on an 18 spin ( $3 \times 3$ ) periodic cluster and track the ground state fidelity and other observables to identify the phase boundaries. The numerically obtained phase diagram is shown in Fig. C.2.

In absence of the Ising term, i.e. the toric code Hamiltonian with a transverse field is self-dual under ( $h_{\text{eff}} \leftrightarrow J_{\text{eff}}^{TC}$ ) which is known to be a first-order transition at  $\epsilon_1 = 0.5$  [67, 68]. Here in our finite-sized system, this transition shows up as a peak in the fidelity susceptibility which does not change remarkably with increasing  $\epsilon_2$  ( $\sim J$ ) suggesting that the transition is stable with increasing  $\epsilon_2$  (see Fig.C.1 (a)). However, strictly our finite size numerics cannot distinguish the order of transition when transiting to either the large  $\Gamma$  phase or the FM. The transition is concomitant with a finite magnetization (along the transverse field) signaling a transition to a paramagnetic (polarized) phase (see Fig.C.1 (b)). In absence of the toric code term, the Ising magnet to paramagnet transition is governed by the Ising transition and occurs at  $h_{\text{eff}} \sim 3J_{\text{eff}}$  [77–80] where the ordered phase spontaneously breaks a  $Z_2$  Ising symmetry operator given by  $\prod_i \tilde{\tau}_i^y$ . This corresponds to  $\epsilon_2 = \frac{\epsilon_1}{3-2\epsilon_1}$  (dashed green) line in the  $\epsilon_1 - \epsilon_2$  phase diagram (see Fig. C.2). Clearly, the numerically obtained phase boundary follows this quite closely especially when the toric code term is small ( $\epsilon_1, \epsilon_2 > 0.5$ ). We find that this second order line and the (expected) first order line (separating the  $Z_2$  QSL and the paramagnet) meet at  $\epsilon_1 \sim 0.5, \epsilon_2 \sim 0.3$ , potentially a multicritical point. The phase boundary between the  $Z_2$  QSL and the Ising ferromagnet (in absence of any magnetic field) (see sections 7.1.1 and 7.2.1) is

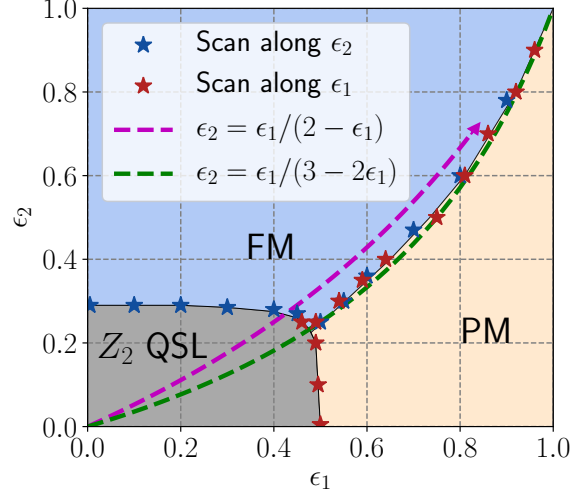


Figure C.2: Phase diagram of Eq. C.3 where we consider a general paramagnetic field along with the toric code and Ising contribution. The three phases are (i) ferromagnet (FM), (ii) Paramagnet (PM), and (iii) toric code spin liquid ( $Z_2$  QSL). The green dashed line indicates the expected phase boundary between the ferromagnetic and the paramagnetic phase in absence of the toric code contribution (see text). The magenta dashed shows the effect of Heisenberg coupling ( $J$ ) on the anisotropic anti-ferromagnetic Kitaev model (see Eq. 3.14).

argued to be a 3D-Higgs transition with mutual Chern Simons term. We find that this transition with increasing  $\epsilon_1$  remains stable and meets both the first order line and the second order Ising transition line again at  $\epsilon_1 \sim 0.5, \epsilon_2 \sim 0.3$ .

Having discussed the phase diagram of the generalized  $J - K$  Hamiltonian (see Eq. C.2) we now specify which intervening phases to expect as we increase the Heisenberg coupling in the anisotropic limit. Given the form of the effective Hamiltonian (see Eq. 3.14) we find that  $h_{\text{eff}} = 2J_{\text{eff}}$  which corresponds to  $\epsilon_2 = \frac{\epsilon_1}{2-\epsilon_1}$  line (shown in a magenta dashed line with an arrow) in Fig. C.2 suggesting a single step transition.

## APPENDIX D

### ADDITIONAL COMMENTS AND RESULTS ON $\Gamma$ -LIMIT OF AFM ANISOTROPIC MODEL

#### D.1 Summary of the 1D cluster phase ( $Z_2 \times Z_2$ SPT)

Here we briefly summarise the essential results for a one-dimensional cluster model for completion. The one-dimensional (on an open chain) cluster model Hamiltonian is given by [81–85, 95]

$$H_{1d} = \sum_{i=2}^{N-1} \mathcal{U}_i \quad (\text{D.1})$$

where  $\mathcal{U}_i = \tau_{i-1}^z \tau_i^x \tau_{i+1}^z$  and we consider  $N \in \text{Even}$ . The Hamiltonian, in particular, is symmetric under a  $Z_2 \times Z_2$  transformation generated by

$$P_1 = \prod_{i=2}^{N/2} \tau_{2i-1}^x = \tau_1^x \tau_2^z \left( \prod_{i=2}^{N/2} \mathcal{U}_{2i-1} \right) \tau_N^z \quad (\text{D.2})$$

$$P_2 = \prod_{i=1}^{N/2} \tau_{2i}^x = \tau_1^z \left( \prod_{i=1}^{N/2-1} \mathcal{U}_{2i} \right) \tau_{N-1}^z \tau_N^x \quad (\text{D.3})$$

The Hamiltonian in Eq. D.1 is exactly solvable since  $[\mathcal{U}_i, \mathcal{U}_j] = 0 \quad \forall i, j$ . Since  $\mathcal{U}_i^2 = 1$ , the ground state,  $|\psi_g\rangle$ , satisfies

$$\mathcal{U}_i |\psi_g\rangle = -|\psi_g\rangle \quad \forall i \quad (\text{D.4})$$

and can be obtained explicitly as

$$|\psi_g\rangle = \prod_i \left[ \frac{1 - \mathcal{U}_{2i-1}}{2} \right] |\tau_{2i}^x = -1\rangle |\tau_{2i\pm 1}^z = 1\rangle \quad (\text{D.5})$$

Therefore for the ground state on the open chain

$$P_1|\Psi_g\rangle = (-1)^{N/2-1}\tau_1^x\tau_2^z\tau_N^z|\Psi_g\rangle \quad (\text{D.6})$$

$$P_2|\Psi_g\rangle = (-1)^{N/2-1}\tau_1^z\tau_{N-1}^z\tau_N^x|\Psi_g\rangle \quad (\text{D.7})$$

Assuming that  $(N/2 - 1) \in \text{Even}$ , We find that the two conserved operators  $P_1$  and  $P_2$  have non-trivial structure at the two edges of the open chain, *i.e.*,

$$P_{1L} = \tau_1^x\tau_2^z \quad P_{2L} = \tau_1^z \quad (\text{D.8})$$

for the left edge and

$$P_{1R} = \tau_N^z \quad P_{2R} = \tau_{N-1}^z\tau_N^x \quad (\text{D.9})$$

for the right edge such that the edge operators anti-commute on the same edge leading to a four-dimensional representation of the ground state manifold generated by

$$|P_{1L} = \pm 1, P_{1R} = \pm 1\rangle, \quad (\text{D.10})$$

with each edge supporting a zero energy spin-1/2 or equivalently a complex fermion mode that transforms under a projective representation of the above  $Z_2 \times Z_2$  symmetry. In fact, due to exact solvability, each energy eigenstate is four-fold degenerate on the open chain [141] The edge modes are a characteristic signature of the one dimensional  $Z_2 \times Z_2$  SPT.

Since the Hamiltonian in Eq. D.3 is invariant under the global spin-flip generated by  $P_1P_2 = \prod \tau_i^x$ , we can map it to a fermionic Hamiltonian via the following one-dimensional Jordan-Wigner transformations [95] :

$$\gamma_i = \left( \prod_{j=1}^{i-1} \tau_j^x \right) \tau_i^z, \quad \tilde{\gamma}_i = \left( \prod_{j=1}^{i-1} \tau_j^x \right) \tau_i^y \quad (\text{D.11})$$

into the Majorana fermions  $\gamma_i$  and  $\tilde{\gamma}_i$  whence we get  $\mathcal{U}_i = i\tilde{\gamma}_{i-1}\gamma_{i+1}$  such that Eq. D.3 becomes

$$H_{1d} = \sum_{j=2} (i\tilde{\gamma}_{j-1}\gamma_{j+1}) \quad (\text{D.12})$$

which is nothing but two stacked Kitaev superconducting chains [142] with a complex fermionic mode at each boundary which is annihilated respectively on the left and right edge by

$$c_L = (\gamma_1 + i\gamma_2)/2 \quad \text{and} \quad c_R = (\tilde{\gamma}_{N-1} + i\tilde{\gamma}_N)/2 \quad (\text{D.13})$$

The generator of the spin-flips is local under the Jordan-Wigner Transformation, *i.e*

$$\tau_i^x = -i\tilde{\gamma}_i\gamma_i \quad (\text{D.14})$$

and is related to the fermion parity operator. Therefore the generators of the  $Z_2 \times Z_2$  symmetry becomes

$$\mathcal{P}_1 = \prod_{j=2}^{N/2} (-i\tilde{\gamma}_{2j-1}\gamma_{2j-1}), \quad \mathcal{P}_2 = \prod_{j=1}^{N/2} (-i\tilde{\gamma}_{2j}\gamma_{2j}) \quad (\text{D.15})$$

which shows that the parity of the even sites and the odd sites are separately preserved. Now following arguments similar to those given above we can find the edge representations of the symmetry in terms of the complex fermions given by Eq. D.13.

Remarkably, the representation in terms of the majorana fermions reveals further rich symmetry structures of the cluster Hamiltonian through its fermionic form [95] which usefully connects to the microscopic symmetries in our case. This is seen by noticing that the fermionic representation of the cluster Hamiltonian in Eq. D.12 is invariant under the following anti-unitary transformations :

$$V_1 = P_1 \prod_{j=2}^{N/2} \mathcal{K}_{2j-1} : \begin{cases} \{\tilde{\gamma}_{2j}, \gamma_{2j}\} & \rightarrow \{\tilde{\gamma}_{2j}, \gamma_{2j}\} \\ \{\tilde{\gamma}_{2j-1}, \gamma_{2j-1}\} & \rightarrow \{\tilde{\gamma}_{2j-1}, -\gamma_{2j-1}\} \end{cases} \quad (\text{D.16})$$

$$V_2 = P_2 \prod_{j=1}^{N/2} \mathcal{K}_{2j} : \begin{cases} \{\tilde{\gamma}_{2j}, \gamma_{2j}\} & \rightarrow \{\tilde{\gamma}_{2j}, -\gamma_{2j}\} \\ \{\tilde{\gamma}_{2j-1}, \gamma_{2j-1}\} & \rightarrow \{\tilde{\gamma}_{2j-1}, \gamma_{2j-1}\} \end{cases} \quad (\text{D.17})$$

$$V_3 = \prod_{j=2}^{N/2} \mathcal{K}_{2j-1} : \begin{cases} \{\tilde{\gamma}_{2j}, \gamma_{2j}\} & \rightarrow \{\tilde{\gamma}_{2j}, \gamma_{2j}\} \\ \{\tilde{\gamma}_{2j-1}, \gamma_{2j-1}\} & \rightarrow \{-\tilde{\gamma}_{2j-1}, \gamma_{2j-1}\} \end{cases} \quad (\text{D.18})$$

$$V_4 = \prod_{j=1}^{N/2} \mathcal{K}_{2j} : \begin{cases} \{\tilde{\gamma}_{2j}, \gamma_{2j}\} & \rightarrow \{-\tilde{\gamma}_{2j}, \gamma_{2j}\} \\ \{\tilde{\gamma}_{2j-1}, \gamma_{2j-1}\} & \rightarrow \{\tilde{\gamma}_{2j-1}, \gamma_{2j-1}\} \end{cases} \quad (\text{D.19})$$

where  $\mathcal{K}_j$  is the complex conjugation operator at site  $j$ . Clearly, the four transformations are related to the microscopic symmetries and the  $Z_2 \times Z_2$  spin-flip symmetries as follows :

$$\begin{aligned} P_1 &= V_1 V_3; & P_2 &= V_2 V_4 \\ \mathcal{T} &= V_1 V_2; & \mathcal{K} &= V_3 V_4 \end{aligned} \quad (\text{D.20})$$

where  $\mathcal{T}$  is the global non-Kramers time reversal defined in Eq. 2.12 and  $\mathcal{K}$  is the global complex conjugation operator. Depending on convenience, we can either use  $(P_1, P_2)$  or  $(\mathcal{T}, \mathcal{K})$  to understand the properties of the  $Z_2 \times Z_2$  SPT and the edge modes. However, the flexibility allows us to study the fate of perturbations.

A transverse field term of the form  $h \sum_i \tau_i^x$  is invariant under the  $Z_2 \times Z_2$  symmetry and hence the SPT is perturbatively stable to it and gives away to a trivial paramagnet polarised in the  $\tau^x$  direction through a quantum phase transition at  $|h| = 1$  [95]. This transition is described by a  $SO(2)_1$  conformal field theory (CFT) with central charge,  $c = 1$  [94].

A transverse field perturbation along  $\tau^y$ , *i.e.*  $h \sum_i \tau_i^y$ , however, it naively appears that the above  $Z_2 \times Z_2$  symmetry is broken. To be precise, we consider the  $(\mathcal{T}, \mathcal{K})$  implementation of the symmetries. While the above term is invariant under  $\mathcal{T}$ , it changes sign under  $\mathcal{K}$ . However, such a change in sign can be rectified by applying unitary global spin-flip  $P_1 P_2$  and thus rendering the above perturbation invariant under the  $Z_2 \times Z_2$  symmetry. Indeed the SPT is perturbatively stable under the above transverse field and gives away to the trivial  $\tau^y$ -polarised phase through the similar critical point as for the  $\tau^x$  case above.

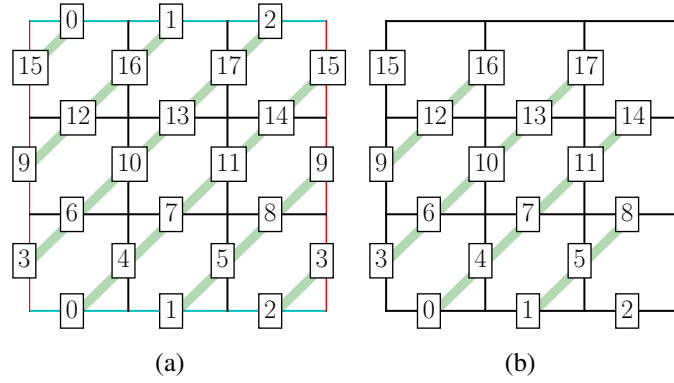


Figure D.1:  $U_{ij}$  are transformations on the bonds (see Eq. 3.24) connected shown in the cluster for (a) PBC, and (b) OBC.

## D.2 $\mathcal{W}$ transformation

To build intuition for the phase diagram in the  $(\lambda_1, \lambda_2)$  plane (Figs. 3.6 and 3.8) and the nature of transitions we summarise the effect of the unitary transformation,  $\mathcal{W}$  (Eq. 3.23), applied on the Hamiltonian (see Eq.3.21). The transformation, defined on a bond  $ij$ , follows  $U_{ij} = U_{ji}^\dagger$ . The bonds involved in a periodic and open system are shown in Fig. D.1. While it is straightforward to see how the periodic Hamiltonian then transforms from  $H_\alpha$  to  $\tilde{H}_\alpha$ , we discuss the same physics in an open system below to understand the intricacies of the boundary modes.

Consider spins  $i$  where  $i \in \mathcal{B}$ ,  $i \in \mathbf{t}$ ,  $i \in \mathbf{b}$ ,  $i \in \mathbf{l}$ ,  $i \in \mathbf{r}$  and  $i \in \mathbf{c}$  represents bulk, top, bottom, left, right boundary and corner of the cluster respectively. For e.g., in the cluster shown in Fig. D.1(b),  $\mathcal{B} = \{4, 5, 6, 7, 10, 11, 12, 13\}$ ,  $\mathbf{t} = \{16, 17\}$ ,  $\mathbf{b} = \{0, 1\}$ ,  $\mathbf{r} = \{14, 8\}$ ,  $\mathbf{l} = \{9, 3\}$ ,  $\mathbf{c} = \{15, 2\}$ . When the transformation  $\mathcal{W}$  is performed on an open problem one obtains (for Hamiltonian  $H$  in Eq. 3.21 in OBC)  $\tilde{H}$  as

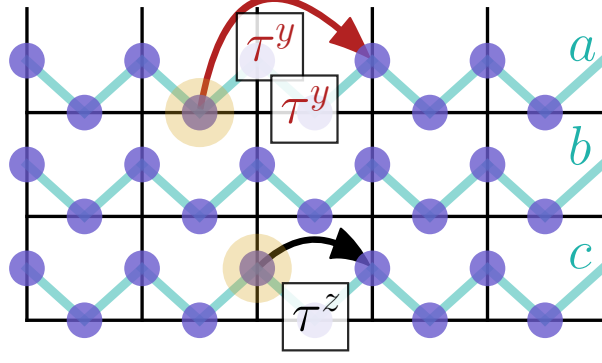


Figure D.2: Excitations of the cluster state and its dynamics in presence of magnetic fields. Three chains labeled by  $a, b, c$  are shown. The orange blob shows the initial position of the  $\langle \tau_{i-d_1}^x \tau_i^z \tau_{i-d_2}^x \rangle = 1$  excitations (on chain  $a$  and  $c$ ) which hop under the action  $\tau^y$  ( $\tau^z$ ) fields to the third (first) neighbor at the second (first) order of perturbation theory.

$$\tilde{H}_1 = \sum_{i \in \mathcal{B}} \tau_i^x \quad (\text{D.21})$$

$$\tilde{H}_2 = \sum_{i \in \mathcal{B}} \tau_i^x \tau_{i+d_1}^z \tau_{i-d_1}^z \tau_{i+d_2}^z \tau_{i-d_2}^z \quad (\text{D.22})$$

$$\begin{aligned} \tilde{H}_3 = & \sum_{i \in \mathcal{V}, \mathcal{B}} \tau_{i-d_1}^z \tau_i^y \tau_{i-d_2}^z - \sum_{i \in \mathcal{H}, \mathcal{B}} \tau_{i+d_2}^z \tau_i^y \tau_{i+d_1}^z \\ & + \sum_{i \in \mathcal{I}} \tau_i^y \tau_{i-d_2}^z + \sum_{i \in \mathcal{R}} \tau_i^y \tau_{i+d_2}^z \end{aligned} \quad (\text{D.23})$$

$$\tilde{H}_4 = \sum_{i \in \mathcal{H}, \mathcal{B}} \tau_{i-d_1}^z \tau_i^y \tau_{i-d_2}^z - \sum_{i \in \mathcal{V}, \mathcal{B}} \tau_{i+d_2}^z \tau_i^y \tau_{i+d_1}^z \quad (\text{D.24})$$

$H_1$  has a set of  $2^{2(L_x+L_y-1)}$  degeneracy which is reflected in the fact that  $\tilde{H}_1$  has no terms which involve boundary spins.  $H_2$  has a set of  $2^{2(L_x+L_y-1)}$  degeneracy given it is an SSPT on an open system.  $\tilde{H}_3$  has free spins on top and bottom boundaries while symmetry-breaking terms on the left and right boundaries. This leads to a degeneracy of  $2^{2L_x}$ . Since  $\tilde{H}_4$  has free spins on boundaries it again as  $2^{2(L_x+L_y-1)}$  degeneracy. These are the exact ground state degeneracies for  $H_1, H_2, H_3, H_4$  when placed in an open system. The analysis, therefore, shows that  $\mathcal{W}$  is suitably defined for both open and periodic systems.

### D.3 Excitations and their dynamics in the pure $\Gamma$ limit

Consider the Hamiltonian

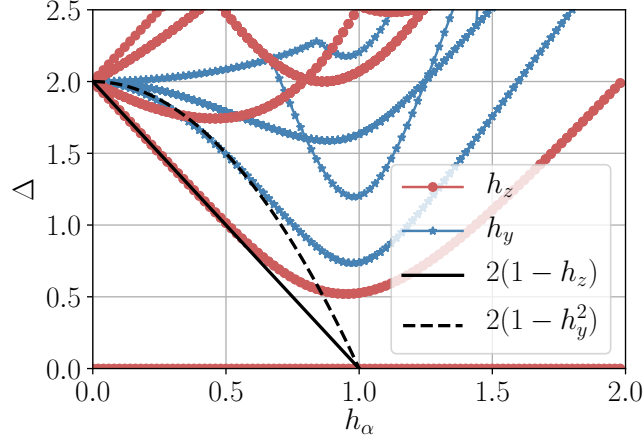


Figure D.3: The low energy spectrum of a one-dimensional cluster state in presence of magnetic fields ( $h_\alpha = \{h_x, h_z\}$ ) (see Eq. D.25) for a 16 site system.

$$\begin{aligned}
H = & \sum_{i \in V} \tau_{i-d_1}^x \tau_i^z \tau_{i-d_2}^x + \sum_{i \in H} \tau_{i+d_2}^x \tau_i^z \tau_{i+d_1}^x \\
& + h_y \sum_{i \in H, V} \tau_i^y + h_z \sum_{i \in H, V} \tau_i^z
\end{aligned} \tag{D.25}$$

which perturbs the cluster Hamiltonian (similar to Eq. D.1) with a magnetic field in  $y$  direction ( $\equiv h_y$ ) and  $z$  direction ( $\equiv h_z$ ). Both these are symmetry allowed and in either field, there exists a second-order transition with  $c = 1$ . Note that in Eq. 3.31 for  $\lambda_1 = \lambda_2 = 0$  the cluster Hamiltonian in  $\tilde{H}_3$  is of the above form where perturbations along  $\tilde{H}_1$  direction is essentially that of a  $y$ -field.

Here we explore the properties of the low energy excitations of the cluster state as the magnetic field is tuned to understand their role in the eventual transition to the trivial paramagnet. The ground state in absence of any fields is characterized by  $\langle \tau_{i-d_1}^x \tau_i^z \tau_{i-d_2}^x \rangle = -1$  for every  $i$ , where an excitation with energy gap = 2 localized at a particular site is given by  $\langle \tau_{i-d_1}^x \tau_i^z \tau_{i-d_2}^x \rangle = 1$ . A  $y$  field can effectively hop a charge by three lattice constants at quadratic order, but a  $z$  field hops it by two lattice constants at linear order (see Fig. D.2).

Therefore the charge gap behaves, for small fields, as  $\Delta \sim 2 - 2h_z$  or  $\Delta \sim 2 - 2h_y^2$  depending on the field direction both going to zero at  $h_z$  (or  $h_y$ ) = 1 signaling that the Ising transition (with  $c = 1$ ) can be understood as the condensation of these excitations. The exact diagonalization spectrum and how the low energy spectrum behaves is shown in Fig. D.3.

Under a unitary rotation ( $\{\tau^x, \tau^y, \tau^z\} \rightarrow \{-\tau^z, \tau^y, \tau^x\}$ ) where the cluster Hamiltonian

gets mapped to Eq. D.1 and perturbation  $h_z(h_y)$  leads to a  $x(y)$  polarized state. Using transformation to Majorana operators (see Eq. D.11) and defining bond complex fermion operators through

$$c_i = \frac{1}{2}(\gamma_{i-1} + i\tilde{\gamma}_{i+1}) \quad (\text{D.26})$$

Eq. D.25 becomes

$$H = \sum_i (2n_i - 1) \quad (\text{D.27})$$

$$+ h_z \sum_i \left( c_{i+1}c_{i-1} + c_{i+1}^\dagger c_{i-1} + c_{i-1}^\dagger c_{i+1} + c_{i+1}^\dagger c_{i-1}^\dagger \right) \\ - h_y \sum_i \prod_j^{i-1} \left( i\gamma_j \tilde{\gamma}_j \right) \left[ i(c_{i-1} - c_{i-1}^\dagger) \right] \quad (\text{D.28})$$

where  $n_i = c_i^\dagger c_i$ . Therefore the ground state of the cluster Hamiltonian ( $h_y = h_z = 0$ ) is given by  $\langle n_i \rangle = 0 \quad \forall i$  while the excitations are given by particles at site  $i$  with  $\langle n_i \rangle = +1$ . Using this fermionic description it is easily seen that  $\tau_i^x$  leads to a hopping process by two lattice sites in the single excitation sector; while a  $\tau_i^y$  operator changes the parity sector (along with a string) leading to the creation of charges. A quadratic action of  $\tau^y$  brings it to the same excitation sector leading to an effective hopping by three lattice sites.

While the magnetic field terms above are ultra-local and cannot lead to any dispersion of a single excitation in the vertical direction for the stacked system (Eq. 3.21) – no interchain couplings of the kind mediated by  $(\tilde{H}_4)$  or by  $(\tilde{H}_2)$  can lead to any vertical dispersion for these single excitations. This leads to the fact that the  $\lambda_2 = 1$  (even at a non-zero  $\lambda_1$ ) transition is extremely anisotropic in character where the spin-spin correlations are expected to be power law only in the  $x$  direction, while continues to remain short-ranged in the  $y$ -direction. At  $\lambda_2 = 0$ ,  $\lambda_1$  direction creates no dynamics in the single excitation sector, but perturbatively brings down the two-excitation sector. However, before the gap to the two-excitation sector closes, a level crossing mediated by an excited state with a host of excitations leads to a first-order transition at  $\lambda_2 = 1$ .

To understand the role of the subsystem symmetries on the dynamics, we consider the cluster term of the Hamiltonian in Eq. D.25 and revisit the above discussion in light of the

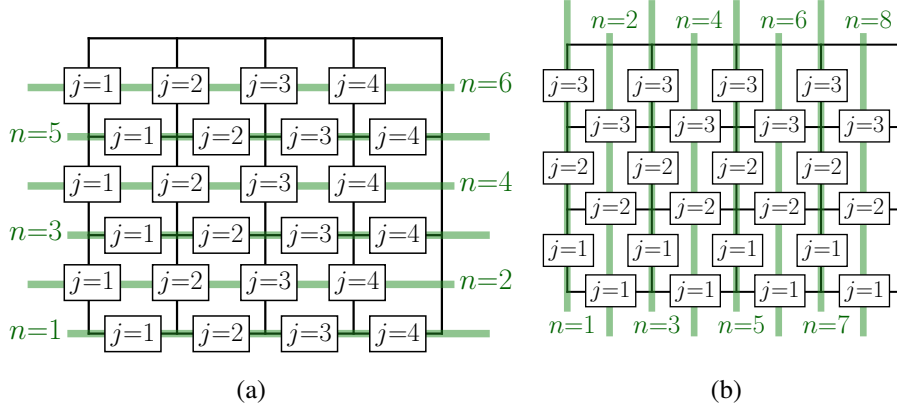


Figure D.4: The horizontal (in (a)) and vertical (in (b)) subsystems symmetries, in an open  $(L_x, L_y) = (4, 3)$  system.

sub-system symmetries. Consider the Hamiltonian given in Eq. D.25 which has two equivalent ways of considering the sub-symmetries which protect the SPT order. (i)  $P_1 = \prod_i \tau_{2i-1}^z, P_2 = \prod_i \tau_{2i}^z$  and (ii)  $P_1 = \prod_i \tau_{2i-1}^z \mathcal{K}_{2i-1}, P_2 = \prod_i \tau_{2i}^z \mathcal{K}_{2i}$ . A  $z$  perturbation preserves both pairs of symmetries (i) and (ii), leading to a sublattice preservation of the excitations. On the other hand, a  $y$  perturbation, given the way time-reversal symmetry behaves in this system, continues to preserve (ii) and does not change the eigenvalues of the horizontal sub-system symmetries with anti-unitary character. It is the same way that the  $y$ -perturbations don't change the eigenvalue of vertical subsystem symmetries (see Eq. 3.33). Therefore, excitations over the cluster state as generated by the  $y$  field are not constrained by horizontal and vertical sub-system symmetries.

#### D.4 Boundary modes of large $\Gamma$ Hamiltonian

Our discussion of the large  $\Gamma$  phase in  $(\lambda_1, \lambda_2)$  plane in section 3.2.3 focused on the bulk system, the corresponding phases, and tentative phase diagram of the same. We now discuss the nature of boundary modes in this system and which symmetries protect them.

We investigate how the subsystem symmetries (see Eq. 3.35) act on the boundaries in the  $(\lambda_1, \lambda_2) = (1, 1)$  point. It is easier to start from the  $\lambda_2 = 0$  line where we have a set of stacked cluster phases. When we are in one of the vertical SPTs (say  $H_3$ ). Interestingly one finds that both in the ground states of  $H_3$  and  $H_4$ ,

$$\{PT_{v_n}, PT_{v_{n+1}}\} = 0 \quad (\text{D.29})$$

on the top and bottom boundaries leading to  $2^{2L_x}$  degeneracies where  $PT_{v_n}$  symmetries are

given in Eq. 3.35 (see Fig D.4) . The corresponding horizontal subsystem symmetries given in Eq. 3.34 commutes leading to no protected boundary modes on the right and left boundaries for  $\tilde{H}_3$ .

Given the  $H_1$  and  $H_2$  perturbations respect the symmetries given in Eq. 3.35, the boundary modes on the top and bottom boundaries remain stable in all of  $(\lambda_1, \lambda_2)$  plane as is found leading to  $2^{2L_x}$  degeneracy even at the  $(1, 1)$  point. Interestingly given the energetics at the  $\lambda_2 = 2$  line, one gets additional boundary modes on the left and right boundaries which increases the degeneracy to  $2^{2(L_x+L_y)}$ .

We now investigate how the symmetries protect the boundary modes at  $\lambda_2 = 2$  line where we have boundary modes on all four boundaries. Here again for  $H_1$  (see Eq. 3.19) each of the vertical and horizontal sub-system symmetries (see Eq. 3.35) can be written as a product of stabilizers where it acts anomalously on the boundaries. For instance, the horizontal subsystem symmetries behave as

$$PT_{h_n}^L = \tau_{j=1+d_2}^z \quad \forall n \in \text{odd} \quad (\text{D.30})$$

$$PT_{h_n}^R = \tau_{j=L_x}^x \tau_{j=L_x-d_1}^z \mathcal{K}_{L_x} \quad \forall n \in \text{odd} \quad (\text{D.31})$$

$$PT_{h_n}^L = \tau_{j=1}^x \tau_{j=1+d_1}^z \mathcal{K}_{j=1} \quad \forall n \in \text{even} \quad (\text{D.32})$$

$$PT_{h_n}^R = \tau_{j=L_x-d_2}^z \quad \forall n \in \text{odd} \quad (\text{D.33})$$

It is easy to see that these anti-commutes on the left and right boundaries. The vertical subsystem symmetries are given by

$$PT_{v_n}^B = \tau_{j=1-d_2}^z \quad \forall n \in \text{odd} \quad (\text{D.34})$$

$$PT_{v_n}^T = \tau_{j=L_y}^x \tau_{j=L_y-d_1}^z \mathcal{K}_{j=L_y} \mathcal{K}_{j=L_y-d_1} \quad \forall n \in \text{odd} \quad (\text{D.35})$$

$$PT_{v_n}^B = \tau_{j=1}^x \tau_{j=1+d_1}^z \mathcal{K}_{j=1} \mathcal{K}_{j=1+d_1} \quad \forall n \in \text{even} \quad (\text{D.36})$$

$$PT_{v_n}^T = \tau_{j=L_y+d_2}^z \mathcal{K}_{j=L_y+d_2} \quad \forall n \in \text{odd} \quad (\text{D.37})$$

Since these anticommute on the top and bottom boundaries they again lead to the  $2^{2L_x}$  degeneracy. This shows why  $H_1$  has a  $2^{2L_x+2L_y-2}$  degeneracy in the system. A similar analysis for  $H_2$  shows the same degeneracy count. Therefore on the  $\lambda_2 = 2$  line the sub-system symmetries (see Eq. 3.35) protect the boundary modes on all the boundaries. Introduction of

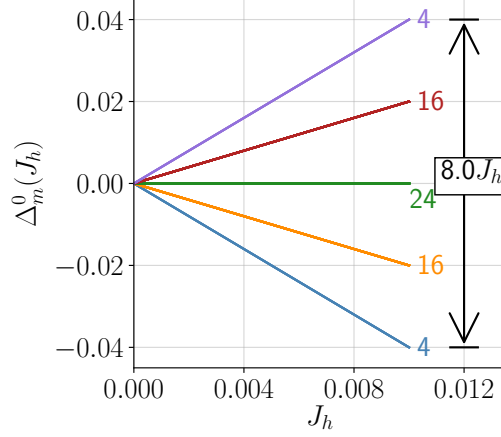


Figure D.5: Evolution of the ground state degeneracy splits in presence of an Ising exchange perturbation, see Eq. D.38. Along the y-axis we plot the energy of the  $m^{\text{th}}$  state after subtracting the  $J_h = 0$  GS energy, *i.e.*  $\Delta_m^0(J_h) = E_m(J_h) - E_0(J_h = 0)$ .

$H_3$  and  $H_4$  even while they do not break the symmetries interfere with the anomalous character of the symmetry operators since the way they behave in the bulk is dependent on the stabilizers. Since  $H_3$  and  $H_4$  couple spins in the vertical direction, they immediately hybridize the free spins which lie on the left and right boundaries leading to the removal of degeneracies stabilized in the  $\lambda_2 = 2$  limit. On the other hand, these same vertical SPTs stabilize free spins on the top and bottom boundaries, as discussed before, and hence do not disturb the degeneracies there. Hence the complete  $(\lambda_1, \lambda_2)$  has exact degeneracies on the top and bottom boundaries. Given these degeneracies are independent of any finite size (or therefore even when the bulk gap is dominated by Kubo gaps), these are stable and occur in all of  $(\lambda_1, \lambda_2)$  plane.

### D.5 Effect of perturbations on the boundary modes

The large  $\Gamma$  phase (see Eq. 3.21), at  $(\lambda_1, \lambda_2) = (1, 1)$  has a degeneracy of  $2^{2L_x}$  in an OBC geometry, see Fig. D.1(b), where  $L_x$  is the length of the top and bottom boundaries. We now study the effect of various perturbations on this ground state degenerate manifold.

**Symmetry allowed Ising perturbation:** When ferromagnetic Ising interactions among the boundary spins are introduced, which are allowed by the microscopic symmetries (see Eq. 2.12), we find that the top and the bottom boundaries behave as one-dimensional Ising Hamiltonians which spontaneously break time-reversal symmetry to order in the  $z$  direction.

More concretely, in a  $3 \times 3$  cluster (see Fig. D.1(b)) whose resulting Hamiltonian is

$$H(J_h) = H(1, 1) - J_h (\tau_0^z \tau_1^z + \tau_1^z \tau_2^z + \tau_{15}^z \tau_{16}^z + \tau_{16}^z \tau_{17}^z) \quad (\text{D.38})$$

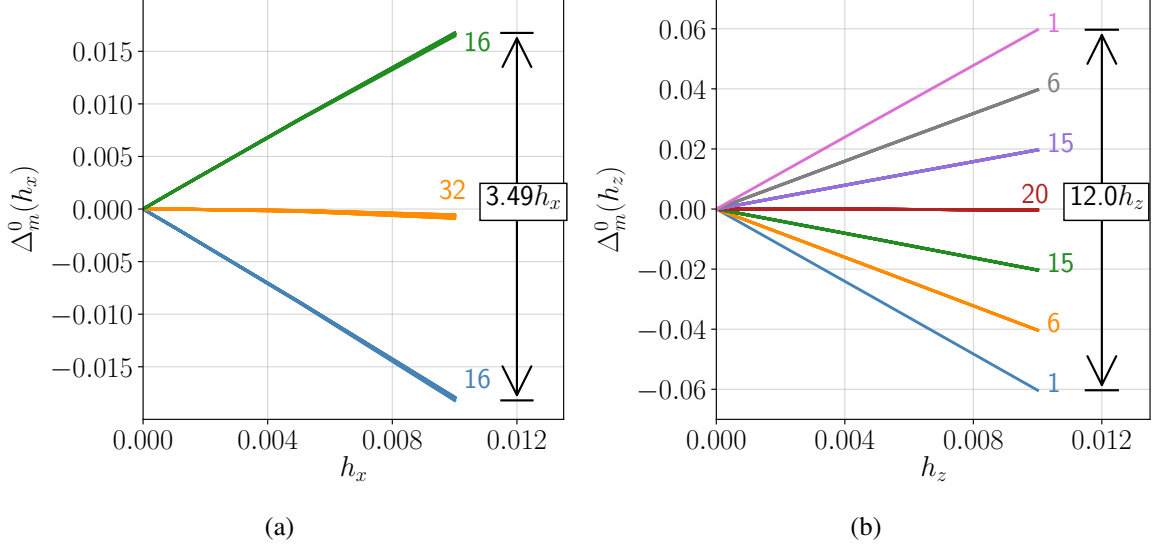


Figure D.6: Splitting of the degeneracy in an OBC geometry of the  $H(1, 1)$  (in Eq. 3.21) in the presence of  $\tau^{x(z)}$ -field as a function of the field strength ( $h_{x(z)}$ ), also see Eq. D.39.

the splitting of the ground state degenerate manifold is shown in Fig. D.5. Clearly among the  $2^{2L_x}|_{L_x=3} = 64$  degenerate states (at  $J_h = 0$ ), four unique states are chosen which correspond to the two Ising symmetry broken states in the top and bottom boundaries.

**Bulk  $\tau^{x(z)}$  field:** Next we apply the symmetry allowed (breaking) bulk  $\tau^{x(z)}$ -field to the  $(\lambda_1, \lambda_2) = (1, 1)$  point of the Hamiltonian in Eq. 3.21 in an OBC geometry. We consider the Hamiltonian:

$$H(h_{x(z)}) = H(1, 1) - h_{x(z)} \sum_i \tau_i^{x(z)} \quad (\text{D.39})$$

In Fig. D.6(a) and D.6(b) we show the corresponding results. Even while a symmetry allowed  $x$ -field splits the 64-fold degeneracy of the same  $3 \times 3$  cluster (see Fig. D.1(b)) into sub-branches, a time-reversal symmetry breaking  $\tau^z$  field immediately polarizes the boundary spins into a unique ground state.

The above analysis shows that even while the large  $\Gamma$  phase has a set of boundary modes (given its proximity to weak SPTs), these modes are extremely susceptible to both symmetry-preserving and symmetry-breaking perturbations, thereby reflecting their fragile character.

## D.6 Additional numerical results for the $\Gamma$ limit

To show that the large  $\Gamma$  phase is indeed smoothly connected to the paramagnet, we tune it to the  $x$ - paramagnet (via parameter  $\delta_1$ ) in presence of Ising perturbation ( $\propto \delta_2$ ) (see Eq. 5.4 in

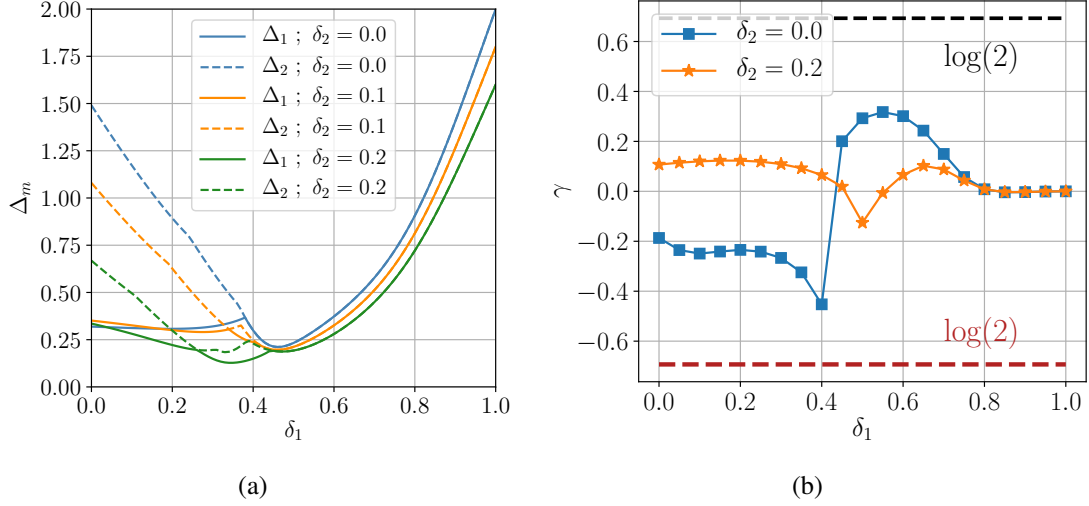


Figure D.7: (a) The first ( $\Delta_1$ ) and the second ( $\Delta_2$ ) gap to the GS energy following the Eq. 5.4 where we keep  $\delta_2$  constant and vary the  $\delta_1$  to tune the  $\Gamma$ -phase ( $\delta_1 = 0$ ) to a  $\tau^x$ -paramagnet ( $\delta_1 = 1$ ). The calculation is done for a system size  $L_x \times L_y = 2 \times 4$ . (b) The behavior of topological correction to the entanglement entropy ( $\gamma$ ) is shown for the Hamiltonian in Eq. 5.4 as a function of  $\delta_1$  for constant  $\delta_2 = 0.0, 0.2$ . The calculation is done in a  $(L_x, L_y) = (4 \times 3)$  lattice.

the main text). While the susceptibility comes down with increasing strength of Ising perturbation (see Fig. 5.8), one finds that the minima of energy gaps ( $\min(\Delta_m) = m^{\text{th}}$  excitation gap) remains finite as a function of  $\delta_1$  for different values of  $\delta_2$  (see Fig. D.7). One also finds that the topological entanglement entropy ( $\gamma$ ) remains close to zero across the complete interpolation showing that the large  $\Gamma$  phase is not a gapped topologically ordered state.

## APPENDIX E

### ADDITIONAL RESULTS IN THE ANISOTROPIC LIMIT OF THE AFM KITAEV MODEL

#### E.1 Additional numerical results for the $KJ\Gamma$ Hamiltonian

Here we present additional results for the behavior of bipartite entanglement for different cuts in the  $KJ\Gamma$  phase diagram (see Fig. 5.5).

Following Eq. 5.3, we calculate the different scaling coefficients of entanglement entropy (dubbed as  $X_{Fit}$ ;  $X = \alpha, \gamma$ ) along with the topological entanglement entropy ( $\gamma$ ) calculated using the Kitaev-Preskil method [64]. The behavior of these quantities in the  $\tilde{t}_2$  direction for  $\tilde{t}_1 = 0.0, 0.6$  is shown in Fig. E.1. Clearly both in FM and  $\Gamma$  phase,  $\gamma \sim 0$  while in  $Z_2$  QSL,  $\gamma \sim \log(2)$ .

#### E.2 Gauge Mean Field Theory

Following the discussions in section 7.1, we start our analysis by decoupling the first term in Eq. 7.86 within gauge mean field theory where the gauge fluctuations have been neglected. The first term in Eq. 7.86 is written using this decoupling as:  $[\mu_a^x \rho_{ab}^z \mu_b^x] [\rho_{bc}^x] \rightarrow \langle \mu_a^x \rho_{ab}^z \mu_b^x \rangle \rho_{bc}^x + \mu_a^x \rho_{ab}^z \mu_b^x \langle \rho_{bc}^x \rangle$ . Thus the Eq. 7.86 becomes:

$$\tilde{\mathcal{H}}_{\Gamma=0}^{AF} \rightarrow \tilde{\mathcal{H}}_{\Gamma=0}^{\text{GMFT}} = \tilde{\mathcal{H}}_{\Gamma=0}^{\text{GMFT}}(e) + \tilde{\mathcal{H}}_{\Gamma=0}^{\text{GMFT}}(m) \quad (\text{E.1})$$

where

$$\tilde{\mathcal{H}}_{\Gamma=0}^{\text{GMFT}}(e) = - \sum_{\langle ab \rangle \in H} J_{ab} \mu_a^x \rho_{ab}^z \mu_b^x - J_{TC} \sum_a \mu_a^z \quad (\text{E.2})$$

describes the  $e$  sector with

$$J_{ab} = J \left[ \langle \rho_{b,b-\hat{y}}^x \rangle + \langle \rho_{b,b+\hat{y}}^x \rangle + \langle \rho_{a,a-\hat{y}}^x \rangle + \langle \rho_{a,a+\hat{y}}^x \rangle \right] \quad (\text{E.3})$$

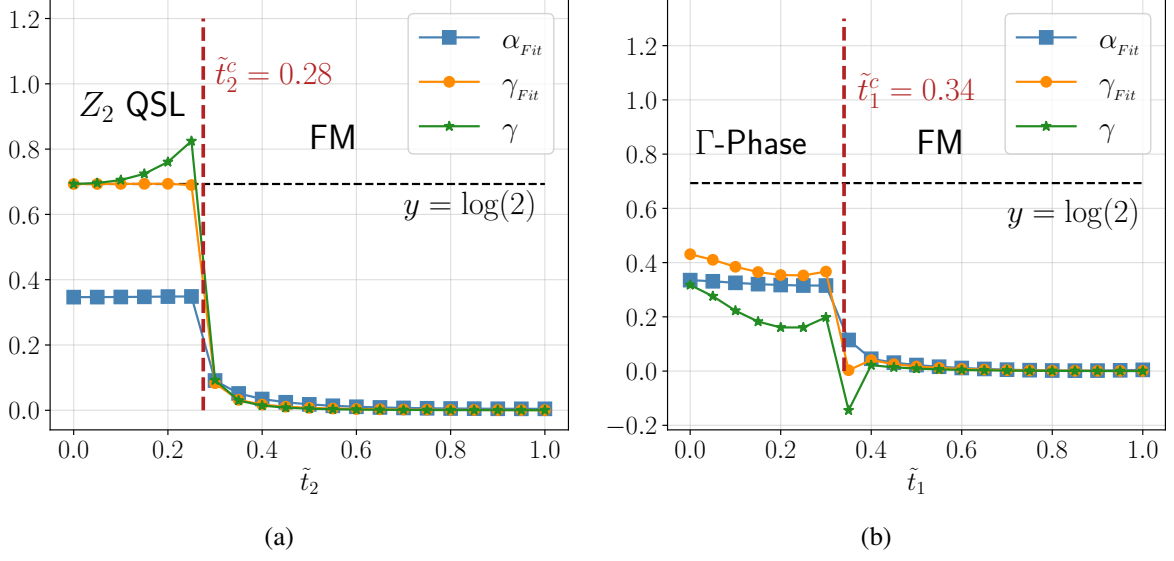


Figure E.1: Following Eq. 5.3 the values of  $\alpha_{Fit}$ ,  $\gamma_{Fit}$ ,  $\gamma$  are shown as we vary  $\tilde{t}_2$  (see Fig. 5.5) for a constant  $\tilde{t}_1 = 0.0$  in (a) and  $\tilde{t}_1 = 0.6$  in (b), the calculations are done in an  $(L_x, L_y) = (4, 3)$  system. Here a perturbing  $\tau^z$  magnetic field has been applied to break the degeneracy between the two-fold symmetry breaking GS manifold.

being the effective coupling and

$$\tilde{\mathcal{H}}_{\Gamma=0}^{\text{GMFT}}(m) = - \sum_{\langle \bar{a}\bar{b} \rangle \in H} J_{\bar{a}\bar{b}} \tilde{\mu}_{\bar{a}}^x \tilde{\rho}_{\bar{a}\bar{b}}^z \tilde{\mu}_{\bar{b}}^x - J_{TC} \sum_{\bar{a}} \tilde{\mu}_{\bar{a}}^z \quad (\text{E.4})$$

describes the  $m$  sector with

$$J_{\bar{a}\bar{b}} = J \left[ \langle \tilde{\rho}_{\bar{b}, \bar{b}-\hat{y}}^x \rangle + \langle \tilde{\rho}_{\bar{b}, \bar{b}+\hat{y}}^x \rangle + \langle \tilde{\rho}_{\bar{a}, \bar{a}-\hat{y}}^x \rangle + \langle \tilde{\rho}_{\bar{a}, \bar{a}+\hat{y}}^x \rangle \right] \quad (\text{E.5})$$

Upto the first order this becomes a series of transverse field Ising chains in the horizontal direction, we choose the following gauge:

$$\rho_{a, a+\hat{x}}^z = \tilde{\rho}_{\bar{a}, \bar{a}+\hat{x}}^z = +1 \quad (\text{E.6})$$

Clearly, in the presence of the Heisenberg term, the single excitation sector of  $e$  &  $m$  acquires a dispersion, the condensation of these soft modes gives rise to  $\langle \mu^x \rangle \neq 0$  and  $\langle \tilde{\mu}^x \rangle \neq 0$  for the respective chains.

For the above gauge, the soft mode develops at zero momentum as shown in Fig. 7.1 for

both the  $e$  and  $m$  sectors. This can be denoted by

$$\hat{\nu}_e^{(1)} = 1; \quad \hat{\nu}_m^{(1)} = 1 \quad (\text{E.7})$$

for the  $e$  ( $m$ ) sector on the direct (dual) lattice.

Time reversal symmetry (see Eq. 6.16) gives the partner soft mode for both the  $e$  and  $m$  sectors as shown in Fig. 7.1 which are given by

$$\hat{\nu}_e^{(2)} = e^{i\pi x}; \quad \hat{\nu}_m^{(2)} = e^{i\pi X} \quad (\text{E.8})$$

for the  $e$  sector and  $m$  sectors. The cartesian coordinates of the direct and dual lattices are given by  $(x, y)$  and  $(X, Y)$  with  $X = x+1/2$  and  $Y = y+1/2$  (red dashed line in Fig. 7.1(a) and 7.1(b)). Since no further soft modes are generated by the remaining symmetry, the transition out of the  $Z_2$ -QSL is described using these soft modes.

### E.3 Symmetry transformations of the soft modes

Now, using the symmetry transformations of the gauge degrees of freedoms in Eqs. 6.14-6.19, the transformations of the complex soft modes in Eqs. 7.89 and 7.90 are obtained:

$$\begin{aligned} \mathbf{T}_{\mathbf{d}_1} &: \begin{cases} \Phi_e \rightarrow \Phi_m \\ \Phi_m \rightarrow \Phi_e^* \end{cases} & \mathbf{T}_{\mathbf{d}_2} &: \begin{cases} \Phi_e \rightarrow \Phi_m^* \\ \Phi_m \rightarrow \Phi_e \end{cases} \\ \mathbf{T}_{\mathbf{x}} &: \begin{cases} \Phi_e \rightarrow \Phi_e^* \\ \Phi_m \rightarrow \Phi_m^* \end{cases} & \mathbf{T}_{\mathbf{y}} &: \begin{cases} \Phi_e \rightarrow \Phi_e \\ \Phi_m \rightarrow \Phi_m \end{cases} \\ \mathcal{T} &: \begin{cases} \Phi_e \rightarrow -i\Phi_e \\ \Phi_m \rightarrow -i\Phi_m \end{cases} & \sigma_v &: \begin{cases} \Phi_e \rightarrow \Phi_e \\ \Phi_m \rightarrow \Phi_m \end{cases} \\ C_{2z} &: \begin{cases} \Phi_e \rightarrow i\Phi_e^* \\ \Phi_m \rightarrow i\Phi_m^* \end{cases} & R_\pi &: \begin{cases} \Phi_e \rightarrow i\Phi_e^* \\ \Phi_m \rightarrow i\Phi_m^* \end{cases} \end{aligned} \quad (\text{E.9})$$

Here we note that the  $\sigma^v$  and  $R_\pi$  symmetries act differently on the soft modes compared to the FM case (section 7.1.1). The gauge invariant spin order parameter in terms of the above soft modes is [75, 108, 114]:

$$\begin{aligned}
\tilde{\tau}_i^z &\sim |\Phi_e|^2 \cos(2\theta^e) \quad \forall i \in \text{Horizontal bonds} \\
\tilde{\tau}_i^x &\sim |\Phi_m|^2 \cos(2\theta^m) \quad \forall i \in \text{Vertical bonds}
\end{aligned} \tag{E.10}$$

Crucially, the two spin order parameters are odd under  $\mathcal{T}$ ,  $C_{2z}$ ,  $R_\pi$  symmetry transformations.

#### E.4 Symmetry transformation of the gauge fields

Following the  $U(1) \times U(1)$  mutual CS formalism, we introduce two internal gauge fields  $A_\mu$  and  $B_\mu$  in Eq. 7.91 that minimally couples to the electric ( $\Phi_e$ ) and magnetic ( $\Phi_m$ ) soft modes respectively. The transformation rules for the gauge fields follow from Eqs. 6.14-6.19.

$$\begin{aligned}
\mathbf{T}_{\mathbf{d}_1} &: \begin{cases} A_\mu \rightarrow B_\mu \\ B_\mu \rightarrow -A_\mu \end{cases} & \mathbf{T}_{\mathbf{d}_2} &: \begin{cases} A_\mu \rightarrow -B_\mu \\ B_\mu \rightarrow A_\mu \end{cases} \\
\mathbf{T}_{\mathbf{x}} &: \begin{cases} A_\mu \rightarrow -A_\mu \\ B_\mu \rightarrow -B_\mu \end{cases} & \mathbf{T}_{\mathbf{y}} &: \begin{cases} A_\mu \rightarrow A_\mu \\ B_\mu \rightarrow B_\mu \end{cases} \\
\mathcal{T} &: \begin{cases} A_\mu \rightarrow -A_\mu \\ B_\mu \rightarrow -B_\mu \end{cases} \\
\sigma_v &: \begin{cases} A_x \rightarrow A_x, A_y \rightarrow -A_y, A_\tau \rightarrow A_\tau \\ B_x \rightarrow B_x, B_y \rightarrow -B_y, B_\tau \rightarrow B_\tau \end{cases} \\
C_{2z} &: \begin{cases} A_x \rightarrow A_x, A_y \rightarrow -A_y, A_\tau \rightarrow -A_\tau \\ B_x \rightarrow B_x, B_y \rightarrow -B_y, B_\tau \rightarrow -B_\tau \end{cases} \\
R_\pi &: \begin{cases} A_x \rightarrow A_x, A_y \rightarrow A_y, A_\tau \rightarrow -A_\tau \\ B_x \rightarrow B_x, B_y \rightarrow B_y, B_\tau \rightarrow -B_\tau \end{cases}
\end{aligned} \tag{E.11}$$

#### E.5 The phases

To capture the phases at the mean-field level, for  $u > 0$ , we have

$$\langle \Phi_e \rangle = \langle \Phi_m \rangle = 0 \quad (\text{E.12})$$

Thus the complex soft modes can be integrated out so that the effective theory is described by  $\mathcal{S}_{CS}$ , which is the  $Z_2$  QSL phase.

For  $u < 0$  both the electric and magnetic modes condense, *i.e.*,

$$\langle \Phi_e \rangle, \langle \Phi_m \rangle \neq 0 \quad (\text{E.13})$$

In this case, due to the Anderson-Higgs mechanism, the gauge fields acquire a mass and their dynamics are dropped. The four-fold terms in Eqs. 7.22 and 7.23 becomes

$$\sim -\lambda (|\Phi_e|^4 \cos(4\theta^e) + |\Phi_m|^4 \cos(4\theta^m)) \quad (\text{E.14})$$

Therefore, for  $\lambda > 0$  the free energy minima occurs for

$$\theta^e, \theta^m = 0, \pm\pi/2, \pi \quad (\text{E.15})$$

which gives the two possible symmetry-broken partner spin-ordered states as:

$$\begin{aligned} \langle \tilde{\tau}_i^z \rangle &\sim \langle |\Phi_e|^2 \cos(2\theta^e) \rangle \sim \pm 1 \quad \forall i \in \text{Horizontal bonds} \\ \langle \tilde{\tau}_i^x \rangle &\sim \langle |\Phi_m|^2 \cos(2\theta^m) \rangle \sim \pm 1 \quad \forall i \in \text{Vertical bonds} \end{aligned} \quad (\text{E.16})$$

Further the state breaks  $\mathcal{T}$ ,  $C_{2z}$  and  $R_\pi$ . In this phase, the interaction between the electric and the magnetic modes (Eq. 7.24) can be written as

$$\mathcal{L}_{em} \sim w |\Phi_e|^2 |\Phi_m|^2 \cos(2\theta^e) \cos(2\theta^m) \quad (\text{E.17})$$

For  $w < 0 (> 0)$ , this results in ferromagnetic (antiferromagnetic) spin ordering in terms of  $\tilde{\tau}^x$  (on horizontal bonds) and  $\tilde{\tau}^z$  (on the vertical bonds). The antiferromagnetic order also breaks translation symmetry under  $\mathbf{T}_{d_1}$  and  $\mathbf{T}_{d_2}$  which interchanges a vertical and horizontal

bond. The above phenomenology suggest  $w \sim \text{sgn}(J)$ . Therefore the above critical theory indeed reproduces the right phases.

## E.6 The details of the mutual $Z_2$ gauge theory formulation

The partition function corresponding to the mutual  $Z_2$  action (Eq. 7.97) is given by

$$\mathcal{Z} = \sum_{\{\rho\}} \sum_{\{\bar{\rho}\}} \int [\mathcal{D}\theta^e] [\mathcal{D}\theta^m] \exp[-\mathcal{S}] \quad (\text{E.18})$$

where  $\mathcal{S}$  is given by Eq. 7.97.

For further manipulation, we re-write the above partition function as

$$\mathcal{Z} = \sum_{\{\bar{\rho}\}} \int [\mathcal{D}\theta^m] \exp[-\mathcal{S}_m] \mathcal{Z}_e \quad (\text{E.19})$$

where

$$\mathcal{Z}_e = \sum_{\{\rho\}} \int [\mathcal{D}\theta^e] \exp[-\mathcal{S}_e - \mathcal{S}_{CS}] \quad (\text{E.20})$$

We now write the electric action,  $\mathcal{S}_e$ , as in Eq. 7.101 and perform standard steps of XY duality in presence of a  $Z_2$  gauge field [138–140]

Starting with writing it down within a Villain approximation as

$$\mathcal{Z}_e = \sum_{\{\rho\}} \sum_{\{m_{ab}\}} \int [\mathcal{D}\theta^e] \exp[-\mathcal{S}_{CS}] \exp[-\mathcal{S}_e^{(1)}] \quad (\text{E.21})$$

$m_{ab}$  is an integer field living on the links of the direct lattice and

$$\mathcal{S}_e^{(1)} = -t \sum_{ab} \left( \theta_a^e - \theta_b^e + \frac{\pi}{2}(1 - \rho_{ab}) + 2\pi m_{ab} \right)^2 \quad (\text{E.22})$$

which we can decouple via an auxiliary link field  $L_{ab}$  to get

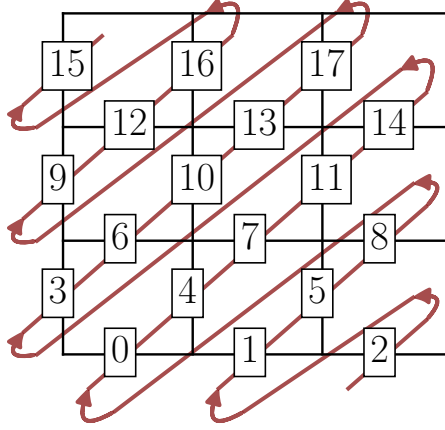


Figure E.2: A single Jordan Wigner string running through the  $H_1$  direction in an open system.

$$\mathcal{Z}_e = \sum_{\{\rho\}} \sum_{\{m_{ab}\}} \int [\mathcal{D}\theta^e] [\mathcal{D}L] \exp[-\mathcal{S}_{CS}] \exp[-\mathcal{S}_e^{(2)}] \quad (\text{E.23})$$

where

$$\mathcal{S}_e^{(2)} = \frac{1}{2t} \sum_{ab} L_{ab}^2 + iL_{ab} \left( \Delta_j \theta_a^e + \frac{\pi}{2} (1 - \rho_{ab}) + 2\pi m_{ab} \right) \quad (\text{E.24})$$

The integer field  $m_{ab}$  can be integrated out and restricts  $L_{ab}$  to an integer leading to Eq. 7.102 in the main text.

## APPENDIX F

### A POSSIBLE TRANSITION BETWEEN THE $Z_2$ QSL AND A CLUSTER SPT

#### F.1 Transition between $Z_2$ QSL and a cluster SPT

It is interesting to consider the phase transition between the  $Z_2$  QSL in the Toric code limit and each of the cluster SPTs given by Eq. 3.20. Such transitions provide examples of yet a new class of novel phase transitions even though presently we do not know a mechanism to stabilize either the cluster SPT phase or this transition in the spin system that we have considered. As we discuss below, this transition is naturally described in terms of Majorana fermions rather than the spins, which makes the transition different from the above class of *bosonic* transitions discussed above—hence we describe them.

In this Appendix, we develop the mean-field theory, in particular, for the transition between the  $Z_2$  QSL with Hamiltonian given by Eq. 3.13 and the stacked cluster SPT  $H_1$ , given by Eq. 3.20 such that the Hamiltonian is given by :

$$H' = \sum_i [\alpha \tau_{i+d_1}^z \tau_i^x \tau_{i-d_1}^z + (1 - \alpha) \tau_{i+d_1}^z \tau_{i-d_2}^z \tau_i^y \tau_{i+d_1-d_2}^y] \quad (\text{F.1})$$

where  $\alpha$  is the parameter that can be tuned to drive the phase transition. For an open system using the Jordan-Wigner transformations of Eq. D.11 as defined in Fig. E.2 the above Hamiltonian becomes

$$H' = \sum_i [\alpha i \tilde{\gamma}_{i-d_1} \gamma_{i+d_1} + (1 - \alpha) \tilde{\gamma}_{i-d_2} \tilde{\gamma}_{i-d_2+d_1} \gamma_i \gamma_{i+d_1}] \quad (\text{F.2})$$

where  $(\tilde{\gamma}_i, \gamma_i)$  are the two Majorana fermions at site  $i$  such that under time-reversal symmetry  $\mathcal{T} : (\tilde{\gamma}_i, \gamma_i) \rightarrow (\tilde{\gamma}_i, -\gamma_i)$ .

In the transformed language, each chain in the stacked cluster SPT at  $\alpha = 0$  is a pair of spin-less topological superconductors whereas the  $Z_2$  QSL is a cluster Mott insulator.

A mean-field decomposition of the four Majorana terms along the time-reversal invariant

channels leads to

$$\begin{aligned}
\tilde{\gamma}_{i-d_2} \tilde{\gamma}_{i-d_2+d_1} \gamma_i \gamma_{i+d_1} &\rightarrow \langle i \tilde{\gamma}_{i-d_2} \gamma_i \rangle i \tilde{\gamma}_{i-d_2+d_1} \gamma_{i+d_1} \\
&+ i \tilde{\gamma}_{i-d_2} \gamma_i \langle i \tilde{\gamma}_{i-d_2+d_1} \gamma_{i+d_1} \rangle \\
&- \langle i \tilde{\gamma}_{i-d_2} \gamma_{i+d_1} \rangle i \tilde{\gamma}_{i-d_2+d_1} \gamma_i \\
&- i \tilde{\gamma}_{i-d_2} \gamma_{i+d_1} \langle i \tilde{\gamma}_{i-d_2+d_1} \gamma_i \rangle
\end{aligned} \tag{F.3}$$

Let us define the following mean-field ansatz:

$$\begin{aligned}
\zeta_1 &\equiv \langle i \tilde{\gamma}_{i-d_2} \gamma_i \rangle ; \quad \zeta_2 \equiv \langle i \tilde{\gamma}_{i-d_2+d_1} \gamma_{i+d_1} \rangle \\
\zeta_3 &\equiv \langle i \tilde{\gamma}_{i-d_2} \gamma_{i+d_1} \rangle ; \quad \zeta_4 \equiv \langle i \tilde{\gamma}_{i-d_2+d_1} \gamma_i \rangle
\end{aligned} \tag{F.4}$$

which we consider as variational parameters and study the spectrum of the quadratic Hamiltonian as a function of  $\alpha$ . Symmetry dictates that  $\zeta_1 = \zeta_2 = \zeta$ ; Fourier transforming and defining  $\Psi^T = (\tilde{\gamma}_k, \gamma_k)$ , where  $k = (k_1, k_2)$  are the reciprocal lattice vectors in  $d_1, d_2$  direction respectively, the Hamiltonian one obtains is

$$H = \sum_k \Psi^\dagger \begin{pmatrix} 0 & f(k) \\ f^*(k) & 0 \end{pmatrix} \Psi \tag{F.5}$$

where

$$f(k) = i e^{-2ik_1} (\alpha + (\alpha - 1) e^{i(k_1 - k_2)}) (\zeta_4 - 2\zeta e^{ik_1} + \zeta_3 e^{2ik_1}) \tag{F.6}$$

If  $\zeta_3 = \zeta_4 = 0$  for a fixed  $\zeta_1 = \frac{1}{2} = \zeta$ ,  $f(k) = i\alpha e^{-2ik_1} - i(\alpha - 1) e^{-ik_2}$  which implies a direct transition with a gap closing along the complete  $k_2 = 2k_1 + \pi$  line when  $\alpha = 0.5$ . With a finite value of  $\zeta_3, \zeta_4$  the nodal line semimetal opens up into a phase with nodal points hosting anisotropic Dirac dispersion. Generically one, therefore, expects an intermediate gapless phase in the finite region of  $\alpha$  when interpolating between a weak SPT and a toric code  $Z_2$  QSL.

## BIBLIOGRAPHY

- [1] A. Auerbach, “Interacting electrons and quantum magnetism,” 1998.
- [2] S. Sachdev, “Quantum phase transitions,” *Physics world*, vol. 12, no. 4, p. 33, 1999.
- [3] D. P. Arovas, E. Berg, S. A. Kivelson, and S. Raghu, “The hubbard model,” *Annual Review of Condensed Matter Physics*, vol. 13, no. 1, pp. 239–274, 2022.
- [4] P. W. Anderson, “Basic notions of condensed matter physics,” 2018.
- [5] T. Senthil, A. Vishwanath, L. Balents, S. Sachdev, and M. P. Fisher, “Deconfined quantum critical points,” *Science*, vol. 303, no. 5663, pp. 1490–1494, 2004.
- [6] T Senthil, L. Balents, S. Sachdev, A. Vishwanath, and M. P. Fisher, “Quantum criticality beyond the landau-ginzburg-wilson paradigm,” *Physical Review B*, vol. 70, no. 14, p. 144 407, 2004.
- [7] L. Savary and L. Balents, “Quantum spin liquids: A review,” *Reports on Progress in Physics*, vol. 80, no. 1, p. 016 502, 2016.
- [8] H. Diep *et al.*, *Frustrated spin systems*. World Scientific, 2013.
- [9] L. Balents, “Spin liquids in frustrated magnets,” *Nature*, vol. 464, no. 7286, pp. 199–208, 2010.
- [10] P. A. Lee, “An end to the drought of quantum spin liquids,” *Science*, vol. 321, no. 5894, pp. 1306–1307, 2008.
- [11] X.-G. Wen, “Quantum orders and symmetric spin liquids,” *Physical Review B*, vol. 65, no. 16, p. 165 113, 2002.
- [12] T Senthil, “Quantum matters: Physics beyond landau’s paradigms,” *International Journal of Modern Physics B*, vol. 20, no. 19, pp. 2603–2611, 2006.
- [13] S.-P. Kou, X.-L. Qi, and Z.-Y. Weng, “Mutual chern-simons effective theory of doped antiferromagnets,” *Phys. Rev. B*, vol. 71, p. 235 102, 23 2005.
- [14] W. Witczak-Krempa, G. Chen, Y. B. Kim, and L. Balents, “Correlated quantum phenomena in the strong spin-orbit regime,” *Annu. Rev. Condens. Matter Phys.*, vol. 5, no. 1, pp. 57–82, 2014.

- [15] G. Jackeli and G. Khaliullin, “Mott insulators in the strong spin-orbit coupling limit: From heisenberg to a quantum compass and kitaev models,” *Phys. Rev. Lett.*, vol. 102, p. 017 205, 1 2009.
- [16] A. Kitaev, “Anyons in an exactly solved model and beyond,” *Annals of Physics*, vol. 321, no. 1, pp. 2–111, 2006.
- [17] P. Anderson, “Resonating valence bonds: A new kind of insulator?” *Materials Research Bulletin*, vol. 8, no. 2, pp. 153–160, 1973.
- [18] P. W. Anderson, “The resonating valence bond state in  $\text{La}_2\text{CuO}_4$  and superconductivity,” *science*, vol. 235, no. 4793, pp. 1196–1198, 1987.
- [19] P. A. Lee, N. Nagaosa, and X.-G. Wen, “Doping a mott insulator: Physics of high-temperature superconductivity,” *Reviews of Modern Physics*, vol. 78, no. 1, p. 17, 2006.
- [20] R. Moessner and S. L. Sondhi, “Resonating valence bond phase in the triangular lattice quantum dimer model,” *Phys. Rev. Lett.*, vol. 86, pp. 1881–1884, 9 2001.
- [21] X.-G. Wen, “Colloquium: Zoo of quantum-topological phases of matter,” *Reviews of Modern Physics*, vol. 89, no. 4, p. 041 004, 2017.
- [22] C Broholm, R. Cava, S. Kivelson, D. Nocera, M. Norman, and T Senthil, “Quantum spin liquids,” *Science*, vol. 367, no. 6475, 2020.
- [23] H. B. Cao *et al.*, “Low-temperature crystal and magnetic structure of  $\alpha\text{-RuCl}_3$ ,” *Phys. Rev. B*, vol. 93, p. 134 423, 13 2016.
- [24] A Banerjee *et al.*, “Proximate kitaev quantum spin liquid behaviour in a honeycomb magnet,” *Nature materials*, vol. 15, no. 7, pp. 733–740, 2016.
- [25] A. Banerjee *et al.*, “Neutron scattering in the proximate quantum spin liquid  $\alpha\text{-RuCl}_3$ ,” *Science*, vol. 356, no. 6342, pp. 1055–1059, 2017.
- [26] S. Trebst, “Kitaev materials,” *arXiv preprint arXiv:1701.07056*, 2017.
- [27] J. Knolle, S. Bhattacharjee, and R. Moessner, “Dynamics of a quantum spin liquid beyond integrability: The kitaev-heisenberg- $\Gamma$  model in an augmented parton mean-field theory,” *Phys. Rev. B*, vol. 97, p. 134 432, 13 2018.
- [28] K. A. Ross *et al.*, “Two-dimensional kagome correlations and field induced order in the ferromagnetic  $XY$  pyrochlore  $\text{Yb}_2\text{Ti}_2\text{O}_7$ ,” *Phys. Rev. Lett.*, vol. 103, p. 227 202, 22 2009.

- [29] K. A. Ross, L. Savary, B. D. Gaulin, and L. Balents, “Quantum excitations in quantum spin ice,” *Phys. Rev. X*, vol. 1, p. 021 002, 2 2011.
- [30] J. Gaudet *et al.*, “Gapless quantum excitations from an icelike splayed ferromagnetic ground state in stoichiometric  $\text{Yb}_2\text{Ti}_2\text{O}_7$ ,” *Phys. Rev. B*, vol. 93, p. 064 406, 6 2016.
- [31] J. D. Thompson, P. A. McClarty, D. Prabhakaran, I. Cabrera, T. Guidi, and R. Coldea, “Quasiparticle breakdown and spin hamiltonian of the frustrated quantum pyrochlore  $\text{Yb}_2\text{Ti}_2\text{O}_7$  in a magnetic field,” *Phys. Rev. Lett.*, vol. 119, p. 057 203, 5 2017.
- [32] A. Scheie *et al.*, “Reentrant phase diagram of  $\text{Yb}_2\text{Ti}_2\text{O}_7$  in a  $\Gamma_1$  magnetic field,” *Phys. Rev. Lett.*, vol. 119, p. 127 201, 12 2017.
- [33] R. Hentrich *et al.*, “Unusual phonon heat transport in  $\alpha$ - $\text{RuCl}_3$ : Strong spin-phonon scattering and field-induced spin gap,” *Phys. Rev. Lett.*, vol. 120, p. 117 204, 11 2018.
- [34] A. Banerjee *et al.*, “Excitations in the field-induced quantum spin liquid state of  $\alpha$ - $\text{RuCl}_3$ ,” *npj Quantum Materials*, vol. 3, no. 1, pp. 1–7, 2018.
- [35] A. N. Ponomaryov *et al.*, “Unconventional spin dynamics in the honeycomb-lattice material  $\alpha$ - $\text{RuCl}_3$ : High-field electron spin resonance studies,” *Phys. Rev. B*, vol. 96, p. 241 107, 24 2017.
- [36] A. Little *et al.*, “Antiferromagnetic resonance and terahertz continuum in  $\alpha$ - $\text{RuCl}_3$ ,” *Phys. Rev. Lett.*, vol. 119, p. 227 201, 22 2017.
- [37] Y. Kasahara *et al.*, “Majorana quantization and half-integer thermal quantum hall effect in a kitaev spin liquid,” *Nature*, vol. 559, no. 7713, pp. 227–231, 2018.
- [38] P. Czajka *et al.*, “Oscillations of the thermal conductivity in the spin-liquid state of  $\alpha$ - $\text{RuCl}_3$ ,” *Nature Physics*, vol. 17, no. 8, pp. 915–919, 2021.
- [39] G. Baskaran, S. Mandal, and R. Shankar, “Exact results for spin dynamics and fractionalization in the kitaev model,” *Phys. Rev. Lett.*, vol. 98, p. 247 201, 24 2007.
- [40] P. M. Chaikin, T. C. Lubensky, and T. A. Witten, *Principles of condensed matter physics*. Cambridge university press Cambridge, 1995, vol. 10.
- [41] S.-P. Kou, M. Levin, and X.-G. Wen, “Mutual chern-simons theory for  $Z_2$  topological order,” *Phys. Rev. B*, vol. 78, p. 155 134, 15 2008.

- [42] M. Freedman, C. Nayak, K. Shtengel, K. Walker, and Z. Wang, “A class of p, t-invariant topological phases of interacting electrons,” *Annals of Physics*, vol. 310, no. 2, pp. 428–492, 2004.
- [43] J. c. v. Chaloupka, G. Jackeli, and G. Khaliullin, “Kitaev-heisenberg model on a honeycomb lattice: Possible exotic phases in iridium oxides  $A_2\text{IrO}_3$ ,” *Phys. Rev. Lett.*, vol. 105, p. 027 204, 2 2010.
- [44] J. G. Rau, E. K.-H. Lee, and H.-Y. Kee, “Generic spin model for the honeycomb iridates beyond the kitaev limit,” *Phys. Rev. Lett.*, vol. 112, p. 077 204, 7 2014.
- [45] M. Hermanns, I. Kimchi, and J. Knolle, “Physics of the kitaev model: Fractionalization, dynamical correlations, and material connections,” *Annual Review of Condensed Matter Physics*, vol. 9, no. 1, null, 2018, ArXiv:1705.01740.
- [46] Y. Singh and P. Gegenwart, “Antiferromagnetic mott insulating state in single crystals of the honeycomb lattice material  $\text{Na}_2\text{IrO}_3$ ,” *Phys. Rev. B*, vol. 82, p. 064 412, 6 2010.
- [47] X. Liu *et al.*, “Long-range magnetic ordering in  $\text{na}_2\text{iro}_3$ ,” *Phys. Rev. B*, vol. 83, p. 220 403, 22 2011.
- [48] Y. Singh *et al.*, “Relevance of the heisenberg-kitaev model for the honeycomb lattice iridates  $A_2\text{IrO}_3$ ,” *Phys. Rev. Lett.*, vol. 108, p. 127 203, 12 2012.
- [49] S. K. Choi *et al.*, “Spin waves and revised crystal structure of honeycomb iridate  $\text{Na}_2\text{IrO}_3$ ,” *Phys. Rev. Lett.*, vol. 108, p. 127 204, 12 2012.
- [50] F. Ye *et al.*, “Direct evidence of a zigzag spin-chain structure in the honeycomb lattice: A neutron and x-ray diffraction investigation of single-crystal  $\text{na}_2\text{iro}_3$ ,” *Phys. Rev. B*, vol. 85, p. 180 403, 18 2012.
- [51] A. Biffin *et al.*, “Unconventional magnetic order on the hyperhoneycomb kitaev lattice in  $\beta$ -  $\text{li}_2\text{iro}_3$ : Full solution via magnetic resonant x-ray diffraction,” *Phys. Rev. B*, vol. 90, p. 205 116, 20 2014.
- [52] A. Biffin *et al.*, “Noncoplanar and counterrotating incommensurate magnetic order stabilized by kitaev interactions in  $\gamma$ -  $\text{li}_2\text{iro}_3$ ,” *Phys. Rev. Lett.*, vol. 113, p. 197 201, 19 2014.
- [53] Z. Nussinov and J. v. d. Brink, “Compass and kitaev models—theory and physical motivations,” *arXiv preprint arXiv:1303.5922*, 2013.

- [54] I. Kimchi and A. Vishwanath, “Kitaev-heisenberg models for iridates on the triangular, hyperkagome, kagome, fcc, and pyrochlore lattices,” *Phys. Rev. B*, vol. 89, p. 014 414, 1 2014.
- [55] E. K.-H. Lee, R. Schaffer, S. Bhattacharjee, and Y. B. Kim, “Heisenberg-kitaev model on the hyperhoneycomb lattice,” *Physical Review B*, vol. 89, no. 4, p. 045 117, 2014.
- [56] J. Reuther, R. Thomale, and S. Trebst, “Finite-temperature phase diagram of the heisenberg-kitaev model,” *Phys. Rev. B*, vol. 84, p. 100 406, 10 2011.
- [57] H.-C. Jiang, Z.-C. Gu, X.-L. Qi, and S. Trebst, “Possible proximity of the mott insulating iridate  $\text{Na}_2\text{IrO}_3$  to a topological phase: Phase diagram of the heisenberg-kitaev model in a magnetic field,” *Phys. Rev. B*, vol. 83, p. 245 104, 24 2011.
- [58] J. Oitmaa, “Phase diagram of the heisenberg-kitaev model at  $T = 0$ ,” *Phys. Rev. B*, vol. 92, p. 020 405, 2 2015.
- [59] R. Schaffer, S. Bhattacharjee, and Y. B. Kim, “Quantum phase transition in heisenberg-kitaev model,” *Phys. Rev. B*, vol. 86, p. 224 417, 22 2012.
- [60] C. C. Price and N. B. Perkins, “Critical properties of the kitaev-heisenberg model,” *Phys. Rev. Lett.*, vol. 109, p. 187 201, 18 2012.
- [61] M. Gohlke, G. Wachtel, Y. Yamaji, F. Pollmann, and Y. B. Kim, “Quantum spin liquid signatures in kitaev-like frustrated magnets,” *Phys. Rev. B*, vol. 97, p. 075 126, 7 2018.
- [62] H.-Y. Lee *et al.*, “Magnetic field induced quantum phases in a tensor network study of kitaev magnets,” *Nature communications*, vol. 11, no. 1, pp. 1–7, 2020.
- [63] D. Gotfryd, K. Wohlfeld, G. Jackeli, J. c. v. Chaloupka, “Phase diagram and spin correlations of the kitaev-heisenberg model: Importance of quantum effects,” *Phys. Rev. B*, vol. 95, p. 024 426, 2 2017.
- [64] A. Kitaev and J. Preskill, “Topological entanglement entropy,” *Physical review letters*, vol. 96, no. 11, p. 110 404, 2 2006.
- [65] M. Levin and X.-G. Wen, “Detecting topological order in a ground state wave function,” *Physical review letters*, vol. 96, no. 11, p. 110 405, 2 2006.
- [66] O. I. Motrunich and T. Senthil, “Origin of artificial electrodynamics in three-dimensional bosonic models,” *Phys. Rev. B*, vol. 71, p. 125 102, 12 2005.

- [67] J. Vidal, R. Thomale, K. P. Schmidt, and S. Dusuel, “Self-duality and bound states of the toric code model in a transverse field,” *Phys. Rev. B*, vol. 80, p. 081 104, 8 2009.
- [68] S. Dusuel, M. Kamfor, R. Orús, K. P. Schmidt, and J. Vidal, “Robustness of a perturbed topological phase,” *Phys. Rev. Lett.*, vol. 106, p. 107 203, 10 2011.
- [69] A. Y. Kitaev, “Fault-tolerant quantum computation by anyons,” *Annals of Physics*, vol. 303, no. 1, pp. 2–30, 2 2003.
- [70] E. Quinn, S. Bhattacharjee, and R. Moessner, “Phases and phase transitions of a perturbed kekulé-kitaev model,” *Phys. Rev. B*, vol. 91, p. 134 419, 13 2015.
- [71] Villain, J., Bidaux, R., Carton, J.-P., and Conte, R., “Order as an effect of disorder,” *J. Phys. France*, vol. 41, no. 11, pp. 1263–1272, 2 1980.
- [72] R Moessner and S. L. Sondhi, “Ising models of quantum frustration,” *Physical Review B*, vol. 63, no. 22, p. 224 401, 2 2001.
- [73] Y.-Z. You, I. Kimchi, and A. Vishwanath, “Doping a spin-orbit mott insulator: Topological superconductivity from the kitaev-heisenberg model and possible application to  $(\text{na}_2/\text{li}_2)\text{iro}_3$ ,” *Phys. Rev. B*, vol. 86, p. 085 145, 8 2012.
- [74] X.-G. Wen, “Quantum orders in an exact soluble model,” *Phys. Rev. Lett.*, vol. 90, p. 016 803, 1 2003.
- [75] C. Xu and S. Sachdev, “Global phase diagrams of frustrated quantum antiferromagnets in two dimensions: Doubled chern-simons theory,” *Physical Review B*, vol. 79, no. 6, p. 064 405, 2 2009.
- [76] E.-G. Moon and C. Xu, “Exotic continuous quantum phase transition between  $\mathbb{Z}_2$  topological spin liquid and néel order,” *Phys. Rev. B*, vol. 86, p. 214 414, 21 2012.
- [77] H. W. J. Blöte and Y. Deng, “Cluster monte carlo simulation of the transverse ising model,” *Phys. Rev. E*, vol. 66, p. 066 110, 6 2002.
- [78] A. F. Albuquerque, F. Alet, C. Sire, and S. Capponi, “Quantum critical scaling of fidelity susceptibility,” *Phys. Rev. B*, vol. 81, p. 064 418, 6 2010.
- [79] B. Blaß and H. Rieger, “Test of quantum thermalization in the two-dimensional transverse-field ising model,” *Scientific Reports*, vol. 6, no. 38185, p. 024 426, 2 2016.
- [80] C.-J. Huang, L. Liu, Y. Jiang, and Y. Deng, “Worm-algorithm-type simulation of the quantum transverse-field ising model,” *Phys. Rev. B*, vol. 102, p. 094 101, 9 2020.

- [81] Y. You, T. Devakul, F. J. Burnell, and S. L. Sondhi, “Subsystem symmetry protected topological order,” *Phys. Rev. B*, vol. 98, p. 035 112, 3 2018.
- [82] X. Chen, Y.-M. Lu, and A. Vishwanath, “Symmetry-protected topological phases from decorated domain walls,” *Nature communications*, vol. 5, no. 1, pp. 1–11, 2 2014.
- [83] W. Son, L. Amico, and V. Vedral, “Topological order in 1d cluster state protected by symmetry,” *Quantum Information Processing*, vol. 11, no. 6, pp. 1961–1968, 2 2012.
- [84] M. A. Nielsen, “Cluster-state quantum computation,” *Reports on Mathematical Physics*, vol. 57, no. 1, pp. 147–161, 2 2006.
- [85] O. Dubinkin and T. L. Hughes, “Higher-order bosonic topological phases in spin models,” *Phys. Rev. B*, vol. 99, p. 235 132, 23 2019.
- [86] M. B. Plenio, “Remarks on duality transformations and generalized stabilizer states,” *Journal of Modern Optics*, vol. 54, no. 13-15, pp. 2193–2201, 2 2007.
- [87] H. Kalis, D. Klagges, R. Orús, and K. P. Schmidt, “Fate of the cluster state on the square lattice in a magnetic field,” *Phys. Rev. A*, vol. 86, p. 022 317, 2 2012.
- [88] H. A. Kramers and G. H. Wannier, “Statistics of the two-dimensional ferromagnet. part i,” *Phys. Rev.*, vol. 60, pp. 252–262, 3 1941.
- [89] W. Son, L. Amico, R. Fazio, A. Hamma, S. Pascazio, and V. Vedral, “Quantum phase transition between cluster and antiferromagnetic states,” *EPL (Europhysics Letters)*, vol. 95, no. 5, p. 50 001, 2 2011.
- [90] R. Raussendorf and H. J. Briegel, “A one-way quantum computer,” *Phys. Rev. Lett.*, vol. 86, pp. 5188–5191, 22 2001.
- [91] M. Pretko, X. Chen, and Y. You, “Fracton phases of matter,” *International Journal of Modern Physics A*, vol. 35, no. 06, p. 2 030 003, 2 2020.
- [92] R. M. Nandkishore and M. Hermele, “Fractons,” *Annual Review of Condensed Matter Physics*, vol. 10, pp. 295–313, 2 2019.
- [93] R. Orús, H. Kalis, M. Bornemann, and K. P. Schmidt, “Bounds on universal quantum computation with perturbed two-dimensional cluster states,” *Phys. Rev. A*, vol. 87, p. 062 312, 6 2013.
- [94] V. Lahtinen and E. Ardonne, “Realizing all  $so(N)_1$  quantum criticalities in symmetry protected cluster models,” *Phys. Rev. Lett.*, vol. 115, p. 237 203, 23 2015.

- [95] R. Verresen, R. Moessner, and F. Pollmann, “One-dimensional symmetry protected topological phases and their transitions,” *Phys. Rev. B*, vol. 96, p. 165 124, 16 2017.
- [96] P. Weinberg and M. Bukov, “Quspin: A python package for dynamics and exact diagonalisation of quantum many body systems part i: Spin chains,” *SciPost Phys*, vol. 2, no. 1, p. 024 426, 2 2017.
- [97] P. Weinberg and M. Bukov, “Quspin: A python package for dynamics and exact diagonalisation of quantum many body systems. part ii: Bosons, fermions and higher spins,” *SciPost Phys.*, vol. 7, no. arXiv: 1804.06782, p. 020, 2 2019.
- [98] W.-C. Yu, H.-M. Kwok, J. Cao, and S.-J. Gu, “Fidelity susceptibility in the two-dimensional transverse-field ising and  $XXZ$  models,” *Physical Review E*, vol. 80, no. 2, p. 021 108, 2 2009.
- [99] J. Eisert, M. Cramer, and M. B. Plenio, “Colloquium: Area laws for the entanglement entropy,” *Rev. Mod. Phys.*, vol. 82, pp. 277–306, 1 2010.
- [100] L. Zou and J. Haah, “Spurious long-range entanglement and replica correlation length,” *Phys. Rev. B*, vol. 94, p. 075 151, 7 2016.
- [101] Q. Luo, J. Zhao, H.-Y. Kee, and X. Wang, “Gapless quantum spin liquid in a honeycomb  $\Gamma$  magnet,” *npj Quantum Materials*, vol. 6, no. 1, pp. 1–8, 2 2021.
- [102] T. Scaffidi, D. E. Parker, and R. Vasseur, “Gapless symmetry-protected topological order,” *Phys. Rev. X*, vol. 7, p. 041 048, 4 2017.
- [103] R. Verresen, N. G. Jones, and F. Pollmann, “Topology and edge modes in quantum critical chains,” *Phys. Rev. Lett.*, vol. 120, p. 057 001, 5 2018.
- [104] R. Thorngren, A. Vishwanath, and R. Verresen, “Intrinsically gapless topological phases,” *Phys. Rev. B*, vol. 104, p. 075 132, 7 2021.
- [105] S. Trebst, P. Werner, M. Troyer, K. Shtengel, and C. Nayak, “Breakdown of a topological phase: Quantum phase transition in a loop gas model with tension,” *Phys. Rev. Lett.*, vol. 98, p. 070 602, 7 2007.
- [106] T. Hansson, V. Oganesyan, and S. L. Sondhi, “Superconductors are topologically ordered,” *Annals of Physics*, vol. 313, no. 2, pp. 497–538, 2 2004.
- [107] T. Senthil and M. P. A. Fisher, “ $Z_2$  Gauge theory of electron fractionalization in strongly correlated systems,” *Phys. Rev. B*, vol. 62, pp. 7850–7881, 12 2000.

- [108] S. Bhattacharjee, “Quantum destruction of spiral order in two-dimensional frustrated magnets,” *Phys. Rev. B*, vol. 84, p. 104 430, 10 2011.
- [109] A. M. Essin and M. Hermele, “Classifying fractionalization: Symmetry classification of gapped  $\mathbb{Z}_2$  spin liquids in two dimensions,” *Phys. Rev. B*, vol. 87, p. 104 406, 10 2013.
- [110] Y. Kamiya, Y. Kato, J. Nasu, and Y. Motome, “Magnetic three states of matter: A quantum monte carlo study of spin liquids,” *Phys. Rev. B*, vol. 92, p. 100 403, 10 2015.
- [111] S. Sachdev, “Topological order, emergent gauge fields, and fermi surface reconstruction,” *Reports on Progress in Physics*, vol. 82, no. 1, p. 014 001, 2 2018.
- [112] G. B. Halász, J. T. Chalker, and R. Moessner, “Doping a topological quantum spin liquid: Slow holes in the kitaev honeycomb model,” *Phys. Rev. B*, vol. 90, p. 035 145, 3 2014.
- [113] L. Savary and L. Balents, “Coulombic quantum liquids in spin-1/2 pyrochlores,” *Phys. Rev. Lett.*, vol. 108, p. 037 202, 3 2012.
- [114] C. Lannert, M. P. Fisher, and T Senthil, “Quantum confinement transition in a d-wave superconductor,” *Physical Review B*, vol. 63, no. 13, p. 134 510, 2 2001.
- [115] J. C. Y. Teo, A. Roy, and X. Chen, “Unconventional fusion and braiding of topological defects in a lattice model,” *Phys. Rev. B*, vol. 90, p. 115 118, 11 2014.
- [116] S.-P. Kou, J. Yu, and X.-G. Wen, “Mutual chern-simons landau-ginzburg theory for continuous quantum phase transition of  $\mathbb{Z}_2$  topological order,” *Phys. Rev. B*, vol. 80, p. 125 101, 12 2009.
- [117] G. V. Dunne, “Aspects of chern-simons theory,” in *Aspects topologiques de la physique en basse dimension. Topological aspects of low dimensional systems*, vol. 95, Springer, 1999, pp. 177–263.
- [118] S. D. Geraedts and O. I. Motrunich, “Monte carlo study of a  $U(1) \times U(1)$  system with  $\pi$ -statistical interaction,” *Phys. Rev. B*, vol. 85, p. 045 114, 4 2012.
- [119] M. E. Peskin, “Mandelstam-’t hooft duality in abelian lattice models,” *Annals of Physics*, vol. 113, no. 1, pp. 122–152, 2 1978.
- [120] C. Dasgupta and B. I. Halperin, “Phase transition in a lattice model of superconductivity,” *Phys. Rev. Lett.*, vol. 47, pp. 1556–1560, 21 1981.

- [121] O. I. Motrunich and A. Vishwanath, “Emergent photons and transitions in the  $O(3)$  sigma model with hedgehog suppression,” *Phys. Rev. B*, vol. 70, p. 075 104, 7 2004.
- [122] M. Levin and T. Senthil, “Deconfined quantum criticality and néel order via dimer disorder,” *Phys. Rev. B*, vol. 70, p. 220 403, 22 2004.
- [123] H. Kleinert, F. S. Nogueira, and A. Sudbø, “Deconfinement transition in three-dimensional compact  $U(1)$  gauge theories coupled to matter fields,” *Phys. Rev. Lett.*, vol. 88, p. 232 001, 23 2002.
- [124] J. Yu, S.-P. Kou, and X.-G. Wen, “Topological quantum phase transition in the transverse wien-plaquette model,” *EPL (Europhysics Letters)*, vol. 84, no. 1, p. 17 004, 2 2008.
- [125] I. S. Tupitsyn, A. Kitaev, N. V. Prokof’ev, and P. C. E. Stamp, “Topological multicritical point in the phase diagram of the toric code model and three-dimensional lattice gauge higgs model,” *Phys. Rev. B*, vol. 82, p. 085 114, 8 2010.
- [126] F. Wu, Y. Deng, and N. Prokof’ev, “Phase diagram of the toric code model in a parallel magnetic field,” *Phys. Rev. B*, vol. 85, p. 195 104, 19 2012.
- [127] J. Vidal, S. Dusuel, and K. P. Schmidt, “Low-energy effective theory of the toric code model in a parallel magnetic field,” *Phys. Rev. B*, vol. 79, p. 033 109, 3 2009.
- [128] E. Fradkin and S. H. Shenker, “Phase diagrams of lattice gauge theories with higgs fields,” *Phys. Rev. D*, vol. 19, pp. 3682–3697, 12 1979.
- [129] S. Dusuel, M. Kamfor, R. Orús, K. P. Schmidt, and J. Vidal, “Robustness of a perturbed topological phase,” *Phys. Rev. Lett.*, vol. 106, p. 107 203, 10 2011.
- [130] G. A. Jongeward, J. D. Stack, and C. Jayaprakash, “Monte carlo calculations on  $Z_2$  gauge-higgs theories,” *Phys. Rev. D*, vol. 21, pp. 3360–3368, 12 1980.
- [131] L. Genovese, F. Gliozzi, A. Rago, and C. Torrero, “The phase diagram of the three-dimensional  $Z_2$  gauge higgs system at zero and finite temperature,” *Nuclear Physics B-Proceedings Supplements*, vol. 119, pp. 894–899, 2 2003.
- [132] M. Campostrini, M. Hasenbusch, A. Pelissetto, P. Rossi, and E. Vicari, “Critical behavior of the three-dimensional XY universality class,” *Phys. Rev. B*, vol. 63, p. 214 503, 21 2001.

- [133] G.-Y. Zhu and G.-M. Zhang, “Gapless coulomb state emerging from a self-dual topological tensor-network state,” *Phys. Rev. Lett.*, vol. 122, p. 176 401, 17 2019.
- [134] C. Xu and S. Sachdev, “Global phase diagrams of frustrated quantum antiferromagnets in two dimensions: Doubled chern-simons theory,” *Phys. Rev. B*, vol. 79, p. 064 405, 6 2009.
- [135] C. Dasgupta and B. I. Halperin, “Phase transition in a lattice model of superconductivity,” *Phys. Rev. Lett.*, vol. 47, pp. 1556–1560, 21 1981.
- [136] M. P. A. Fisher and D. H. Lee, “Correspondence between two-dimensional bosons and a bulk superconductor in a magnetic field,” *Phys. Rev. B*, vol. 39, pp. 2756–2759, 4 1989.
- [137] J Villain, “Spin glass with non-random interactions,” *Journal of Physics C: Solid State Physics*, vol. 10, no. 10, pp. 1717–1734, 2 1977.
- [138] T. Senthil and M. P. A. Fisher, “Competing orders, nonlinear sigma models, and topological terms in quantum magnets,” *Phys. Rev. B*, vol. 74, p. 064 405, 6 2006.
- [139] T Senthil and M. P. A. Fisher, “Fractionalization and confinement in the  $U(1)$  and  $Z_2$  gauge theories of strongly correlated systems,” *Journal of Physics A: Mathematical and General*, vol. 34, no. 10, pp. L119–L125, 2 2001.
- [140] S. Bhattacharjee, “Quantum destruction of spiral order in two-dimensional frustrated magnets,” *Phys. Rev. B*, vol. 84, p. 104 430, 10 2011.
- [141] P. Fendley, “Strong zero modes and eigenstate phase transitions in the xyz/interacting majorana chain,” *Journal of Physics A: Mathematical and Theoretical*, vol. 49, no. 30, 30LT01, 2 2016.
- [142] A. Y. Kitaev, “Unpaired majorana fermions in quantum wires,” *Physics-Uspokhi*, vol. 44, no. 10S, pp. 131–136, 2 2001.